Implementation of fibre reinforcement in between the layers of 3D concrete printing

van Brunschot, M.C.A.J.

Award date:
2019

IMPLEMENTATION OF FIBRE REINFORCEMENT IN BETWEEN THE LAYERS OF 3D CONCRETE PRINTING

GRADUATION THESIS

M.C.A.J. VAN BRUNSCHOT

Eindhoven University of Technology

Department of the Built Environment

Master	Architecture, Building and Planning
Specialisation	Structural Design

Title	Implementation of fibre reinforcement in between the layers of 3D concrete printing

Report number	A-2019.269
Version	Final
Date	May 10, 2019

Student	M.C.A.J. (Maikel) van Brunschot
Student number	0742208
E-mail	m.c.a.j.v.brunschot@student.tue.nl maikel-van-brunschot@live.nl

Graduation committee	Prof. dr. ir. T.A.M. (Theo) Salet Dr. ir. F.P. (Freek) Bos Z.Y. (Zeeshan) Ahmed M.Arch

PREFACE

This graduation thesis concludes my graduation project on the topic of implementing fibre reinforcement in between the layers of 3D concrete printing. It is the final project before completion of the master program 'Architecture, Building and Planning', with the specialisation 'Structural Design' at the Eindhoven University of Technology. This study is part of the research group on 3D concrete printing.

First of all, I want to express my gratitude towards the graduation committee, Theo Salet, Freek Bos, and Zeeshan Ahmed. Over the course of this project they supported me with their knowledge and feedback helping me to get to the final result as it now is. In times when the research might end up in a dead end, the provided me with practical solutions and new approaches to solve the problems.

Secondly, I want to thank the personnel of the Structural Laboratory at the Eindhoven University of Technology. Their years of experience is highly appreciated and deemed helpful during the performed experimental program. Also with regard to the development of the device which was needed to succeed my graduation project, they were always available to make or repair tools which were required for the 3D concrete printer.

Finally, I want to thank my fellow students from the 3D concrete printing group for their help at the 3D concrete printer and their feedback during my graduation. Without the mutual collaboration my research and the overall research on 3D concrete printing would never been possible.

Maikel van Brunschot,

Waalwijk, May 2019

ABSTRACT

The production method of 3D concrete printing is gaining interest in the construction industry, nevertheless the majority of the printed concrete structures are unreinforced resulting in a lack of tensile capacity. The aim of this study is to analyse the possibility to implement fibre reinforcement in between the layers of printed concrete. In general reinforcement is entrained inside the concrete, however the layered manufacturing technique enables this alternative approach of reinforcing printed concrete structures. A device is developed to transport and deposit the fibres on top of the concrete layers without significantly influencing the printing process. Additionally, the influence on the structural capacity due to the addition of fibres is examined in an analytical model and an experimental program.

Firstly, a device is developed to automate the process of adding fibres to the concrete printing process. This device transports the fibres by means of an air flow from a storage bucket towards the robot arm. A test program is developed to examine the workability of this device, in here the consistency of the output and the influence on the depositing method of the concrete layers is observed. Several adaptions are made to this device resulting in an improved control over the output quantity of the fibres. By observing the printing parameters it is concluded that the nozzle type and printing offset directly influence the possibility to add fibres in between the concrete layers. A reduction in the printing offset results in a negative influence on the fibre distribution. In addition to this, the nozzle type could negatively influence the fibre distribution while it can push the fibres aside.

Simultaneously, an analytical model is proposed to analyse the influence on the structural capacity. By calculating internal equilibrium, a load-deflection diagram is obtained. In conventional casted concrete the fibre distribution is, in general, unknown which makes it difficult to give an accurate prediction of the structural behaviour. The layered manufacturing technique of 3D concrete printing makes this possible, by conducting an image analysis the fibre distribution is known for each layer. Based on the pull-out behaviour of a single fibre, the contribution of the fibres in the cracked section can be taken into account. Hereby the load bearing capacity can be determined for any given vertical deflection.

Besides the analytical model, an experimental study is conducted in which the influence on the flexural strength is observed. From this it can be concluded that the interfacial bond between the fibre and the concrete matrix and the geometry of the fibre are important aspects. The bond between the tested alkali resistant glass fibre and the concrete matrix seems to improve the peak strength, however further testing is needed to support this assertion. The post-peak behaviour is directly influenced by the shape of the fibre, an increase in fracture energy is observed for the deformed fibre types. Although in most cases a positive influence is obtained for the structural behaviour, it is shown from a proof of concept print that an excessive use of fibres can reduce the bond strength in the interface. Rupture in the interface occurred once a too large coverage percentage was applied, further testing is required in order to define the upper limit of fibre quantity in between the layers. Finally, a comparison is made between the experimental results and the proposed analytical model. In here several assumptions are made for the pull-out response of the fibres. By implementing a distribution factor, which takes several parameters into account, a good agreement can be found between the analytical and experimental output.

In summary, from the study is can be concluded that fibre reinforcement in between the concrete layers can be of additional value for the 3D concrete printing process. However, the currently tested fibres and concrete mixture result in a strain softening behaviour, thus it cannot be used as primary reinforcement at this moment.

TABLE OF CONTENTS

NOTATION

Greek symbols:

α	Distribution factor	-
β	Overlap factor	-
δ	Vertical deflection	mm
ΔL	Elongation/Shortening of beam	mm
ε_c	Compressive strain in concrete	‰
ε_{c3}	Compressive strain in concrete at 1.75 ‰	‰
ε_{cr}	Tensile strain in concrete at cracking	‰
ε_{ct}	Tensile strain in concrete	‰
ε_{cu3}	Ultimate compressive strain in concrete	‰
θ	Rotation at supports	Rad
κ	Curvature	/m
ρ_{cov}	Coverage percentage	%
σ_c	Compressive stress in concrete	N/mm^2
σ_{ct}	Tensile stress in concrete	N/mm^2
τ_{av}	Average bond stress	N/mm^2

Roman symbols:

$A_{c;t}$	Concrete surface	mm^2
A_f	Cross sectional area of fibre	mm^2
$A_{f;t}$	Surface of single fibre	mm^2
b	Width of beam	mm
c	Height of compressive zone	mm
d_f	Diameter of fibre	mm
E_{cm}	Secant modulus of elasticity of concrete	N/mm^2
f_{cd}	Design value of concrete compressive strength	N/mm^2
f_{ctm}	Mean value of axial tensile strength of concrete	N/mm^2
f_{cm}	Mean value of concrete cylinder compressive strength	N/mm^2
f_{Fy}	Tensile strength of fibre	N/mm^2
f_{Lk}	Characteristic value of nominal strength	N/mm^2
F_p	Pull-out force	N
f_{R1k}	Post-cracking residual strength at serviceability limit state	N/mm^2
F_{R3k}	Post-cracking residual strength at ultimate limit state	N/mm^2
G_f	Fracture energy	N/mm
h	Height of beam	mm
h_{cr}	Height of crack	mm
h_i	Layer height	mm
L	Length of span	mm
L_e	Embedment length	mm
M_e	Moment capacity	Nmm
m_f	Mass of single fibre	g
N_c	Compressive force concrete	N
$N_{f;i}$	Tensile force fibres	N
n_i	Number of fibres	-
N_t	Tensile force concrete	N

O_{blower}	Output of blower	g
w	Crack opening	mm
x	Height of uncracked tensile zone	mm
$x_{N;c}$	Distance from neutral axis compressive zone	mm
$x_{N;fi}$	Distance from neutral axis fibres	mm
$x_{N;t}$	Distance from neutral axis uncracked tensile zone	mm

1. INTRODUCTION

1.1 SCOPE OF RESEARCH

Nowadays 3D concrete printing is gaining a lot of interest in the construction industry, as the first show cases are being constructed using this additive manufacturing technology. However until now most structures are unreinforced and thus unable to withstand tensile forces. Therefore the next step in the development of this additive manufacturing technique is the application of reinforcement. In the last couple of years the principle of printing concrete has been researched at Eindhoven University of Technology. This relatively new manufacturing technique has a great freedom in designing concrete structures. In order to print concrete structures a 4-axis gantry robot is used, which can move in x-, y-, and z-direction and rotate around its z-axis. A layered manufacturing process is used to build the element, to do so a thixotropic concrete is used. In the mixing chamber of the pump dry-mix and water are added, which is continuously sheared to avoid a thixotropic build-up of the concrete. Hereafter a rotor-stator pump is used to pump the material through a hose, a continuous flow of material is obtained by using this type of pump. At the end of the hose a nozzle is fixed to the gantry robot which moves over a print path. The set-up of the system is shown in figure 1.1 a more elaborate description of the printing process is described by Bos et al. [7].

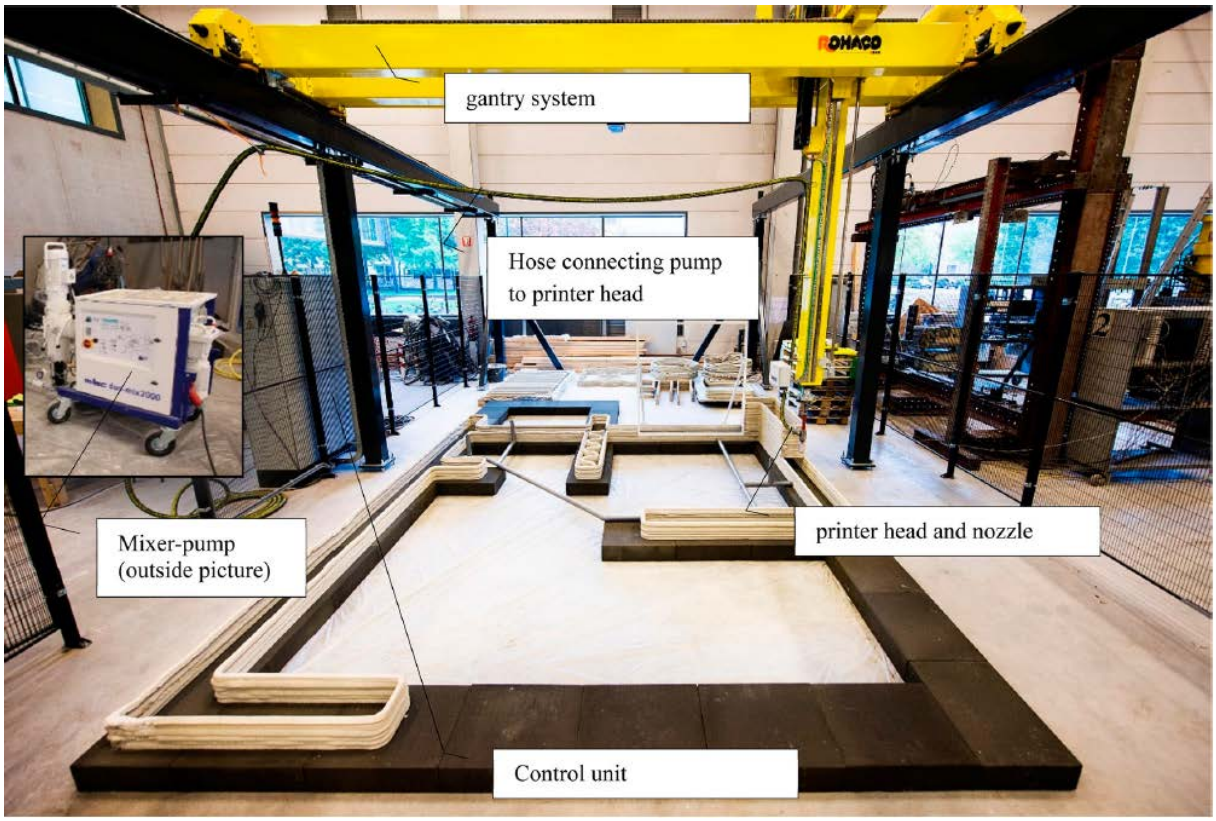

Figure 1.1: 3D Concrete printing facility at the Eindhoven University of Technology. (Bos et al. [7])

Concrete as a material is able to withstand relatively large compressive forces, on the other hand the tensile capacity of the material is rather low. By adding reinforcement to the concrete the tensile capacity of the material is increased. The conventional way of adding reinforcement is by placing rebar in the elements. For printed concrete structures rebar can be placed between the layers of concrete, this method is analysed by Goris [19] (figure 1.2). Steel bars with different diameters are tested to investigate the compatibility with printing of concrete. From this research it can be stated that the position of placement of the rebar highly affects the bond between the bar and the concrete.

Furthermore, the bar diameter is of great influence for the bond, while for larger diameters air pockets occurred near the rebar resulting in a decrease in contact area. When the placement method is observed it can be said that conventional rebar might restrict the freedom in design, which is one of the benefits of printing concrete. Another disadvantage is the labour intensity of placing rebar in printed structures, up till now rebar has to be placed by hand in each layer. This process can later be automated, however in general rebar is not very flexible. This might restrict the freedom in motion and printing shape which can be obtained by concrete printing. A second option for reinforcing printed concrete is the use of a steel cable, which is investigated by Jutinov [22] and Dezaire [15] at the Eindhoven University of Technology (figure 1.2). This method has similarities with conventional rebar, however a cable is flexible so the freedom in design is not restricted. A device is developed which embeds the cable simultaneously during printing, which reduces the labour intensity compared to conventional rebar. Also for this research the bond between the cable and the concrete showed difficulties, especially with regard to the placing method. The material has a low viscosity as long as it is continuously sheared or pumped through the hose, hereby it flows around the cable during placement. Once the material is placed on the previous layer is regains it thixotropic behaviour, thus the material will not flow beneath the cable and result in an air gap. This air gap leads to a reduction in contact surface between the cable and the concrete and thus reduces the bond between the reinforcement and the concrete matrix. A third option of reinforcement is to add fibres to the concrete, by doing so a composite material is created which has a post-cracking residual tensile strength [16]. Adding fibres to printing concrete can be less labour intensive compared to regular rebar as reinforcement, it is also less influencing with regard to the freedom of design. Earlier research at Eindhoven University of Technology has shown that the addition of fibres to printed concrete can be beneficial for the flexural strength [38]. In the current research the possibility of adding fibres to the process of printing concrete is further analysed.

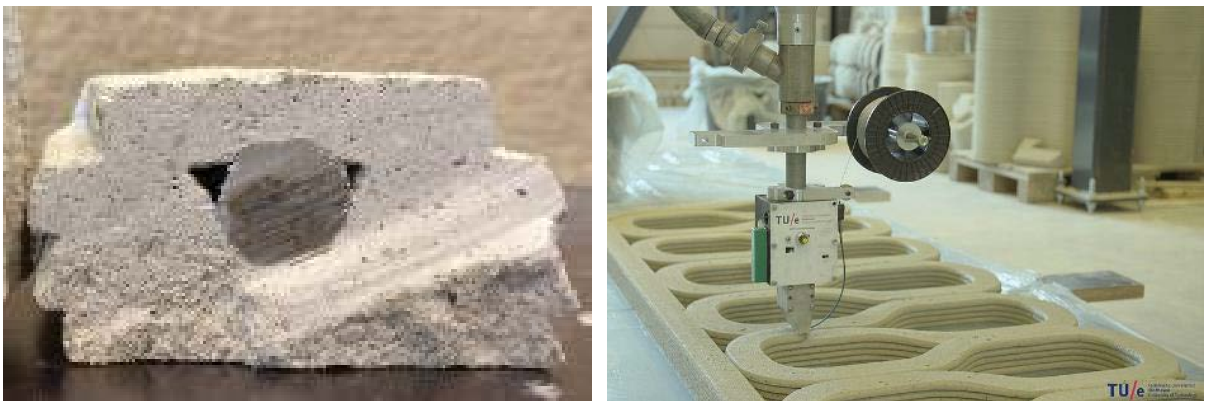

Figure 1.2: *Section of rebar in printed concrete (Left); Printing of cable reinforced concrete (Right). (Goris [19]; Dezaire [15])*

In practice the fibres are added to the concrete during mixing, in a concrete drum the fibres are dispersed to get a homogeneous material. In the concrete printer water and a dry-mix are added in a mixing chamber, from here the material is pumped through a rotor-stator pump from which a hose leads to the printing nozzle. The rotor-stator pump builds up the pressure to pump the material through the hose, however due to this pump a limitation of particle size is obtained. For the dry-mix a maximum grain size of approximately 4 millimetre [50] is allowed, the same size limitation holds for the fibres which can go through this pump. In practice there are microfibres which can be transported by the rotor-stator pump, and can thus be added in the dry-mix or the mixing chamber. Synthetic micro fibres are already added to the dry-mix to reduce the plastic shrinkage of the material, however these have little to no influence on the structural behaviour. In order to add the fibres a more generic addition method is required which is able to implement different fibre types. Thus to add fibres a

different solution needs to be found to print fibre reinforced concrete, in which the fibres are added after the rotor-stator pump. The first possibility is to add the fibres in the concrete hose, hereby the pressure created by the rotor-stator pump is lost. It is thus needed to design an additional device for this option to transport the material further towards the nozzle. A second option is to design a nozzle in which the concrete and fibres are mixed, however by doing so a short mixing time is obtained. This could lead to an inhomogeneous mixture of fibres and concrete. Another option can be to look at the system from a different approach. In general the fibres are premixed with the concrete before an element is created. However due to the layered manufacturing technique it is also possible to add the fibres after the concrete is deposited, hereby the fibres are placed in between the layers of concrete. This means that in general there are two options to add the fibres: 1.) fibres inside the concrete and 2.) fibres in between the layers (figure 1.3). When a fibre reinforced element is observed it is desired that the fibres are distributed evenly over the element. By printing concrete an element is created layer by layer, so the positioning of the fibres can easily be controlled over the height of the element for both options. Due to the small layer height compared to the height of an element this control of position can be precise.

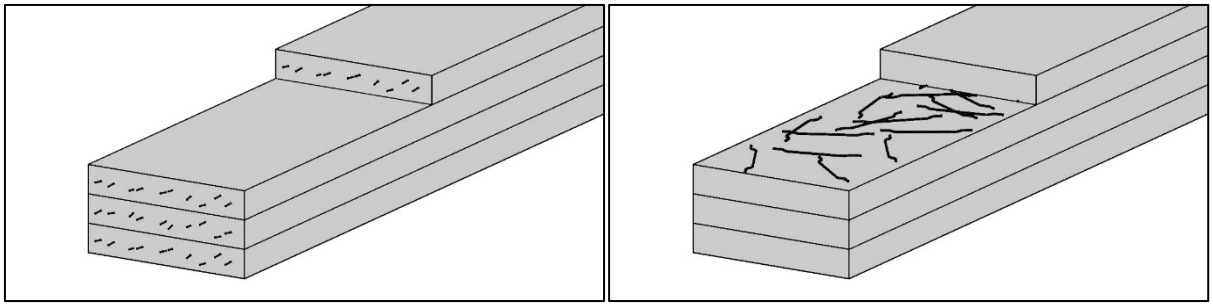

Figure 1.3: *Options of fibre location by layered manufacturing technique; 1.) Fibres mixed inside the concrete (Left); 2.) Fibres in between the layers of printed concrete(Right).*

By comparing the two methods of adding fibres the opportunities and challenges of both options can be balanced against each other. Some differences between the two method can be listed, the first thing is the freedom in type of the fibre. When the fibres are mixed with the concrete, the size is limited by the dimensions of the concrete hose and the nozzle which is used. This size limitation does not hold for sprinkling fibres in between the layers of concrete. Additionally, the option of using deformed fibres is easier for sprinkling fibres in between the layers, while fibre balling can occur once deformed fibres are pumped through a small concrete hose. With the ability of using a large variety of fibre types, the possibility of achieving a specific structural behaviour increases. This structural behaviour of the composite material is dependent on the type of fibre which is used.

Another factor which differs for the two methods is the workability of the material. When a low dosage of fibres, less than 0.25% by volume, is added to concrete, the mixture does not necessarily has to change [3]. However to obtain an improved structural capacity these amounts are too little. In general, the water-cement ratio can be increased once fibres are added to the concrete or the quantity of water-reducing admixture is increased. For printing concrete the layered manufacturing method is of great importance, the material has to be stiff enough to print on the previous layer. Therefore there is a certain limitation in what can be changed in the material composition like the water-cement ratio or the addition of plasticisers. When fibres are sprinkled between the layers the material composition does not has to change, so the process of printing concrete remains the same. This means that the printing process does not significantly has to be altered.

Furthermore, it is also expected that there will be a difference with regard to orientation of the fibres between the two methods. From research done by Raedts [38] it was shown that almost all fibres in

the printed concrete were orientated parallel to the printing direction. This orientation is most likely due to the flow of the material, fibres are added to the concrete and are pumped along for a certain distance through the concrete hose. The orientation of the fibres for the option where the fibres are placed in between the layers is expected to be more random. While there is no influence of the concrete flow, the fibres will be randomly orientated in the 2D plane perpendicular to the print direction. For both cases it is expected that the fibres will not be orientated parallel to the printing direction, hereby an inhomogeneous material is obtained. The mechanical behaviour of the material will thus be dependent of the test direction.

Finally, when the interface between the layers is observed, the addition of fibres in between the layers might have an influence on the bond strength. Several tests are performed on the interface of plain concrete to analyse the homogeneity of the printed elements at the Eindhoven University of Technology [17][43]. From this research it is concluded that several parameters have an influence on the bond strength between the layers, for instance test direction and time interval. If the test direction is observed, it can be concluded that the tensile strength for samples tested perpendicular to the print direction is less compared to samples which are tested parallel to the printing direction. The same holds for the cases in which the printing time is increased, here a reduction in strength is obtained. If the time interval between the two printing layers is increased the bond between the interfaces is reduced. For the case where fibres are added between the layers a new parameter is introduced. It is expected that for an excessive amount of fibres a reduction in bond strength is obtained, particularly if an overlap of fibres occurs. In the case for which fibres are mixed within the concrete it is expected that the influence on the interface strength is of less influence. Even though it might be needed to adjust certain printing settings, no fibres are directly added at the interface level.

In conclusion, both reinforcing methods do have their opportunities and challenges and it can be interesting to analyse their compatibility with the printing process. In the current research the method to deposit the fibres in between the layers is further analysed. The freedom in type of fibre and the low influence on the 3D concrete printing process show potential to improve the structural behaviour of the concrete material.

1.2 RESEARCH GOAL AND METHODOLOGY

To determine whether fibre reinforcement can be of additional value for 3D concrete printing, a study is conducted. In this study the manufacturing method and the influence on the structural capacity are analysed. The main goal of this research is to analyse whether it is possible to implement fibre reinforcement in between the layers of 3D printed concrete. By adding fibre reinforcement to the printed concrete, the ductility of the material can be improved. Different fibre types can also improve the tensile capacity compared to the plain concrete. This research goal can be divided into two main research questions, for which the first can be stated as follow.

"How can fibre reinforcement be deposited in between the layers in the 3D concrete printing process?"

To answer the first question, the manufacturing method of fibre reinforced concrete is observed. A study is conducted to understand how fibres are handled in the conventional concrete industry. During this research a device is developed which can deposit the fibres on top of the printed concrete layers. Hereby the compatibility with the concrete printing process has been considered. Different methods are analysed, and a test program is conducted to gain control over the deposition method. By the addition of fibre reinforcement in between the layers a new parameter is introduced to the concrete printing process, which can influence the depositing method of the concrete layers. To analyse the influence on the printing parameters an empirical study is conducted. Besides the possibility to add fibres to the printed concrete it is also of interest to analyse the influence on the mechanical behaviour. To do so the impact of fibre reinforcement on printed concrete has to be understood, thus the second part of research is related to the influence on the mechanical behaviour.

"What is the impact on the structural capacity of fibre reinforcement in between the layers of printed concrete?"

To predict the influence on the strength an analytical model can be made in which the contribution of the fibres is taken into account. Hereby the structural behaviour will be dependent on the type of fibre which will be used. In practice a large variety of fibre types are available, with respect to length, geometry, material, etc. In literature the influence on conventional casted concrete is already analysed, however it cannot be stated with certainty that this also holds for printed concrete. Different fibre types are experimentally tested to observe the influence on the flexural behaviour of printed concrete.

At the end of this study an overview can be given about the opportunities and challenges of fibre reinforcement in between the layers of printed concrete. With the development of a transportation/depositing device, the process of printing fibre reinforced concrete can be automated. Additionally, an understanding about the influence of different fibre types on printed concrete is obtained by the analytical and experimental study which is conducted.

1.3 THESIS OUTLINE

In this thesis the possibility to reinforce printed concrete structures with fibres in between the layers is analysed. Nowadays a lot of research is conducted towards using fibre reinforcement for printed concrete structures, however this research is still in its early stage. Therefore, it is needed to start from scratch to understand what the influence is of adding fibres to the concrete printing process. To get a first understanding a brief literature study is conducted in the second chapter. In this study the behaviour of conventional fibre reinforced concrete is analysed, starting from the fibre properties on a small scale towards the overall behaviour of the material. Subsequently, the influence of the printing technique is observed for plain concrete and fibre reinforced concrete. Based on this a selection can be made regarding the most important parameters.

The influence of adding fibres to the printing process is analysed in the third chapter, here the depositing method and the printing process are observed. From these analyses a device is developed to transport and deposit the fibres in between the layers of printed concrete. A test program is conducted to determine the influence on the manufacturing method. The adaptions are described which are made to improve the consistency of the device. An analysis is given about the compatibility with the current printing process of the device which is developed.

Next, an analytical model is proposed to analyse the influence of fibre reinforcement in between the layers on the structural behaviour. The concept and implementation of this model is described in chapter four. Based on some theoretical assumptions a first prediction can be given about the structural capacity. Additionally, an experimental study is conducted to analyse the influence on the structural behaviour. In chapter five the material properties and the test set-up are described. The results of this study are discussed in chapter six, in here the influence of different fibre types is observed.

Finally, the conclusions and recommendations following from this research are discussed in chapter seven. The addition method of fibres is analysed, and the development of a transportation/depositing device is assessed. Also, the influence of fibre reinforcement in between the layers is analysed based on the conducted experimental study. In this research the possibility of adding fibre reinforcement is investigated, recommendations are given for future research to continue this research topic.

2. LITERATURE STUDY

First the available information is analysed to see what research has already been done into fibre reinforced concrete. From the pull-out behaviour of a single fibre to a concrete element reinforced with steel fibres, the influence on the material properties is analysed. Hereafter, the production process is analysed, while different parameters are of importance for printed concrete compared to casted concrete.

2.1 FIBRE REINFORCED CONCRETE

The concept of reinforcing brittle material by means of fibres is already used for centuries. Natural products such as straw and horse hair could be used to reinforce masonry mortar and plaster. In the last decades extensive research has been done towards improving cementitious composites by means of fibres. In the late 1950s, research started towards the possibility to add glass fibres to concrete. It was quickly discovered that the alkaline environment of concrete destroyed the ordinary glass fibres. This resulted in the development of alkali resistant glass fibres which are still used today. The first research into adding steel fibres to concrete also started at this time. It followed from research that the toughness of concrete increased by the addition of the steel fibres [2].

Nowadays fibre reinforced concrete mixtures can consist of a large variety of fibre types, most classifications given by codes are based on the material of the fibre. In Europe NEN-EN-14889 is commonly used which makes a division in two categories, steel fibres and polymeric fibres. The group of steel fibres consists of carbon, galvanised steel, and stainless-steel fibres and makes a subdivision based on the manufacturing method. Fibres can be made by using different processes such as cold drawn wire, cut from sheets, melt extracted, shaved cold drawn wire, or milled from steel blocks. Also, for the polymeric fibres a subdivision is made, however this is related to the size of the fibre. The first category consists of microfibres (Polymer I) which have an equivalent diameter which is smaller than 0.3 millimetre. Here a distinction can be made between a monofilament (Polymer IA) and fibrillated fibres (Polymer IB) which consists of multiple strands. The second type of polymeric fibres are the macrofibres (Polymer II) which have a diameter larger than 0.3 millimetre. Polymer type I fibres are generally used for non-structural applications while steel fibres and polymer type II can be suitable for structural use. ACI 544.1R-96 [2] is commonly used in America to make a classification of fibre types. Also this code is based on the material of the fibre, however in this code four groups are distinguished. Here a distinction is made between steel, glass, synthetic, and natural fibres. Each fibre type will result in a different type of structural behaviour. By adding fibres, the amount of conventional reinforcement might be reduced or in some cases even completely eliminated. Microfibres can be used to reduce the amount of cracking due to early-age shrinkage, which has a positive effect on the durability of the element [52]. The selection of fibre type, or combination of fibres, is dependent on the structural capacity which is required.

To date, the application of fibre reinforced concrete in the construction industry is rather limited. Fibre reinforcement is mainly used to limit the crack width or to increase the toughness. Due to the distribution in the concrete a more diffused crack pattern can be developed [11]. Industrial floor, sewage pipes, tunnel linings, etc. are examples for which steel fibres can be added to a concrete mixture [27]. Examples for which alkali resistant glass fibres can be used are façade panels and building restorations due to their relative low weight [2]. To avoid plastic shrinkage in concrete elements low amounts of synthetic fibres can be added to the mixture. Another option is to use fibre reinforcement in combination with conventional rebar. Here it can be used as (partial) replacement for stirrups or to

replace a part of the conventional reinforcement [11]. For structures in which fibres and conventional rebar is combined, it is usually required to design the structure such that the rebar is able to bear the total load. This is due to the random distribution and orientation of the fibres in the concrete. Until now no calculation rules are adopted in Eurocode 2 for structures only reinforced with fibres, although they are currently under development. The fib Model Code 2010 [16] prescribes that conventional rebar can only be fully substituted by fibres if the following relationships are fulfilled:

- $f_{R1k}/f_{Lk} \geq 0.4$
- $f_{R3k} / f_{R1k} \geq 0.5$

In which:

f_{R1k} = post-cracking residual strength at serviceability limit state
f_{R3k} = post-cracking residual strength at ultimate limit state
f_{Lk} = characteristic value of the nominal strength

These parameters describe the material behaviour in the serviceability limit state and in the ultimate limit state. The residual strength values are obtained by performing a Crack Mouth Opening Displacement test. These relationships make sure that a brittle behaviour of fibre reinforced concrete is avoided in structural elements.

2.2 PULL-OUT BEHAVIOUR

To get a first insight in the behaviour of fibre reinforced concrete as a material, the behaviour of a single fibre has to be understood. When the tensile strength of plain concrete is reached, small cracks appear which result in failure of the concrete element. By adding fibres to the concrete, the fibres will bridge these cracks, resulting in a post-cracking behaviour. The ductility of the brittle material concrete is increased [8], while the stresses are transferred across the cracks by the fibres. The fibres which cross the cracks will also delay crack propagation [8][21], thus the properties will improve. According to Robins et al. [39] the pull-out behaviour of a steel fibre can be divided into three bond mechanisms:

- Adhesion; Elastic shear bond.
- Friction; Frictional shear bond.
- Mechanical anchorage; Creates localised load transfer points between fibre and matrix.

The first two bond mechanisms are valid for all type of fibres, mechanical anchorage is only present for deformed fibres. In research done by Marković [27] these three bond mechanisms are described. The adhesion is directly related to the strength of the concrete in the interface transition zone, which is the concrete area surrounding the fibre. When the pull-out behaviour of a fibre is observed it can be said that debonding occurs in the interface transition zone and not at the surface of the fibre. Due to the wall effect around the fibre a non-efficient packaging of aggregates leads to a higher porosity in this zone. With a higher porosity the strength and stiffness are reduced compared to the bulk material. The width of this interface transition zone varies from 20-75 μm [13] (see figure 2.1).

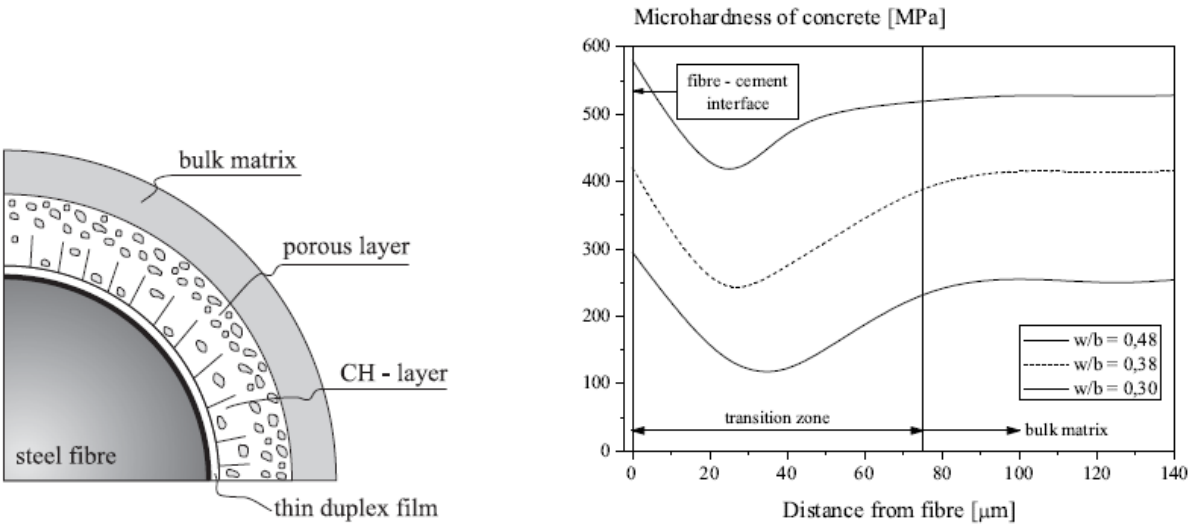

Figure 2.1: *Cross section through steel fibre, interface transition zone (Left); Results of microhardness test (Right). (Cunha et al. [13])*

At a certain pull-out force the debonding process of a fibre ends and there is no adhesion anymore. From this point the pull-out resistance is obtained due to the frictional bond of the fibre. In this process frictional stresses occur along the interfacial zone during slip of the fibre. This slip results in abrasion and a compaction process along the interfacial zone. This abrasion lead to a smoother surface and thus less frictional resistance of the matrix surface once a fibre is pulled out further. The shape of a fibre is also important for the pull-out behaviour, when a hooked-end fibre is observed an extra bond mechanism occurs know as mechanical anchorage. Due to the hook a mechanical interlock is created, when a fibre is pulled-out a plastic deformation occurs. This means that a higher amount of energy is needed, thus higher pull-out force, for the fibre to be pulled-out. Mechanical anchorage occurs after the adhesion mechanism, once the hook is straightened the pull-out behaviour is again governed by friction [27]. In practice it is usually observed that the hooks of a fibre are not completely straightened, which results in larger frictional stresses.

For a straight fibre the pull-out behaviour is only governed by adhesion and friction of the fibre, in figure 2.2 this process is shown. Adhesion is the first bond mechanism which occurs, this is shown in step a and b. After fully debonding the final step c occurs, where the pull-out resistance is obtained by friction between the fibre and the concrete matrix. The debonding process for a hooked-end fibre is shown in steps figure 2.2. In steps a and b the fibre is debonding, after which step c and d show the deformation of the fibre, mechanical anchorage. After the fibre is straightened the pull-out behaviour is governed by friction, which is similar to the behaviour of a straight fibre [27].

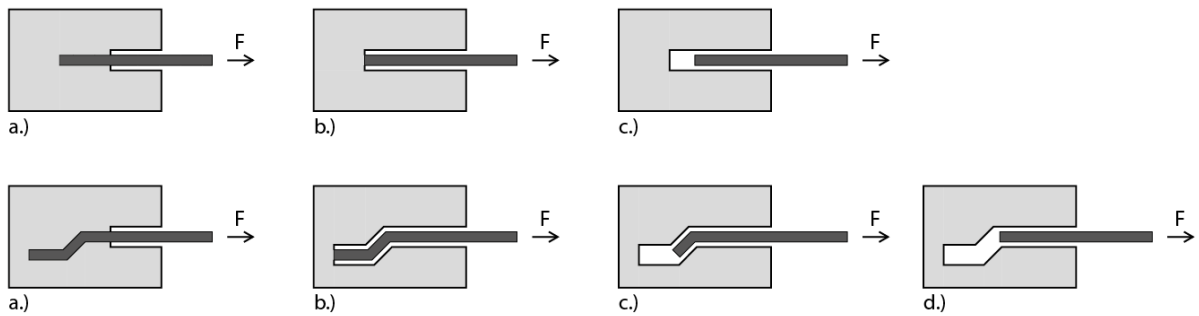

Figure 2.2: *Pull-out process of straight fibre (Top); Pull-out process of hooked-end fibre (Bottom). (Marković [27]) (Modified)*

When the load-slip relation of fibre pull-out is observed, these different stages can be described. In figure 2.3 a load-slip diagram of a straight fibre and a hook-end fibre are shown [26]. Adhesion of the fibre results in a linear, ascending branch (OA), after which debonding of the fibre starts (AB). After debonding of the fibre, the fibre will be pulled out of the concrete. In this stage the pull-out behaviour is governed by frictional stresses (BF). For a hooked-end fibre, deformation of the hook will occur after the debonding phase. The mechanical anchorage results in an increase for the pull-out force (BC), after this stage plastic deformation of the hook takes place (CE). Once the hook of the fibre is straightened the fibre will act as a straight fibre, from this point frictional stresses will define the pull-out behaviour (EF).

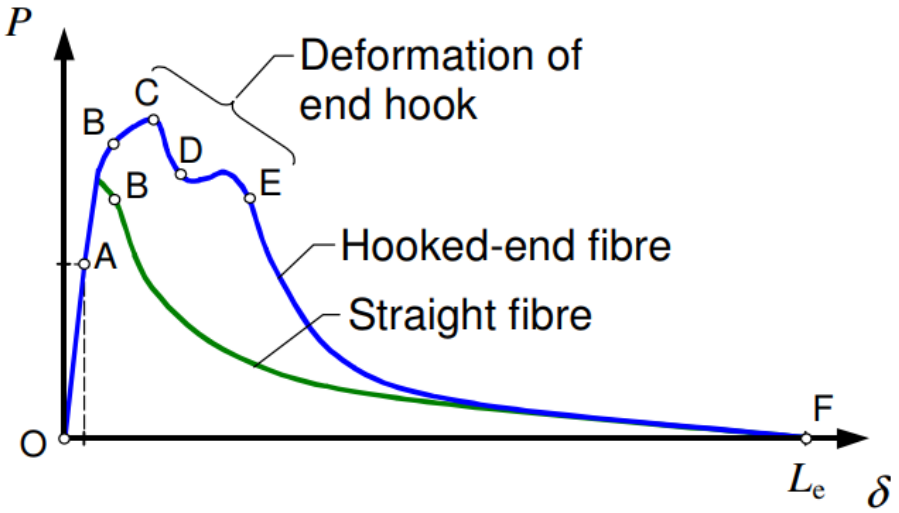

Figure 2.3: *Typical fibre pull-out relationship of straight and hooked-end fibre. (Löfgren [26])*

Several parameters have been investigated to determine the influence on the mechanical properties of fibre reinforced concrete. This influence can be divided into two main categories, the properties of the fibre and the properties of the cement matrix. When the properties of the fibres are observed a variation can be made regarding the shape, fibre orientation, embedment length and material. For the properties of the cement matrix the type of concrete that is used can be of importance. In appendix A an elaborate literature study is conducted for each parameter.

2.3 Material behaviour

The influence of adding fibres to concrete can also be observed from a material point of view instead of by observing the pull-out behaviour of a single fibre. Fibres have, in most cases, a positive effect on the mechanical properties like the tensile and compressive strength. Additionally, a reduction in shrinkage and creep deformations is obtained by the addition of fibres [4][9]. Fibre reinforced concrete can be seen as a unique composite material based on experimental results. According to di Prisco et al. [16] the characteristics of this material depend mainly on the location and orientation of the fibres, which are in general difficult to determine. While these factors are unknown it is rather difficult to give a reliable prediction for the behaviour of the overall material. The material properties are influenced by the aspect ratio and the fibre ratio according to Yazici et al. [47]. In general, a value between 50 and 100 is chosen for the aspect ratio, for the fibre ratio there is often chosen for a volume percentage between 0.5% and 2.5%.

When the length of the fibres is observed a distinction can be made between short (6-13mm) and large (30-60mm) fibres. The short fibres bridge the micro cracks in the first stage, they increase the tensile strength of the material in the pre-peak stage. In general, a large quantity of small fibres is used which

results in a small distance between these fibres, once a crack starts growing the micro fibres are pulled out of the matrix and they lose their function. The long fibres are activated once a macro crack occurs, these fibres increase the ductility of the material by bridging the cracks [27]. In figure 2.4 this situation is shown, where a mixture of short and long fibres is loaded in tension. The option to combine different types of fibres has also been investigated. Research done by Pakravan et al. [34] states that the use of multiple fibres has an advantage, regarding strength and costs, compared to individual fibre reinforce concrete. For a hybrid fibre reinforced concrete, the tensile capacity is increased due to the micro fibres and the ductility is improved by the macro fibres.

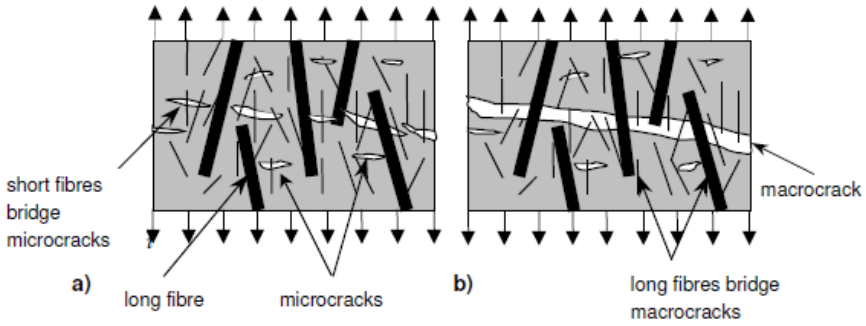

Figure 2.4: *Influence of short and long fibres. (Marković [27])*

2.4 PRINTED CONCRETE

All abovementioned research is based on conventional casted concrete, however the 3D concrete printing process also has some parameters to be considered. First the process of printing plain concrete structures is analysed. According to Le et al. [23] the most critical fresh properties are the workability and the open time of the material. In the current research fibres will be added to the interface between the layers of concrete, therefore the influence of the layered manufacturing process is of interest. Earlier conducted research at the Eindhoven University of Technology has already done research towards the influence of the layered manufacturing process. It should however be noted that the concrete mixture is changed for this research, thus the results cannot directly be interpreted for the current research. The direction of the layers does not seem to have a direct influence on the compressive strength on the material according to Doomen [17]. Although there is a reduction in compressive strength compared to the casted samples, this is most likely due to the absence of compaction is the printing process. If the flexural strength is observed a slight reduction can be found for the samples which are loaded parallel to the direction of the layers. Here a reduction of about 30% could be observed compared to the other test directions. This is most likely due to the fact that the layers are pulled of each other. The importance of open time as mentioned by Le et al. [23] is also observed in research done at the Eindhoven University of Technology. In research done by Doomen [17] and Slager [43] a reduction in strength could be observed if a longer open time between the printing of layers is maintained. Similar research is conducted at the Loughborough University, were the influence of the open time is analysed by Le et al. [24] (figure 2.5).

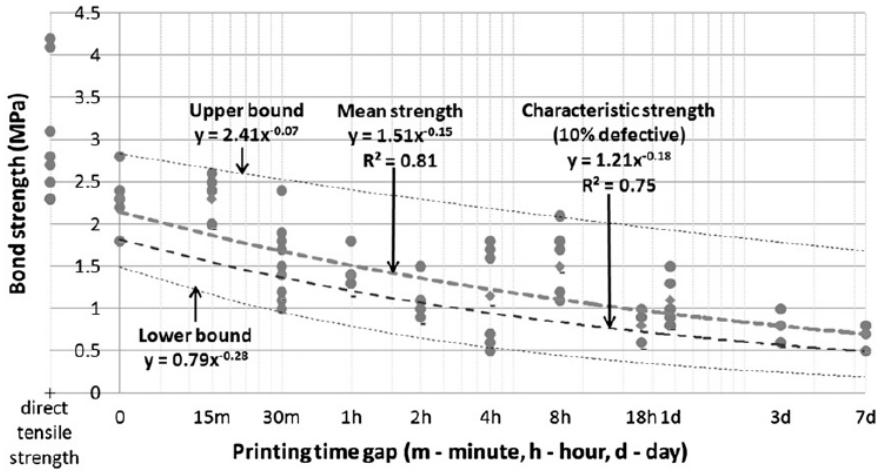

Figure 2.5: *Influence of printing time gap on bond strength of printed concrete. (Le et al. [24])*

2.5 PRINTED FIBRE REINFORCED CONCRETE

The first step towards reinforcing printed concrete with fibres at the Eindhoven University of Technology has already been made, in research done by Raedts [38] the possibility of adding fibres to the concrete is observed. In this research two types of high-strength steel fibres, 6 and 13 millimetres, are tested to analysing the influence on the flexural strength. Samples are printed with a dimension of 40x40x160mm and tested with a Crack Mouth Opening Displacement test. From these results it could be observed that the addition of 6 millimetre steel fibres resulted in a large increase of peak strength, with a factor of approximately 5 compared to plain concrete. Additionally, a post-peak behaviour is obtained in which a strain-softening behaviour is observed due to the pulling out of the fibres. For the 13 millimetre steel fibres no test samples could be printed due to clogging at the nozzle. A nozzle opening of 10x60 millimetre was used, which seemed too small to make a continuous print. This shows that the printing parameters could set certain limitations of what can be printed. This was also observed by Hambach et al. [20], here micro fibres with a length of 3-6 millimetre were printed with a nozzle diameter of 2 millimetre. From testing it could be concluded that the maximum fibre ratio which was printable had a fibre volume percentage of less than 1.5%. Once the amount of fibres was increase clogging of the nozzle occurred more frequently. This shows that there seems to be a limitation in the ratio of fibre length/ratio to nozzle diameter.

In addition, different research has developed cementitious composites reinforced with fibres which are printable. Panda et al. [35] have tested different lengths of glass fibres, for varying fibre contents. A geopolymer mortar is developed with a thixotropic behaviour, which is tested to determine its mechanical properties. From this research it is concluded that for an increasing fibre ratio, the flexural strength of the specimen increases. From the results it could also be stated that in general a larger fibre resulted in a larger flexural strength. If the compressive strength of the samples is analysed little to no influence could be observed for the different fibre length or the different contents. Another printable concrete mixture is developed by Hambach et al. [20], for which different type of fibres are mixed to analyse its influence. In this research three types of micro fibres are tested which are made from a different material, carbon, glass, and basalt fibres. By observing the flexural strength of the test specimen it can be stated that the use of 1% of carbon fibres results in an increase of peak flexural strength of a factor 3. For the other two types of fibres the peak strength remains more or less the same compared to plain concrete. However, when the post-peak behaviour is observed, the glass and basalt fibres show a strain-softening behaviour. On the other hand, no significant influence on the post-peak behaviour is observed by the application of the carbon fibres. The peak flexural strength of

the samples with glass and basalt fibres does not increase due to the low Young's modulus of these fibres according to Hambach et al. [20]. Also, from this research it can be seen that the compressive strength of concrete hardly changes once fibres are added to the mixture.

From research it also followed that the printing process has an influence on the orientation of the fibres. It could be seen that the majority of the fibres have an alignment parallel to the printing direction (see figure 2.6), so the flow of concrete seems to be of importance. For the casted samples a more random fibre orientation could be seen [31][35][38], this directional dependency also seems to have an influence on the strength of the specimen. From the results from Raedts [38] a similar behaviour could be found for the printed and casted samples. For this it should be noted that the casted samples were compacted, thus less air voids should be present in these samples. For Ogura et al. [31] an improvement in strain hardening behaviour for the printed specimen compared to the casted specimen could be found. In this research no compaction was applied for the casted samples. In this research two possible conclusions are stated for this difference between printed and casted samples. Due to the extrusion process during printing compaction of the material could occur at the nozzle, reducing the are voids in the printed samples. The second possibility is the aligned orientation of the fibres, which are parallel to the test direction.

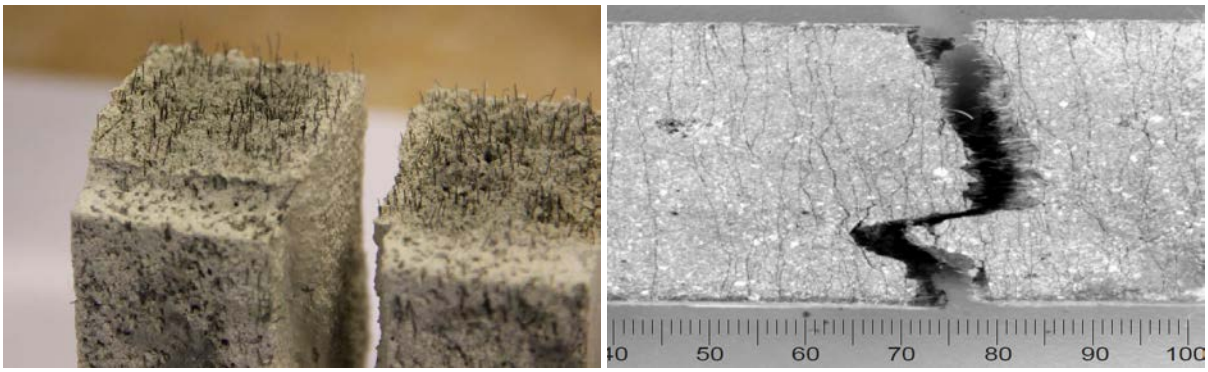

Figure 2.6: *Alignment of fibres parallel to printing direction (Left); crack pattern with alignment of fibres (Right). (Raedts [38]; Ogura et al. [31])*

In general, it follows from research that the flexural strength of the printed concrete increases by the addition of fibres. The same conclusion is drawn from research conducted by Nematollahi et al. [29], in here three different types of synthetic fibres are tested. For all tested samples an increase in flexural strength is observed compared to the printed geopolymer without fibres. However, also the inter-layer bond strength is tested in this research. By the addition of fibres to a mixture the material properties change, this led to a reduction in interlayer bond strength compared to the plain geopolymer samples. An increase in stiffness of the fresh mixture was observed, hereby the deformation capacity of the layers reduced which led to a more porous interface [29]. It is stated that further research is needed to confirm this statement.

2.6 Discussion

At present, a lot of research is been going on to see whether fibre reinforcement can be implemented in the 3D concrete printing process. In the majority of these studies micro fibres are used, while the printing process limits the size of the fibres. Using larger fibres results in general to blockage at the nozzle opening. From literature it is concluded that micro fibres could increase the peak tensile strength, however at already small crack openings they lose their function. In this study a different approach is adopted, the fibres are placed in between the layers. Therefore, the size limitation due to the nozzle is removed, creating the possibility to use fibres to increase the ductility of the material. A

large range of fibre types is available in practice, with varying size, shape, material and so on. Their contribution to the strength in conventional casted concrete has already been proven. However, it is unknown whether the results from casted concrete guarantee the same results for printed concrete. Due to the layered manufacturing technique the fibres can be placed in between the printed layers, however it followed from literature that the interface between the layers is often the weakest link. The addition of fibres in between the layers should not lead to a reduction in bond strength between these layers. Therefore, the compatibility with the printing process need to be analysed in this study. By printing plain concrete structures no significant negative influence is obtained for a relative short time interval. However, by adding fibres in between the layers a new parameter is added to the printing process which is not analysed yet.

3. MANUFACTURING PROCESS

To determine the amount of fibres a percentage based on weight per volume is taken in practice. In the past extensive research has been done to determine the proper weight percentages which will not crucially influence the workability of the material. For this research a different method of applying fibres is used, therefore the standard weight percentages from practice cannot directly be applied in this case. This is while the volume at which the fibres are added is much smaller compared to the conventional manner. If a similar number of fibres from practice is added between the interfaces, the layers will be completely covered with fibres. Where in practice the fibres are added to a volume of concrete, the fibres are in this case added to a surface of concrete. To quantify the amount of fibres the weight per area is used, from this a percentage from the surface which is covered with fibres can be calculated

At this moment there are no guidelines with respect to which fibres and what amount of fibres can be added. Therefore, the first step is to create certain boundary conditions, from this a fibre type and ratio can be selected. To begin with, the manufacturing method has to be observed to analyse what is possible with respect to producibility. To do so the depositing method of fibres and the printing process will be analysed in the following section. After this the amount of fibres need to be quantified, to get an idea of this image analysis has been used.

3.1 DEPOSITING METHOD OF FIBRES

For conventional fibre reinforced concrete the fibres are added in the mixer, this can be done after the concrete is mixed or during the addition of the aggregates. When adding fibres after the concrete is mixed, a long enough mixing time should be attained to get a uniform mixture. By adding fibres simultaneously with the aggregates a proper dispersion can be obtained, however in this case fibres should not be able to pile up before entering the mixer. Fibres can be added to the concrete in several ways, conveyor belts, blowers, chutes, loss-in weight dispensers, and pneumatic tubes can be used for example [3] (figure 3.1). To obtain a homogeneous concrete mix the fibres should be added gradually, otherwise fibre balling might occur. Many fibre manufactures have special pre-packed batches of fibres to easily add the right quantity to a batch of concrete.

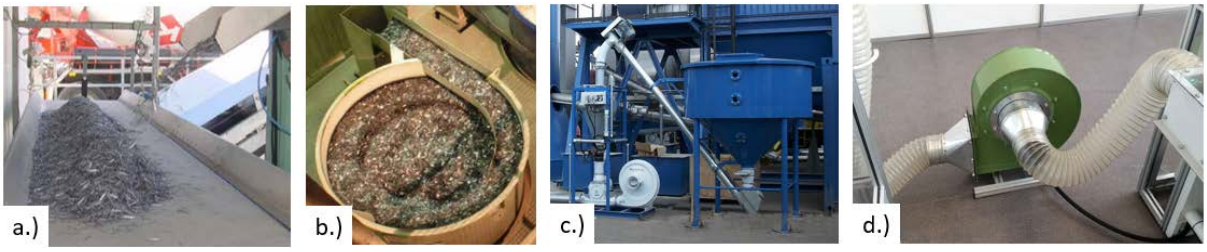

Figure 3.1: *Batching and transport of fibres, a.) Conveyor belt; b.) Bulk fibre disperser; c.) Loss-in weight dispenser; d.) Blower. (Incite AB [49]; Ramella [51]; Uygar endüstri [53])*

For the investigated application the mixing of fibres is less of interest, however the transportation of fibres might be implemented as it is done in the conventional industry. In general, the fibres are transported by a conveyor belt or a blower. For 3D concrete printing a flexible system is required with regard to manoeuvrability, as the robot gantry is in constant motion. With these criteria the blower seems the most viable option, while a hose can be flexible. A conveyor belt on the contrary is more static which makes it more difficult to comply with the movement of the robot. A device is developed which is able to transport the fibres from a storage point towards the nozzle, the fibre blower (see figure 3.2). A rotor blade inside an aluminium chamber (figure 3.2b) creates an air flow which draws

the fibres from a bucket. This rotor blade is powered by a DC motor for which the revolutions per minute can be controlled by a potentiometer (figure 3.2a). By adjusting the settings of the DC motor, it is possible to control the quantity of fibres which are required. An input hose, with a diameter of 60 millimetre, is fixed at the bottom of the chamber and is placed inside a bucket. Inside this bucket a funnel is created which collects all the fibres in the centre of this bucket (figure 3.2c). A continuous vibration is applied to the bucket to avoid fibre balling, and therefore clogging of the device (figure 3.2d). At the side of the chamber another hose of 50 millimetre in diameter is connected through which the fibres are blown further towards the robot arm (figure 3.2e), this hose is flexible so it can follow the movement of the robot. The end of the hose is fixed at a certain height from the print path to assure that the wind flow will not affect the concrete layers. For this research a distance of approximately 200 millimetre from the print path is maintained, no direct influence of the wind flow is observed for this distance. During the research several adjustments are made with respect to the device to improve the results, these are described in detail in appendix B.

Figure 3.2: *Final set-up of fibre blower; a.) Motor and wattage meter; b.) Rotor blade inside aluminium casing; c.) Fixation of input hose and funnel; d.) Vibration bucket; e.) Fixation of output hose at robot arm.*

3.2 WORKABILITY BLOWER

The opportunities and challenges of the blower are analysed by designing a test program which is used to quantify the output. To select which fibres are suitable for sprinkling between the layers, several criteria have to be fulfilled. The first question which should be asked is if the fibres are able to pass through the blower. The smallest hose has a diameter of 50 millimetre, if the length of the fibres is larger clogging of the device may occur. It is also possible that the fibres become useless while they

might get damaged during transport through the device. Inside the chamber of the blower a steel rotor blade creates an air flow to transport the fibres, however the fibres might get sliced or deformed when they are pulled against this blade. If too much damage is done by the rotor blade the fibre might become useless. Subsequently, a constant output of the blower is required to implement the blower in practice, because a constant or controlled fibre ratio over the length of an element needs to be guaranteed. This consistency of the blower needs to be fulfilled for different settings while different fibre ratios might be needed for varying applications. Another parameter which is of importance is the compatibility with the current printing process. By placing the fibres between the layers, the interface between the concrete might be affected. An analysis should be made to see if and in what order this might result in a negative impact on the bond between the layers. The last parameter is related to the structural influence on the element, the goal is to improve the tensile capacity and/or ductility of the printed concrete. If a fibre fulfils all these criteria it can be applied as reinforcement between the layers, if this is not the case the fibre type can be declined as possible reinforcement (figure 3.3) or can be selected as not suitable for the current fibre blower.

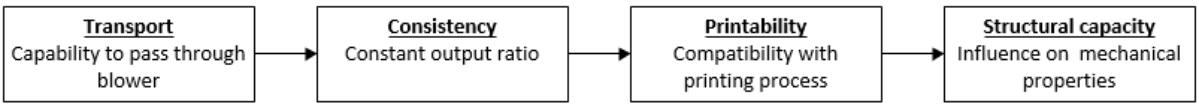

Figure 3.3: *Workability parameters of blower.*

3.2.1 TRANSPORTATION

To test the workability of the blower twenty different fibre types are tested, they are all analysed based on the first criteria given in the previous paragraph. A selection is made in which fibre geometry, length, and material vary, a full list of all fibre types is given in appendix B. In order to analyse whether the fibres are able to pass through the blower a simple test is performed. Over a short period of time different settings of the blower are tried, in between the minimum and maximum settings. Hereby testing the capability of the fibres to be transported for different settings. After testing the inside of the blower chamber is checked to see whether any fibres got stuck inside the device. Almost all fibre types are able to pass through the blower, only two types of fibres get clogged due to the length of the fibre. The hose diameter of the blower is too small for Synmix SP55 and Cem-FIL Minibars 43mm (figure 3.4), so these fibres cannot be applied with the current device. The length of these fibres is 55 millimetre and 43 millimetre respectively, the smallest hose diameter is 50 millimetre.

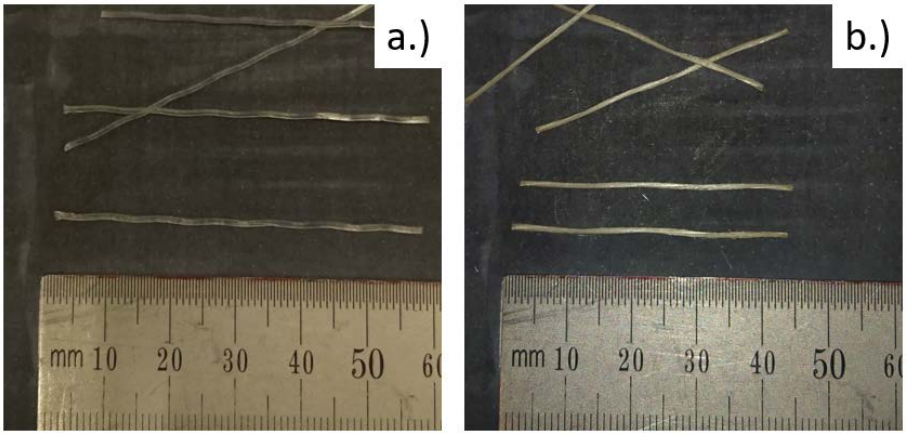

Figure 3.4: *Fibres which resulted in clogging of the device; a.) Synmix SP55; b.) Cem-FIL Minibars 43mm.*

Although most fibres went through the blower, a lot of fibre types got damaged or deformed due to the steel rotor blade. A minority of the Dramix 3D fibres got deformed due to contact with the rotor

blade, the fibres were bend or the hooks were straightened (figure 3.5a). When the Fibraflex fibres are observed it could be seen that a small amount got sliced, due to the small thickness of the fibre some of them broke when sucked into the chamber (figure 3.5b). Another deformation which occurred was the unbundling of the wires, this happened for fibre types which consists of strands of thin wires. This phenomenon happened for three different type of fibres, Duomix M12 (figure 3.5c), Turbobuild AC-12-300/D and Uncoated chopped fibres (figure 3.5d).

Figure 3.5: *Deformation of fibre types due to rotor blade; a.) Dramix 3D RC-4530-BL; b.) Fibraflex FF/30L6; c.) Duomix M12; d.) Uncoated chopped fibres.*

For the Dramix 3D and Fibraflex fibres only a minority of the fibres got deformed, however still an acceptable amount of fibres went through the blower which is expected to still have a positive influence on the material properties. The three types of fibres for which the wires unbundled on the other hand cannot be used for this application. Due to the unbundling of the wires the volume of the fibres increased significant, and due to the low weight the wires are blown in all directions. Hereby the majority of the fibres will not be sprinkled on top of the layer, and the fibres which lands on the layer will be pushed aside by the nozzle printing the next layer. In some cases, the Dramix 3D fibre resulted in clogging of the device, this occurred more frequently for a higher setting of the blower. The reason for this is most likely due to the hooked-end of the fibres which results in entanglement of multiple fibres. For a higher setting of the blower a larger number of fibres are inside the blower thus increasing the possibility of entanglement. This phenomenon was not observed for straight fibres. In order to further improve the device there is chosen to select two types of fibres which are used for testing. One of those is an alkali-resistant glass fibre, Cem-FIL Minibars 24mm, which has a spherical shape. The other is composed out of high-strength steel, Fibraflex FF/15E0, and has a flat shape (figure 3.6a &b). Both fibre types were able to pass through the blower without getting clogged or getting significantly damaged. Based on literature research it is expected that both fibre types can have a positive influence on the structural capacity. In the first stages of testing two other fibre types are also tested, Dramix OL 6/.16 and Dramix OL 13/.20 (figure 3.6c & d), however due to safety reasons these two type of fibres are excluded. The needle like shape can result in scratches and cuts during handling, moreover it is expected that the influence on the structural capacity is less compared to the other two selected fibre types.

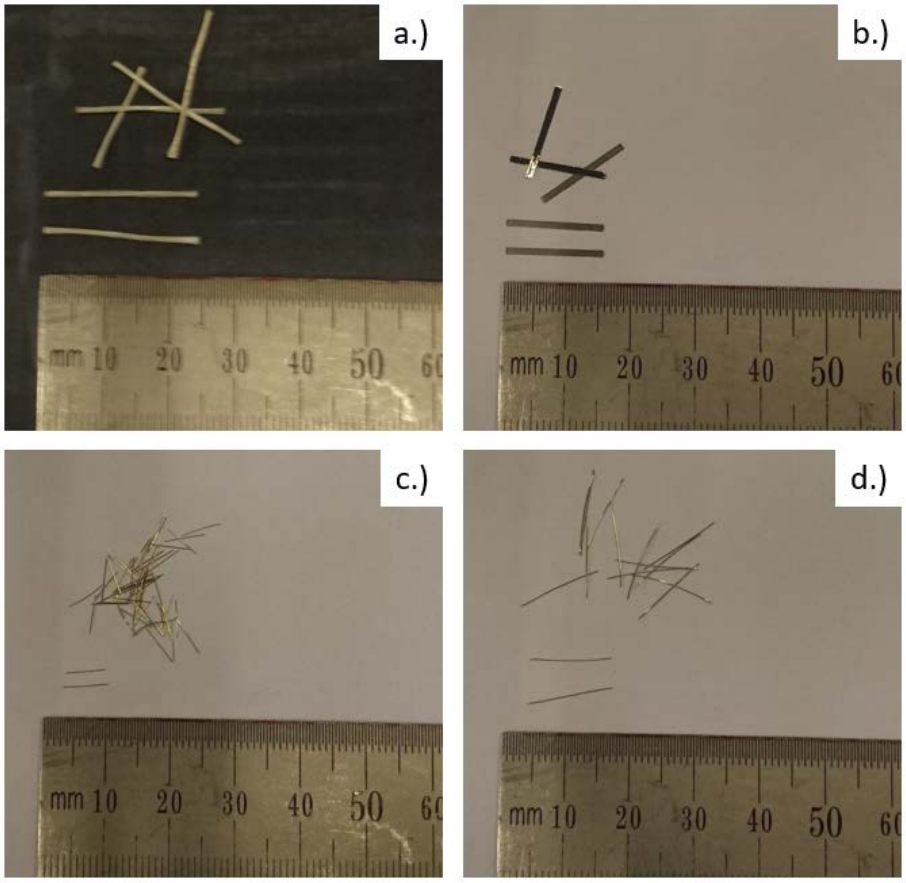

Figure 3.6: *Tested fibre types for workability test blower; a.) Cem-FIL Minibars 24mm; b.) Fibraflex FF/15E0; c.) Dramix OL 6/.16 (Excluded); d.) Dramix OL 13/.20 (Excluded).*

3.2.2 CONSISTENCY OF OUTPUT

To obtain a certain structural capacity the fibre ratio is of importance, therefore the output of the blower should be able to match a required amount of fibres. At the start of this research it is difficult to give an exact number of fibres which is required, however a certain range can be given. As mentioned at the start of this chapter, the number of fibres can be quantified by a coverage percentage. With the dimensions and weight of a single fibre, it is possible to calculate the required output per coverage percentage. By observing the printed layer from the top the concrete area can be calculated, a print path of 50 millimetre in width and 6000 millimetre in length is considered. With the adopted printing speed of 100 mm/sec this resembles a total printing time of 1 minute. From the dimensions of the fibre the total number on top of the layer can be calculated, this multiplied by the weight of a single fibres gives the total output of the blower. It should be noted that this only holds if all fibres are placed neatly next to each other. This is not the case once the fibres are distributed by the blower, hereby an overlap between fibres is created. To take this overlap into account a factor β is added to the formula. The exact value of this factor can differ per fibre type, for a first assumption this factor is taken equal to 1. However by performing further research a closer approximation of this value can be given.

$$O_{blower} = \frac{1}{\beta} \cdot \left(\frac{\rho_{cov} \cdot A_{c;t}}{A_{f;t}} \right) \cdot m_f \qquad [3.1]$$

In which:

O_{blower} = Output of blower (g)
β = Overlap factor
ρ_{cov} = Coverage percentage
$A_{c;t}$ = Concrete surface (mm^2)
$A_{f;t}$ = Surface of single fibre (mm^2)
m_f = Mass of single fibre (g)

Two different fibre types are selected which are used to improve the blower, for both fibre types a range is given in table 3.1. Here the output per minute of the blower is given for three different coverage percentages. At this stage of the research the optimum coverage percentage is still unknown, therefore a range between 5% and 50% is taken. It is assumed that by using less fibres the influence on the structural capacity can be neglected. On the other hand, if more than half of the concrete surface is covered the fibres might have a negative influence on the bond between the interface. For the first optimisation of the blower this range should suffice.

Table 3.1: *Output of blower*

Fibre type	Coverage percentage	Output per minute
Cem-FIL Minibars 24mm	5 %	18.8 g/min
	25 %	94.0 g/min
	50 %	188.0 g/min
Fibraflex FF/15E0	5 %	3.0 g/min
	25 %	15.2 g/min
	50 %	30.3 g/min

To start a bucket test is done (figure 3.7), where the fibres are collected in a bucket over a certain period of time. By weighing the output the weight per surface can be calculated, as well as a check on the consistency of the output can be done. By performing this stationary test the influence of different parameters can be observed. During the development of the device several parts are substituted to improve the output, by performing multiple tests the influence of these parameters can be observed. Once the fibre blower is connected to the concrete printer another parameter is added, movement of the robot arm. To check whether this has an influence on the output of the blower a chamber test is performed (figure 3.7). Here the printer will move over a simple print path which is surrounded by wooden boards. As the robot arm is moving, the fibres are collected in the four compartments. The compartments have a length of approximately 1 metre, which corresponds to a printing time of 10 seconds with the adopted printing speed. These fibres can be collected and weighed to determine the output per time interval.

Figure 3.7: *Set-up bucket test (Left); Set-up chamber test (Right).*

3.2.2.1 Bucket test

Multiple tests are done to improve the device and the adaptions which are made are described in detail in appendix B. To improve the consistency of the blower it is necessary to have a gradual input at the storage point. Hereby fibre balling should be avoided while this can lead to clogging of the device. The first improvement made at this point is the addition of a vibration bucket, the continuous motion avoids entanglement of the fibres in the storage bucket. From a visual analysis it can be concluded that the number of times for which clogging of the device occurred is reduced. Inside this vibration bucket a funnel is created, which collects all the fibres in the centre of the bucket. At this point the input hose is fixed, by doing so the variation of input per test and time interval is reduced while the same position is kept for all tests.

Besides the input of the blower, the used DC motor has a direct influence on the consistency. To control the settings of this motor a wattage meter is added, by doing so the settings of the tests can be reproduced. Different settings of the motor are tested to quantify the output, in figure 3.8 the results can be seen for the two tested fibre types. The fibres are blown through the device and for a time interval of 15 seconds the fibres are collected. The amount of fibres is weighed and from this number, based on a layer dimension of 60x10mm, the weight per volume, weight per area and output per minute can be calculated.

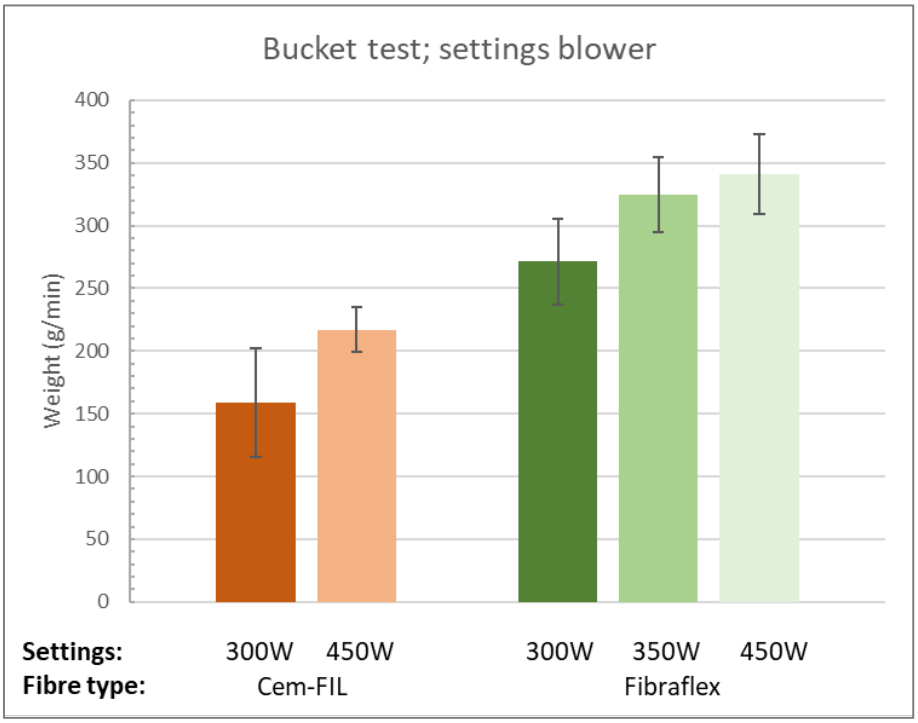

Figure 3.8: *Bucket test, Variation of blower settings.*

From this graph it can be seen that the output of the blower is reduced by lowering the settings of the blower, as could be expected. However, the relative standard deviation increases for a lower setting for both fibre types. Especially for the Cem-FIL Minibars a larger increase in scatter is observed, this is most likely due to the weight of a single fibre. By lowering the power of the device the weight of the fibres becomes more important, while the wind flow might be too weak to transport the fibres. This relative standard deviation is also partly due to the fact that only five tests are performed per setting.

In the previous paragraph (table 3.1) a certain range is given for the output of the blower based on the coverage percentage of the concrete layers. In case of the Cem-FIL fibres it can be seen that for a blower setting of 450 Watts, this range is exceeded. However, if a lower setting of 300 Watts is used,

the output of the blower is within this range. On the other hand, if the output of the Fibraflex fibres is observed, a large difference can be found between the real output and the given range from table 3.1. At the lowest setting which is tested, 300 Watts, an average output of 271.3 g/min is obtained. For a coverage percentage of 50% the output of the blower is equal to 30.3 g/min, which is about 9 times less. Although the overlap of fibres is not considered for the calculation of the given range in the previous paragraph, the coverage percentage will much likely be larger than 50%. From the tests it can be observed that a lower output can be obtained by reducing the blower settings, however the standard deviation also increases for a lower setting.

At this point no direct relation can be found between the settings of the blower and the output per minute. To see whether this relation exists it is required to gain a better control over several parameters. From the performed tests it can be concluded that for instance the input quantity and position of the hose have a major influence on the output. During the development of the device it is tried to keep these parameters as constants, however even a slight variation results in a difference in output.

3.2.2.2 Chamber test

From the chamber test the influence due to movement can be observed, these results are given in figure 3.9. This test is performed for both fibre types and a comparison is made with the stationary bucket test. As explained, a box is made to collect the fibres which are blown over the print table. Two test runs are performed for both fibre type, from these eight results are obtained over which the average value is taken. During the test runs the print path is completed three times, thus the obtained value per chamber is already an average value over thirty seconds. From this the weight per volume, weight per area, and output per minute can be calculated. Also in this case a concrete layer dimension of 60 millimetre in width and 10 millimetre in height is considered. The chamber test is only performed for a single setting of the blower, 300 Watts. Although it showed from the bucket test that the standard deviation increases for a lower setting, the quantity of fibres is closer to the required range (table 3.1).

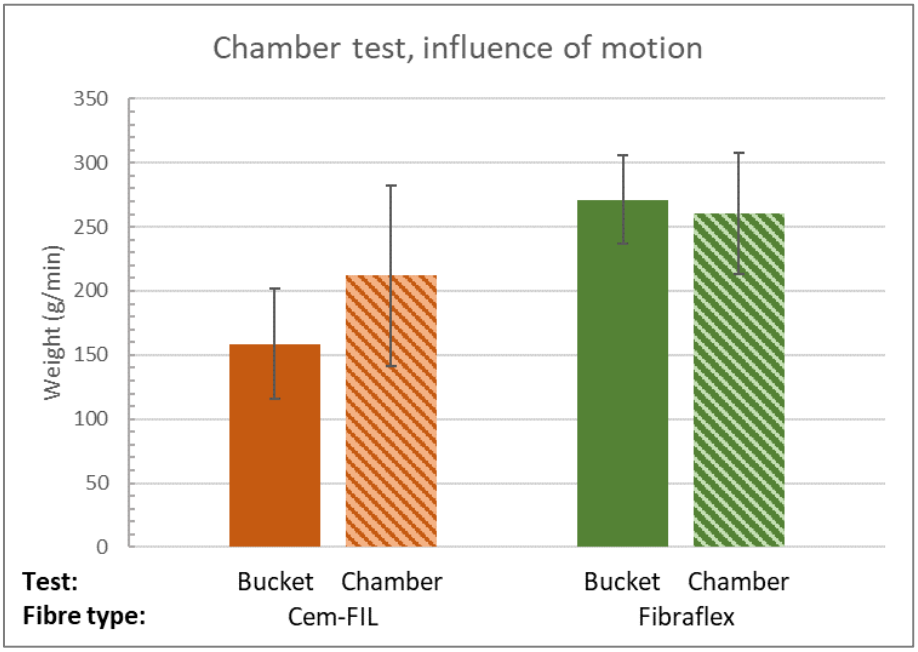

Figure 3.9: *Chamber test, Test to define influence of motion.*

For the Cem-FIL fibres an increase in output can be seen for the chamber test, while the quantity of Fibraflex fibres remains more or less constant for both tests. During testing several parameters are of importance, for instance the input of fibres and the position of the hose will affect the output of fibres.

Although it is tried to perform all test in a similar manner, it is difficult to control all parameters at this stage of the development. On the other hand, for both fibre types an increase in standard deviation can be found for the chamber test. It is likely that this is due to the movement of the hose. For the bucket test the hose does not move, in case of the chamber test the hose is continuously stretched and bended. It is assumed that the resistance inside the hose is less for a straight hose compared to a curved hose. Therefore, the output of the blower will be larger if the hose is completed stretched compared to the situation for which the hose is curved. These extra curves, and thus larger resistance, inside the hose can lead to fibre balling and even clogging of the hose which occurred twice for the Cem-FIL fibre type. In these cases the results of the chamber test are neglected and redone. However, this shows that the position of the hose is of great importance and can significantly affect the output of the blower.

In the chamber test explained above the total output of the blower is considered, however these numbers are not equal to the quantity of fibres deposited on the concrete layers. With the current depositing method the fibres are blown at a certain distance from the concrete layers, by doing so a part of output is blown next to the print path. To define the quantity of fibres which is blown next to the print path the chamber test is redone, however this time a concrete layer will be printed. In order to obtain the number of fibres on top of the concrete layers the amount of fibres next to the layers is subtracted from the total amount of fibres obtained from the previous test. The results can be found in figure 3.10, here the total amount of fibres is divided in fibres on top of the print path and fibres next to the print path.

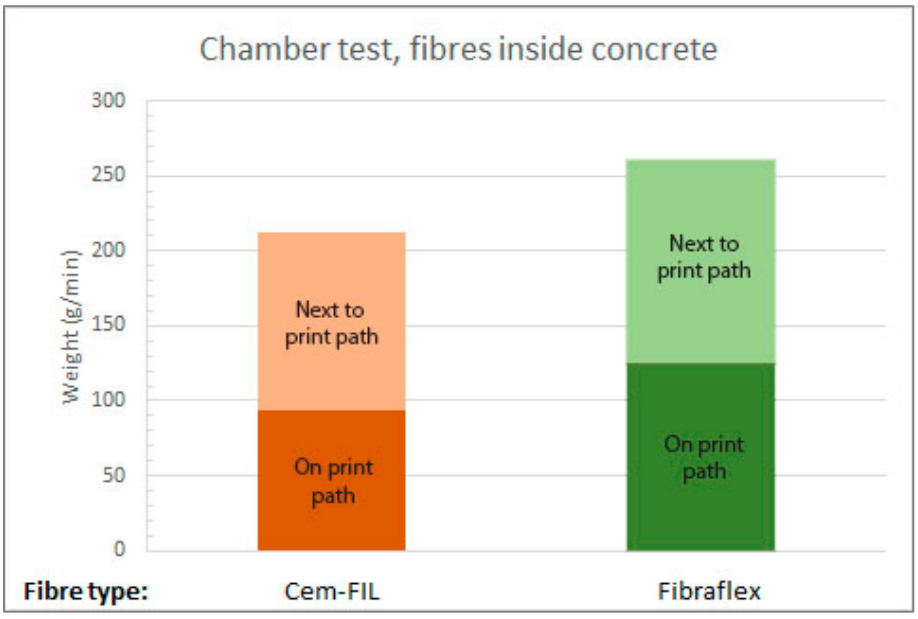

Figure 3.10: *Chamber test; spread of output blower.*

In both cases a comparable ratio is found between the fibres on top of the print path and the total amount. For the Cem-FIL fibres approximately 44% of the fibres landed on top of the concrete, for the Fibraflex fibres this number is about 48%. It should be noted that these numbers are an assumption while the total number of fibres and the fibres next to the layers are obtained from different tests. A relatively large standard deviation is obtained for the different chamber tests, so it is needed to further analyse the output to obtain the real number of fibres inside the concrete. For the fibres next to the print path no standard deviation is shown while the test is only performed once, even though an average value is obtained per chamber while the print path is completed five times.

Once again, the results from the chamber test are compared with the given range based on the coverage percentage (table 3.1). For the Cem-FIL fibre type an increase is observed if the chamber test is compared to the bucket test. However as mentioned not all fibres will be deposited on top of the printed layers. For this test a result of approximately 118.9 g/min is obtained, this value is within the given range from table 3.1. For the Fibraflex fibres a comparable result is found between the bucket test and chamber test, also for this test about half of the fibres are blown next to the print path. About 135.6 g/min is deposited on top of the printed layer, this number still exceeds the given range from table 3.1. For a coverage percentage of 50% the output of the blower is equal to 30.3 g/min, this is a factor 4.5 less compared to the real output.

3.2.3 PRINTING PARAMETERS

Once the fibres can be transported from a storage bucket towards the robot arm, the printing process needs to be analysed. By sprinkling the fibres on top of the printed concrete layers, several parameters have to be considered. The fibre distribution on top of the concrete should not be affected by the process of printing concrete. In a trial print different fibre types are sprinkled by hand on top of the printed concrete layers, in this print a hybrid nozzle is used. During printing it is observed that a major part of the fibres is dragged along by the robot arm and thus a negative influence on the fibre distribution is obtained. From this observation a study is conducted to analyse the compatibility of fibre reinforcement in between the layers with the concrete printing technique. Overall the 3D concrete printing process can remain unaltered, only the deposition of layers should be analysed. The flow of material or the robot arm might interfere with the sprinkled fibres on top of the layers. Different parameters need to be taken into account, type of nozzle, printing offset, printing speed, fibre geometry, fibre ratio, and material behaviour of the concrete are of importance (figure 3.11).

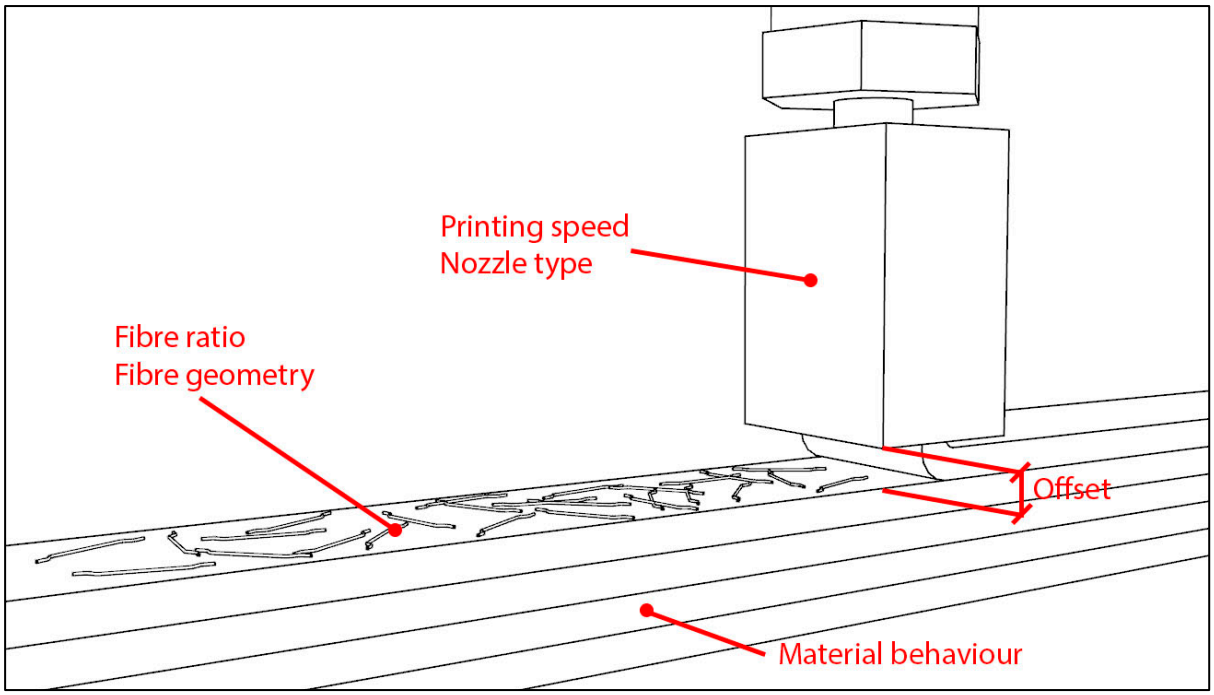

Figure 3.11: *Printing parameters*

The type of nozzle determines the flow of material, the way in which the concrete is deposited on the previous layer. In general, two types of nozzle are used at the Eindhoven University of Technology, a back-flow and down-flow nozzle (see figure 3.12), a third option which is designed is a hybrid nozzle. For the back-flow nozzle the concrete is deposited from the back of the nozzle, the offset between the previous layer and the nozzle is minimal. This nozzle is mainly developed for the cable reinforcement, with this nozzle a horizontal entrainment of the cable can be achieved. However, from research

performed by Salet et al. [40] it was discovered that the interface between the layers is affected if the nozzle is designed improperly. For this nozzle no fluidic pressure is applied, which reduces the bond between the layers disastrously. The second type of nozzle is the down-flow nozzle, here the material is deposited from the top on the previous layers. A third type of nozzle is designed which is a hybrid of the two other versions, for this nozzle the outlet of a back-flow nozzle is slightly altered. The bottom part and the sides of the outlet are removed, by doing so the nozzle will not scrape material from the previous layer. By leaving the front plate intact it is still possible to entrain cable reinforcement in the concrete layers. Besides the use of the standard nozzles, it is also possible to design different accessories to the current nozzle. One of these is the addition of a small roller in front of the nozzle (See figure 3.12). This roller should push the fibres slightly in the concrete to make sure the nozzle does not touch the fibre, thus affecting the fibre distribution. From the trial print it is observed that a hybrid nozzle might interfere with the fibre distribution, by the addition of the roller the fibres should be pushed down into the previous concrete layer. Hereby the negative impact of the hybrid nozzle should be avoided. If a hybrid nozzle can be used for printing fibre reinforced concrete, the possibility arises to combine this reinforcement method with cable reinforcement. This combined reinforcing method is out of the scope of this research, however while this might be interesting for future research the compatibility with this type of nozzle is analysed.

Figure 3.12: *Different nozzle types used at the Eindhoven University of Technology; Back-flow nozzle; Hybrid nozzle; Down-flow nozzle; Roller attachment (From left to right).*

Secondly the settings of the printer are of importance, while the printing offset and the printing speed define the way in which the concrete layers are deposited. The printing offset has an influence on the level of compression of the printed layers. For a low offset the concrete layer is pushed in the previous layer, this is not the case for a larger offset. However, for a too large offset the strength of the interface might be reduced. In research by Wolfs et al. [46] three different printing offsets are tested, from flexural tensile tests no direct relation regarding strength is observed. On the other hand, an increase of scatter was obtained by deviating from the standard print settings. For the case in which the printing offset is kept equal to the nozzle opening the lowest scatter was obtained. By increasing or decreasing this offset, an increase in scatter is observed. This is most likely due to the uncontrolled depositing manner of the concrete layers. Also in research performed by Panda et al. [36] the same phenomenon is observed, by deviating the printing offset from the layer height an increase in scatter is obtained. Whereas no direct influence of printing offset is observed by Wolfs et al. [46], a reduction of bond strength is observed for larger printing offsets in research by Panda et al. [36]. A balance needs to be found in which the fibre distribution is not altered and the reduction in interface strength is as low as possible. The flow of concrete can also alter the distribution of fibres, this is partly dependent on the printing speed. For a high printing speed the fibres might get dragged along the printing path due to the movement of the robot.

Also the fibres could be seen as unfit for sprinkling on top of the layers of concrete, hereby the fibre geometry is of most importance. A fibre with a large diameter is more susceptible for being dragged

along by the concrete, if parts are sticking out due to the geometry the same holds. Hereby the printing offset of the nozzle is in fact reduced with regard to the fibres. This is mainly the case by using a hybrid nozzle, while for this type of nozzle the offset regarding the previous layer is smaller compared to a down-flow nozzle. Also for the bond between the layers the geometry can have an influence. The concrete should be able to properly flow around the fibre, for complex geometries, e.g. a spiral shaped fibre, air gaps might occur between the layers. In earlier conducted research at the Eindhoven University of Technology this phenomenon is observed for different reinforcing methods. Goris [19] conducted a study towards the application of rebar in printed concrete structures. Hereby the position of the rebar is analysed, for which the reinforcement is placed on top or pushed inside the previous layer. For all tested positions and bar diameters air pockets can be observed near the rebar. A similar study with respect to location of reinforcement is conducted by Dezaire [15], in this research cable reinforcement is entrained in the printed concrete. From the results it is observed that the concrete flow is diverted around the cable, leaving a void underneath this cable. It is concluded that by entrainment of the cable at the bottom of the layer resulted in the smallest void. If air gaps are present near the reinforcement, the contact area with the concrete is reduce which will lead to a reduction in bond strength. For a large fibre ratio the possibility of fibres overlapping each other increases. When two fibres are stacked the total height increases which could again result in fibres being dragged along with the nozzle.

Finally, the workability of the concrete could affect the fibre distribution. For 3D concrete printing the thixotropic behaviour of the material is of great importance. The viscosity of the material is reduced as long as a shear stress, mixing, is applied, the flowability is increased for a reduced viscosity. Once this shear stress is removed from the process the viscosity is recovered resulting in the material becoming stiffer. This phenomenon makes sure that it is possible to print several layers on top of each other. As mentioned above, the high viscosity of the material can result in air gaps near the reinforcement. This will give a reduction in contact area, thus bond strength, between the fibre and concrete.

To define the influence of the printing parameters on the output, an empirical study is conducted. In this research two different nozzle types, hybrid and down-flow nozzle, are tested to determine its influence on the fibre distribution, also the roller accessory is tested. Secondly the printing offset could be of great influence, different starting heights are chosen for both nozzle types. In figure 3.13 a sketch is given of the side of the nozzle, both nozzle types have an outlet opening of 12x60mm. Here the distance from which the offset is measured is shown. For each layer which is printed, the robot arms moves 12 millimetre up for the next layer. Three different fibre geometries are used, spherical, deformed, and flat, to analyse which fibres might be suitable to use as reinforcement between the layers (figure 3.14). It is chosen to keep the other parameters which might be of importance fixed for this research. For the current manufacturing method the printing speed has a standard setting of 100 mm/sec, it is assumed that the variation of this speed will be low. The concrete mixture is also kept fixed, while changing this parameter is out of the scope of this research. To take the fibre ratio into account there is chosen to take a large quantity of fibres during this empirical research. If the distribution for a large ratio is not altered during printing, then it is assumed that the fibre distribution for a lower amount of fibres also will remain unaltered. The different tests which are executed are listed in table 3.2.

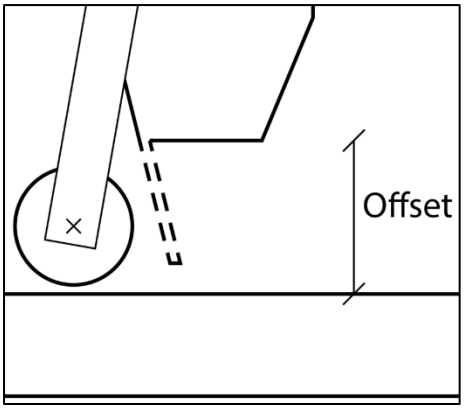

Figure 3.13: *Distance offset nozzle*

Table 3.2: *Empirical research*

Nozzle type	**Offset**			
	14 mm	15 mm	16 mm	17 mm
Hybrid nozzle		x	x	x
Hybrid nozzle + roller		x		
Down-flow nozzle	x	x	x	x

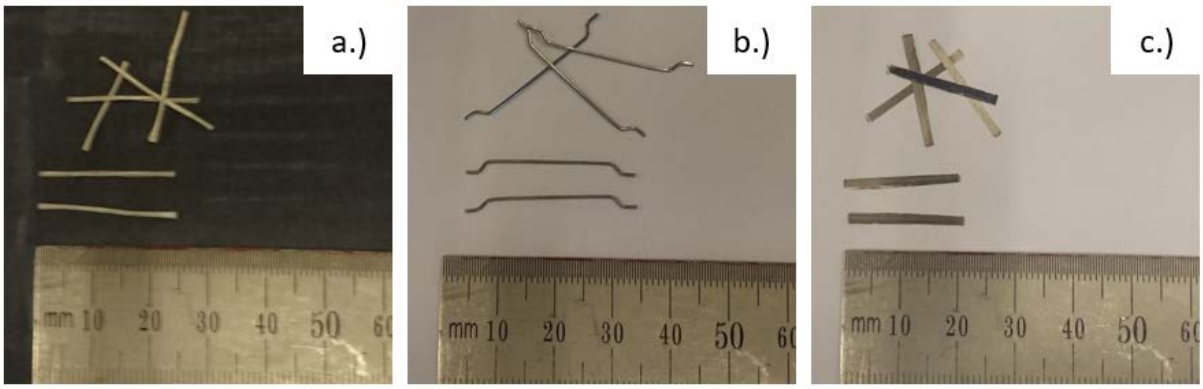

Figure 3.14: *Fibre types; a.) Cem-FIL Minibars 24mm; b.) Dramix 3D RC-4530-BL; c.) Fibraflex FF/20L6.*

From this empirical research it followed that the type of nozzle which is used can make a large difference. By observing the two nozzle types the only difference is the plate in front of the hybrid nozzle, which is designed to entrain cable reinforcement into the concrete. It could be seen that for a lower offset concrete accumulated against this plate, which resulted in fibres being dragged along (figure 3.15). This makes sense while the real offset regarding the previous layer is much smaller than the measured 15 millimetre. The front plate which has a length of 12 millimetre reduces this minimum offset to 3 millimetre. In theory this distance should be enough for the nozzle to hover over the fibres, however in reality this offset can be smaller at certain locations. This is due to the relation between the output of the pump and the print settings which are of great importance. During printing the robot arms goes up by 12 millimetre every layer, which should relate to the printed layer height. If this actual printed layer height is 12 millimetre everything should be fine, however if the actual printed layer height is larger the tolerance between the nozzle and the previous layer reduces for every layer which is printed. By cutting some of the samples this phenomenon could be observed (see figure 3.16), a saw cut was made from the top to the bottom parallel to the printing direction. All fibres are sprinkled by hand in between the black dotted lines, however it could be seen that also outside this region fibres could be found. For the down-flow nozzle no influence on the fibre distribution could be observed, however the tolerance with regard to the hybrid nozzle is much larger. Thus, the next layer is printed

on top of the fibres without horizontal movement, so the fibres remain at the same position. By applying the roller in front of the nozzle the fibres should be pushed down. However, no improvement could be seen compared to the hybrid nozzle without roller attachment. Once concrete gets stuck on the roller, the wheel gets jammed and the attachment loses its function.

Figure 3.15: *Scraping of fibres by using a hybrid nozzle.*

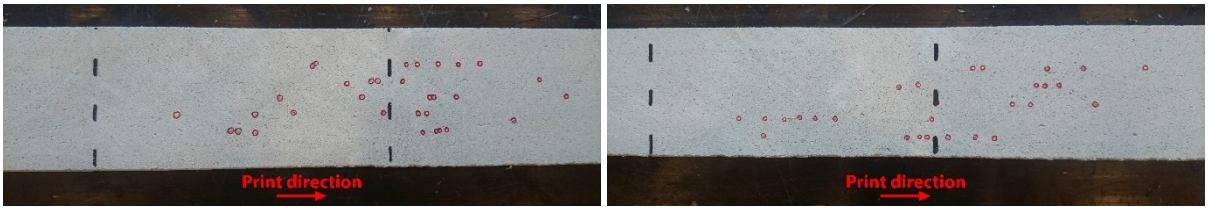

Figure 3.16: *Saw cut parallel to printing direction, distortion of fibre distribution due to printing.*

3.2.4 IMAGE ANALYSIS

In practice the fibre ratio can be given as a percentage per volume, hereby the weight of the fibres is given as a percentage of the total weight. For the case were fibres are sprinkled between the layers of printed concrete, the fibres will only be located on a 2D surface instead of a 3D volume. Therefore, it is possible to give a percentage of concrete which is covered by the fibres instead of the volume percentage. This can be done while the layer height with which can be printed is variable, therefore a volume percentage does not necessarily give a proper indication of the fibre distribution over the height. To perform this image processing techniques are applied to give a percentage of the surface which is covered. With this technique it is possible to determine the location and orientation of the fibres in an element layer by layer. By taking a photo from the top of the layer an image processing toolbox can be used, for this research the program MATLAB is used. Image analysis uses algorithms to extract data from a photo, here the contrast between the fibres and the concrete is used to select which pixels are fibres and which are concrete.

To predict the structural behaviour of the experimental research, a study is conducted in which different fibre distributions are analysed based on their coverage percentage, orientation and distribution. For all tested fibre types a certain number of fibres is selected, which are sprinkled over an area of 50x200 millimetre. An example of such a distribution can be seen in figure 3.17a, where the Cem-FIL fibres are shown. By running the algorithm in MATLAB, a distinction can be made between the pixels which are fibres and which are background. With these algorithms' pixels with the same colour intensity can be combined which relates to the orientation of the fibres. In figure 3.17b the selection of fibres can be seen, in which a line is drawn between the start and endpoints of the fibres. To determine the amount of fibres in a crack surface, three straight lines are taken to calculate the

amount of fibres crossing this line. One of the lines is in the centre of the picture, the other two lines are located at a quarter from the left side and a quarter from the right side.

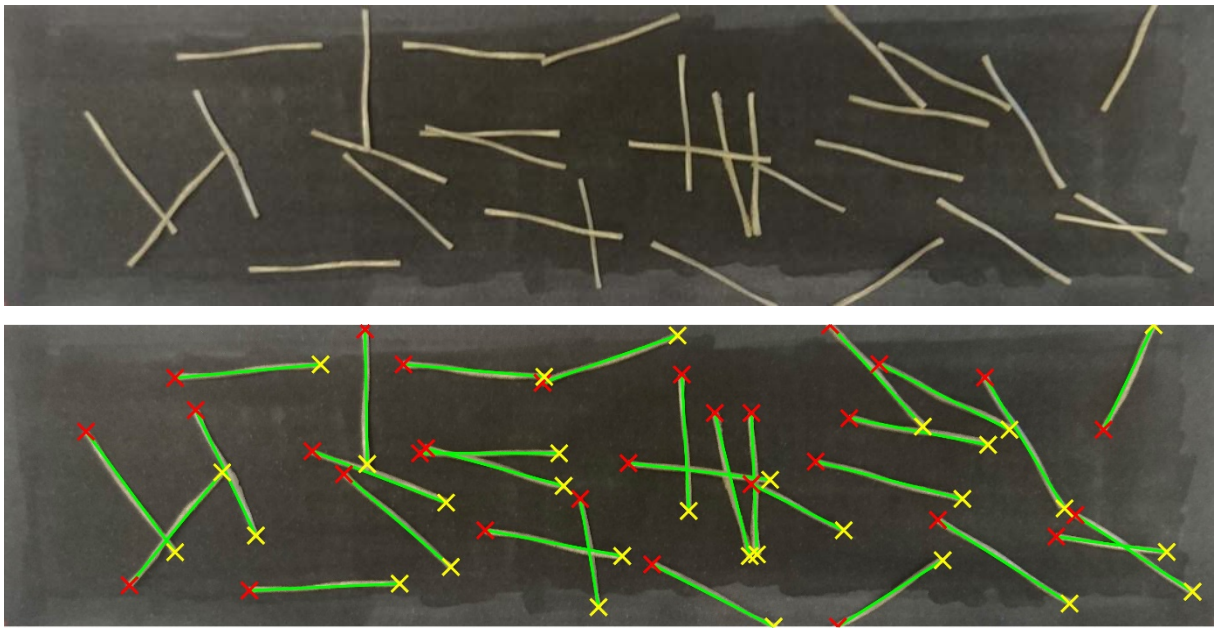

Figure 3.17: *Image analysis; Fibre distribution (Top); Output image analysis (Bottom).*

For each type of fibres two fibre quantities are selected, which are analysed in a similar manner. From this data a prediction can be made for the experimental program, all results can be found in appendix C. The percentage of concrete which is covered by the fibres is given in table 3.3, this ratio can be used to define the amount of fibres on a 2D surface. As can be seen from the results an increase in percentage can be seen from ratio A to B, which makes sense while more fibres will cover a larger area. This percentage will not rise linearly with the amount of fibres which are added to the concrete surface, the reason for this is that for a higher amount of fibres more overlap between the fibres will occur. There is chosen to analyse 10 different distributions per fibre type/ratio, from the standard deviation it can be seen that the percentage is more or less constant for each distribution. Which should be the case while the amount of fibres which is sprinkled on the surface remains the same.

Table 3.3: *Fibre coverage*

Fibre type	Ratio	Average coverage (%)	Standard deviation (%)
Cem-FIL Minibars 24mm	A	6.6	(0.5)
	B	8.1	(0.3)
Dramix 3D RC-4530-BL	A	8.0	(0.5)
	B	9.9	(0.5)
Fibraflex FF/20L6	A	13.7	(0.5)
	B	17.7	(0.4)

Another aspect which is analysed is the amount of fibres which is crossing a crack, these fibres will be important when the structural capacity of an element is observed. In table 3.4 the average number of fibres over all three sections is taken. From this data it can be seen that the amount of fibres crossing a section increases for a larger fibre ratio. This is desired for the experimental program while a different number of fibres per crack will most likely result in a difference in post-peak behaviour. The standard deviation shows that there might be a difference in number of fibres per cross-section for a similar fibre ratio. However, this does not necessarily mean that an inconsistent result will be obtained. For

an increasing number of layers, and thus interfaces with fibres, the overall amount of fibres crossing a section will be more or less the same while the average is obtained.

Table 3.4: *Fibres per cross section*

Fibre type	Ratio	No. fibres per cross section	Standard deviation (No.)
Cem-FIL Minibars 24mm	A	3	(1.20)
	B	4	(1.35)
Dramix 3D RC-4530-BL	A	2	(0.94)
	B	4	(1.03)
Fibraflex FF/20L6	A	4	(1.55)
	B	5	(1.31)

The last parameter which is observed with the image analysis technique is the orientation in a 2D plane. As already mentioned in the introduction, the orientation for printed fibre reinforced concrete where the fibres are embedded in the concrete is dependent on the material flow. This is not the case if the fibres are sprinkled between the layers. In table 3.5 the orientation of the fibres can be seen, here an angle of 0^{o} means it is aligned with the printing direction. From the results it can be concluded that the fibre orientation is indeed random as already expected. For each fibre type and ratio the amount of fibres in a particular direction varies, also a large standard deviation can be observed. This large standard deviation shows that there is a large difference per fibre distribution, which is in line with the random dispersion of fibres in conventional concrete.

Table 3.5: *Fibre orientation*

Fibre type	Ratio	0°-15°	15°-30°	30°-60°	60°-90°
Cem-FIL Minibars 24mm	A	5.8 (2.3)	5.8 (1.5)	11.3 (3.2)	7.1 (2.1)
	B	9.6 (2.7)	7.3 (1.9)	13.5 (3.3)	10.5 (2.7)
Dramix 3D RC-4530-BL	A	5.5 (2.1)	5.1 (2.3)	7.6 (2.2)	2.8 (1.1)
	B	8.7 (1.7)	7.0 (2.6)	8.5 (2.3)	5.1 (1.6)
Fibraflex FF/20L6	A	9.9 (3.2)	10.5 (2.6)	12.7 (4.8)	9.0 (2.1)
	B	15.3 (3.1)	11.5 (4.0)	19.0 (3.8)	13.2 (4.8)

3.3 Discussion

Based on the workability of the blower, the literature study and the image analysis three types of fibres are selected. For all three type of fibres two different ratios will be tested experimentally to determine the influence on the material properties. From the workability test of the blower the Cem-FIL fibres and the Fibraflex fibres showed the largest potential, both type of fibres were able to pass through the blower without significant damage or deformation. To further develop and improve the blower regarding consistency of the output, these two fibre types are selected. From these tests it followed that the output for the Cem-FIL fibre type is within the selected range. Although the influence of motion which is tested by the chamber test resulted in an increase of standard deviation. The relative standard deviation obtained from the tests of the Fibraflex fibre is lower compared to the Cem-FIL fibres, however these numbers have a large deviation from the selected range. From the performed bucket test it can be observed that the quantity of fibres reduces for a lower setting, thus by reducing the power output a quantity should be obtained which is closer to the required range. Further testing is necessary while it could be seen that the relative standard deviation slightly increases for a lower setting of the blower.

The Cem-FIL Minibars and the Fibraflex fibre types showed good compatibility with the device and therefore there is chosen to further analyse these two types of fibres. From literature research it

followed that for fibre pull-out, mechanical anchorage is the most important mechanism. Therefore, there is also chosen to test the Dramix 3D fibre, with hooked-ends. Although it is not yet possible to obtain a constant output with the blower for this type of fibre, structurally these might be of interest. With the current selection a broad spectrum of fibres will be analysed, with respect to different material and different shapes. Two different fibre materials will be tested, alkali resistant glass and high-strength steel fibres. Also the shape of the fibres differs for all three fibres, the glass fibres are slightly twisted which should be able to produce resistance against pull-out. For the Dramix 3D fibres the deformation capacity will be obtained due to the straightening of the hooked-ends and the large contact area of the Fibraflex area should be able to give a high friction resistance.

3D concrete printing showed to be a sensitive process, by changing several aspects on a small scale a large difference in output could be obtained. By using a back-flow nozzle a negative influence on the fibre distribution could be seen, for the down-flow nozzle this effect did not occur. Moreover, regarding the printing offset an influence could be seen, in which 1 or 2 millimetre already showed a large difference. These challenges need to be solved in order to print fibre reinforced concrete in which the fibres are sprinkled between the layers. The ratio between the material output of the printer and the offset in the code is of great importance. In an ideal situation the actual layer height and the printing offset should be the same. However, it follows from practice that this is difficult to achieve, to further optimise the printing process control needs to be gained over this ratio.

From the image analysis different fibre ratios are selected, to create a starting point the amount of fibres per cross section is analysed. For all three fibres types two ratios are selected, the amount of fibres crossing a section varies for all three fibres. With a varying number of fibres bridging the crack, it is assumed that the post-peak resistance should differ for the selected ratios. In figure 3.18 all fibre types are shown, the related fibre ratios are given in table 3.6. To calculate the weight per area, the amount of fibres on a surface of 50x200 millimetre is taken as a reference. To be able to compare the number of fibres with fibre reinforced concrete for which the fibres are mixed in the concrete, the volume percentage is taken based on a layer height of 10 millimetre. The volume percentages for the chosen ratios appear to be on the low side if compared to literature. However, it is expected that an increase of fibres might have a negative influence on the interface. All fibres which are mixed over the total volume in the case of casted concrete, are all located at the interface for the option of fibres in between the layers. It might thus not be realistic to compare the amount of fibres which are used one on one for both options. Therefore, it is chosen to quantify the amount of fibres as weight per area in this study.

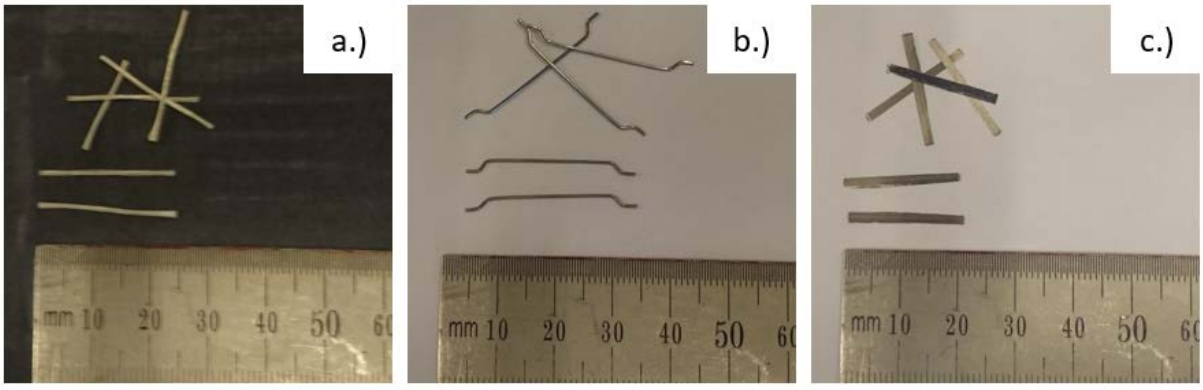

Figure 3.18: *Fibre types; a.) Cem-FIL Minibars 24mm; b.) Dramix 3D RC-4530-BL; c.) Fibraflex FF/20L6.*

Table 3.6: *Fibre ratio*

Fibre type		Fibre ratio	Weight per area (kg/m^2)	Volume percentage (%)
F1	Cem-FIL Minibars 24mm	A	0.0632	0.32
		B	0.0842	0.42
F2	Dramix 3D RC-4530-BL	A	0.1559	0.78
		B	0.2227	1.11
F3	Fibraflex FF/20L6	A	0.0259	0.13
		B	0.0388	0.19

The abovementioned fibre ratios will be used in the experimental program, to test the influence on the mechanical properties. Although the consistency of the blower is improved during this research, there is still chosen to apply these fibre ratios by hand. By doing so a better control is obtained over the number of fibres per test specimen. If the blower is used it cannot be guaranteed at this point that the same number of fibres is obtained over the entire print path. Also the exact required number of fibre coverage is still unknown, therefore reference samples are made by sprinkling the fibres by hand. In the end a proof of concept test is performed for which the blower is used to sprinkle the fibres in between the layers.

4. ANALYTICAL MODEL

To predict the behaviour of printed fibre reinforced concrete, an analytical model is proposed in this chapter. Based on the pull-out behaviour and the position of the fibres, a prediction can be made on the structural behaviour of a printed element. The results obtained by the analytical model can be compared by the experimental research.

4.1 CONCEPT

Until now no design rules are adopted in the Eurocode for fibre reinforced concrete, however different models have been proposed by multiple researchers. One example is the Model Code 2010 [16] in which two simplified stress-crack opening laws are proposed. These laws are able to describe the residual post-cracking behaviour of a fibre reinforced element. The two laws can be defined as a rigid-plastic model or a linear post-cracking model which can represent a strain-softening or strain-hardening material (figure 4.1). The residual post-peak response is characterised by performing three-point bending tests according to NEN-EN 14651. In this research the continuous mechanics is related to the fracture mechanics by taking a structural characteristic length into account. In case of a strain hardening material this length can be taken equal to the spacing between the cracks, if a strain softening behaviour is present the beam depth can be taken as structural characteristic length. In this research the proposed constitutive models are validated by experimental research, which showed similar results.

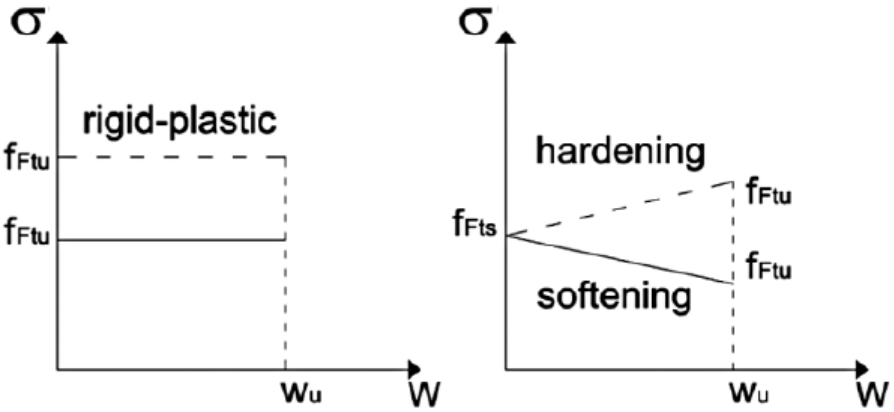

Figure 4.1: *Simplified constitutive laws according to the Model Code 2010. (di Prisco et al. [16])*

Another option is to calculate the internal equilibrium in the cracked section, the crack bridging response can be obtained from a single fibre pull-out behaviour [45]. From this a mode I constitutive law is obtained for the crack opening behaviour of the fibres. In here all fibre pull-out forces at a specific crack opening are combined, the total contribution is divided over the cracked surface. A semi-analytical model is used to take the parameters into account which are of influence, like the inclination angle and embedment length (figure 4.2). The random fibre distribution is taken into account by considering different intervals for the orientation and embedment length of a fibre. Hereby different pull-out curves can be obtained which show a reliable accuracy and for which on the other hand a reasonable calculation time is maintained. By doing so the tensile response of the material can be expressed as a function of the crack opening, for which the fibre orientation, embedment length and fibre strength as well as the concrete strength are used. From the research conducted by Soetens et al. [45] a good agreement is found between the analytical model based on single fibre pull-out and a model based on inverse analysis of flexural bending tests.

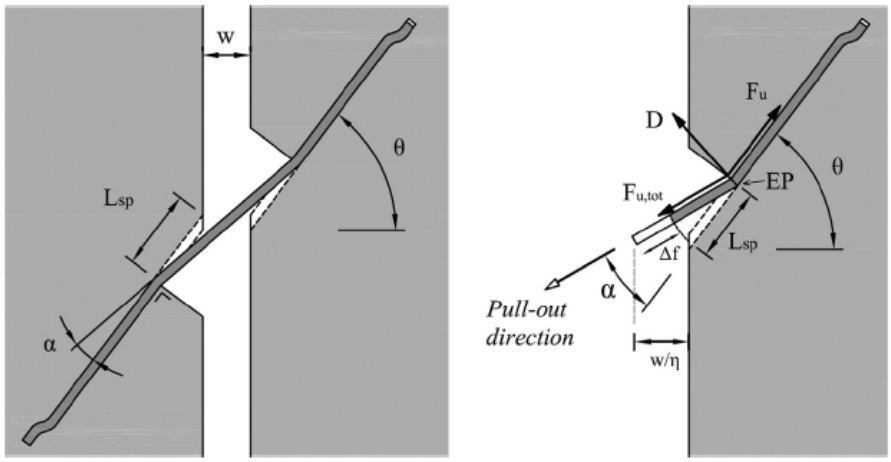

Figure 4.2: *Schematic pull-out behaviour of inclined fibre. (Soetens et al. [45])*

It is difficult to apply this method for conventional fibre reinforced concrete because the number and location of the fibres in the cracked surface is in general unknown. Also, the orientation and embedment length are of importance, which are in general randomly dispersed in conventional casted concrete. Prudencio Jr. et al. [37] proposed to perform flexural bending tests to obtain an average pull-out behaviour of the fibres in the cracked section. Hereby it is not necessary to know the exact dispersion of fibres over the element. In figure 4.3 a cracked section is shown which can be divides into three zones: a compression zone, an uncracked tension zone and a cracked tension zone. In the cracked tension zone a further distinction can be made between an aggregate bridging zone, a fibre bridging zone and a traction free zone. If the forces in all these zones are known, the stress over the element can be calculated for a given deflection. Hereby the moment equilibrium can be calculated from which a load-deflection diagram can be obtained. In the research by Prudencio Jr. et al. [37] it is assumed that the crack will occur at mid-span, which shows similarity with a failure mode in which a plastic hinge is assumed at mid-span. A rigid body motion is assumed while the elastic deflection in relatively small compared to the analysed deflections. Also in this research an experimental program is conducted for which a good agreement is found with the results obtained for the analytical model.

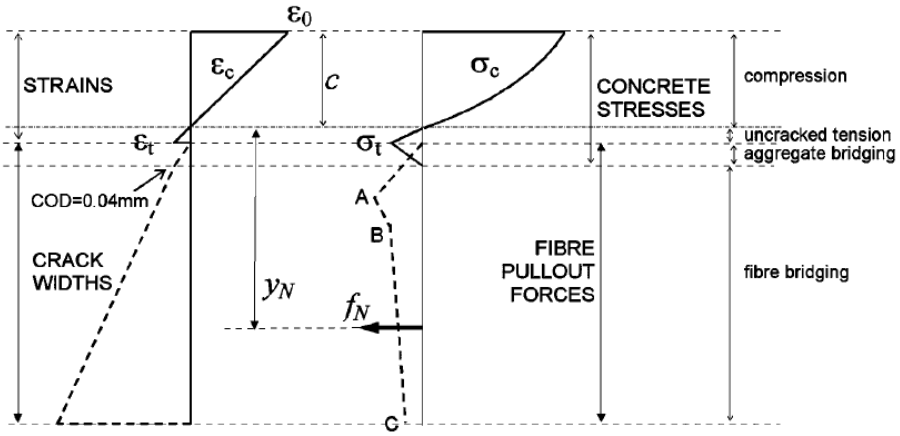

Figure 4.3: *Stress-Strain and Force-Crack width relation at critical cracked section. (Prudencio Jr. et al. [37])*

All models described above are based on conventional casted fibre reinforced concrete or sprayed fibre reinforced concrete elements. In general, a random fibre distribution is obtained due to the manufacturing process of these applications. Therefore, an average tensile contribution is taken for the influence of the fibre pull-out behaviour in the different models. Even in Soetens et al. [45] for which the pull-out response of a single fibre is considered, the total contribution is averaged over the total cracked surface. Contrary to conventional fibre reinforced concrete structures, the control over

the location of the fibres for printed elements is much larger. Due to the layered manufacturing technique the fibres are deposited on top of the layers, thus the location is known. Regarding the fibre orientation, a random distribution is obtained in the 2D plane parallel to the printing direction. However, by using the image analysis described in the previous chapter, this orientation of fibres is also known. Hereby it is possible to take a single fibre pull-out response into account at the location where the fibres are deposited.

In this research an analytical model is proposed which calculates the internal equilibrium of the cracked section. The analytical models of Prudencio Jr. et al. [37] and Soetens et al. [45] described above are taken as a starting point. It is assumed that the crack will occur at mid-span, and that the two broken halves will behave as rigid bodies (figure 4.4). This assumption can be made while the vertical deflections are a factor of 10 to 100 larger compared to the elastic deflections of the sample [37]. Once a crack occurs a distinction is made between three different zones at the critical section, a compression zone, an uncracked tension zone, and a cracked tension zone. In the compression zone a linear stress-strain relationship is taken into account for concrete in compression. Also for the uncracked tension zone a linear elastic stress-strain relationship is assumed until the maximum cracking strain is reached. After this point a crack will occur, and the concrete will have no more contribution to the load bearing capacity. In this cracked tension zone the contribution of the pull-out behaviour of the fibres is taken, which is dependent on the crack opening at mid-span. The contribution of the fibres is based on the number and orientation of the fibre distribution obtained from the image analysis performed in chapter 3.2.4. From figure 4.4 the rotation at the supports can be determined for any given deflection at mid-span (equation 4.1).

$$\theta = \frac{\delta}{L/2} \qquad [4.1]$$

The axial shortening at the top of the beam is calculated based on the rotation at the support and the height of the compressive zone (equation 4.2). At a vertical deflection of zero the beam is still uncracked, thus the height of the compressive zone is taken equal to half of the total beam height at the start. Once the deflection starts to increase a crack occurs which leads to a new internal equilibrium. By satisfying this internal equilibrium a new height is obtained for the compressive zone, which can be taken as input for the next incremental step.

$$\Delta L = 2\theta c \qquad [4.2]$$

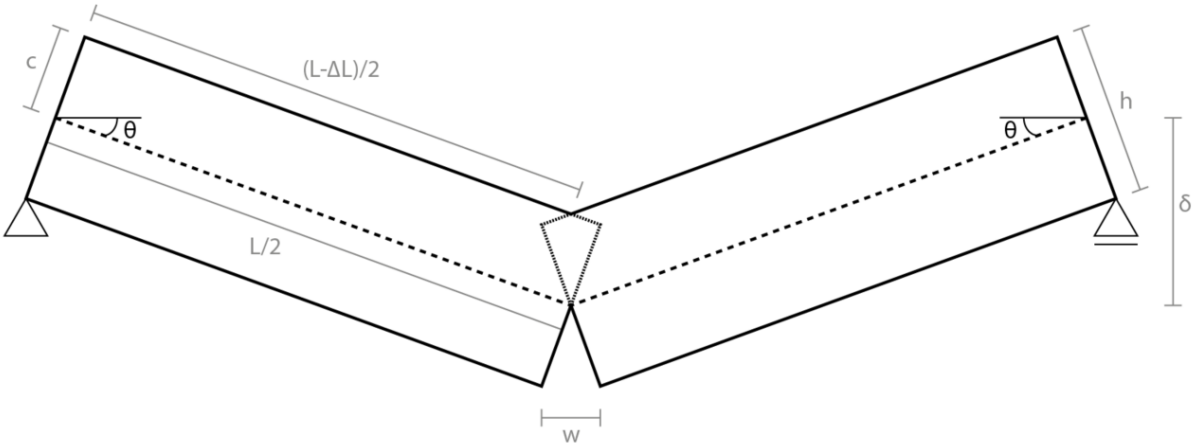

Figure 4.4: *Rigid body motion of two beam ends.*

The compressive strain at the top of the beam can be derived from the total axial shortening. By assuming a linear strain distribution over the height the curvature can be obtained. For an increasing deflection, the strain at the top and bottom of the beam will increase until a crack occurs. By applying Hooke's law, the strain at which a crack occurs can be calculated from the tensile strength and the Young's modulus (equation 4.3). The average values of the tensile strength and the Young's modulus for all concrete strength classes are given in NEN-EN 1992, another option is to perform material tests to obtain these values.

$$\varepsilon_{cr} = \frac{f_{ctm}}{E_{cm}} \qquad [4.3]$$

With the maximum strain at the bottom of the beam known, it is possible to calculate the height of the crack. The height of the uncracked tension zone can be determined by dividing the maximum strain by the curvature. This uncracked zone cannot be larger than half of the total height of the beam (equation 4.4). Consequently, the height of the crack can be calculated by subtracting the height of the compressive zone and the height of the uncracked tensile zone from the total height of the beam.

$$x = \min \begin{cases} x = \frac{h}{2} \\ x = \frac{\varepsilon_{cr}}{\kappa} \end{cases} \qquad [4.4]$$

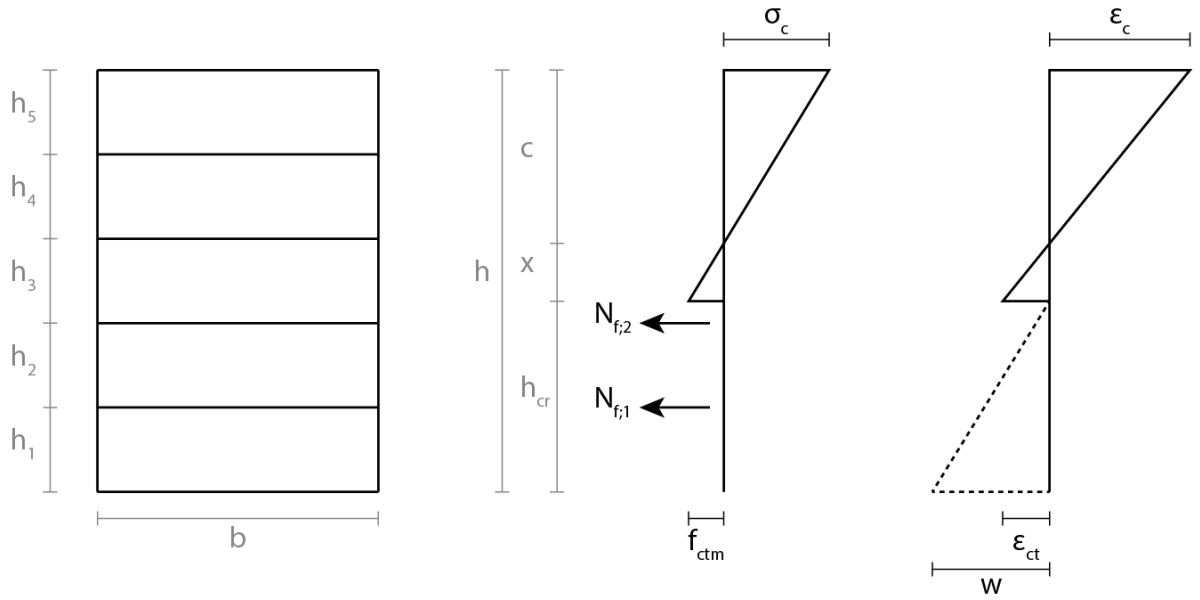

Figure 4.5: *Dimensions of cross sections and schematic drawing of stress-strain/crack width diagram.*

By satisfying the internal equilibrium the load carrying capacity at any given vertical deflection can be calculated (figure 4.5). The contribution of the three different zones can be multiplied by their distance from the neutral axis to obtain the moment equilibrium. The contribution of the concrete in compression, and the uncracked concrete in tension is given in respectively equation 4.5 and 4.6.

$$N_c = \frac{1}{2} \cdot b \cdot c \cdot \sigma_c \qquad [4.5]$$

$$N_t = \frac{1}{2} \cdot b \cdot x \cdot \sigma_{ct} \qquad [4.6]$$

The contribution of the fibres is based on its pull-out behaviour multiplied by the number of fibres per cross-section. This pull-out behaviour is dependent on the type of fibre which is used and can be calculated with equation 4.7. If the fibre is pulled out of the concrete matrix equation 4.7a is valid, in here to bond stress is multiplied by the perimeter and embedment length of the fibre. A factor α is added to the equation to take the random distribution into account, as not all fibres in the interface

have the same embedment length and inclination angle. If fibre rupture occurs equation 4.7b can be used, here the pull-out force is based on the strength of the fibre. The tensile strength of a fibre is multiplied by the cross-section to obtain the rupture force of a single fibre. Also in this case the force is multiplied by the number of fibres per interface. Fibre rupture only occurs if the pull-out force due to friction is larger compared to the rupture force, it is thus possible that for short embedment lengths these fibres are still pulled out of the concrete matrix. Also for these type of fibres the inclination angle and embedment length are of importance, therefore also in this equation a factor α is implemented.

$$N_{f;i} = \alpha \cdot n_i \cdot \tau_{av} \cdot \pi d_f \cdot L_e \quad [4.7a]$$

$$N_{f;i} = \alpha \cdot n_i \cdot f_{Fy} \cdot A_f \quad [4.7b]$$

Once a fibre is pulled out of the concrete matrix the embedment length reduces, hereby the pull-out force of the fibre reduces. The reduction of the embedment length is equal to the increase in crack opening. Thus by calculating the width of the crack at the different interfaces, the reduction in pull-out force is known. The crack width at the bottom of the sample can be determined by equation 4.8, to obtain the crack width at the different interfaces the crack height needs to be reduced by the layer height.

$$w = 2 \cdot h_{cr} \cdot \sin[\theta] \quad [4.8]$$

The contribution of fibres is only taken into account if the crack height exceeds the height of the interface, the fibres located in the uncracked concrete are not yet taken into account. The moment equilibrium can be calculated with equation 4.9.

$$M_e = N_c \cdot x_{Nc} + N_t \cdot x_{Nt} + \sum N_{f;i} \cdot x_{N;fi} \quad [4.9]$$

From the moment equilibrium the load can be calculated which then can be converted to a flexural stress by the basic mechanics. By increasing the deflection stepwise a stress-deflection diagram is obtained by equilibrium of forces at the critical section. With an increasing crack height, the height of the compression zone also changes. This new height can be calculated by observing equilibrium in the cracked section based on the forces of the concrete and fibres (equation 4.5 – 4.7). In equation 4.10 this calculation is shown which gives the new height of the compression zone which has to be implemented in equation 4.2 for the next incremental step of the deflection.

$$c = \frac{b \cdot x \cdot \sigma_{ct} + 2\sum N_{f;i}}{b \cdot \sigma_c} \quad [4.10]$$

4.2 Implementation of model

The stress-strain relationship of the concrete material which is used is assumed to have a bi-linear shape (figure 4.6a). The strength in compression and tension, with the corresponding strains, are taken from NEN-EN 1992, according to the manufacturer of the dry-mix the strength class of concrete is equal to C35/45 (table 4.1). Also the Young's modulus of the material is calculated with the formula given in NEN-EN 1992 chapter 3.1.3 (equation 4.11).

$$E_{cm} = 22000 \cdot \left(\frac{f_{cm}}{10}\right)^{0.3} \quad [4.11]$$

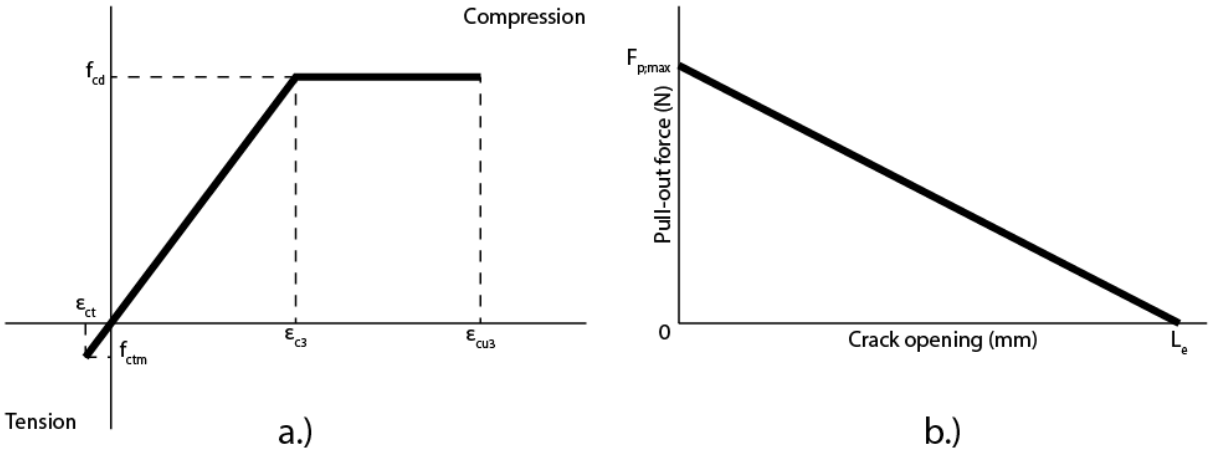

Figure 4.6: *Assumptions material behaviour a.) Bi-linear stress-strain diagram of concrete; b.) Pull-out force-crack opening diagram (In case of fibre pull-out).*

Table 4.1: *Assumed material properties; concrete*

f_{cd}	23.33	N/mm^2
f_{ctm}	3.21	N/mm^2
ε_{c3}	1.75	‰
ε_{cu3}	3.5	‰
ε_{ct}	0.09	‰
E_{cm}	34077.15	N/mm^2

Table 4.2: *Assumed material properties; fibres*

Cem-FIL Minibars 24mm	τ_{av}	8.0	N/mm^2
	d_f	0.70	mm
	L_e	12	mm
Dramix 3D RC-4530-BL	τ_{av}	11.4	N/mm^2
	d_f	0.62	mm
	L_e	15	mm
Fibraflex FF/20L6	f_{Fy}	1400	N/mm^2
	A_f	0.0464	mm^2

The aim of the analytical model is to give a prediction of the flexural strength of printed fibre reinforced concrete. In this research an experimental program is conducted in which a four-point bending test is performed, this experimental program is discussed in the chapter 6. To compare the results the dimensions are based on this experimental program. The samples which are tested have a size of 40x60x600mm and are printed with a layer height of 12 millimetre. The four-point bending test has a span of 450 millimetres with the two loading rollers evenly distributed over the length.

In chapter 3.2.4 an image analysis is conducted to predict the fibre distribution, the results of this study are used as input for the analytical model. In this study different fibre types and distributions are analysed, from this the number of fibres per cracked section are determined (table 4.3). The value of the pull-out load of these fibres can be calculated by using equation 4.7. For the case in which the fibre is pulled out of the concrete matrix, the force reduces for an increasing crack opening (figure 4.6b). The exact frictional bond stress of the fibre types is unknown, therefore there is chosen to make an assumption based on pull-out tests performed in literature [8][41][44]. If fibre rupture is the governing pull-out mechanism the cross-section of the fibre is multiplied by its tensile strength. The fibre strength

and dimensions are taken from the declaration of performance given by the manufacture of the fibres. Once the crack opening at the fibre location exceeds 0.1 millimetre, the contribution of the fibre is neglected. It is assumed that at this point the fibre breaks and is further unable to transfer any loads. The values of the investigated fibre types are listed in table 4.2. In both cases a factor α is added to the equation to take the random fibre distribution into account. In Prudencio Jr. et al. [37] a similar parameter is considered, in here a value of 0.5 is adopted for a random 3D fibre distribution. The same value is taken for α in this analytical model, from experimental validation the exact value can be obtained. For every deflection the force equilibrium in the critical section is calculated, from this the height of the crack can be determined. As long as the interface is within the uncracked concrete, the contribution of the fibres is neglected. Once the crack exceeds the height of the interface the contribution of the fibres is applied in the force equilibrium.

Table 4.3: *Fibres per cross section*

Fibre type	Ratio	No. fibres per cross section
Cem-FIL Minibars 24mm	A	3
	B	4
Dramix 3D RC-4530-BL	A	2
	B	4
Fibraflex FF/20L6	A	4
	B	5

By implementing the analytical model, the stress-deflection graphs are obtained as shown in figure 4.7. In here it can be seen that all samples show a similar behaviour up to the first crack, which should be the case while the contribution of the fibres is not taken into account in the uncracked phase. After the sample breaks a reduction in strength can be observed for an increasing vertical deflection. The bending stiffness of the cracked section is reduced with respect to the uncracked section. Once the crack height passes an interface a new layer of fibres is activated, these locations can clearly be seen in the graph. In the case for which the fibres are pulled-out of the matrix a small increase in stress can be observed. The stress remains constant for an increasing deflection while the contribution of the fibres stays more or less equal. A slight reduction of pull-out force is implemented in the pull-out model due to the reducing embedment length. This reduction is based on the increase of crack width at the interfaces, which is rather small for the given deflections. On the other hand a continuous reduction in stress can be observed in the case for which fibre rupture occurs. For both the Fibraflex ratios a sudden drop can be observed if the crack passes an interface. If the crack width at the interface exceeds 0.1 millimetre it is assumed that all fibres break, resulting in a sudden reduction of load bearing capacity. In the current model all fibres in a certain interface break at the same time, which explains the sudden drop. Also in the case for which fibre pull-out is observed a sudden impact of the fibres can be observed. In here the pull-out behaviour of the fibres after the maximum load is assumed, hereby the contribution of the fibres goes from zero to maximum.

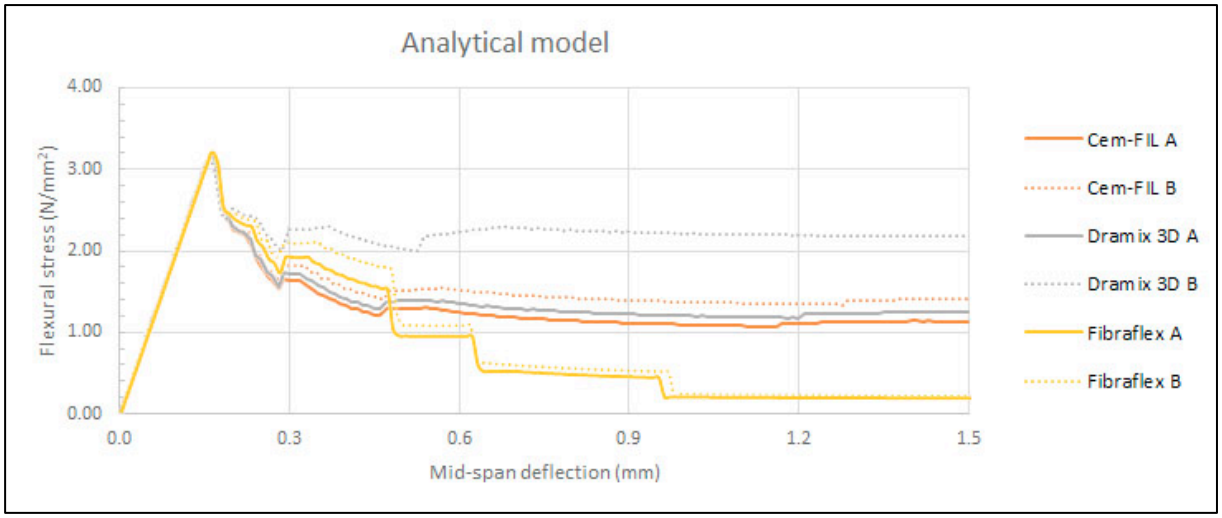

Figure 4.7: *Prediction stress-deflection diagram of four-point bending test using analytical model with input from image analysis.*

4.3 Discussion

The outcome of the analytical model seems to give a reasonable behaviour of a fibre reinforced sample in a four-point bending test. As mentioned in the previous paragraph, the location at which the fibres are activated can clearly be seen in the graph. This is due to the manner in which the fibres are implemented in the model. Once the crack height passes an interface, the fibres are suddenly activated based on their maximum pull-out load. In reality this load will have a more gradual build-up, thus it is assumed that a smoother graph will be obtained once a more realistic pull-out behaviour is implemented. The same holds for the case in which fibre rupture occurs, in here the fibres break once the crack width exceeds a certain value. This leads to a sudden drop in the stress-deflection diagram while the contribution of the fibres suddenly becomes zero. In reality it is assumed that not all fibres break at the exact same moment, thus a smoother drop should be obtained.

For all three fibre types which are implemented in the model it can be seen that a larger number of fibres results in an increase of post-peak behaviour. This should also be the case while the contribution of the single fibres is added for each interface. In figure 4.7 it is assumed that the contribution due to the fibres is the same for each interface, however this can be different in reality. The distribution and orientation of the fibres is random as is observed from the image analysis in paragraph 3.2.4. Thus it is most likely that the number of fibres per interface differs in the cracked section. For simplicity, all fibre contributions are taken the same, however it is possible to implement a different quantity of fibres per interface.

5. EXPERIMENTAL PROGRAM

The goal of adding fibres to the concrete is to improve the tensile capacity of the material, therefore an experimental is conducted. A selection of fibres is made based on the performed literature research and the workability tests of the blower described in the respectively chapter 2 and 3. In this section the test program is described which is performed to obtain the influence on the mechanical behaviour.

5.1 MATERIAL PROPERTIES

The concrete which is used is made available by Saint Gobain Weber Beamix, a cement dry-mix is created by this company which is specially crafted for printing concrete. Due to the thixotropic behaviour of the concrete, the material has a good flowability when energy is applied. Once the material leaves the nozzle there is no more energy added due to which the material becomes stiff. The code for the dry-mix which is used is Weber 3D 145-2, the water/dry-mix ratio which is used is approximately 0.162. According to Saint Gobain Weber Beamix the strength of the material is comparable to C35/45. The material is produced in accordance with EN 206, the specifications are given in table 5.1.

Table 5.1: *Concrete specifications*

Label:	Weber 3D 145-2
Concrete class:	C35/45
Workability:	Consistency class F3
Largest grain size:	1 mm
Cement type:	CEM I

Different types of fibres are used to test the impact on printed concrete, three fibre types are tested experimentally. These three fibres are selected based on their geometry and compatibility with the manufacturing method. The first fibre which will be tested is the Cem-FIL Minibars 24mm produced by Owens Corning, this fibre is made of alkali resistant glass with a thermoset resin [54]. The second fibre is the Dramix 3D RC-4530-BL produced by Bekaert, due to the hooked-ends mechanical anchorage will play a major role during pull-out of the fibre [55]. The third fibre is produced by Saint Gobain SEVA, Fibraflex FF/20L6, this fibre should have a good adhesion to the concrete matrix due to the large surface area [56]. All three fibre types are shown in figure 5.1, the dimensions of the fibres can be found in table 5.2.

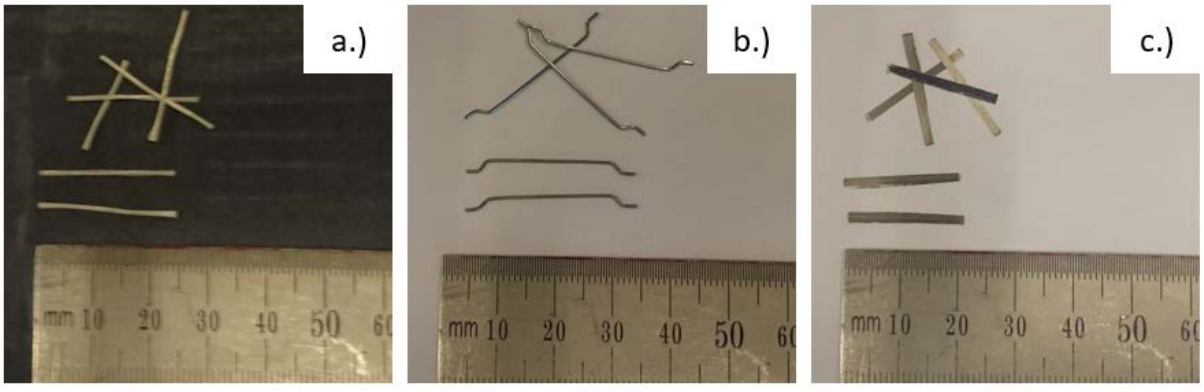

Figure 5.1: *Fibre types; a.) Cem-FIL Minibars 24mm; b.) Dramix 3D RC-4530-BL; c.) Fibraflex FF/20L6.*

Table 5.2: *Fibre properties*

Fibre type		Shape	Length (mm)	Diameter (mm)	Tensile strength (N/mm^2)
F1	Cem-FIL Minibars 24 mm	Twisted	24	0.70	1000
F2	Dramix 3D RC-4530-BL	Hooked-end	30	0.62	1270
F3	Fibraflex FF/20L6	Flat	20	0.029	1400

5.2 Test series

5.2.1 Test program

Different testing methods are available to analyse the influence of fibres on the material properties. In general flexural tests are used as a standard method, this is because they are easily performed. These flexural tests are mainly designed as a three-point (NEN-EN 14651) bending test or a four-point bending test (ASTM 1609, JCI-FS4)[10], for which the beam can be notched. Model Code 2010 [16] prescribes a notched three-point bending test (NEN-EN14651) as a standard method to test fibre reinforced concrete, however it accepts different testing methods if proper correlation factors can be given [10]. In research done by Conforti et al. [10] and Paegle et al. [33] different test methods are compared to analyse if there is a correlation between these test methods. In research done by Conforti et al. [35] three different flexural tests are performed, a three-point bending test on a notched beam (EN 14651), and two different four-point bending test (ASTM 1609, JCI-SF4). For the three-point bending test the crack width is measured, in order to compare the results from the other two tests a clip was fixed to the centre part of the four-point bending tests. This clip needs to span the centre part while the exact location of the crack is unknown at the beginning of the test. By comparing the post-peak response of all tests it can be concluded that the behaviour is similar, the only difference was due to experimental scatter. Also the variation of the independent test is comparable between the different tests. For this research a linear correlation could be found between the vertical deflection and the crack width, so all three test methods should give reliable results. A comparison between different test methods is also made in research done by Paegle et al. [33], similar results were found. From the results in this research, a four-point bending test is recommended. It is concluded that a notched three-point bending test cannot be used for a strain hardening material while only a single crack can occur. Additionally, in some cases this test set-up might also not be valid for strain softening materials. By implementing a notch the stresses around the notch tip are disturbed which leads to a diffuse cracking pattern. A modified set-up of a four-point bending test should be used, were the slenderness ratio (a/h) of the beam needs to be 2 or higher. This to minimise the influences of shear stresses in the beam.

To get an overview of the impact of adding fibres in between layers different parameters are observed during testing. There is chosen to test three types of fibres, as mentioned in the chapter 3 this is done based on the geometry of the fibre and workability of the blower. Also the fibre ratio is varied to check the influence of the amount of fibres. The material properties are tested by performing a flexural test, a modified four-point bending test should give proper results as stated above. By performing a four-point bending test the specimen is fully subjected to bending stress in the centre part of the specimen. A slenderness ratio of 150 / 60 = 2.5 will be maintained. The samples will be tested perpendicular to the printing direction, by doing so the fibres should be orientated in such a manner that they will be able to bear the tensile loads. From the experiments a load-deflection diagram will be obtained. By subjecting the specimen to a flexural load it is expected that the fibres are activated once a crack occurs. From this point the tensile capacity of the material should improve compared to plain concrete.

5.2.2 Specimen preparation

The print settings of the pump are kept constant for all test specimen, for both the hybrid nozzle and down-flow nozzle a nozzle opening of 12x60 millimetre is used. The layers are deposited by the robot arm which was set to a speed of 100 mm/sec. The frequency of the pump is set to approximately 24 Hertz, which relates to the output of the material. With these settings a layer dimension of approximately 12 millimetre in height and a width of 60 millimetre could be printed of good quality. At this stage of the research the blower is not yet fully operational, therefore there is chosen to add the fibres manually (figure 5.2). From the different fibre ratios selected in chapter 3.3 the quantity of fibres is calculated based on the layer width, these are sprinkled by hand on top of the printed layers. Due to practical reason it is impossible to sprinkle fibres by hand over the entire print path, therefore there is chosen to only distribute the fibres over a length of 200 millimetre. Theoretically the crack in the samples will occur in between the loading rollers, which are 150 millimetres apart. Thus if the specimens are carefully sawn and placed in the test set-up, it should not matter that the outer ends of the beam are unreinforced. From the image analysis performed in chapter 3.2.4 it is concluded that the fibre orientation of the blower is random, during sprinkling it is tried to replicate this random fibre orientation over the length. Finally, one proof of concept test is performed for which the blower is used to deposit the fibres over the print path, the same print settings are maintained.

Figure 5.2: *Specimen preparation, sprinkling of fibres by hand*

All specimens are stored and cured according to NEN-EN 12390-2, in this code the manufacturing and curing of concrete specimen is described. Only the manufacturing method differs from this code, the samples are printed instead of casted. The specimens are printed according to the standard procedure, where layer after layer is printed. After the samples are printed they are covered with a plastic foil for one day. After a day the samples are removed from the printing table, after this they are sealed in plastic and stored at room temperature. To get the right dimensions the samples are wet sawn during the curing time, for the four-point bending test a dimension of 40x60x600mm is required.

5.3 Experimental test set-up

5.3.1 Four-point bending test

For the four-point bending test an Instron test bench is used (see figure 5.3). To obtain the post-peak behaviour it is needed to perform the test under displacement control. The speed of the test bench is set at 0.05 mm/min, this test speed is maintained until the specimen has reached its peak strength. Once a stable post-peak behaviour is obtained the test speed is increased to 0.15 mm/min. In order to properly obtain the behaviour at the peak, the test speed needs to be kept low. After cracking of the specimen the fibres will be pulled out of the concrete and a higher test speed can be used. For the

span of the test a distance of 450 millimetre is used, with a spacing between the loading rollers of 150 millimetres (figure 5.4). For the supporting rollers one of the two should be able to rotate, the same holds for the loading rollers. This is required to even out any eccentricities of the specimen. During the test the vertical deflection of the beam is measured, this is done by placing two LVDTs. To do so a wooden frame is made which can be clamped onto the beam, the LVDTs can be fitted into this frame. The vertical deflection is measured at one side of the beam, both under the loading rollers. By fixing the LVDTs directly onto the specimen the deformation of the test bench itself is not measured, hereby the obtained deflection is only from the beam itself.

Figure 5.3: *Test set-up four-point bending test; Overall set-up (Left); Location of LVDTs (Right).*

The location of the crack is different for each test sample, therefore there is chosen to measure the deflection at the position of the loading rollers. By doing so an approximation can be made about the location of the crack and thus the maximum deflection. This is done by creating a hinge at the location of the crack, it is assumed that the rest of the beam remains rigid (figure 5.4). The vertical deflection at the support rollers is zero, from the data obtained through the LVDTs the rotation at both supports can be calculated. While both beam ends should come together in the hinge, the distance x can be calculated (equation 5.1). Once this point is known the deflection at the crack can be calculated, which should be the maximum deflection (equation 5.2). This calculation will be performed for all test data to be able to compare the behaviour of the beams.

$$x = \frac{150 \cdot (2 \cdot \delta_2 - \delta_1)}{\delta_1 + \delta_2} \qquad [5.1]$$

$$\delta_{max} = \frac{3 \cdot \delta_1 \cdot \delta_2}{\delta_1 + \delta_2} \qquad [5.2]$$

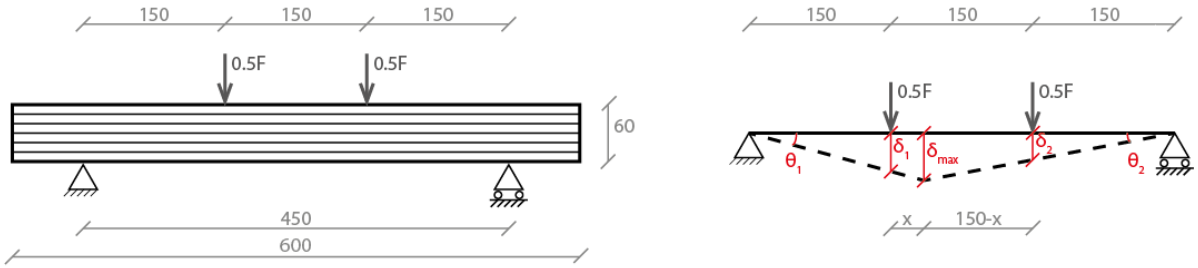

Figure 5.4: *Schematic drawing of test set-up four-point bending test; Dimensions (Left); Determination of maximum vertical deflection (Right).*

To analyse and compare the post-peak behaviour of the different samples the fracture energy is calculated. This is the energy which is required for the crack to grow and can be obtained by integrating the stress over the deflection after the crack has occurred. If a sample has a post-peak behaviour the fracture energy is considered, the area under the curve is shown in figure 5.5. The fracture energy is taken from the crack initiation until a vertical deflection of 1.5 millimetre.

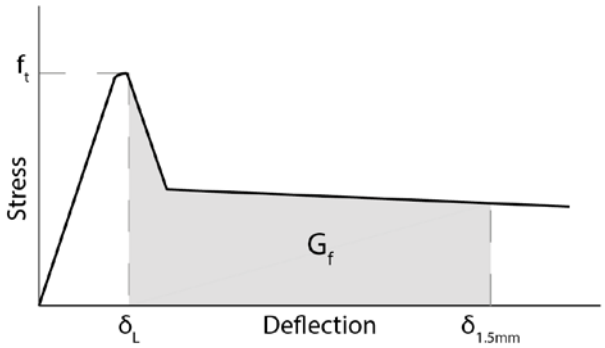

Figure 5.5: *Fracture energy.*

Different parameters are observed in this experimental study, which are fibre type, fibre ratio, and nozzle type. The results will be discussed in three different test series, the first is printed with a hybrid nozzle for which the fibres are sprinkled by hand on the concrete layers. The second test series is printed with a down-flow nozzle, also in this case the fibres are sprinkled by hand. The last test series is again printed with a down-flow nozzle, however for this proof of concept the blower is used to deposit the fibres on top of the concrete layers. For all test series a reference test is printed with plain concrete, to analyse the influence of the fibre reinforcement three different fibres are applied which are given in paragraph 5.1. For all fibre types two fibre ratios are selected, due to practical reason not all combinations of fibre type and fibre ratios are tested in each series. A total list of all performed tests is given in table 5.4, the results from the four-point bending test are labelled according to the following protocol.

[FX]_[ρ]_[n]

Table 5.3: *Experimental labels*

Fibre type	(FX)	F0	No fibres
		F1	Cem-FIL Minibars 24mm
		F2	Dramix 3D RC-4530-BL
		F3	Fibraflex FF/20L6
Fibre ratio	(ρ)	A - C	
Specimen number	(n)	1 - 10	

Table 5.4: *Test series*

Test series	**Fibre type**		**Fibre ratio**		
Hybrid nozzle	F0	Plain concrete	-	kg/m^2	(A)
	F1	Cem-FIL Minibars 24 mm	0.0632	kg/m^2	(A)
	F2	Dramix 3D RC-4530-BL	0.1559	kg/m^2	(A)
			0.2227	kg/m^2	(B)
	F3	Fibraflex FF/20L6	0.0259	kg/m^2	(A)
			0.0388	kg/m^2	(B)
Down-flow nozzle	F0	Plain concrete	-	kg/m^2	(A)
	F1	Cem-FIL Minibars 24mm	0.0842	kg/m^2	(B)
	F2	Dramix 3D RC-4530-BL	0.2227	kg/m^2	(B)
	F3	Fibraflex FF/20L6	0.0388	kg/m^2	(B)
Proof of concept	F0	Plain concrete	-	kg/m^2	(A)
	F1	Cem-FIL Minibars 24mm	0.2485	kg/m^2	(C)

6. EXPERIMENTAL RESULTS

Different test series are performed to analyse the influence on the mechanical behaviour, in this section the results from the bending tests are discussed. In this study two series of four-point bending tests are performed, printed with two different nozzles to analyse the influence of the printing parameters. Hereby it should also be possible to draw a conclusion regarding the compatibility with different reinforcing methods. Additionally, a proof of concept print is conducted in which the blower is used to create test samples. Finally, the experimental output is compared to the proposed analytical model explained in chapter 4.

6.1 HYBRID NOZZLE

Although it followed from the observations of the printing parameters that a hybrid nozzle can influence the fibre distribution, there is chosen to perform a test series printed with this nozzle. For future research it could be interesting to combine several reinforcing methods. This combined option is out of the scope of this research, however by doing this series the compatibility with different reinforcing options can be analysed. The dimensions of all specimens are measured to translate the obtained load to a flexural stress, these dimensions can be found in appendix E. Only the average results per test series will be given in this chapter, the results of all independent tests can be found in appendix F.

To analyse the influence of the addition of fibres, several plain concrete specimens are printed as a reference value. In figure 6.1 the stress-deflection diagram of the tested samples is shown, the average values can be found in table 6.1. The overall behaviour of the samples is similar, the load is increased until a crack is initiated. After the samples are cracked the load drops to zero while the unreinforced concrete is unable to resist the flexural stresses, this shows the brittle failure behaviour of the material concrete. When the lines are analysed individually it can be seen that two out of six samples showed a larger moment of rupture. It should be noted that not all samples are printed on the same date due to practical reasons. Although it is tried to keep all the printing parameters constant, a change of environmental conditions is unavoidable. It is assumed that the deviation in these samples is due to differences in the printing process. When the overall material behaviour is compared a similar trend can be observed between the different test series.

Table 6.1: *Average results; plain concrete, ratio A*

Maximum stress (N/mm^2)	Deflection at max stress (mm)	Fracture energy (N/mm)
3.68 (0.59)	0.18 (0.03)	- (-)

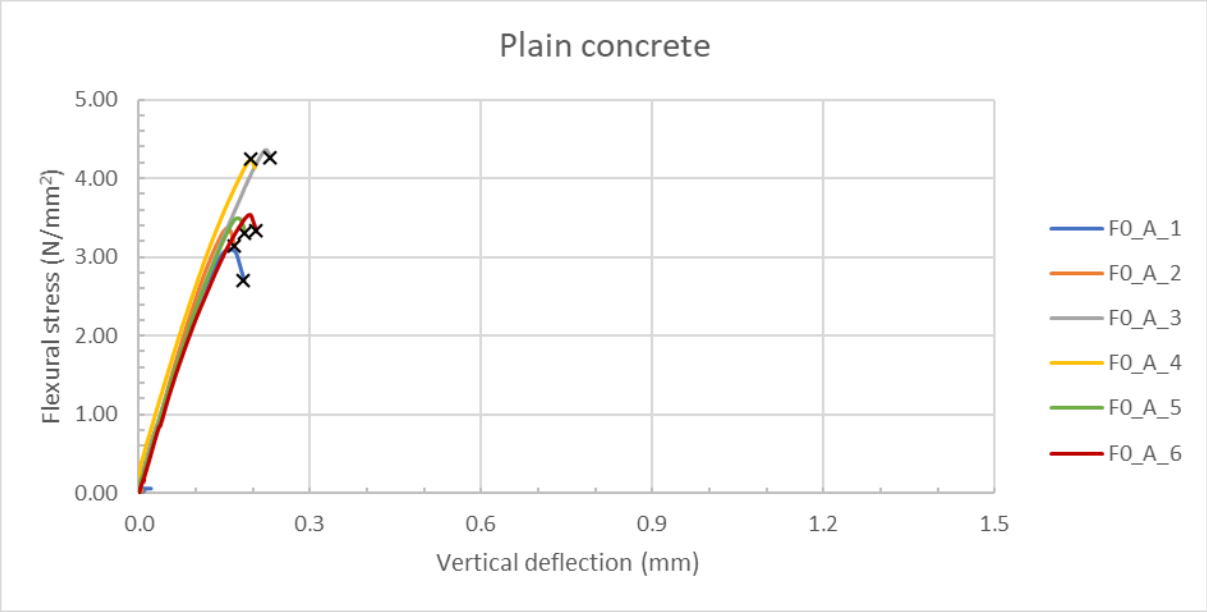

Figure 6.1: *Stress-Deflection diagram, Plain concrete.*

The first fibre which is tested is the alkali resistant glass fibre, Cem-FIL Minibars 24mm. The results are shown in figure 6.2 and the average values are given in table 6.2. Although only four lines are shown in the graph, five samples are tested. For one case the data of the vertical deflection gave incorrect values, the measurement of the load however showed correct results. The peak stress of the tested samples is comparable, only for one value a slightly lower strength is obtained. The overall behaviour of this sample is similar to the rest, no direct explanation can be found for this reduction in strength. The peak strength is slightly higher compared to plain concrete, however it cannot be stated with certainty that this is due to the addition of the glass fibres. By analysing the descending branch of the samples a strange trend could be observed for some of the samples, namely F1_A_2 and F1_A_4. Here a gentle slope could be observed, however after analysing the data points it can be said that the vertical deflection showed a large jump. After the crack is initiated an abrupt jump can be seen for the vertical deflection, also a sudden load drop is observed. While this sudden drop does not properly represent the real behaviour a dotted line is given for this load drop. The speed of the test bench is most likely the cause of this sudden drop, while the machine was not able to collect enough data points on the softening branch of these samples. After the crack is initiated the load does not drop to zero, but a little post-peak behaviour is obtained due to bridging of the fibres. After analysing the crack surfaces it can be seen that only 1 or 2 fibres bridged the crack. This explains the low post-peak behaviour while the load bearing capacity of a single fibres is small. Even in the case of one sample, F1_A_3, no fibres could be observed in the crack surface. This sample immediately broke after the crack was initiated, behaving as plain concrete. The fracture energy could only be calculated for a single sample, so no standard deviation is given.

Table 6.2: *Average results; Cem-FIL Minibars 24mm, ratio A = 0.0632 kg/m²*

Maximum stress (N/mm²)	Deflection at max stress (mm)	Fracture energy (N/mm)
4.00 (0.57)	0.20 (0.01)	1.000 (-)

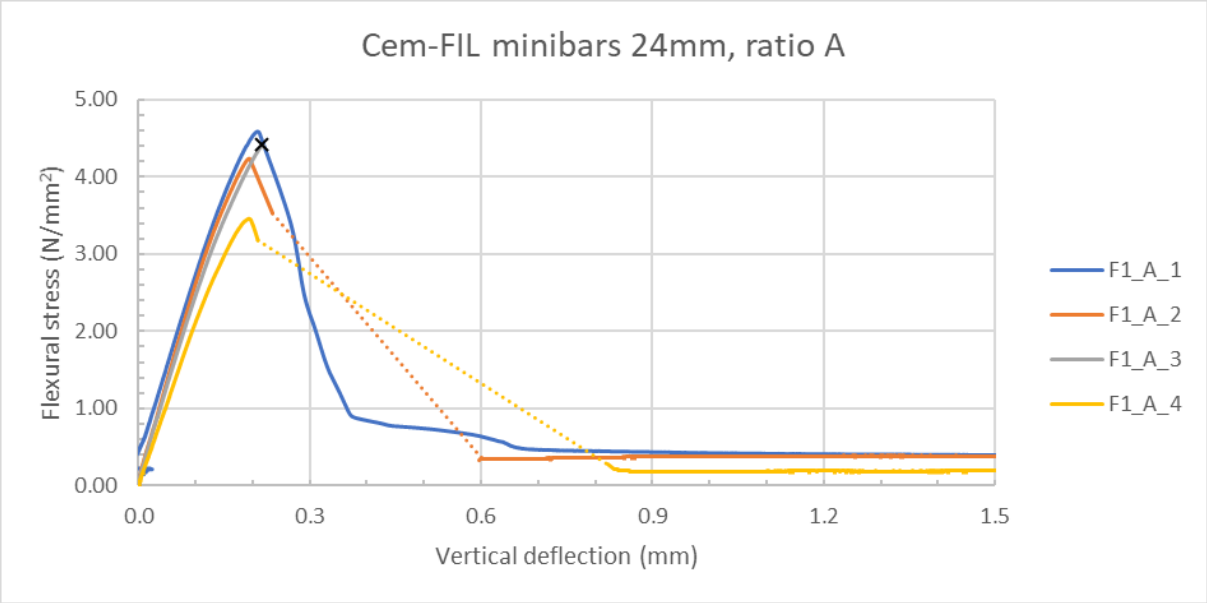

Figure 6.2: *Stress-Deflection diagram, Cem-FIL Minibars 24mm, ratio A = 0.0632 kg/m².*

The second type of fibre is a deformed high-strength steel fibre, Dramix 3D with hooked ends. From the results two different trends could be observed in the stress-deflection diagrams shown in figure 6.4. For three out of five cases sudden rupture occurred after the initiation of a crack. By analysing the crack surfaces of these samples no fibres could be found, thus is makes sense that these samples behaved as plain concrete. In the other two samples a post-peak behaviour can be observed, after the crack a stable post-peak behaviour of about 0.5 N/mm² can be found. For both these samples a single fibre was found in the crack surface. Contrary to the pull-out behaviour of the glass fibres, the pull-out capacity of the high-strength steel fibres is obtained due to mechanical anchorage. In both cases the hooked-end of the fibre was straightened (figure 6.3), as should be the case according to literature. No direct influence can be observed on the peak strength compared to plain concrete, the maximum flexural stress and deflection are within the same range. This can be explained by the pull-out mechanism of the high-strength steel fibre, which is mechanical anchorage. The pull-out resistance of the fibre is obtained due to deformation of the hooked-end, and this will only happen for an increasing crack opening resulting in the fibre being pulled out. Also for the high-strength steel fibres a slight improvement in ductility is achieved, however only a single fibre is bridging the cracks. No standard deviation of the fracture energy is calculated, the reason for this is that only two samples showed a post-peak behaviour.

Figure 6.3: *Straightening of hooked-end of Dramix 3D fibre.*

Table 6.3: *Average results; Dramix 3D RC-4530-BL, ratio A = 0.1559 kg/m²*

Maximum stress (N/mm²)	Deflection at max stress (mm)	Fracture energy (N/mm)
3.83 (0.25)	0.21 (0.02)	1.011 (-)

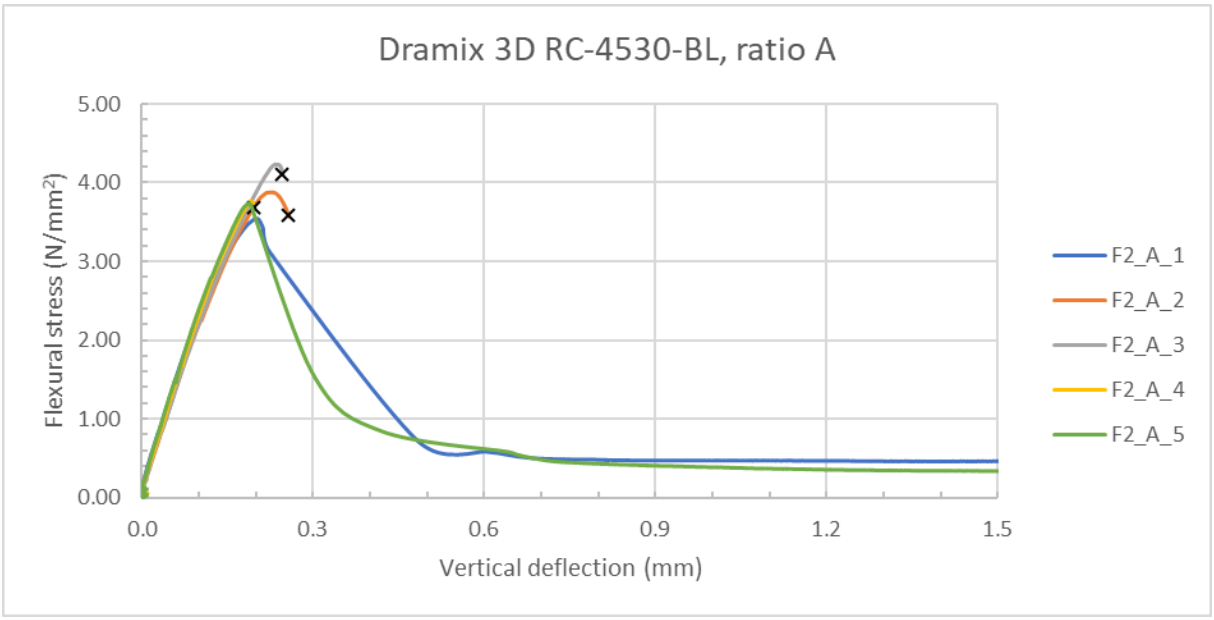

Figure 6.4: *Stress-Deflection diagram, Dramix 3D RC-4530-BL, ratio A = 0.1559 kg/m².*

Two different fibre ratios are tested in this series for the deformed high-strength steel fibre, the results are given in figure 6.5 and table 6.4. A similar behaviour can be found as compared to the lower fibre ratio, for this case two out of five samples showed a brittle behaviour. For both samples no fibres could be found in the crack surface, thus the behaviour is comparable to plain concrete. For the other three samples an improvement in ductility is obtained. Also in this case no significant influence in the peak strength can be observed compared to plain concrete. This is most likely due to the pull-out mechanism of the used fibre type as explained before. A reduction in load bearing capacity can be observed after the crack is initiated, a stable branch of about 0.7 – 0.8 N/mm² is obtained. This is a small improvement compared to ratio A, for which a post-peak behaviour of approximately 0.5 N/mm² is obtained. By observing the crack surfaces of the samples, it could be seen that the post-peak behaviour is obtained due to the pull-out of two fibres. Again in these cases straightening of the hooked-end could be observed. Also the fracture energy of the test samples is slightly increased, this is due to the stable post-peak branch. The area under the curve is larger due to a higher post-peak load.

Table 6.4: *Average results; Dramix 3D RC-4530-BL, ratio B = 0.2227 kg/m²*

Maximum stress (N/mm²)	Deflection at max stress (mm)	Fracture energy (N/mm)
3.57 (0.32)	0.21 (0.01)	1.144 (0.101)

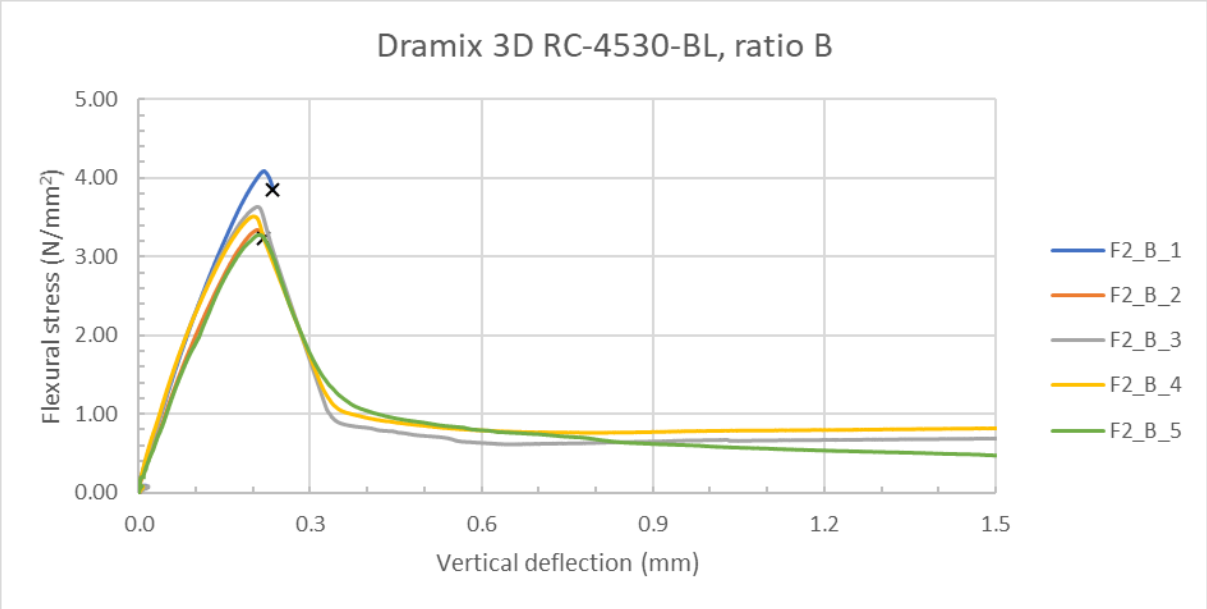

Figure 6.5: *Stress-Deflection diagram, Dramix 3D RC-4530-BL, ratio B = 0.2227 kg/m².*

Finally, a third type of fibre is tested which is made of high-strength steel, Fibraflex FF/20L6. For all five tested samples a similar behaviour could be found, only in one case the test bench was not able to produce enough data points in the descending branch (figure 6.6). This is most likely, as already explained before, due to the test speed. For the first fibre ratio which is tested a reduction of 17% can be found in peak strength compared to plain concrete. This reduction in strength is most likely due to the large surface area of the fibres. Although this large surface area can be beneficial in conventional fibre reinforced concrete due to the large frictional capacity, it seems that a negative influence is obtained for this reinforcing method. Due to the overlap of the fibres the bond between the layers is reduced, while a steel to steel surface shows no bond strength. The influence on the post-peak behaviour differs from the other two type of fibres, only for a small deflection a post-peak behaviour is obtained. For a larger deflection the load bearing capacity of the samples drops to zero. This is due to the pull-out mechanism of this fibre type, which is fibre rupture instead of pull-out. Due to the small thickness of the fibres the tensile capacity is reached before the fibre is pulled out due to friction. Once the fibre ruptures it is no longer able to bear any tensile forces, thus the load capacity is gone for small crack openings. This also leads to a lower fracture energy compared to the other two types of fibres, while the post-peak behaviour is much shorter.

Table 6.5: *Average results; Fibraflex FF/20L6, ratio A = 0.0259 kg/m²*

Maximum stress (N/mm²)	Deflection at max stress (mm)	Fracture energy (N/mm)
3.05 (0.15)	0.20 (0.02)	0.576 (0.070)

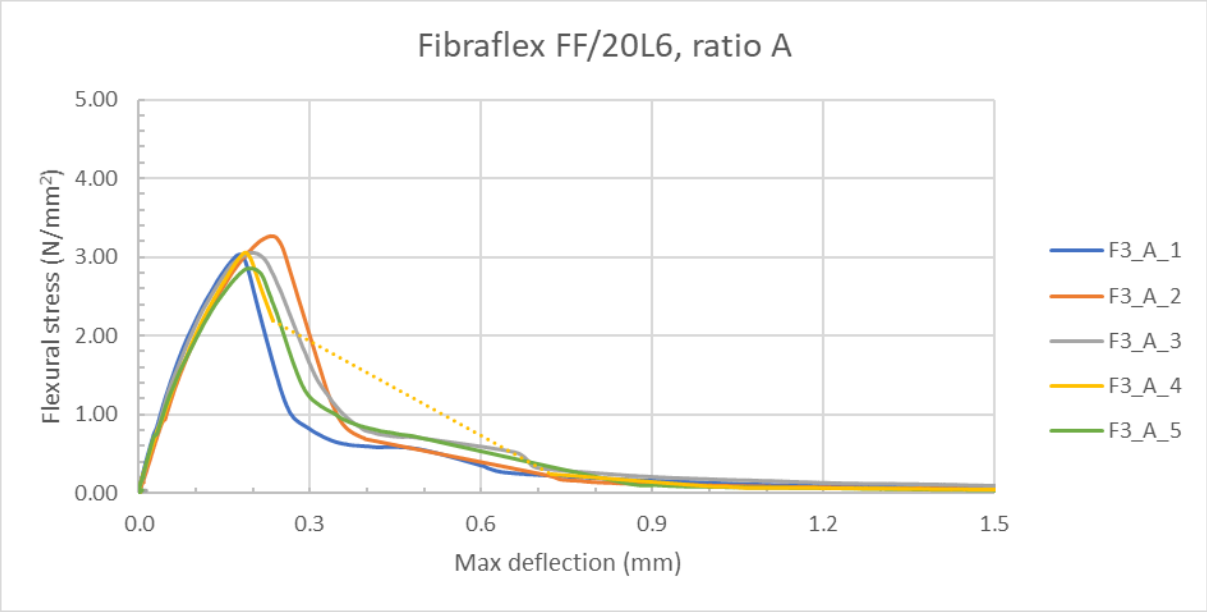

Figure 6.6: *Stress-Deflection diagram, Fibraflex FF/20L6, ratio A = 0.0259 kg/m².*

Also for this type of fibre a larger fibre ratio is tested to analyse the influence of the amount of fibres, the results are shown in figure 6.7 and table 6.6. It seems that a larger amount of fibres further reduces the peak strength of the samples, a reduction of 22% compared to plain concrete can be found for the average maximum stress. The overlap of fibres, resulting in a reduction in bond strength, seem to be the cause for this reduction in maximum stress. The samples in this test series also show a little influence on the post-peak behaviour for small deflections. This is due to the failure mechanism of the fibres which is fibre rupture. Once the crack opening starts to grow the fibres rupture, resulting in a loss of its load bearing capacity. The fracture energy is slightly increased for a larger amount of fibres, presumably more fibres are bridging the crack resulting in a slightly higher pull-out capacity. However the fracture energy is still significantly lower compared to the other fibre types which are tested.

Table 6.6: *Average results; Fibraflex FF/20L6, ratio B = 0.0388 kg/m²*

Maximum stress (N/mm²)	Deflection at max stress (mm)	Fracture energy (N/mm)
2.89 (0.26)	0.21 (0.02)	0.618 (0.106)

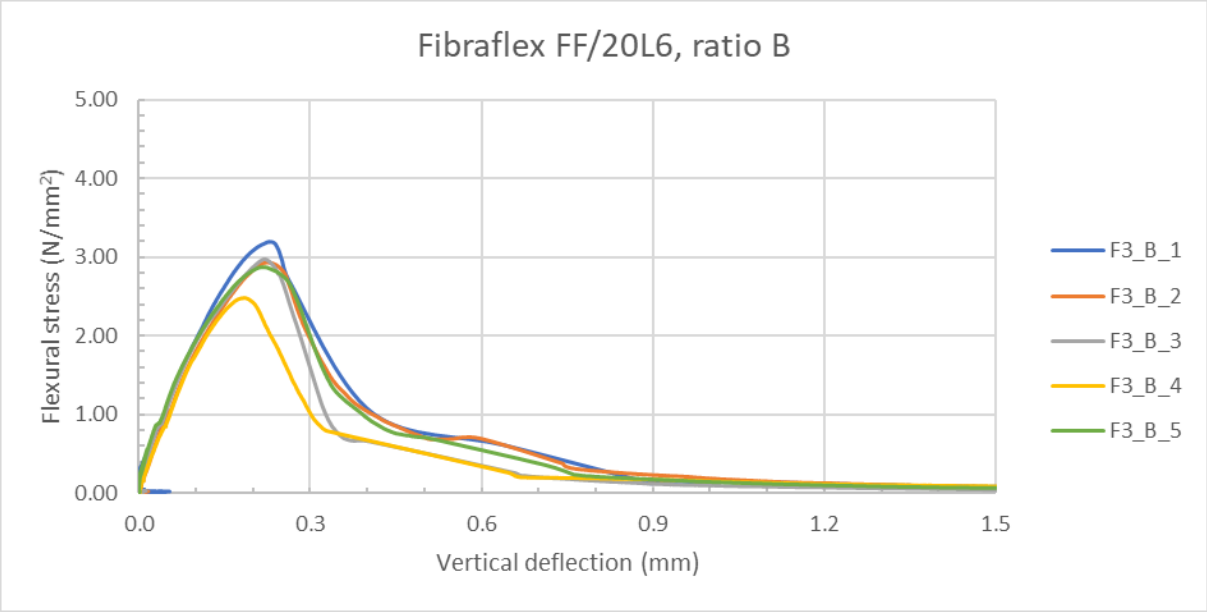

Figure 6.7: *Stress-Deflection diagram, Fibraflex FF/20L6, ratio B = 0.0388 kg/m².*

During the manufacturing process the influence of the printing parameters on the possibility to add fibres in between the layers of printed concrete already became visible. It could be seen that in several cases the fibres were dragged along the printing path, thus influencing the fibre distribution on top of the layers. The same conclusion follows from the experimental results, while the actual fibres per cross section do not comply with the fibre ratios obtained from the image analysis from chapter 3.2.4 (table 3.4). In the worst cases scenario, all fibres got dragged along resulting in plain concrete samples without any fibres in the cross section. To further analyse the compatibility with different reinforcing methods, the printing parameters are of importance. While in theory the fibre distribution should be unaltered, it followed during the manufacturing process that the nozzle offset was too small. This phenomenon is also dependent on the fibre type which is used, while for the Cem-FIL and Dramix type of fibres a larger influence could be observed. The diameter of these two types of fibres is larger compared to the Fibraflex type of fibres, thus making them more susceptible to being dragged along the printing path.

Although the fibre distribution is altered for all samples, some conclusions can be drawn regarding the obtained results. For the Cem-FIL and Dramix fibres no significant influence can be observed for the peak strength, the maximum values are within the same range as plain concrete as can be seen in figure 6.8. However for the tested samples the crack is only bridged by 1 or 2 fibres. It is assumed that the impact on the crack propagation for such low number of fibres per cross section is negligible. In the case for the Fibraflex fibres the printing process could be of influence, due to the scraping of fibres. Although the phenomenon of scraping was less visible for these flat fibres, it is likely that the distribution is also altered for this fibre type. If a large amount of overlap between the fibres is obtained, the bond strength between the layers is significantly reduced. Hereby the connection between the layers is decreased, resulting in small beams working independently. A small influence on the post-peak behaviour could be observed, in most of these cases 1 or 2 fibres were bridging the crack. This can also be seen from the required fracture energy which is needed to break the samples (figure 6.8). It is expected that if the amount of fibres per cross section can be increased, the influence

on the post-peak behaviour can be improved. This holds mostly for the Cem-FIL and Dramix type of fibre, the Fibraflex fibres showed only little improvement for the post-peak behaviour due is pull-out mechanism, fibre rupture. Although an improvement could be observed for a larger fibre ratio, it is expected that the impact on the post-peak behaviour is limited compared to the other type of fibres. However it should be noted that it is difficult to determine the amount of Fibraflex fibres crossing the crack. Due to their small cross section and rupture mechanism it is difficult to perceive the exact number of fibres crossing the crack.

Table 6.7: *Average results*

Fibre type	Ratio (kg/m^2)		Max stress (N/mm^2)		Deflection at max stress (mm)		Fracture energy (N/mm)	
Plain concrete	A	-	3.68	(0.59)	0.18	(0.03)	-	(-)
Cem-FIL Minibars 24mm	A	0.0632	4.00	(0.57)	0.20	(0.01)	1.000	(-)
Dramix 3D RC-4530-BL	A	0.1559	3.83	(0.25)	0.21	(0.02)	1.011	(-)
	B	0.2227	3.57	(0.32)	0.21	(0.01)	1.144	(0.101)
Fibraflex FF/20L6	A	0.0259	3.05	(0.15)	0.20	(0.02)	0.576	(0.070)
	B	0.0388	2.89	(0.26)	0.21	(0.02)	0.618	(0.106)

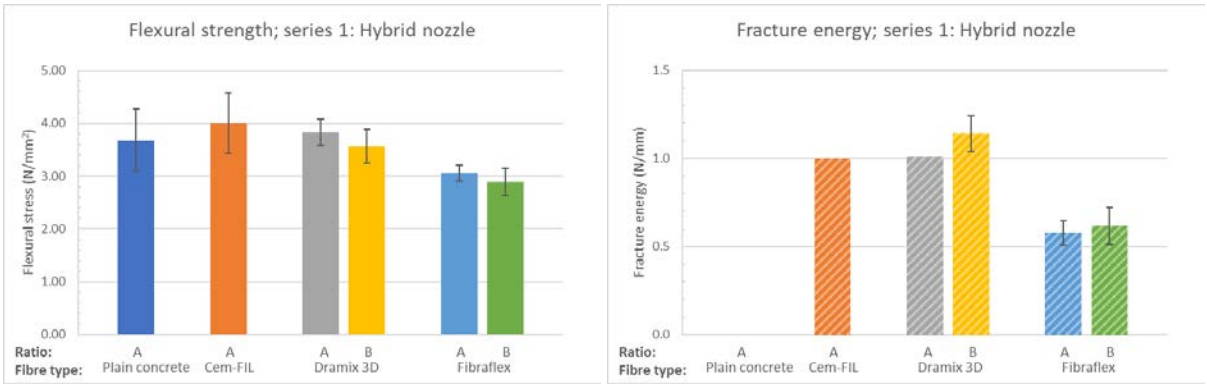

Figure 6.8: *Average flexural strength (Left); Average fracture energy (Right).*

6.2 DOWN-FLOW NOZZLE

The second test series is printed with a different nozzle type, the down-flow nozzle. Also for this test series a four-point bending test is performed to define the influence of the fibres on the flexural capacity. Little to no influence on the fibre distribution could be observed from the study on the printing parameters for this type of nozzle. In this paragraph the average results for the different test series are analysed, the results from all tests can be found in appendix F. Also in this case the dimensions of all samples are measured to translate the obtained load to a flexural stress and are listed in appendix E.

Again for this test series several plain concrete samples are printed to obtain a reference value. Although the print settings are kept the same compared to the previous series, the environmental conditions on the different printing dates can be of influence. By observing the graphs in figure 6.9, the brittle behaviour of concrete can be observed. An increase of flexural strength is obtained until the crack is initiated, after this point all three samples broke into two parts. The overall material behaviour of the three samples is similar, however a relatively large standard deviation can be found. This is most likely due to the small sample size while no direct relation could be observed from a visual analysis.

Table 6.8: *Average results; plain concrete, ratio A*

Maximum stress (N/mm^2)	Deflection at max stress (mm)	Fracture energy (N/mm)
2.41 (0.34)	0.15 (0.02)	- (-)

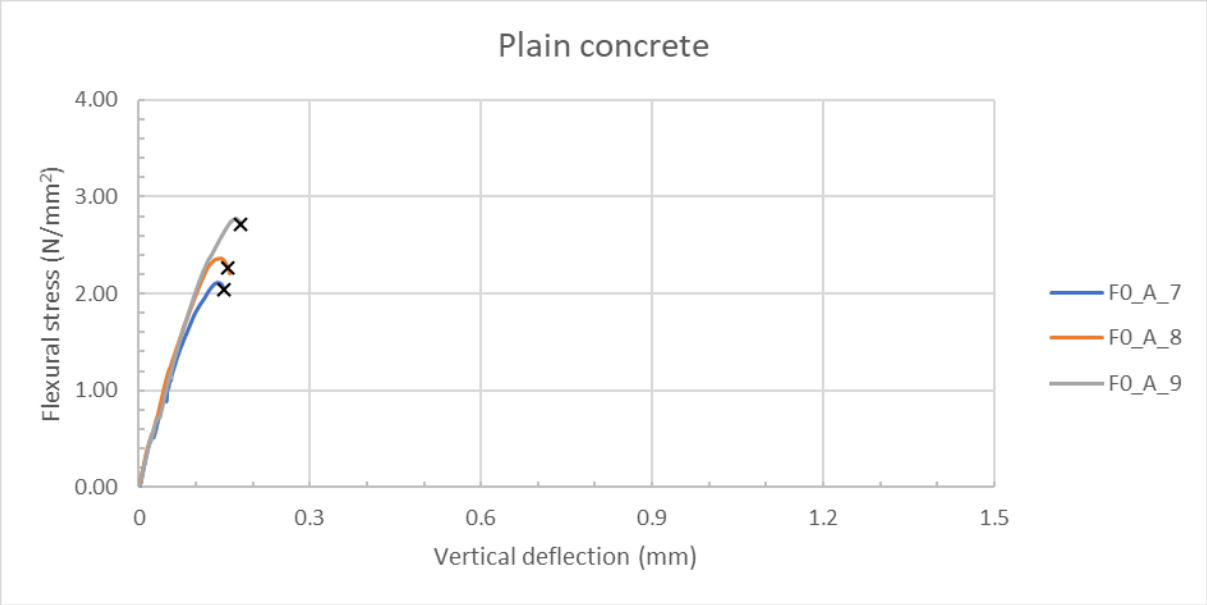

Figure 6.9: *Stress-Deflection diagram, Plain concrete.*

First the Cem-FIL Minibars 24mm are added to the print, the results are shown in figure 6.10 and table 6.9. The overall material behaviour of the five samples is similar, for the post-peak behaviour it seems that the scatter between the samples increases slightly. By comparing the peak strength to plain concrete an increase can be found of approximately 30%. Thus it seems that the glass fibres improve the cracking strength of the material. This might be due to the interfacial bond between the glass fibre and the concrete matrix. Also for the post-peak behaviour an improvement can be found in comparison to plain concrete. Where for plain concrete no strength was obtained after crack initiation, a post-peak strength in between 0 N/mm^2 and 1 N/mm^2 can be observed. The level of the post-peak behaviour is dependent on the amount of fibres per crack surface. By observing the samples it can be said that those samples with more fibres resulted in a higher post-peak behaviour. Which makes sense while the amount of energy which is needed is related to the amount of fibres which are pulled out.

Table 6.9: *Average results; Cem-FIL Minibars 24mm, ratio B = 0.0842 kg/m²*

Maximum stress (N/mm²)	Deflection at max stress (mm)	Fracture energy (N/mm)
3.12 (0.33)	0.16 (0.01)	0.774 (0.275)

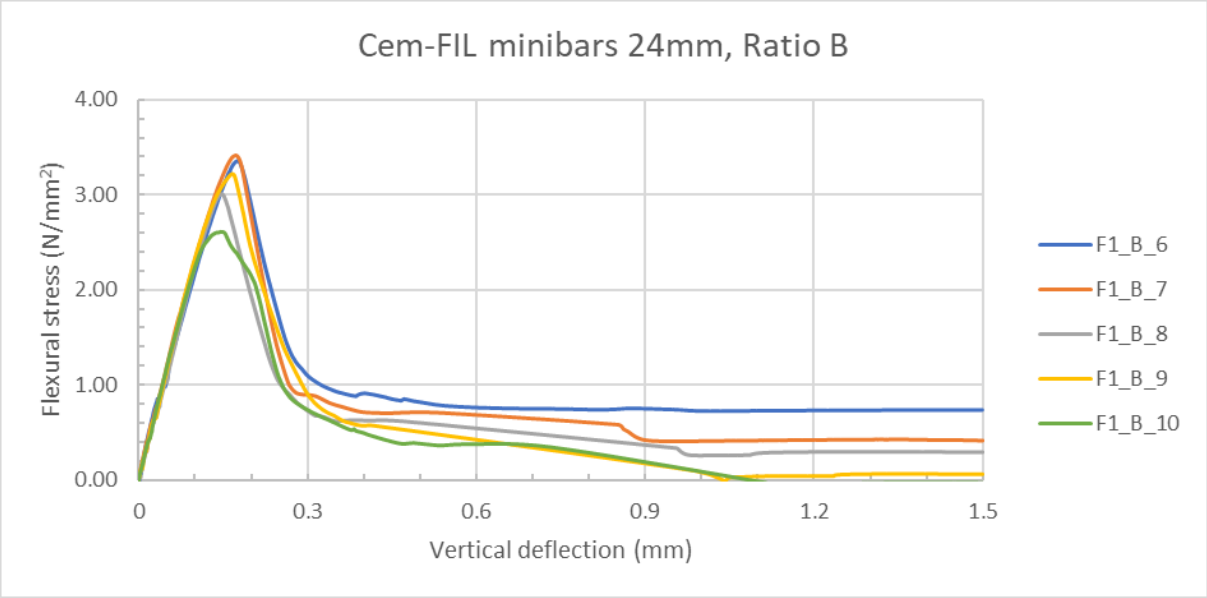

Figure 6.10: *Stress-Deflection diagram, Cem-FIL Minibars 24mm, ratio B = 0.0842 kg/m².*

In this test series also a high-strength steel deformed fibre is tested, the Dramix 3D type of fibre, the results can be found in figure 6.11 and table 6.10. For these samples no significant influence on the peak strength can be observed compared to the plain concrete samples. All results are within the same range compared to the plain concrete samples shown at the start of this paragraph. This is as expected while the main pull-out mechanism of these fibres is mechanical anchorage, and for this phenomenon to occur the crack opening needs to increase. This straightening of the hooked-ends did however have a significant influence on the post-peak behaviour of the samples. After the crack has initiated the load still drops, however the fracture energy is doubled compared to the tested glass fibres. Also for these type of fibres it can be observed that the amount of fibres is directly related to the level of post-peak behaviour. For an increasing number of fibres a larger post-peak behaviour is obtained. This high variation in number of fibres per cross section results in a relatively large standard deviation of fracture energy. Although the graph is only shown until a vertical deflection of 1.5 millimetre, it followed from the raw data that the post-peak behaviour remained constant for quite a while. This shows that the influence of the embedment length is inferior to the mechanical anchorage as could be concluded from the literature research. There is chosen to show the post-peak behaviour up to 1.5 millimetre of vertical deflection, in general a stable trend is observed for the behaviour.

Table 6.10: *Average results; Dramix 3D RC-4530-BL, ratio B = 0.2227 kg/m²*

Maximum stress (N/mm²)	Deflection at max stress (mm)	Fracture energy (N/mm)
2.56 (0.22)	0.19 (0.03)	1.430 (0.536)

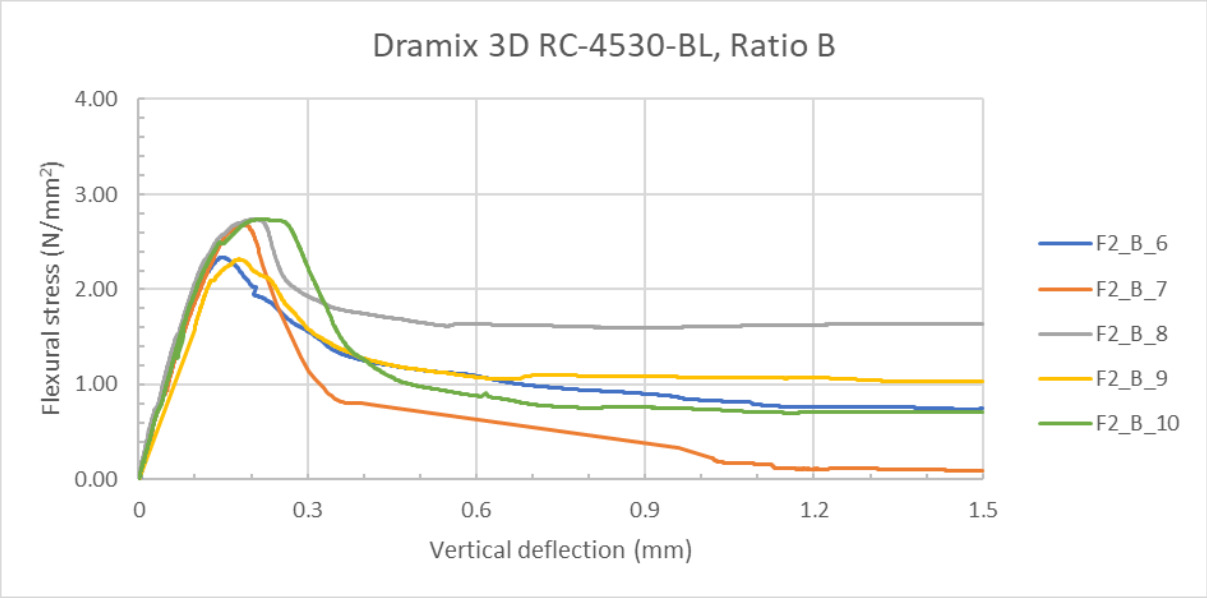

Figure 6.11: *Stress-Deflection diagram, Dramix 3D RC-4530-BL, ratio B = 0.2227 kg/m².*

The last fibre type which is tested in this test series is the Fibraflex FF/20L6, a high-strength steel flat fibre. Also for this type of fibre no significant influence can be observed regarding the peak strength, the average value is in the same range as for plain concrete. For small deflections a post-peak behaviour is obtained, however the load drops to zero for larger deflections. This is due to the pull-out mechanism, which is fibre rupture. Due to the large surface area the friction of this type of fibre is large, the tensile capacity will be reached first. Once the fibre breaks, it is unable to bridge the crack and thus unable to bear any loads. For one sample fibre rupture occurred already in an early stage, F3_B_8, resulting in fracture of the sample at approximately 0.4 millimetre of vertical deflection.

Table 6.11: *Average results; Fibraflex FF/20L6, ratio B = 0.0388 kg/m²*

Maximum stress (N/mm²)	Deflection at max stress (mm)	Fracture energy (N/mm)
2.65 (0.20)	0.21 (0.05)	0.746 (0.291)

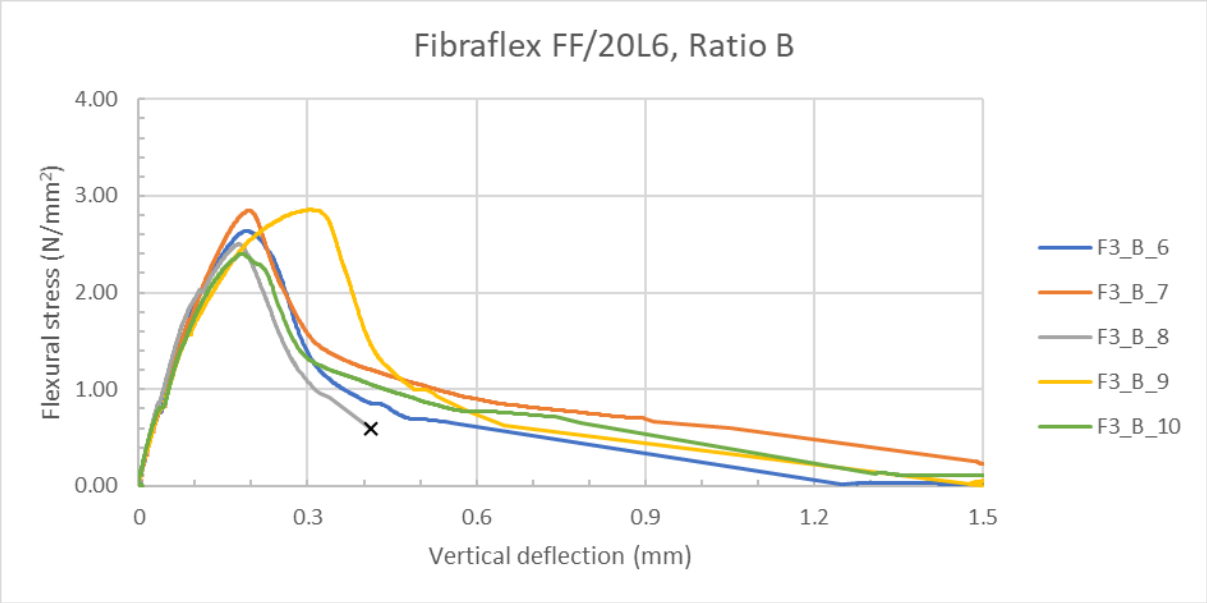

Figure 6.12: *Stress-Deflection diagram, Fibraflex FF/20L6, ratio B = 0.0388 kg/m².*

In summary, it can be concluded that by the addition of fibres in between the layers a post-peak behaviour can be obtained (figure 6.13). For all three tested fibre types crack propagation is obtained due to fibres bridging the crack. The highest fracture energy can be obtained by adding Dramix 3D fibres, which is about double the amount compared to the other two types of fibres. From literature this can be explained by the pull-out mechanism, which is governed by mechanical anchorage for this type of fibre. Also for deflections larger than 1.5 millimetre a stable post-peak behaviour could be observed, which is not the case for the other two type of fibres. Although the fracture energy for the Cem-FIL fibre and Fibraflex fibre are comparable, a difference can be seen in their behaviour. For all samples reinforced with Fibraflex fibres, the post-peak behaviour reduced to zero at a vertical deflection of about 1.5 millimetre. For the Cem-FIL fibre a stable post-peak behaviour could be observed, however this is in a lesser extent compared to the Dramix fibre.

If the peak strength of the samples is compared to plain concrete it seems that by the addition of the Cem-FIL fibre a slight increase in strength can be obtained (figure 6.13). On average a peak strength which is 30% higher is obtained from the experimental tests. This could be due to the bond between the fibre and the concrete matrix. For the other two type of fibres no significant influence on the peak strength can be observed, these fibres are only activated after the crack has initiated. By analysing the crack surface it also seems that, for the glass fibres, more fibres result in a higher peak strength.

Table 6.12: *Average results*

Fibre type	Ratio		Max stress		Deflection at max stress		Fracture energy	
		(kg/m²)		(N/mm²)		(mm)		(N/mm)
Plain concrete	A	-	2.41	(0.34)	0.15	(0.02)	-	(-)
Cem-FIL Minibars 24mm	B	0.0842	3.12	(0.33)	0.16	(0.01)	0.774	(0.275)
Dramix 3D RC-4530-BL	B	0.2227	2.56	(0.22)	0.19	(0.03)	1.430	(0.536)
Fibraflex FF/20L6	B	0.0388	2.65	(0.20)	0.21	(0.05)	0.746	(0.291)

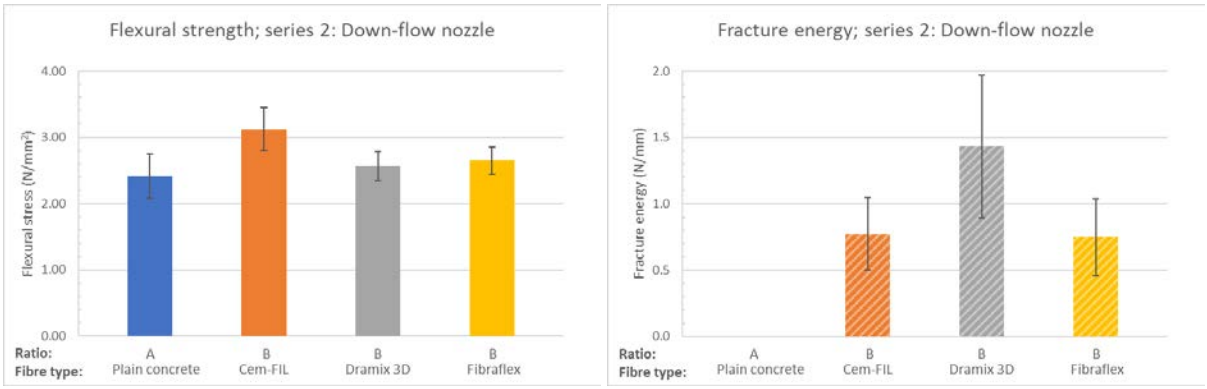

Figure 6.13: *Average flexural strength (Left); Average fracture energy (Right).*

Also for this test series a comparison is made between the real number of fibres per cross section and the predictions based on the image analysis from chapter 3.2.4. From a visual analysis it can be concluded that these numbers do not correspond, a lower quantity of fibres is observed in the crack surfaces. A more elaborate analysis about the comparison of number of fibres is given in paragraph 6.4.

6.3 PROOF OF CONCEPT

For the previous two test series, the fibres are still sprinkled by hand in order to maintain control over the amount of fibres. In practice this process needs to be automated, a device is developed which is already described in chapter 3. At the start of this research a test program is designed to improve the output of the blower. Although further research is still needed to improve this device, a test series is conducted to analyse the applicability of the blower. From the test program two types of fibres were selected, Cem-FIL Minibars 24mm and Fibraflex FF/20L6. These two fibre types are also tested with a four-point bending test to analyse their influence on the structural capacity. The samples are printed with a down-flow nozzle, while it followed from the printing parameters that this type of nozzle has the least influence on the fibre distribution.

The first fibre type which is tested is the Cem-FIL Minibars 24mm, for the settings of the blower a power of 300 Watts is taken. Based on the workability test of the blower described in chapter 3.2, this gives approximately a coverage percentage of 30% without taking fibre overlap into account. Although this number might reduce the bond between the layers, there is chosen to test with these settings while the standard deviation increases for a lower blower setting. The results of the bending test can be found in figure 6.15, the average results are given in table 6.13. During manufacturing of the samples the distribution of fibres over the length of the print path seemed constant (figure 6.14). This also followed from the experimental results, while the scatter of the three samples is low. For the peak strength a relative standard deviation of less than 2% is obtained. However it should be noted that only three samples are tested, a larger test series needs to be conducted to further analyse the consistency of the blower. Although this test series is treated independently, it is printed at the same date as the test series which is printed with the down-flow nozzle and where the fibres are sprinkled by hand (previous paragraph). Therefore those tested plain concrete samples can also be used as a reference to analyse the influence of the addition of fibres for this test series. An increase in peak strength can be observed of about 25% compared to plain concrete. It is assumed that this increase in flexural strength is due to the bond between the fibre and the concrete matrix. The addition of the glass fibres also has a positive influence on the post-peak behaviour. Instead of a brittle behaviour, a post-peak strength of approximately 0.5 N/mm^2 is obtained.

Figure 6.14: *Fibre distribution over print path (Left); Fibre distribution in cross section (Right).*

Table 6.13: *Average results; Cem-FIL Minibars 24mm, ratio C = 0.2485 kg/m² (Blower)*

Maximum stress (N/mm²)	Deflection at max stress (mm)	Fracture energy (N/mm)
3.02 (0.05)	0.17 (0.02)	0.931 (0.226)

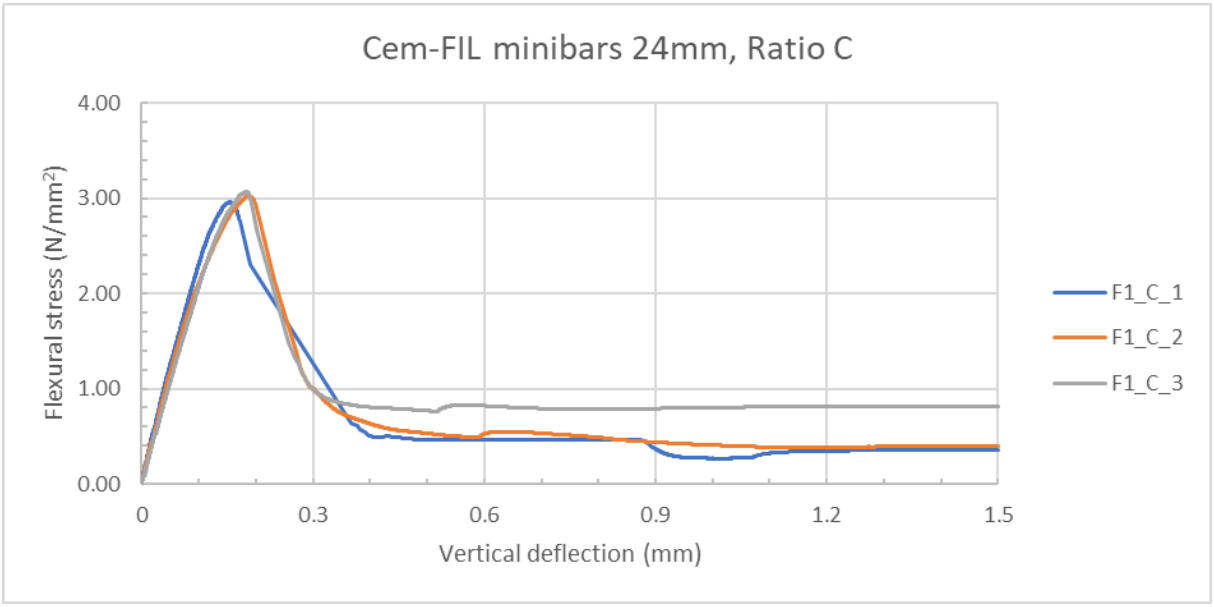

Figure 6.15: *Stress-Deflection diagram, Cem-FIL Minibars 24mm, ratio C = 0.2485 kg/m².*

The second fibre type which is tested is the Fibraflex FF/20L6, also for this test the power of the blower is set at 300 Watts. Although it followed from the workability test in chapter 3.2 that for these settings the coverage percentage is significantly out of range, there is chosen to use the same settings as is done for the Cem-FIL fibre type. By further reducing the blower settings it is observed that the scatter of the blower output increases, resulting in inconsistent results. Further control needs to be gained over this output consistency to test the blower for lower settings. From this print series no samples could be made, while a failure of bond occurred for the samples. The amount of fibres in between the layers was such that separation of the concrete filaments occurred as can be seen in figure 6.17. By removing the samples from the print table several cracks occurred parallel to the print direction. This is most likely caused due to overlap of the fibres. A steel to steel connection has little to no bond strength, thus reducing the total bond strength between the layers significantly. If too much overlap occurs a laminated beam is created which easily fails in the direction perpendicular to the print direction. From this it can be concluded that there is an upper limit with regard to the quantity of fibres which can be added in between the layers. The influence on the bond behaviour might be taken as a parameter to define the amount of fibres which can be added while this bond should not be reduced.

Figure 6.17: *Failure in interface due to excessive overlap of fibres.*

As mentioned, the test series printed with the down-flow nozzle (paragraph 6.2) is printed on the same date as the current test series. Therefore it is possible to compare the samples which are made with the blower with the samples for which the fibres are sprinkled by hand. The average results of the tests are shown in table 6.14 and figure 6.18. Although the fibre ratio is significantly larger compared to fibre ratio B, the peak strength of the samples is in the same range. The addition of a larger quantity of fibres does not show a direct influence on the maximum flexural strength. The number of fibres in the cross section might give an explanation for this. While the ratio increases significantly, this is not the case for the fibres bridging the crack. From a visual analysis only about 1.5 times as many fibres are found in the crack surface. This increase in fibres does lead to an improvement in fracture energy. If more fibres are bridging the crack, a larger fracture energy is required to bend the samples. This should make sense while more fibres need to be pulled out of the concrete, a larger sample size needs to be tested to further analyse this statement.

Table 6.14: *Average results*

Fibre type	**Ratio** (kg/m²)		**Max stress** (N/mm²)		**Deflection at max stress** (mm)		**Fracture energy** (N/mm)	
Plain concrete	A	-	2.41	(0.34)	0.15	(0.02)	-	(-)
Cem-FIL Minibars 24mm	B	0.0842	3.12	(0.33)	0.16	(0.01)	0.774	(0.275)
	C	0.2485	3.02	(0.05)	0.17	(0.02)	0.931	(0.226)

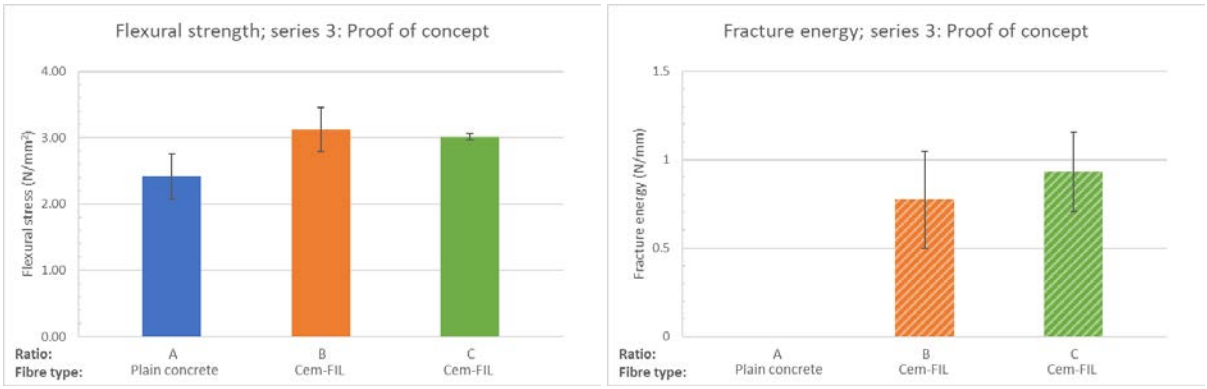

Figure 6.18: *Average flexural strength (Left); Average fracture energy (Right).*

In the first two print series the fibres are sprinkled by hand on top of the printed layers, the selected fibre ratios are analysed using image analysis. The fibre ratio obtained by using the blower can also be processed by using image analysis, this in order to be able to compare the ratio between the different test series. In chapter 3.2.4 the procedure of the image analysis is already described, the results are given in table 6.15 till 6.17. The two selected ratios for the Cem-FIL Minibars from chapter 3.3 are also given in these tables. Only the output for the Cem-FIL Minibars is analysed, because no test samples

could be made from the trial print performed with the Fibraflex fibres. The first thing which can be noticed is that the output by the blower is much larger compared to the first two selected ratios. The coverage of ratio C obtained by the blower is twice as much compared to the other two selected ratios. This can also be seen from the fibres per cross section, also this number increases. The relative standard deviation on the other side also increases for the ratio obtained by the blower, however it should be noted that only three images are used for the analysis. The fibre orientation for all three ratios is comparable, this shows that also the output of the blower gives a random orientation for the fibres. The number of fibres on the concrete layers can also be obtained from the image analysis. This number is multiplied by the weight of a single fibre to obtain the weight per area and a volume percentage. The selected area has a dimension of 50x200 millimetre, the volume is calculated by taking a layer height of 10 millimetre. The values can be found in table 6.18, here also the other two ratios selected at the start of this research can be found for comparison.

Table 6.15: *Fibre coverage*

Fibre type	Ratio	Average coverage (%)	Standard deviation (%)
Cem-FIL Minibars 24mm	A	6.6	(0.5)
	B	8.1	(0.3)
	C	17.9	(2.5)

Table 6.16: *Fibres per cross section*

Fibre type	Ratio	No. fibres per cross section	Standard deviation (No.)
Cem-FIL Minibars 24mm	A	3	(1.20)
	B	4	(1.35)
	C	6	(3.71)

Table 6.17: *Fibre orientation*

Fibre type	Ratio	0°-15°	15°-30°	30°-60°	60°-90°
Cem-FIL Minibars 24mm	A	5.8 (2.3)	5.8 (1.5)	11.3 (3.2)	7.1 (2.1)
	B	9.6 (2.7)	7.3 (1.9)	13.5 (3.3)	10.5 (2.7)
	C	22.7 (6.4)	22.3 (4.7)	37.0 (5.2)	36.0 (6.2)

Table 6.18: *Fibre ratio*

Fibre type	Fibre ratio	Weight per area (kg/m^2)	Volume percentage (%)
Cem-FIL Minibars 24mm	A	0.0632	0.32
	B	0.0842	0.42
	C	0.2485	1.24

6.4 COMPARISON WITH ANALYTICAL MODEL

In chapter 4 an analytical model is proposed with which a prediction is given for the stress-deflection diagram. The results of the experimental program can be compared with this outcome, to do so the number of fibres per cracked section are counted for all samples (table 6.19). A more elaborate distinction of the number of fibres per interface is given in appendix D. What immediately can be observed is that the number of fibres per interface is significantly lower compared to the predictions made by the image analysis in chapter 3.2.4 (see also table 6.20). This can also be seen from the experimental results, the post-peak behaviour of all performed test is less compared to the predictions made by the analytical model. For the test series printed with the hybrid nozzle the fibre distribution

was affected by the printing process, this was not observed for the two print series printed with a down-flow nozzle. However, still a significant deviation is observed regarding the number of fibres compared with the prediction from the image analysis. By evaluating the image analysis it might be possible that an incorrect prediction is given. The number of fibres per cross section are calculated at a fixed position of the image, hereby an average number is obtained. However if a sample is subjected to a bending test, the crack occurs at the weakest section which in general has the lowest number of fibres. The section with the least number of fibres is not necessarily on the same location as the selected section from the image analysis. Hence it is plausible that with the method used in the image analysis an incorrect value is obtained. Further analysis of the printing process and image analysis technique is required to improve the accuracy of the prediction of fibres per cross section.

Table 6.19: *Manual count of fibres in cracked section per interface (Average number)*

Fibre type	Ratio	Interface			
		1	2	3	4
Cem-FIL Minibars 24mm	B	1.2	0.8	0.2	0.6
	C	2.0	2.5	1.8	2.8
Dramix 3D RC-4530-BL	B	1.4	1.6	1.4	0.8
Fibraflex FF/20L6	B	1.2	1.2	1.0	1.4

Table 6.20: *Fibres per cross section based on results image analysis*

Fibre type	Ratio	No. fibres per cross section	Standard deviation (No.)
Cem-FIL Minibars 24mm	B	4	(1.35)
	C	6	(3.71)
Dramix 3D RC-4530-BL	B	4	(1.03)
Fibraflex FF/20L6	B	5	(1.31)

By implementing the real number of fibres obtained by manually counting these, the analytical model explained in chapter 4 can be validated. In this model several assumptions are made, especially with regard to the pull-out behaviour of the tested fibres. In equation 4.7a and 4.7b a distribution factor (α) is implemented in the formula to take the random fibre dispersion into account. Also the exact value for the bond stress (τ_{av}) is unknown, therefore literature is used to find a value for this bond stress. By counting the number of fibres per cross section, it is observed that there is a large scatter in embedment length and orientation between the fibres. In the used equations, the contribution per fibre is based on a fixed value for the embedment length and orientation which is multiplied by the number of fibres. As this is not the case, there is chosen to adjust the value for α to take this random distribution into account. It is noted that also the value for the bond stress is not exact at this moment due to missing experimental data. However it is chosen to keep this value fixed at this moment, any discrepancies from the real bond stress are corrected by the distribution factor.

For all performed tests a comparison is made with the analytical model, by a trial and error analysis the correct value of α is determined for each curve. In figure 6.19 some examples are given in which the experimental and analytical curves are compared. To determine the correct value of the distribution factor a comparison is made at multiple vertical deflection points. From this it can be observed that by adjusting the distribution factor, a good agreement can be found between the analytical and experimental curves. In appendix D all experimental curves are compared with the analytical model.

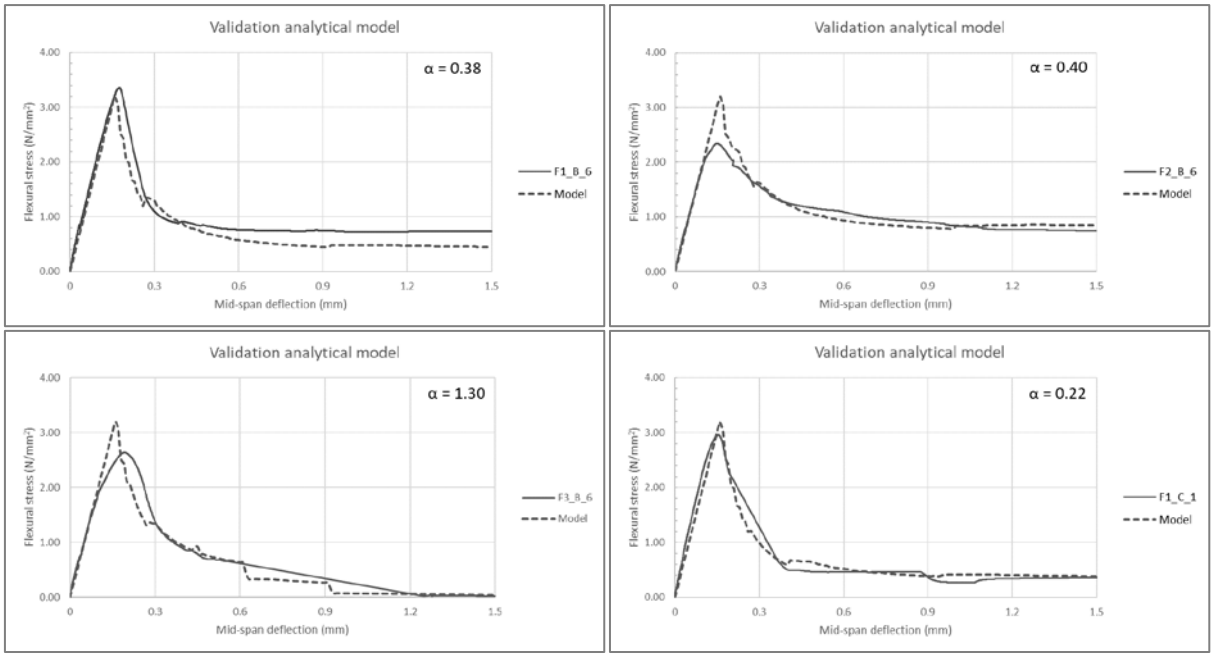

Figure 6.19: *Validation of analytical model; Cem-FIL Minibars 24mm, ratio: 0.0842 kg/m^2, fibres sprinkled by hand (Top left); Dramix 3D RC-4530-BL, ratio: 0.2227 kg/m^2, fibres sprinkled by hand (Top right); Fibraflex FF/20L6, ratio: 0.0388 kg/m^2, fibres sprinkled by hand (Bottom left); Cem-FIL Minibars 24mm, ratio: 0.2485 kg/m^2, fibres sprinkled by blower (Bottom right).*

Although in general a good comparison is obtained between the curves from the derived value for the distribution factor, in some cases a large scatter is obtained between the different experimental curves. This is most likely due to the importance of the embedment length and orientation of the fibres. For the cases in which the Cem-FIL Minibars and Fibraflex fibre types are used, a large deviation is observed of approximately 50% between the different distribution factors. In contrast to this large difference for these two fibre types, a constant factor is obtained for the samples reinforced with the Dramix 3D fibres. From this fibre type a distribution factor of 0.40 is obtained, which showed good agreement for all experimental curves. A relative standard deviation of about 5% is obtained for the distribution factor. For this fibre type mechanical anchorage is the most important pull-out mechanism, which seems less dependent on embedment length and orientation. It is assumed that this is the reason for the constant value of the distribution factor.

For almost all curves a good agreement between the analytical and experimental curves is found for the post-peak behaviour. However if the peak strength of the samples is observed a deviation can be observed in some cases. This is most likely due to the implemented concrete strength, which is based on a prescribed number from the manufacturing company. Also for the tested plain concrete samples a lower flexural tensile strength is obtained, extensive material testing is required to define the correct concrete strength values. Hereby it should be possible to give a more accurate prediction with the analytical model.

6.4.1 Application analytical model

For all three fibre types which are implemented in the model it can be seen that a larger number of fibres results in an increase of post-peak behaviour. This should also be the case while the contribution of the single fibres is added for each interface. Until now all results, analytical and experimental, are based on certain given limitations by the concrete printing process. From the proof of concept print described in paragraph 6.3 it is observed that there is an upper limit with regard to the number of fibres which can be added in between the layers of concrete. An extensive amount of Fibraflex fibres

resulted in fracture between the interface due to a reduction of bond strength between the layers. By reducing the layer height, the number of interfaces increases for the same element dimensions. For now it is assumed that a standard layer height is 12 millimetre, however by reducing this height it is possible to obtain a more homogeneous fibre distribution over the height. Hereby it is possible to apply the same number of fibres over a larger number of interfaces.

Instead of performing an extensive experimental program, which is time consuming and expensive, the analytical model can be used to give a first prediction of the influence on the structural behaviour. In figure 6.20 an example is given for which the Cem-FIL Minibars are taken as a reference. The same four-point bending test is observed which is used in the experimental program, for the distribution factor a value of 0.38 is applied. The solid line (Cem-FIL h12 n4) represents a four-point bending test with a layer height of 12 millimetre and 4 fibres per interface. By reducing the layer height a more homogeneous fibre distribution is obtained over the height. If a sample is printed with a layer height of 6 millimetre, it is possible to reduce the number of fibres to 2 in order to obtain the same number of fibres per cross-section. This is shown by the dotted line in figure 6.20 (Cem-FIL h6 n2). A more or less similar behaviour is obtained which should be the case while the same number of fibres is used. What can be seen is that the sudden drop due to the activation of the fibres becomes less visible. It is also possible to apply the same number of fibres per interface and to reduce the height of the printed layer. Hereby the number of fibres per cross-section increase, which should result in an increase in post-peak behaviour. An example is shown in figure 6.20, in which the dashed line (Cem-FIL h6 n4) represents a sample with a layer height of 6 millimetre and 4 fibres per interface. From this it seems that it should even be possible to obtain a plastic post-peak behaviour by using this reinforcing method. In figure 6.21 a sketch is given which a visualisation of the examples is shown. Although these results seem promising, care should be taken while further validation is required to define whether the analytical model also yields reliable results for different test series.

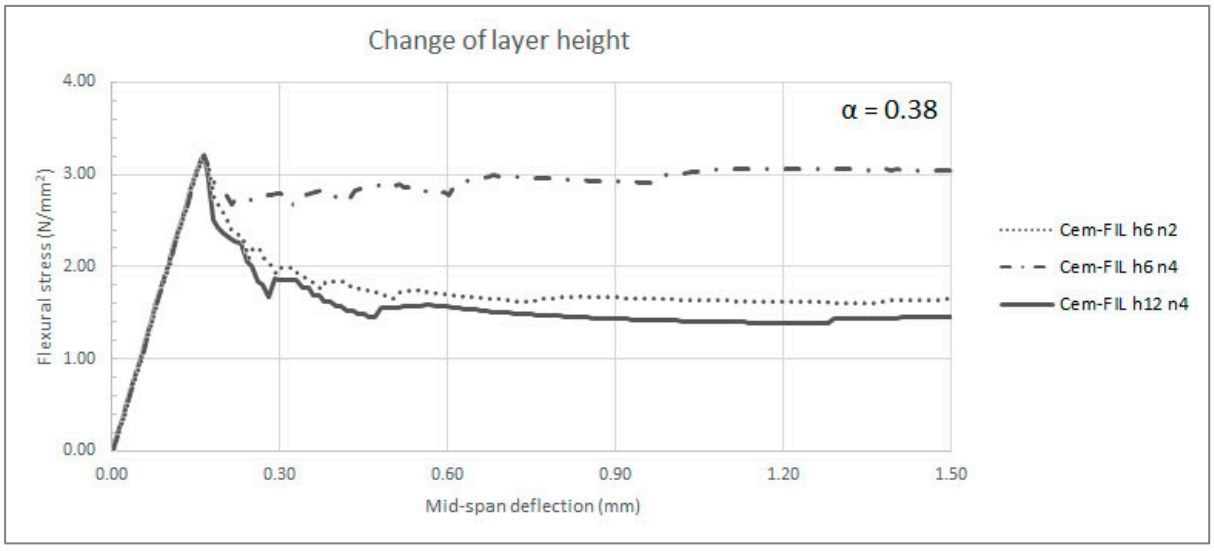

Figure 6.20: *Prediction stress-deflection diagram of four-point bending test using analytical model change of layer height and/or number of fibres per interface.*

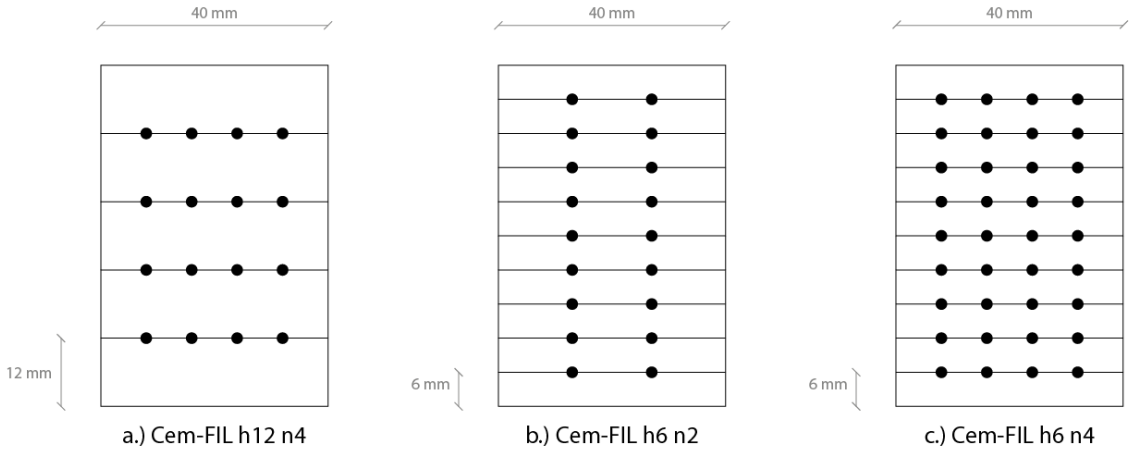

Figure 6.21: *Sketch of given examples; a.) Layer height: 12mm, number of fibres per interface: 4; b.) Layer height: 6mm, number of fibres per interface: 2; Layer height: 6mm, number of fibres per interface: 4.*

6.5 Discussion

In all performed test series a strain softening behaviour is obtained, after crack initiation a load drop can be observed. In most cases a post-peak behaviour is obtained, for which the amount of fracture energy is directly related to the quantity of fibres crossing the crack. If the different test series are observed a similar overall material behaviour can be seen for the tested fibre types. The first type of fibre which is observed is an alkali-resistant glass fibre with a thermoset resin coating, the Cem-FIL Minibars 24mm. For this type of fibre it seemed that an increase of about 25% to 30% in flexural strength can be obtained compared to plain concrete. This is most likely due to the bond between the fibre and the concrete matrix, however further research is required to confirm this assertion. When the high-strength steel Dramix 3D fibre with hooked-ends are observed no direct influence on the flexural capacity is observed. This is because the pull-out mechanism is activated after the first crack has occurred. Although the peak strength is not affected by this type of fibre, an impact on the fracture energy could be observed. This is due to the deformation of the hooked-end, which requires much more energy compared to adhesion and friction which also followed from literature. A stable post-peak behaviour is obtained for almost all samples reinforced with this type of fibre, also for a relatively large vertical deflection in contrast to the other tested fibre types. Finally another high-strength steel fibre is tested, Fibraflex FF/20L6 which has a flat shape. For this type of fibre a different pull-out mechanism is obtained compared to the other two type of fibres, fibre rupture. This only resulted in a post-peak behaviour for small deflection, for larger deflections all fibres ruptured. Also for this type of fibre no significant influence is observed regarding the flexural strength, only for the test series which are printed with the hybrid nozzle. Here a reduction is obtained for the flexural strength which is most likely caused by an excessive overlap of the fibres. This overlap is caused by the printing process, while no significant influence is observed for the second test series. While it is noted that the overall material of the different test series is similar, a significant difference in peak strength is observed between the plain concrete samples. It is assumed that this is due to the environmental conditions during hardening of the samples. This might be possible while the fibre reinforced concrete samples printed with a down-flow nozzle also show a lower peak strength compared to the plain concrete samples printed with a hybrid nozzle. However if the samples are compared to the plain reference samples in the same print series a comparable effect is observed.

If the analytical model is compared to the experimental curves it can be concluded that overall a good agreement is found. By adjusting the distribution factor for the fibres and counting the number of fibres per cross section a good prediction can be given of the material behaviour. In the model internal

equilibrium is calculated to define the load bearing capacity for a given deflection. In here the contribution of the fibres is taken into account based on the pull-out behaviour of the fibres. By determining the correct values of the distribution factor, it is concluded that the embedment length and orientation of the fibres is of great importance for the value. In case of the straight Cem-FIL Minibars and flat Fibraflex fibre types a large variety of values for the distribution factor is obtained. In the case of the Dramix 3D fibre this dependency on the embedment length and orientation is less significant. This is most likely due to the pull-out mechanism which is mechanical anchorage. Here the energy required for the deformation of the hook is much more of importance compared to the adhesion and friction, therefore the embedment length and inclination angle are of less importance. Until now several assumptions are done for the analytical model, like the pull-out behaviour of the fibres, the strength of the concrete and the rigid body motion of the beam. Further analysis is required to obtain more accurate input which should result in a better prediction for the structural behaviour.

For the analysed reinforcing method it can be stated that the tested fibre types are not (yet) applicable as primary reinforcement. In all cases a strain softening behaviour is obtained which will lead to structurally unsafe structures. Further research should be conducted to aim for a strain hardening material. With the analytical model an example is given in which a plastic material behaviour can be obtained by implementing Cem-FIL fibres. However, it should be noted that these results are not validated, experimental research is required in order to define whether the model yields reliable results. However it is also possible to combine the fibres in between the layers with a different reinforcing method. Hereby the fibres in between the layers can act as a secondary reinforcement to improve the structures. An example might be a combination with conventional rebar or cable reinforcement. By the addition of fibres crack propagation is obtained which will increase the compressive zone of the element, hereby the dimensions of the element can be reduced. It is also possible to combine the fibre reinforcement in between the layers with fibres mixed inside the concrete. Hereby a hybrid fibre reinforced element can be created in which the fibres are distributed over the entire element, different types of fibres can be used which are suitable to the desired structural behaviour.

7. CONCLUSIONS & RECOMMENDATIONS

In general this research can be divided into two parts, on the one hand the development of a transportation/depositing device to place fibre reinforcement in between the layers of printed concrete. On the other hand an analysis is made about the influence on the structural capacity of fibre reinforcement in printed concrete. In this final chapter the conclusions are formulated, based on the findings of the development of the device and on the analytical and experimental research which is conducted. The research towards printed fibre reinforced concrete is still at an early stage, therefore recommendations are given in the end to improve and continue this research topic.

7.1 CONCLUSION

Based on the workability test of the blower a device is developed which is capable of depositing fibre reinforcement in between the layers of the printed concrete layers. Multiple adaptions are made during this research to improve the output of this device. At this stage of the research it seems that the fibre blower is compatible with the 3D concrete printing process adopted at the Eindhoven University of Technology. A first test series is printed for which a flow of fibres is obtained without clogging of the device. However further improvement of this device is still necessary, while the standard deviation of the output is relatively large. Until now a flexible hose is used to guide the fibres from the storage bucket towards the robot arm. By using a flexible hose the movement of the robot arm leads to stretching and bending of the hose. This leads to a difference in internal resistance inside the hose, thus it is likely that a varying output is obtained based on the location on the print table. Another important parameter which is related to the output of the blower is the input of the device. At this moment the input hose is fixed in the vibration bucket and a funnel is created in order to collect all the fibres. With the current settings of the blower all the fibres are rapidly sucked into the blower chamber, no matter how many fibres are accumulated. This does not lead to a gradual input and thus it can be expected that the consistency of the output is also affected. For practical applications a good control over the fibre ratio is required, this to ensure the structural safety of the printed element.

Also the printing process is observed during the workability tests of the blower, hereby it can be concluded that several parameters can affect the possibility to deposit fibres in between the concrete layers. The most important parameter is the offset with regard to the previous printed layer. To improve the structural capacity the fibres are placed in between these layers, this fibre distribution should not be affected by the printing process. By using a down-flow nozzle no direct influence on the distribution could be observed during printing, however a hybrid nozzle can have a negative impact. The printed layer height is in theory equal for each print session, however this can differ in reality. The output of the pump can be different due to several factors, for example starting offset and printing speed. Also the rotor-stator pump can be of influence, tightening of this pump is done by hand which can result in a slightly different concrete flow. The relation between the real layer height and the programmed input for the layer offset can result in a tolerance of the print offset.

Besides the possibility to add fibres to the concrete printing process, the influence on the structural capacity is observed. To do so an analytical model is proposed with which a stress-deflection diagram can be obtained by calculating internal equilibrium. In here the contribution of the fibres is based on the pull-out behaviour of a single fibre. By implementing a distribution factor a good agreement is found with the experimental curves, hereby it seems that a good prediction can be given of the structural behaviour. Especially in the case for the Dramix 3D fibres for which mechanical anchorage is the main pull-out mechanism. Hereby the embedment length and fibre orientation are of less

importance, resulting in a more constant value for the distribution factor. In the case of the Cem-FIL Minibars and the Fibraflex fibres a larger scatter is observed for the distribution factor.

Finally the structural capacity of the printed fibre reinforced concrete is observed experimentally, the goal of adding fibre reinforcement is to improve the tensile capacity and/or ductility of the material. To obtain an understanding about the influence of fibre reinforcement for printed concrete, three different fibre types are tested. From the workability test of the blower and a literature study, three fibre types are selected with varying material and geometries. For all performed test a strain softening behaviour is obtained, however a post-peak behaviour is obtained. If the different test series are observed per fibre type, it can be concluded that the overall material behaviour is comparable. The impact on the structural capacity is dependent on the number of fibres per cross section, which makes sense while a sample with a larger number of fibres requires more energy to deform. Based on the different fibre types which are tested it can be concluded that the geometry and material have a direct influence on the structural behaviour, which also follows from the conducted literature research. The moment at which the fibres are activated determines its influence on the flexural capacity. The bond between the alkali resistant glass fibres and the concrete matrix results in propagation of the crack, this is not observed for the other two high-strength steel fibres. Hereby it seems that the fibre reinforced material is able to bear a slightly larger load compared to the plain concrete. The geometry is of importance if a post-peak behaviour is required, the hooked-end fibres showed a stable post-peak behaviour. The fracture energy for the other two straight fibres is much lower compared to the deformed fibre.

7.2 Recommendations

During this research the depositing method of the fibres is analysed and the fibre blower is developed. The blower seems to be compatible with the 3D concrete printing process, however it still needs to be improved in order to be applicable in practice. The main challenges are related to the constant output of the device, which is affected by parameters such as the position of the hose and the input of the fibres. Due to the movement of the robot arm, a flexible hose is required to comply with this motion. At this point a fully flexible hose is used, however it seems that stretching and bending of the hose affects the output. By partly changing the flexible hose to rigid pipes, the resistance inside the hose becomes more constant. If these rigid pipes are able to rotate and move, they can be connected by flexible parts to retain the possibility to follow the movement of the robot arm. Another option to improve to consistency of the output is by obtaining a gradual input of fibres. Until now the fibres are deposited by hand in the storage bucket, however this quantity varies over time. By using a system like a loss-in weight dispenser or a bulk fibre dispenser as used in the conventional concrete industry a more gradual input might be obtained. Until now the settings of the blower are used to control the fibre ratio, however in general an increase in standard deviation is obtained for lower settings. By controlling the quantity of fibres at the storage bucket, the settings of the blower are of less importance. These might even be increased which results in an increase in consistency and a smaller possibility of fibre clogging.

Besides the consistency of the output it is also needed to analyse the distribution of fibres over the print table. The current device is applicable for experimental research, however due to the spread of the fibres about half of the quantity of fibres is lost. Also the sides of the printed element are fully covered with fibres which might be undesirable for practical purposes. For future research it might be valuable to reduce or even avoid this spread of fibres. Multiple options can be used to avoid this spread over the print table, a worthwhile option might be to separate the wind flow from the fibres. Hereby

the fibres are dropped vertically due to gravity, this principle can be achieved by using a cyclone separator.

For the analytical model several assumptions are made, to improve the accuracy of the prediction these input values need to be known. The contribution of the fibres is based on the pull-out behaviour of a single fibre, however an assumption is made for this relation. By performing pull-out tests on single fibres a pull-out curve can be obtained which might be implemented into the model. The same holds for the material properties of the concrete, which are until now based on values from NEN-EN 1992. What also followed from the analytical model is that it might be interesting to improve the fibre dispersion over the height of the element. A reason might be that the quantity of fibres which is deposited on top of the layers can result in a reduction of bond strength between the interfaces. In chapter 6.4.1 an example is given in which the layer height is reduced, hereby a finer fibre distribution is obtained over the height of an element. This simple example showed that it might be possible to obtain a plastic post-peak behaviour by improving the dimensions with which are printed and optimising the fibre distribution.

As mentioned, the bond between the layers might be reduced due to an excessive use of fibres. If too much overlap occurs between the fibres a reduction in bond strength is obtained as shown for the Fibraflex fibres in chapter 6.3, which should be avoided. In the current research no experimental tests are performed too analyse the influence on the interface. However the influence on the interface is a topic which might be interesting for future research. By performing an experimental or numerical study an upper boundary with respect to fibre quantity might be found.

If the fibre dispersion is observed it can be noted that this is unknown for conventional casted fibre reinforced concrete, by 3D concrete printing this dispersion over the element can be controlled. Image analysis is used for this research to select different fibre ratios which are tested experimentally. However it can also be used in practice as a quality control tool, by checking the fibre distribution over the entire element the structural safety of this element can be guaranteed. Additionally, the image analysis can be used as a tool to predict the strength of an element. By giving a prediction of the number of fibres per cross section input is generated for the analytical model. This can be used to give a first approximation of the structural behaviour of the printed element.

With the current concrete mixture and the tested fibres it is not likely that a strain hardening material can be obtained, therefore it cannot be used in a structural element yet. However it can be interesting to combine the fibres in between the layers with different reinforcing methods. For instance by also mixing fibres inside the printed concrete, hereby a hybrid fibre reinforced concrete can be obtained. By mixing microfibres inside the concrete the tensile capacity might be increased and the macrofibres in between the layers can improve the ductility. Another reinforcing method applied at the Eindhoven University of Technology is the use of cable reinforcement. This has similarities with fibre reinforced concrete in combination with rebar. By using fibres the crack width is reduced and the compressive height of the element is increased, hereby the height of an element might be reduced.

BIBLIOGRAPHY

REFERENCES

[1] Abrishambaf, A., Barros, J., Cunha, V., & Frazão, C. (2017). Time dependent behaviour of fibre pull-out in self-compacting concrete. *Cement and Concrete Composites, 77*, 14-28.

[2] ACI Committee 544 (2002). *Report on fiber reinforced concrete*. ACI Report 544.1R-96.

[3] ACI Committee 544 (2008). *Guide for specifying, proportioning, and production of fiber-reinforced concrete.* ACI Report 544.3R-08.

[4] Afroughsabet, V., Biolzi, L., & Ozbakkaloglu, T. (2016). High-performance fiber-reinforced concrete: a review. *Journal of Materials Science, 51*(14), 6517-6551.

[5] Austin, S., Robins, P., & Pan, Y. (1995). Tensile bond testing of concrete repairs. *Materials and Structures, 28*, 249-259.

[6] Babafemi, A., & Boshoff, W. (2017). Pull-out response of macro synthetic fibre from concrete matrix: Effect of loading rate and embedment length. *Construction and Building Materials, 135*(15), 590-599.

[7] Bos, F., Wolfs, R., Ahmed, Z., & Salet, T. (2016). Additive manufacturing of concrete in construction: potentials and challenges of 3D concrete printing. *Virtual and Physical Prototyping, 11*(3), 209-225.

[8] Breitenbücher, R., Meschke, G., Song, F., & Zhan, Y. (2014). Experimental, analytical and numerical analysis of the pullout behaviour of steel fibres considering different fibre types, inclinations and concrete strengths. *Structural concrete, 15*, 126-135.

[9] Carpinteri, A., Fortese, G., Ronchei, C., Scorza, D., & Vantadori, S. (2017). Mode I fracture toughness of fibre reinforced concrete. *Theoretical and applied fracture mechanics, 91*, 66-75.

[10] Conforti, A., Minelli, F., Plizzari, G., & Tiberti, G. (2017). Comparing test methods for the mechanical characterization of fiber reinforced concrete. *Structural Concrete, 19*(3), 656-669.

[11] Conforti, A., Zerbino, R., & Plizzari, G. (2018). Influence of steel, glass and polymer fibers on the cracking behavior of reinforced concrete beams under flexure. *Structural Concrete, 20*(1), 133-143.

[12] Cotterel, B., & Mai, Y. (1996). *Fracture mechanics of cementitious materials.* Glasgow, Scotland: Blackie Academic & Professional.

[13] Cunha, V., Barros, J., & Sena-Cruz, J. (2010). *Pullout behaviour of hooked-end steel fibres in self-compacting concrete*. Retrieved from https://www.researchgate.net/publication/266042589_Pullout_behavior_of_hooked-end_steel_fibres_in_self-compacting_concrete

[14] Demeke, A., & Tegos, I. (1994). Steel fiber reinforced concrete in biaxial tension-compression conditions. *ACI Materials Journal, 91*(5), 579-584.

[15] Dezaire, S. (2018). *Study on bond capacity of 3D printed concrete with cable reinforcement* (Master thesis). Retrieved from https://research.tue.nl/en/studentTheses/study-on-bond-capacity-of-3d-printed-concrete-with-cable-reinforc

[16] di Prisco, M., Colombo, M., & Dozio, D. (2013). Fibre-reinforced concrete in fib Model Code 2010: principles, models and test validation. *Structural Concrete, 14*, 342-361.

[17] Doomen, C. (2016). *The effect of layered manufacturing on the strength properties of printable concrete* (Master thesis). Retrieved from https://research.tue.nl/en/studentTheses/the-effect-of-layered-manufacturing-on-the-strength-properties-of

[18] Elfgren, L. (1989). *Fracture mechanics of concrete structures; From theory to applications*. London, England: Chapman and Hall Ltd.

[19] Goris, D. (2018). *Traditional reinforcement in 3D concrete printed structures* (Master thesis). Retrieved from https://research.tue.nl/en/studentTheses/traditional-reinforcement-in-3d-concrete-printed-structures

[20] Hambach, M., & Volkmer, D. (2017). Properties of 3D-printed fiber-reinforced Portland cement paste. *Cement and Concrete Composites, 79*, 62-70.

[21] Hao, Y., & Hao, H. (2017). Pull-out behaviour of spiral-shaped steel fibres from normal-strength concrete matrix. *Construction and Building materials, 139*, 34-44.

[22] Jutinov, E. (2017). *3D concrete printing: research and development of a structural reinforcement system for 3D printing with concrete* (Master thesis). Retrieved from https://research.tue.nl/en/studentTheses/3d-concrete-printing

[23] Le, T., Austin, S., Lim, S., Buswell, R., Gibb, A., & Thorpe, T. (2012). Mix design and fresh properties for high-performance printing concrete. *Materials and Structures, 45*(8), 1221-1232.

[24] Le, T., Austin, S., Lim, S., Buswell, R., Gibb, A., & Thorpe, T. (2012). Hardened properties of high-performance printing concrete. *Cement and Concrete Research, 42*(3), 558-566.

[25] Li, V., Wang, Y., & Backer, S. (1990). Effect of inclining angle, bundling and surface treatment on synthetic fibre pull-out from a cement matrix. *Composites, 21*(2), 132-140.

[26] Löfgren, I. (2005). *Fibre-reinforced concrete for industrial construction – a fracture mechanics approach to material testing and structural analysis* (Doctoral dissertation). Retrieved from https://core.ac.uk/download/pdf/70560762.pdf

[27] Marković, I. (2006). *High-performance hybrid-fibre concrete: Development and utilisation* (Doctoral dissertation). Retrieved from http://resolver.tudelft.nl/uuid:44ed51cd-fc27-4353-ab81-cf8348f52443

[28] Meng, Y., Chengkui, H., & Jizhong, W. (2006). Characteristics of stress-strain curve of high-strength steel fiber reinforced concrete under uniaxial tension. *Journal of Wuhan University of Technology – Materials Science edition, 21*(3), 132-137.

[29] Nematollahi, B., Xia, M., Sanjayan, J., & Vijay, P. (2018). Effect of type of fiber on inter-layer bond and flexural strengths of extrusion-based 3D printed geopolymer. *Materials Science Forum, 939*, 155-162.

[30] Nieuwoudt, P., & Boshoff, W. (2017). Time-dependent pull-out behaviour of hooked-end steel fibres in concrete. *Cement and Concrete Composites, 79*, 133-147.

[31] Ogura, H., Nerella, V., & Mechtcherine, V. (2018). Developing and testing of strain-hardening cement-based composites (SHCC) in the context of 3D-printing. *Materials, 11*(8), 1375-1392.

[32] Olesen, J. (2001). Fictitious crack propagation in fiber-reinforced concrete beams. *Journal of Engineering Mechanics, 127*(3), 272-280.

[33] Paegle, I., Minelli, F., & Fischer, G. (2016). Cracking and load-deformation behaviour of fiber reinforced concrete: Influence of testing method. *Cement and Concrete Composites, 73*, 147-163.

[34] Pakravan, H., Latifi, M., & Jamshidi, M. (2017). Hybrid short fiber reinforcement system in concrete: a review. *Construction and Building Materials, 142*, 280-294.

[35] Panda, B., Paul, S., & Tan, M. (2017). Anisotropic mechanical performance of 3D printed fiber reinforced sustainable construction material. *Materials Letters 209*, 146-149.

[36] Panda, B., Paul, S., Mohamed, N., Tay, Y., & Tan, M. (2018). Measurement of tensile bond strength of 3D printed geopolymer mortar. *Measurement, 113*, 108-116.

[37] Prudencio Jr., L., Austin, S., Jones, P., Armenlin, H., & Robins, P. (2006). Prediction of steel fibre reinforced concrete under flexure from an inferred fibre pull-out response. *Materials and Structures, 39,* 601-610.

[38] Raedts, W. (2017). *Investigation into properties of fibre reinforced concrete in extrusion based adaptive manufacturing* (Master thesis). Retrieved from https://research.tue.nl/en/studentTheses/investigation-into-properties-of-fibre-reinforced-concrete-in-ext

[39] Robins, P., Austin, S., & Jones, P. (2002). Pull-out behaviour of hooked steel fibres. *Materials and Structures, 35*(7), 434-442.

[40] Salet, T., Ahmed, Z., Bos, F., & Laagland, H. (2018). Design of a 3D printed concrete bridge by testing. *Virtual and Physical Prototyping, 13*(3), 222-236.

[41] Scheffler, C., Zhandarov, S., & Mäder, E. (2017). Alkali resistant glass fiber reinforced concrete: Pull-out investigation of interphase behavior under quasi-static and high rate loading. *Cement and Concrete Composites, 84,* 19-27.

[42] Simões, T., Costa, H., Dias-da-costa, D., & Júlio, E. (2017). Influence of fibres on the mechanical behaviour of fibre reinforced concrete matrixes. *Construction and Building Materials, 137*, 548-556.

[43] Slager, G. (2017). *Influence of the interface between layers on the tensile properties of 3D printed concrete* (Master thesis). Retrieved from https://research.tue.nl/en/studentTheses/influence-of-the-interface-between-layers-on-the-tensile-properti

[44] Soetens, T., Van Gysel, A., Matthys, S., & Taerwe, L. (2013). A semi-analytical model to predict the pull-out behaviour of inclined hooked-end steel fibres. *Construction and Building Materials, 43*, 253-265.

[45] Soetens, T., & Matthys, S. (2014). Different methods to model the post-cracking behaviour of hooked-end steel fibre reinforced concrete. *Construction and Building Materials, 73,* 458-471.

[46] Wolfs, R., Bos, F., & Salet, T. (2019). Hardened properties of 3D printed concrete: The influence of process parameters on interlayer adhesion. *Cement and Concrete research, 119,* 132-140.

[47] Yazici, Ş, Inan, G., & Tabak, V. (2007). Effect of aspect ratio and volume fraction of steel fiber on the mechanical properties of SFRC. *Construction and Building Materials, 21*(6), 1250-1253.

[48] Zhu, H., Yan, M., Wang, P., Li, C., & Cheng, Y. (2015). Mechanical performance of concrete combined with a novel high strength organic fiber. *Construction and Building Materials, 78*, 289-294.

WEBSITES

[49] Incite AB – Fibre dosing, For all types of steel and synthetic fibres. Available online: http://incite.se/images/pdf/generalleafletENG0318_webs.pdf (Accessed online March 2019).

[50] M-tec plastering machine Duo Mix 2000 – Product information. Available online: http://www.kai-trade.com/en/m-tec-machines/m-tec-duo-mix-plastering-machine-2000.html (Accessed online March 2019).

[51] Ramella – Centrifugal fan with double configuration. Available online: http://www.ramella.com/picker.php (Accessed online March 2019).

[52] Sikafiber – Fibre reinforced concrete. Available online: https://sikaconcrete.co.uk/products-systems/fibre-reinforced-concrete/ (Accessed online March 2019).

[53] Uygar endüstri – Fiber dosing systems. Available online: https://www.uygarendustri.com.tr/en/products/fiber-dosing-systems (Accessed online March 2019).

PRODUCT DATA SHEETS

[54] Cem-FIL Minibars 24mm – Owens Corning. *Declaration of performance*. Available online: http://www.ocvreinforcements.com/pdf/library/10021900_Cem_FIL_MiniBars_product_sheet_ww_01_2018_Rev1_EN.pdf (Accessed online April 2019).

[55] Dramix 3D RC-4530-BL – Bekaert. *EC Declaration of performance Dramix® 3D 45/30BL*. Available online: https://www.bekaert.com/en/product-catalog/content/dop/dramix-3d-technical-documents?filterLanguage=en&filterText=4530BL (Accessed online April 2019).

[56] Fibraflex FF/20L6 – Saint-Gobain SEVA. *Declaration of performance.* Available online: http://www.fibraflex.fr/sites/fibraflex.com/files/pdf/qfa-ddp-ffx-en_0.pdf (Accessed online April 2019).

STANDARDS

ASTM C1609/C1609M. *Standard test method for flexural performance of fiber-reinforced concrete (Using beam with third-point loading)*. American standard: ASTM International, West Conshohocken, United States of America.

JCI-SF4. *Method of tests for flexural strength and flexural toughness of fiber reinforced concrete.* Japanese standard: Japan Concrete Institute, Tokyo, Japan.

NEN-EN 12390-2:2009. *Testing hardened concrete – Part 2: Making and curing specimens for strength tests*. European standard: CEN, Brussels, Belgium.

NEN-EN 14651:2005+A1:2007. *Test method for metallic fibered concrete – Measuring the flexural tensile strength (limit or proportionality (LOP), residual)*. European standard: CEN, Brussels, Belgium.

NEN-EN 14889-1:2006. *Fibres for concrete – Part 1: Steel fibres – Definitions, specifications and conformity*. European standard: CEN, Brussels, Belgium.

NEN-EN 14889-2:2018. *Fibres for concrete – Part 2: Polymer fibres – Definitions, specifications and conformity*. European standard: CEN, Brussels, Belgium.

NEN-EN 1992-1-1:2005. *Eurocode 2: Design of concrete structures – Part 1-1: General rules and rules for buildings.* European standard: CEN, Brussels, Belgium.

NEN-EN 206:2014. *Concrete – Specification, performance, production and conformity.* European standard: CEN, Brussels, Belgium.

APPENDICES

APPENDIX A – LITERATURE STUDY

A.1 FIBRE PULL-OUT

To get a first insight in the behaviour of fibre reinforced concrete as a material, the behaviour of a single fibre has to be understood. When the tensile strength of plain concrete is reached, small cracks appear which result in failure of the concrete element. By adding fibres to the concrete the fibres will bridge these cracks, resulting in a post-cracking behaviour. The ductility of the brittle material concrete is increased [8], while the stresses are transferred across the cracks by the fibres. The fibres which cross the cracks will also delay crack propagation [8][21], thus the properties will improve. According to Robins et al. [39] the pull-out behaviour of a steel fibre can be divided into three bond mechanisms:

- Adhesion; Elastic shear bond.
- Friction; Frictional shear bond.
- Mechanical anchorage; Creates localised load transfer points between fibre and matrix.

The first two bond mechanisms are valid for all type of fibres, mechanical anchorage is only present for deformed fibres. In research done by Marković [27] these three bond mechanisms are described. The adhesion is directly related to the strength of the concrete in the interface transition zone, which is the concrete area surrounding the fibre. When the pull-out behaviour of a fibre is observed it can be said that debonding occurs in the interface transition zone and not at the surface of the fibre. Due to the wall effect around the fibre a non-efficient packaging of aggregates leads to a higher porosity in this zone. With a higher porosity the strength and stiffness are reduced compared to the bulk material. The width of this interface transition zone varies from 20-75 µm [13] (see figure A.1).

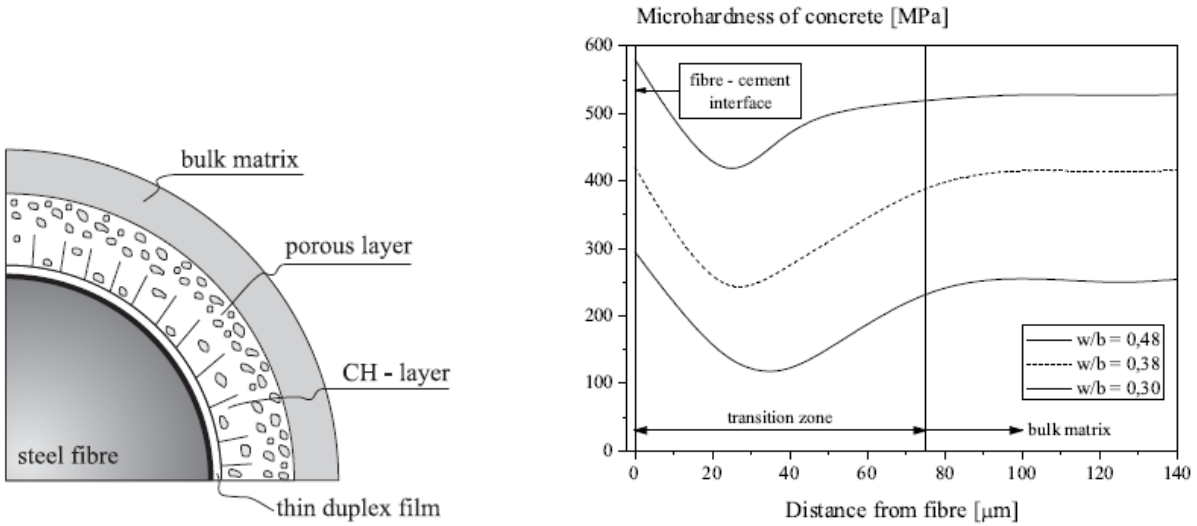

Figure A.1: *Cross section through steel fibre, interface transition zone (Left); Results of microhardness test (Right). (Cunha et al. [13])*

At a certain pull-out force the debonding process of a fibre ends and there is no adhesion anymore. From this point the pull-out resistance is obtained due to the frictional bond of the fibre. In this process frictional stresses occur along the interfacial zone during slip of the fibre. This slip results in abrasion and a compaction process along the interfacial zone. This abrasion leads to a smoother surface and thus less frictional resistance of the matrix surface once a fibre is pulled out further. The shape of a fibre is also important for the pull-out behaviour, when a hooked-end fibre is observed an extra bond mechanism occurs know as mechanical anchorage. Due to the hook a mechanical interlock is created, when a fibre is pulled-out a plastic deformation occurs. This means that a higher amount of energy is

needed, thus higher pull-out force, for the fibre to be pulled-out. Mechanical anchorage occurs after the adhesion mechanism, once the hook is straightened the pull-out behaviour is again governed by friction. In practice it is usually observed that the hooks of a fibre are not completely straightened, which results in larger frictional stresses.

For a straight fibre the pull-out behaviour is only governed by adhesion and friction of the fibre, in figure A.2 this process is shown. Adhesion is the first bond mechanism which occurs, this is shown in step a and b. After fully debonding the final step c occurs, where the pull-out resistance is obtained by friction between the fibre and the concrete matrix. The debonding process for a hooked-end fibre is shown in steps figure A.2. In steps a and b the fibre is debonding, after which step c and d show the deformation of the fibre, mechanical anchorage. After the fibre is straightened the pull-out behaviour is governed by friction, which is similar to the behaviour of a straight fibre [27].

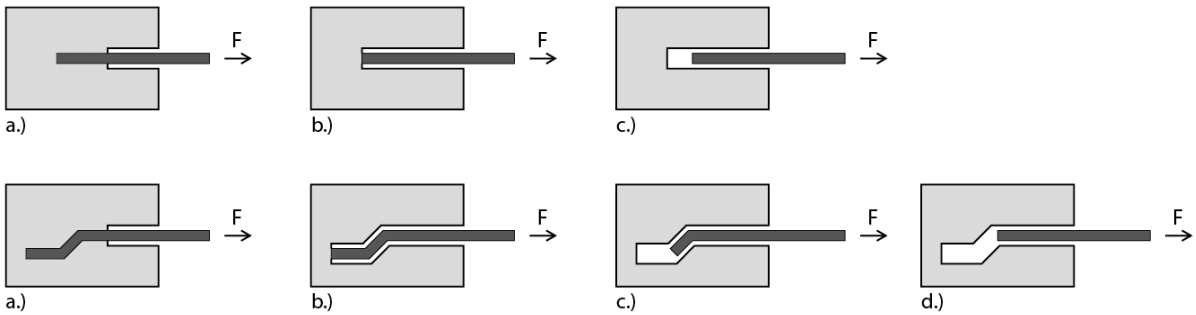

Figure A.2: *Pull-out process of straight fibre (Top); Pull-out process of hooked-end fibre (Bottom). (Marković [27]) (Modified)*

When the load-slip relation of fibre pull-out is observed, these different stages can be described. In figure A.3 a load-slip diagram of a straight fibre and a hook-end fibre are shown [26]. Adhesion of the fibre results in a linear, ascending branch (OA), after which debonding of the fibre starts (AB). After debonding of the fibre, the fibre will be pulled out of the concrete. In this stage the pull-out behaviour is governed by frictional stresses (BF). For a hooked-end fibre, deformation of the hook will occur after the debonding phase. The mechanical anchorage results in an increase for the pull-out force (BC), after this stage plastic deformation of the hook takes place (CE). Once the hook of the fibre is straightened the fibre will act as a straight fibre, from this point frictional stresses will define the pull-out behaviour (EF).

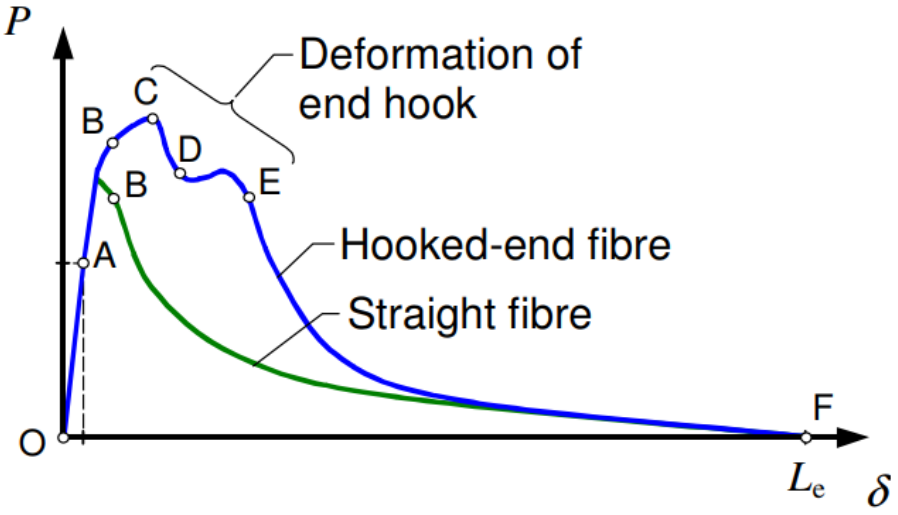

Figure A.3: *Typical fibre pull-out relationship of straight and hooked-end fibre. (Löfgren [26])*

Several parameters have been investigated to determine the influence on the mechanical properties of fibre reinforced concrete. This influence can be divided into two main categories, the properties of the fibre and the properties of the cement matrix. When the properties of the fibres are observed a variation can be made with regard to the shape, fibre orientation, embedment length and material. For the properties of the cement matrix the type of concrete that is used can be of importance. In the following paragraphs these aspects will be analysed to determine their influences on fibre reinforced concrete as a material.

A.1.1 FIBRE SHAPE

Fibres can be found in all kind of shapes, each with a different pull-out behaviour. In research done by Breitenbücher et al. [8] four different types are observed, straight, hooked-end, crimped and twin-coned fibres. Even spiral shaped fibres are observed by Hao et al. [21] whereby the influence on the ductility and energy absorption is observed. Hooked-end fibres are also tested in this research to make a comparison between the influence of the different type of fibres.

When the pull-out behaviour of a straight fibre is observed, this can be divided into three stages: bonded state, debonding stage and pull-out phase. The adhesion to the concrete matrix and the friction between the fibre and the matrix are the two aspects that play a role in the pull-out behaviour for a straight fibre. Once the bond of the fibre is fully gone the maximum pull-out load drops as can be seen from figure A.4. When the deformed fibres are observed the maximum pull-out load still increases after debonding, this is due to the mechanical anchorage. In the experiments executed by Breitenbücher et al. [8] the crimped and twin-coned fibres showed more or less the same behaviour. After the ultimate load was exceeded all fibres ruptured, in contrast to the hooked-end fibres. For these fibres the hooks straightened after which they were being pulled out of the concrete. When the fibres are compared it can be seen that the twin-coned fibres have the highest tensile capacity, however the displacement at which rupture occurs is rather small. Rupture after a small displacement is undesirable, to obtain a better ductility it is more desirable that the fibre is being pulled out of the matrix.

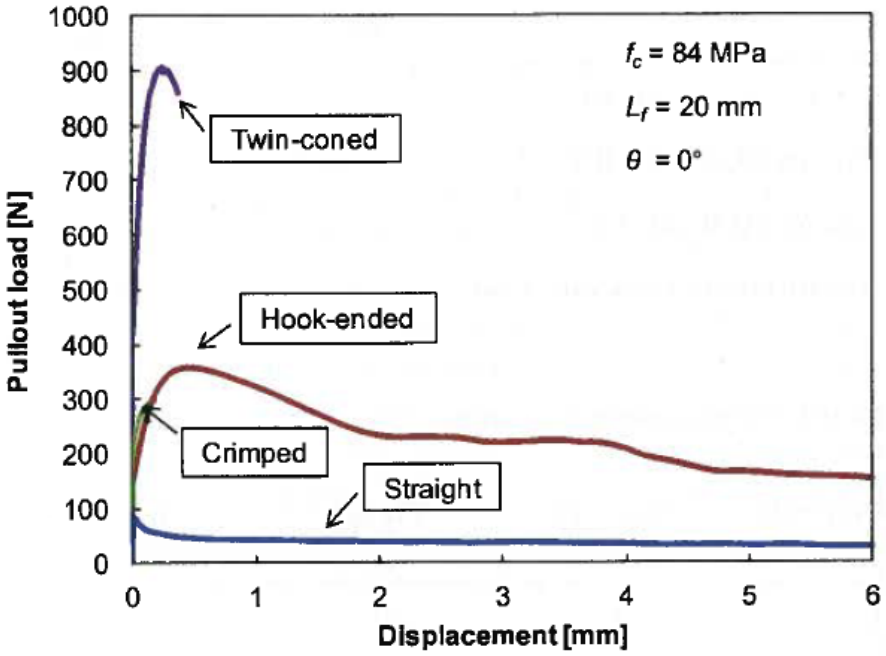

Figure A.4: *Influence of fibre shape on pull-out process. (Breitenbücher et al. [8])*

The spiral shaped fibres, observed by Hao et al. [21], showed an increased frictional force when compared to hooked-end fibres. There are also multiple peaks observed in the force-slip curve, see

figure A.5, which is due to the fibre being pulled out in a circular manner. When the spiral-shaped fibres are compared with the hooked-end fibres it is noted that the spiral-shaped fibres absorb a greater amount of energy, which is beneficial for the ductile behaviour. On the other hand is the initial resistance against the pull-out force lower compared to hooked-end fibres. Thus first there has to be a certain amount of slip before the spiral-shaped fibres have an advantage over hooked-end fibres.

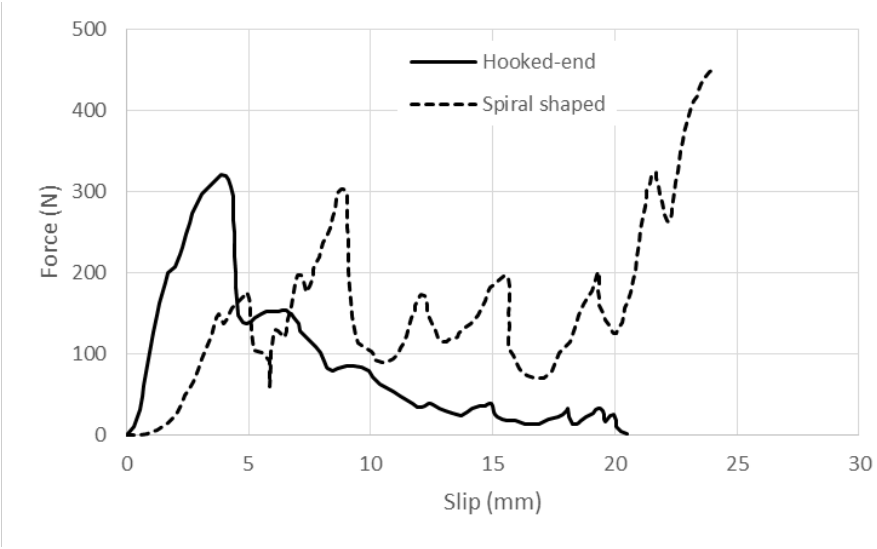

Figure A.5: *Force-slip relation of hooked-end and spiral shaped fibre. (Hao et al. [21]) (Modified)*

A.1.2 FIBRE ORIENTATION

If a fibre has a certain inclination angle the force does not always act in the longitudinal direction of this fibre. When this phenomenon is observed in general there can be said that by an increase in inclination angle, the displacement at the ultimate load increases. The pull-out force exerts an additional stress at the point where the fibre exits the matrix. Due to the stress concentration at this point the concrete starts crushing and spalling off. By increasing the inclination angle the fibres were also more likely to break, from experiments done by Breitenbücher et al. [8] 75% of the test specimen with an inclination angle of 60^{o} resulted in fibre fracture. Also from the results by Robins et al. [39] and Abrishambaf et al. [1] it can be stated that by an increasing inclination angle the percentage of specimen that resulted in fibre fracture increased. Steel fibres with a hooked-end were tested by Soetens et al. [44], the results showed that for an inclination angle between 15^{o} and 40^{o} an optimum in pull-out energy could be found. However only a slight increase in maximum pull-out load was found. Not only steel fibres show an increase in pull-out force, also for synthetic fibres a larger inclination angle results in a higher pull-out force. In experiments done by Li et al. [25] polypropylene and nylon fibres are loaded under different inclination angles. For an inclination angle up to 45^{o} an increase in pull-out force could be found. When the inclination angle further increases the scatter of the results also increases and even lower values of the pull-out force were found. This can be explained by the spalling of the concrete, which results in a shorter embedment length.

Also the long-term behaviour regarding the inclination angle has been observed, Abrishambaf et al. [1] stated that the effect on long-term slip is dependent on the fibre orientation. This difference is explained by the occurring failure modes, fibres with 0^{o} inclination angle were pulled out while fibres under an angle fractured. Fibres with a 0^{o} inclination angle are only loaded by a direct tensile load, which leads to fibre pull-out. For fibres loaded under an angle a normal stress field arises at the fibre exit point, which lead to extra shear friction.

A.1.3 EMBEDMENT LENGTH

The embedment length of a fibre is related to the total length of a fibre, while the maximum embedment length can only be half of the total length. If straight fibres are observed, the embedment length is of importance for the maximum pull-out force [26]. The required pull-out energy, due to debonding and friction, will increase for a longer fibre. This energy keeps increasing up to a certain length for which fibre rupture will occur. If deformed fibres are observed, it can be seen that debonding and friction are often inferior to mechanical anchorage. Therefore the embedment length of deformed fibres is of less importance if the maximum pull-out energy is observed. By testing different embedment lengths it was shown that for a length larger than approximately 15 millimetre no significant difference could be found in the pull-out load [21][39]. This is shown in figure A.6, where the different embedment lengths are shown for an inclination angle of 0^o. Only the fibre with an embedment length of 5 millimetre has a different pull-out behaviour, the other fibres have a more or less identical behaviour. If the total energy of a deformed fibre is observed, it can be noted that the total pull-out energy increases for a larger embedment length. This is due to the fact that once the fibre is deformed, the pull-out energy is governed by friction. For a longer embedment length the pull-out curve will be longer, thus an increase in total pull-out energy is obtained.

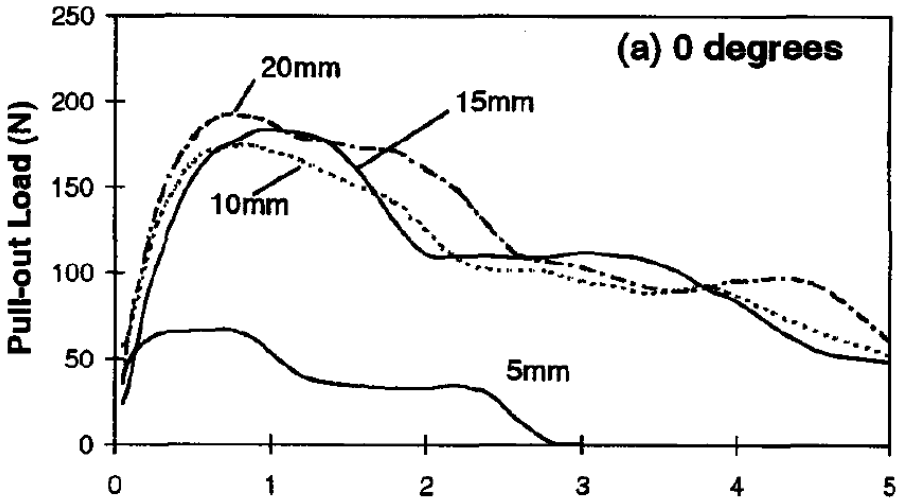

Figure A.6: *Influence of fibre embedment length on pull-out behaviour. (Robins et al. [39])*

A.1.4 FIBRE MATERIAL

The most common material for a fibre is steel, however also different materials can be used in fibre reinforced concrete. As already mentioned in chapter 2.1, the European and American codes make a distinction based on the material of which the fibre is composed. In general a distinction is made between four material classes, steel, glass, synthetic, and natural fibres. The tensile strength and Youngs modulus of steel fibres in general is relatively high compared to the other fibre types. The material of which the fibre is composed can have certain advantages in different environmental conditions. Steel fibres for instance show good performance in high temperature refractory situations. If on the other hand a structure is subjected to a high moisture content, the steel fibres start to corrode. Glass fibres have a better resistance against this large humidity, however these need to be protected from the alkaline environment of the concrete. Standard glass fibres show a reduction in strength and ductility over a period of time. This is due to the formation of hydration products which results in embrittlement and chemical attack. New methods are developed in order to counteract these phenomena, which is usually done by applying a coating or changing the concrete mixture [2]. The variety of synthetic fibres is large while these are man-made, this type of fibre is made from organic polymers. This leads to a large variety in material properties for the different synthetic fibres, like tensile strength and Youngs modulus for instance. For synthetic fibre types the pull-out behaviour is

obtained due to mechanical anchorage or friction, there is no adhesion since there is no chemical bond. The hydrophobic nature of the material is the reason for this. In experiments by Babafemi et al. [6] photos of synthetic fibres are made by scanning electron microscopy. From these pictures it could be seen that there was no adhesion of cement on the fibres. Natural fibres can either be processed or unprocessed, however the influence on the mechanical properties is in general lower compared to the other fibre types. The option of using natural fibres on the other hand is suitable for low-cost construction due to the availability world-wide.

When the loading rate of the experiments is observed no significant effect on the pull-out load could be seen for steel fibres. In experiments done by Nieuwoudt et al. [30] the pull-out rate was varied from 0.0001 mm/s to 10 mm/s, the scatter of maximum force was minimal. On the other hand, when synthetic fibres are observed the loading rate does have an influence on the pull-out force. Babafemi et al. [6] did tests on straight synthetic fibres regarding the loading rate and the embedment length. The conclusion that could be drawn from this research is that a higher pull-out load was found for an increase in loading rate, see figure A.7.

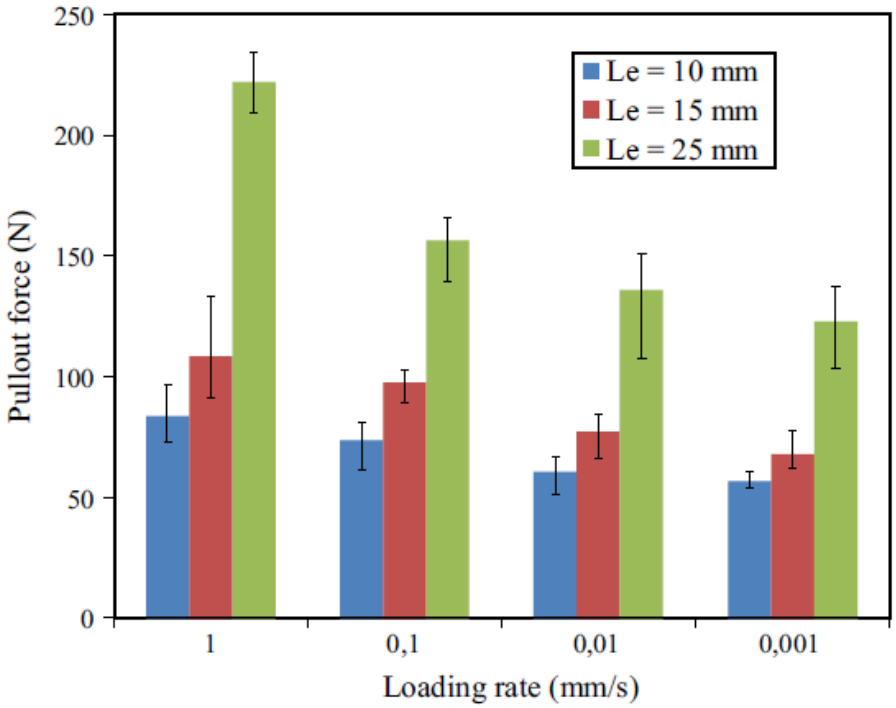

Figure A.7: *Effect of loading rate on pull-out load for different embedment lengths. (Babafemi et al. [6])*

This phenomenon can be explained by the clamping pressure of the concrete to the fibre surface. An increase in friction can be found due to the acceleration of material points in the near area of the fibre. For a large pull-out rate the area close to the fibre is rapidly immobilised, resulting in a high resistance. For a low pull-out rate the confining pressure of the fibre can be reduced due to the Poisson's contraction of the synthetic fibre.

A.1.5 CONCRETE MATRIX

Not only the fibre properties are of influence for the behaviour of fibre reinforced concrete, also the type of concrete is of influence for the material behaviour. In general there can be found that for the use of steel fibres a higher concrete strength results in a higher pull-out strength, this due to the increase in friction [8][44] (See figure A.8). However when synthetic fibres are observed, an insignificant difference in pull-out strength is found by Li et al. [25]. From these results it can thus be said that the bond strength between the fibre and the concrete does not change. It should be noted

that these results are based on an inclination angle of 0°. Different inclination angles are also observed in this research, for an inclination angle of 60° the pull-out load increased by a factor of two. This increase in pull-out load can be explained by the matrix spalling which is not present for an inclination angle of 0°. For a high strength concrete the resistance due to concrete spalling is larger than for normal strength concrete.

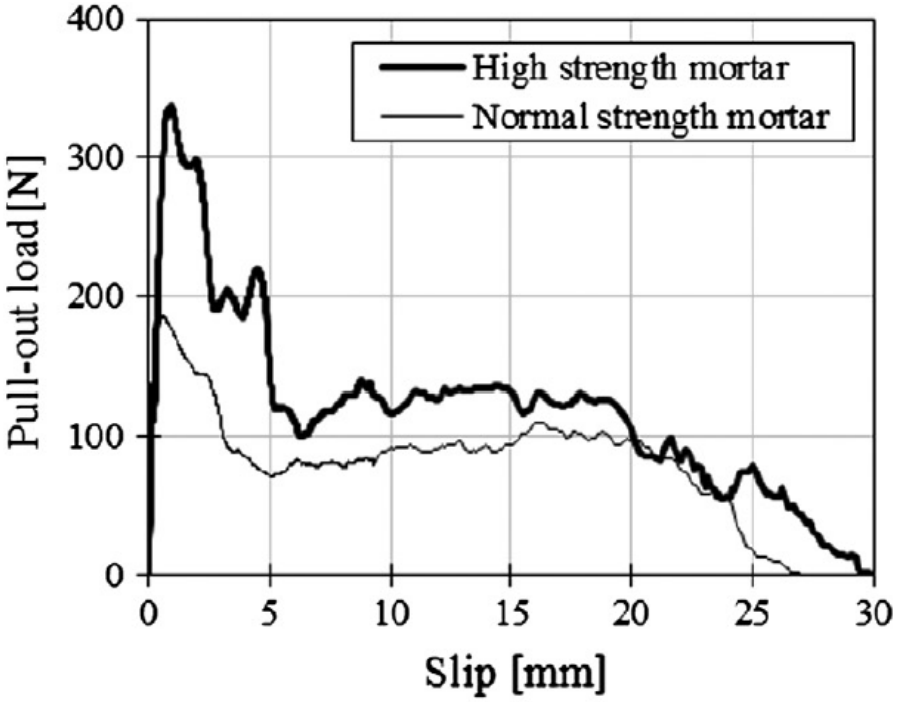

Figure A.8: *Influence of concrete matrix, high strength mortar vs. normal strength mortar. (Soetens et al. [44])*

When different types of fibres are observed, with regard to the concrete strength, a difference can be found between normal strength and high strength fibres. In Breitenbücher et al. [8] normal strength fibres showed a similar behaviour when tested in normal strength concrete and high strength concrete. This was not the case when high strength fibres were applied, here a higher concrete strength results in a higher pull-out load. It could also be seen that for a lower concrete strength the hooked-end of the fibre was not fully straightened, thus the pull-out energy was lower.

By increasing the concrete strength the failure mode might change from fibre pull-out to fibre fracture. Soetens et al. [44] stated that with a higher concrete strength the effect of mechanical anchorage can improve, thus increasing the pull-out load. While by increasing the concrete strength an improvement of the pull-out behaviour can be obtained, some things should be kept in mind. According to Li et al. [25] a larger fibre volume might be needed when using a high strength concrete. From an economical point of view it is also not wise to use high strength fibres to a low strength concrete, so during design the properties of the fibres and the concrete should be in relation with each other.

A.2 Fibre reinforced concrete

The influence of adding fibres to concrete can also be observed from a material point of view instead of by observing the pull-out behaviour of a single fibre. Fibres have, in most cases, a positive effect on the mechanical properties like the tensile and compressive strength. Also a reduction in shrinkage and creep deformations is obtained by the addition of fibres [4][9]. Fibre reinforced concrete can be seen as a unique composite material based on experimental results. According to Di Prisco et al. [16] the characteristics of this material depend mainly on the location and orientation of the fibres, which are

in general difficult to determine. While these factors are unknown it is rather difficult to give a reliable prediction for the behaviour of the overall material. The material properties are influenced by the aspect ratio and the fibre ratio according to Yazici et al. [47]. In general a value between 50 and 100 is chosen for the aspect ratio, for the fibre ratio there is often chosen for a volume percentage between 0.5% and 2.5%.

When the length of the fibres is observed a distinction can be made between short (6-13mm) and large (30-60mm) fibres. The short fibres bridge the micro cracks in the first stage, they increase the tensile strength of the material in the pre-peak stage. In general a large number of small fibres is used which results in a small distance between these fibres, once a crack starts growing the micro fibres are pulled out of the matrix and they lose their function. The long fibres are activated once a macro crack occurs, these fibres increase the ductility of the material by bridging the cracks [27]. In figure A.9 this situation is shown, where a mixture of short and long fibres is loaded in tension. The option to combine different types of fibres has also been investigated. Research done by Pakravan et al. [34] states that the use of multiple fibres has an advantage, regarding strength and costs, compared to individual fibre reinforce concrete. For a hybrid fibre reinforced concrete the tensile capacity is increased due to the micro fibres and the ductility is improved by the macro fibres.

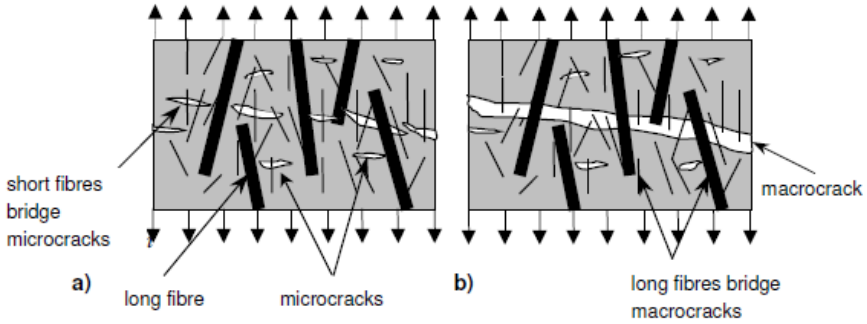

Figure A.9: *Influence of micro and macro fibres. (Marković [27])*

A.2.1 COMPRESSIVE STRENGTH

From literature it follows that in general the compressive strength improves when fibres are added to concrete, however there are some contradictory results. Up to a fibre ratio of 1.5%-2.0% the compressive strength increases [4][41], when a larger ratio is applied it is most likely that the compressive strength will reduce. This is due to the reduced workability for a larger fibre ratio, also the porosity increases due to the extra fibres. In research done by Simões et al. [41] fibres of different materials are tested, polypropylene, glass and steel fibres are tested for different fibre ratios. In figure A.10 the difference in percentage with regard to plain concrete can be seen, steel fibres with a ratio of 1.5% had a maximum increase of approximately 30%.

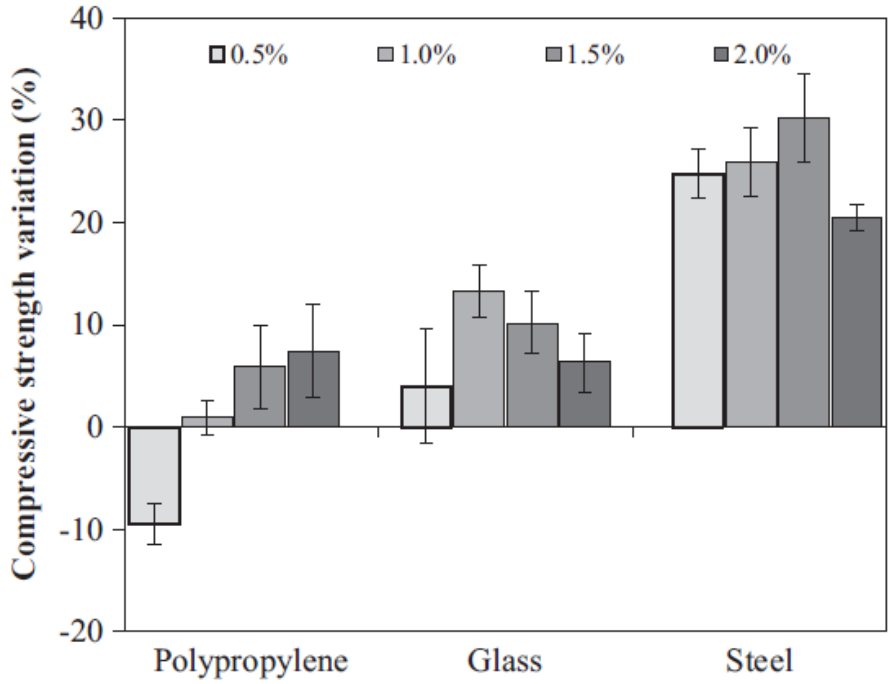

Figure A.10: *Variation of compressive strength for different fibre types and ratios. (Simões et al. [41])*

While the previous examples showed an increase in compressive strength there is also research that states that fibres have little to no effect on the compressive strength. In an experimental study done by Demeke et al. [14] the increase in compressive strength, in comparison to plain concrete, is less than 5%, whereby this effect is neglected. In some research there is even a reduction in compressive strength when fibres are added. In research done by Zhu et al. [48] an organic modified polypropylene fibre is tested. When this research is compared to the results of the polypropylene fibres used by Simões et al. [41] the maximum fibre percentage used by Zhu et al. [48] is 1.15%. So it could be possible that if a larger volume percentage is used the fibres can results in an improvement compared to plain concrete.

A.2.2 TENSILE STRENGTH

Due to the addition of fibres to concrete the tensile capacity increases, according to Afroughsabet et al. [4] this is caused by the ability of the fibre which:

- Restricts the crack extension.
- Reduces the stress concentration at the crack tip.
- Bridges micro and macro cracks.
- Anchoring mechanism (for deformed fibres).

The literature research done by Afroughsabet et al. [4] observed the influence of the fibre ratio. For a low fibre content, $V_f < 0.5\%$, an increase of tensile strength of 9% - 50% compared to plain concrete can be found. When this fibre content is increased to 2% the tensile capacity even increased by 90% - 143% according to several researchers. All these papers focused on the influence of steel fibres, however also other fibre types can be observed. Also by the addition of PVA fibres a significant increase in tensile strength can be found, up to 32.5% compared to plain concrete. However the fibre ratio applied when using PVA fibres is much lower than with steel fibres. A larger ratio than 0.25% of PVA fibres did not lead to an improvement of tensile strength, however the ductility of the material did increase for an increasing fibre content. The PVA fibres are more beneficial in energy absorption and crack control, while the influence on the maximum load bearing capacity is much lower.

From research done by Meng et al. [28] it can also be concluded that for an increase in matrix strength, the ratios of ultimate tensile strength varied dissimilarly depending upon the fibre type. This variation is explained by the varying strength of the different fibres. For the combination of a high matrix strength and a low fibre strength, the failure mode was due to rupture of the fibres.

A.2.3 STRESS-STRAIN CURVE

By the addition of fibres the stress-strain curve of plain concrete changes, the material is able achieve a much higher strain. A comparison of high strength concrete in compression with and without fibres is given in figure A.11 (Left). In figure A.11 (Right) a type of concrete, C30, is tested in tension with and without fibres.

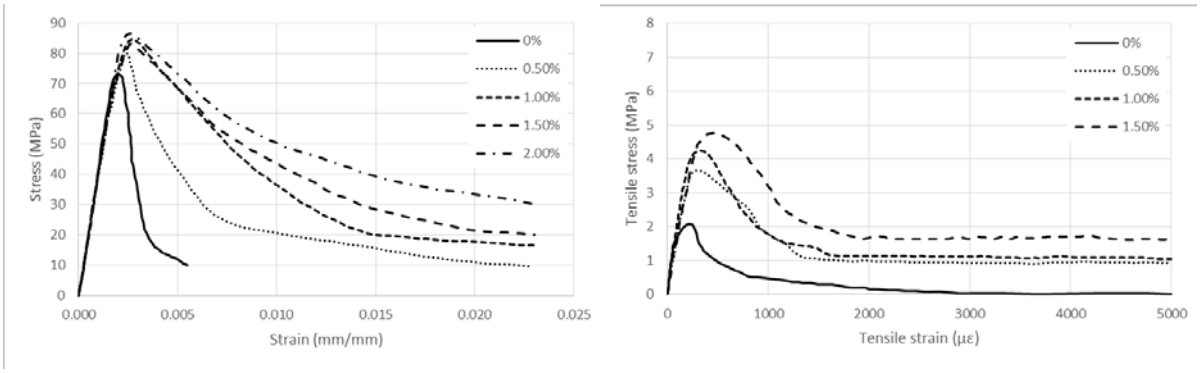

Figure A.11: *Stress-strain curve for high strength concrete in compression (Left); Stress-strain curve for normal strength concrete in tension (Right). (Afroughsabet et al. [4]; Meng et al. [28])*

The low fracture toughness of plain concrete is significantly increased by adding fibres, this is due to the increased resistance against crack propagation. The high energy absorption of fibre reinforced concrete is due to the effect called fibre bridging [9]. The energy absorbed up until failure can be defined as the toughness of the material, the value can be found by the integration of the stress-strain curve. The fracture toughness improves for an increasing fibre volume, this can also be seen from the curves in figure A.11. There is also a change in the post-peak behaviour, as mentioned by Afroughsabet et al. [4] the slope of the descending part decreases when the fibre volume increases. This increase in toughness is described by Simões et al. [41], where it is stated that an increase in fibre volume results in more fibres linking their boundaries. The energy absorption capacity increases due to this and therefore the toughness index grows. In this research the toughness index for steel fibres decreased for a fibre volume of 2%, even while the load and deformation capacity of the material is still increasing for this fibre volume. This is explained by the increase of the cracking point for a higher fibre volume. This results in a decrease of the toughness index while the total absorbed energy still increases.

Another parameter that can be derived from the stress-strain curve is the Young's modulus, which is based on the slope of the curve. As can be seen from figure A.11 the addition of fibres to concrete has hardly an effect on the modulus of elasticity. Different types of fibres are observed in a literature review done by Afroughsabet et al. [4], in this research it is stated that the majority of tests resulted in a modulus of elasticity that is comparable to plain concrete. Some researchers state that fibres do have a beneficial effect on this property, however the increase was in these cases minimal.

A.2.4 FRACTURE ENERGY

Once a fibre reinforced concrete element is loaded in tension it will start to crack after a certain load, the behaviour of the material surrounding the crack can be described by using fracture mechanics. The fracture energy of a material is equal to the area under the σ-w curve, this is the energy required to form a crack. In figure A.12(a) a load-deflection diagram is given which could be obtained through experimental testing. For fibre reinforced concrete the stress increases almost linear elastic up to the

maximum tensile strength, at this point a fracture zone starts to develop. This relation can be visualised by a stress-strain diagram which is sketched in figure A.12(b). After this point the material starts to crack, for a softening material the stress will decrease while the crack width starts to increase. To describe this behaviour the strain cannot be used anymore, however a stress-crack opening diagram can be used (See figure A.12(c)). The strain cannot be used anymore while there is no uniform distribution over the element in contrast to an uncracked element. Once a crack occurs the strain outside the fracture zone will decrease, the total elongation within the fracture zone can be described as the sum of the strain and the crack width [32]. According to Olesen [32] the stress-crack opening relation needs to be at least of a bi-linear form in order to describe the material behaviour. This is due to the fact that in the first part fracture of the concrete matrix is governing. Once the fibres are activated the material behaviour is dominated by the fibres being pulled out.

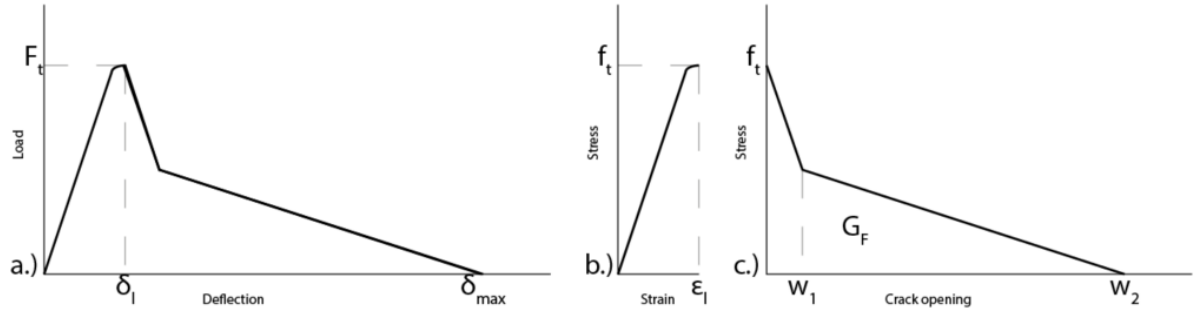

Figure A.12: *Schematic representation of material behaviour.*

Two simplified stress-crack opening relationships are proposed by the Model Code 2010 [16], a rigid-plastic model and a linear post-cracking model (figure A.13). For the rigid-plastic model a constant strain is assumed for an increasing crack width. When the linear post-cracking model is assumed there are two different options. The material can behave as a strain softening material, here the ductility of the material is increased. However the maximum tensile load cannot be further increased for this material. The bearing capacity for a strain hardening material on the other hand can be further increased after cracking.

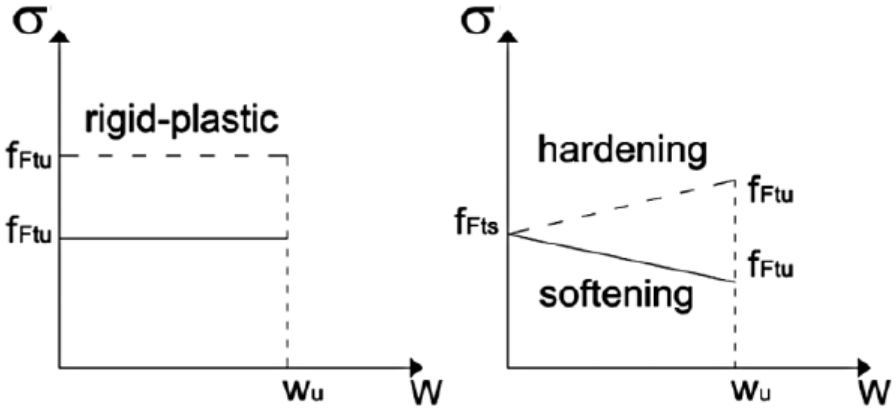

Figure A.13: *Simplified constitutive laws according to the Model Code 2010. (di Prisco et al. [16])*

Since fibre reinforced concrete is an anisotropic material the behaviour in different directions may vary. It is possible that a material which has strain softening in one direction, shows a strain hardening behaviour in the other direction. This is mainly due to the dispersion and alignment of the fibres in the matrix. According to di Prisco et al. [16] this difference in behaviour can also be the result of the used test method. When a bending test is conducted the material cracks before the peak load is reached. This can cause a stable crack propagation while the same element might show a strain softening behaviour when it is tested in uniaxial tension.

In the Model Code 2010 [16] a relation is proposed to connect the continuous mechanics, σ-ε relation, with the fracture mechanics, σ-w relation. To do so a structural characteristic length is introduced which converts the crack opening to a strain, $\varepsilon = w/l_{cs}$. The structural characteristic length is taken equal to the crack spacing when multiple cracking occurs or the depth of the beam when a single crack occurs. By translating the crack width to a strain, the crack is smeared out over the characteristic length. This could be useful if one is designing a model to predict the behaviour of fibre reinforced concrete.

When cracking of the matrix is observed a distinction can be made between two different zones, the fibre bridging zone and the fracture process zone. The fracture process zone can also be observed for cracking of plain concrete, the fibre bridging zone develops due to the addition of fibres. The fracture process zone is located at the tip of the crack, at this location microcracking and debonding of the aggregates and cement takes place [12]. For cementitious materials the stress further reduces for an increasing crack opening. Both the material properties and geometry and size of the element are of influence on the critical size of the fracture process zone. The fibre bridging zone is located after the fracture process zone, here the strain softening behaviour is obtained due to the pull-out of the fibres. A reduction of stress can be found as the fibres are pulled out further. The fibre bridging zone is mainly dependent on the aspect ratio of the fibres and the size and geometry of the specimen. In figure A.14 a sketch is given of a crack in a fibre reinforced concrete element, also a stress distribution over the depth is given. In the stress distribution the bilinear form of the post cracking behaviour can be observed.

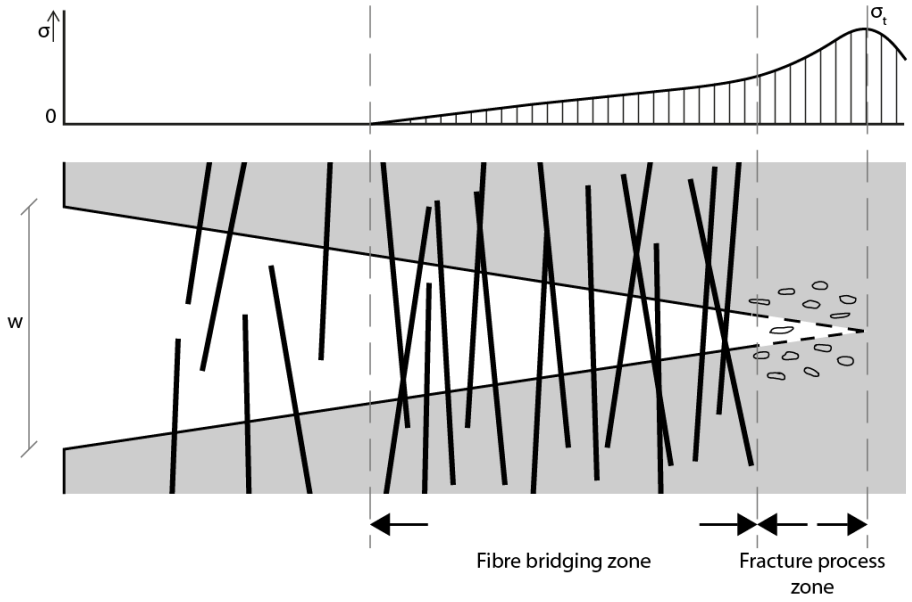

Figure A.14: *Fibre bridging zone and fracture process zone in crack. (Cotterell [12]) (Modified)*

In fracture mechanics different models can be used to describe the behaviour in the crack. For concrete there are two methods which are applied in general, a band model and a crack model. In figure A.15 an example is given of both methods, for the band model the crack width is distributed over a certain band thickness where for the crack model the strain is located at a point. When taking a band model into account one can apply a stress-strain relationship for both softening and hardening materials. For a crack model a stress-strain relationship can also be used when observing a hardening material, however a stress-crack width relationship should be used for softening materials [18].

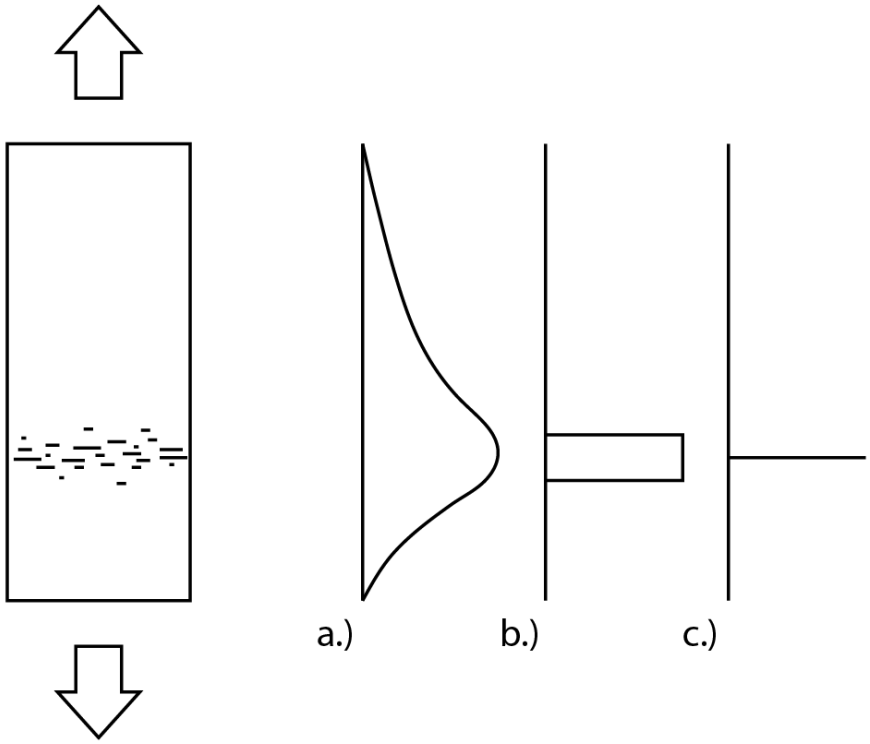

Figure A.15: *Modes of strain localisation; a.) Smooth, arbitrary shape strain localisation; b.) Localisation within band; c.) Localisation into crack-line. (Elfgren [18])*

For both models some basic assumptions can be made according to Elfgren [18], in which some differences can be found between the two models. An isotropic linear elastic behaviour is assumed for the bulk material, this holds for both models. The behaviour until fracture is also assumed to be similar, here the behaviour can be described as elastic. After fracture some differences can be found, for a band model uniformly distributed cracks occur over a certain band thickness. For a crack model a cohesive crack develops at a single location, in both cases the crack develops perpendicular to the direction of the maximum tensile stress. Once the crack starts to develop the stress and strain tensor are uniform over a band thickness for a band model. For a crack model the stress depends on the crack opening instead of the strain. When observing the band model some limitations can be found, the first one is the fact that there is no experimental evidence of a uniform stress and strain over the band thickness. Another limitation is that the band model does not agree with classical continuum mechanics, while it assumes that the behaviour at a certain point is dependent on the behaviour of the material in the band. Also the crack model has its limitations, the theory is well suited to describe a single crack. However in the case that multiple cracks occur a minimum crack spacing needs to be used. This crack spacing is theoretically almost similar to the band thickness used in a band model, so the same problem is created. In order to apply a crack spacing it is also needed that the cracks are orientated parallel with respect to each other, for diverging or converging cracks the crack spacing cannot be used. Another limitation for the crack model is the fact that until now it can only be applied for a pure opening mode.

A.3 PRINTED CONCRETE

Printing concrete, compared to casting concrete, requires several parameters to be considered. According to Le et al. [23] the most critical fresh properties are the ability to extrude the material through the hose and the ability to build an element layer by layer. These parameters have a direct relation with the workability and the open time of the concrete. The Eindhoven University of

Technology in cooperation with Weber Beamix has chosen a type of concrete which fulfils these criteria.

A.3.1 EFFECT OF LAYERED MANUFACTURING

During the past years research has been done at the Eindhoven University of Technology regarding the possibilities of printing concrete. Several subjects have been investigated to optimise this new manufacturing technique, from optimising the design possibilities to testing the material properties. For this graduation thesis the research into the material properties are of interest, especially the behaviour of the interface between the layers. The effect of layered manufacturing is analysed by Doomen [17], in this research the material is tested by a compression test and direct tensile test. The compression and tension tests are subdivided into two different test sets, a strength development test and a time interval test. With a strength development test the build-up of strength in time is determined. By executing a time interval test a conclusion can be drawn about the influence of time on the strength between the printed layers. For each set three different test directions are observed, two parallel and one perpendicular to the printed layers. For the sets parallel to the printed layers a distinction is made between one set parallel to the printing direction and one set perpendicular to the printing direction (see figure A.16).

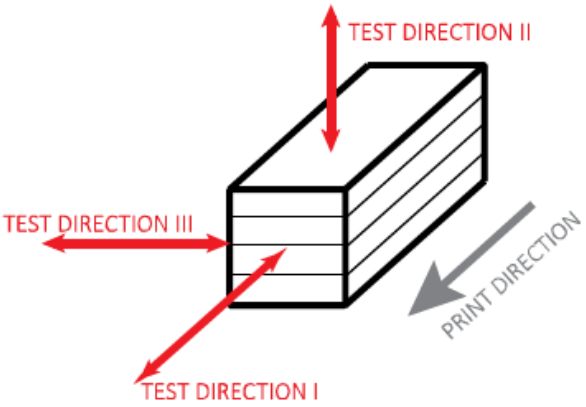

Figure A.16: *Influence of test direction on material behaviour. (Doomen [17])*

When the results are observed it can be stated that the layer direction does not influence the compressive strength. The different test series for the strength development test as well as the time interval test are comparable. Compared to a casted specimen a reduction in compressive strength can be seen, the printed concrete has a reduction of 23% of compressive strength. This is most likely due to the compaction of casted elements, which is not done for printed elements.

The tensile strength on the other hand is depended on the layer direction, test direction II shows a reduction in tensile capacity compared to the other two directions. For the strength development test a reduction of 30% of tensile strength can be observed if compared to the other two directions. This is due to the layers of concrete being pulled of each other, which is not the case for the other two directions. Also for the time interval test an average reduction of 30% can be observed, which even increases for a larger time interval.

When the strength development is observed printed concrete differs from normal concrete. In the strength development test the strength increases rapidly, after which the increase after three days is minimal. This phenomenon happened for all three test directions and is likely caused by the temperature. Due to the manufacturing method the temperature at the pump is high, which influences the strength development of the material. Also the strength development for the time interval test differed. For test direction I and III the strength remains rather constant for a different time interval.

This is not the case for test direction II, here the strength decreases 44% of its initial value over a time interval of 24 hours.

A.3.2 INFLUENCE OF THE INTERFACE

Another research with respect to the influence of the interface on the tensile properties is done by Slager [43]. In this research a direct tensile test is executed to obtain the material properties, four different test series can be distinguished. Two series consisting of six layers of 40x10 millimetre, where one series is printed consistently (figure A.17(a)) and the other has an interval of 7 days (figure A.17(b)) One series of one layer printed with a nozzle of 45x45 millimetre (figure A.17(c)). And the last series which has two layers of 45x45 millimetre with an interval of 7 days between printing the layers (figure A.17(d)). The printed elements are later sawn to obtain test specimen and loaded parallel to the layer direction.

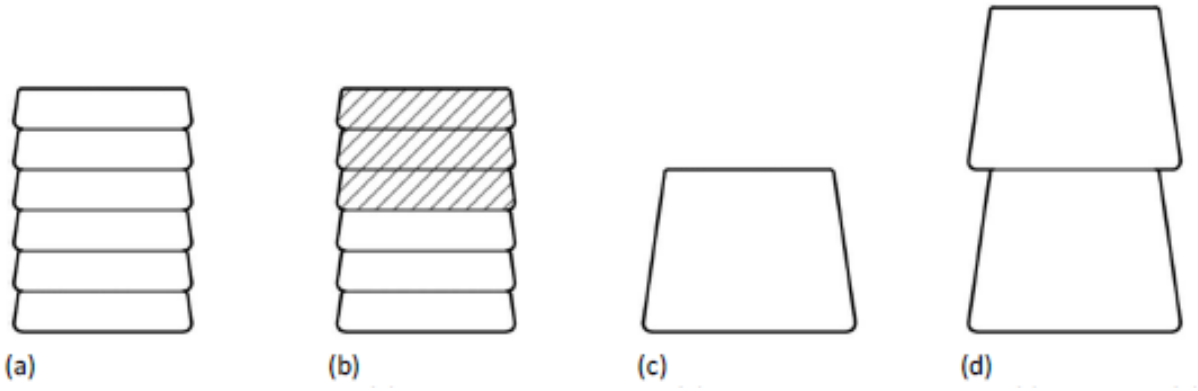

Figure A.17: *Test samples to analyse influence of the interface. (Slager [43])*

When the results of the research are observed it can be said that an increase in time interval results in a decrease of tensile strength, which is comparable to results from Doomen [17]. A 7-day interval between printing the layers results in a reduction of 56% regarding the tensile strength. The difference in tensile strength between the specimen consisting of one or multiple layers is small. The influence of time on the interface can be seen in the specimen in figure A.18. Here the crack surface of a specimen of four layers can be seen, figure A.18(a) shows a specimen printed without interval and figure A.18(b) is a specimen with an interval of 7 days between printing. It can clearly be seen that the specimen with a 7-day interval failed in the interface due to the smooth crack surface.

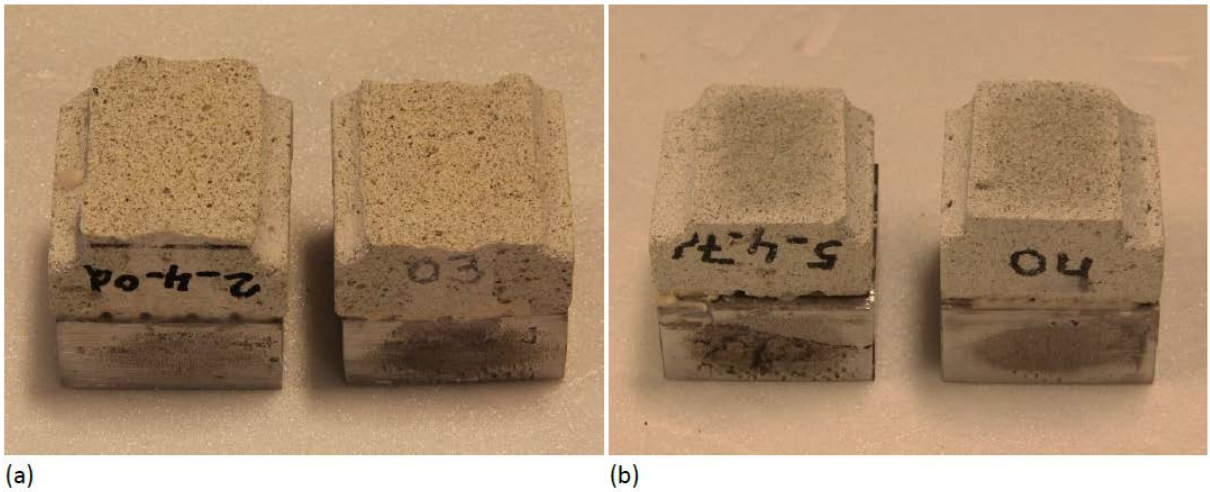

Figure A.18: *Crack surface of test samples with 4 layers; a.) Without time interval; b.) with 7-day time interval. (Slager [43])*

Other material properties like the density of printed concrete are comparable to casted concrete [17][43], the obtained results are comparable thus the manufacturing technique does not seem to have an influence on this parameter even though the printed concrete is not compacted. By changing the test direction the Young's modulus stays the same [17], also the interface between the different layers has no influence on the Young's modulus [43].

A.3.3 BOND STRENGTH

When the production process, printing of concrete, is observed it can be mentioned that the bond strength between the layers is the most important parameter. Research with respect to the bond strength is also executed at the Loughborough University, where Le et al. [24] stated that by printing concrete it is possible that stress concentrations are induced due to potential flaws between extrusions. The adhesion between the layers is important, which is mainly dependent on time. Several experiments are conducted with a varying time gap between printing the layers, the results can be seen in figure A.19. Results showed that for all specimen with a time gap greater than 15 minutes a failure of the interface occurred. For a time gap of 7 days a reduction in bond strength of 77% could be found compared to the specimen without a time gap.

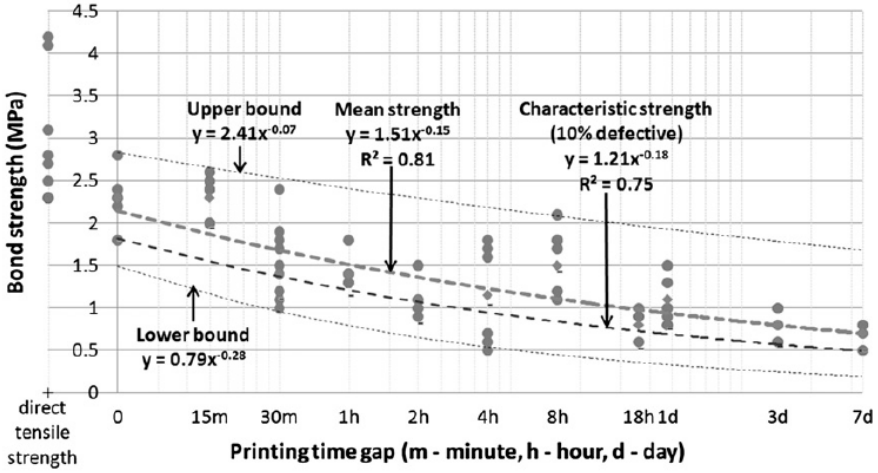

Figure A.19: *Influence of printing time gap on bond strength of printed concrete. (Le et al. [24])*

Adhesion is not the only parameter that is of importance for the strength of the bond, mechanical interlocking can also affect the bond strength [5]. The quality, and directly related the strength, of the bond is dependent on the characteristics of the surface. According to Austin et al. [5] the surface roughness, soundness, cleanliness and moisture condition are the most important characteristics. An increase in roughness of the surface results in an increase of the bond strength [5]. This makes sense while a rougher surface has a larger contact area, hereby the bond strength and fracture energy are improved.

A.3.4 PRINTED FIBRE REINFORCED CONCRETE

The first step towards reinforcing printed concrete with fibres at the University of Technology Eindhoven has already been made, in research done by Raedts [38] the possibility of adding fibres to the concrete is observed. In this research two types of high-strength steel fibres, 6 and 13 millimetres, are tested to analysing the influence on the flexural strength. Samples are printed with a dimension of 40x40x160mm and tested with a Crack Mouth Opening Displacement test (CMOD test). From these results it could be observed that the addition of 6 millimetre steel fibres resulted in a large increase of peak strength, with a factor of approximately 5 compared to plain concrete. Also a post-peak behaviour is obtained in which a strain-softening behaviour is observed due to the pulling out of the fibres. For the 13 millimetre steel fibres no test samples could be printed due to clogging at the nozzle.

A nozzle opening of 10x60 millimetre was used, which seemed too small to make a continuous print. This shows that the printing parameters could set certain limitations of what can be printed. This was also observed by Hambach et al. [20], here micro fibres with a length of 3-6 millimetre were printed with a nozzle diameter of 2 millimetre. From testing it could be concluded that the maximum fibre ratio which was printable had a fibre volume percentage of less than 1.5%. Once the amount of fibres was increase clogging of the nozzle occurred more frequently. This shows that there seems to be a limitation in the ratio of fibre length/ratio to nozzle diameter.

Also in different research cementitious composites with fibres are developed which are printable. Panda et al. [35] have tested different lengths of glass fibres, for varying fibre contents. A geopolymer mortar is developed with a thixotropic behaviour, which is tested to determine its mechanical properties. From this research it is concluded that for an increasing fibre ratio, the flexural strength of the specimen increases. From the results it could also be stated that in general a larger fibre resulted in a larger flexural strength. If the compressive strength of the samples is analysed little to no influence could be observed for the different fibre length or the different contents. Another printable concrete mixture is developed by Hambach et al. [20], for which different type of fibres are mixed to analyse its influence. In this research three types of micro fibres are tested with made from a different material, carbon, glass, and basalt fibres. By observing the flexural strength of the test specimen it can be stated that the use of 1% of carbon fibres resulted in an increase of the peak flexural strength with a factor 3. For the other two types of fibres the peak strength remains more or less the same compared to plain concrete. However when the post-peak behaviour is observed, the glass and basalt fibres show a strain-softening behaviour. On the other hand, no significant influence on the post-peak behaviour is observed by the application of the carbon fibres. The peak flexural strength of the samples with glass and basalt fibres does not increase due to the low Young's modulus of these fibres according to Hambach et al. [20]. Also from this research it can be seen that the compressive strength of concrete hardly changes once fibres are added to the mixture.

From research it also followed that the printing process has an influence on the orientation of the fibres. It could be seen that the majority of the fibres had an alignment parallel to the printing direction (see figure A.20), so the flow of concrete seems to be of importance. For the casted samples a more random fibre orientation could be seen [31][35][38], this directional dependency also seems to have an influence on the strength of the specimen. From the results from Raedts [38] a similar behaviour could be found for the printed and casted samples. For this it should be noted that the casted samples were compacted, thus less air voids should be present in these samples. For Ogura et al. [31] an improvement in strain hardening behaviour for the printed specimen compared to the casted specimen could be found. In this research no compaction was applied for the casted samples. In this research two possible conclusions are stated for this difference between printed and casted samples. Due to the extrusion process during printing compaction of the material could occur at the nozzle, reducing the are voids in the printed samples. The second possibility is the aligned orientation of the fibres, which are parallel to the test direction.

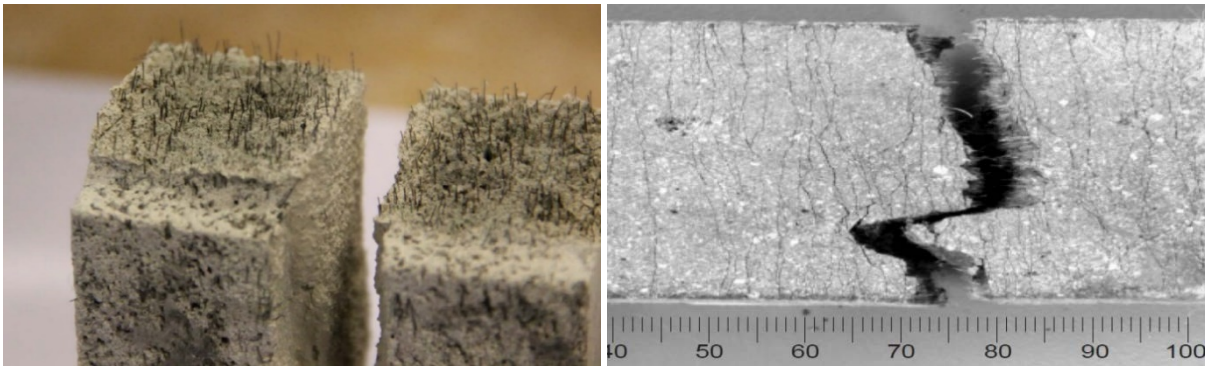

Figure A.20: *Alignment of fibres parallel to printing direction (Left); Crack pattern with alignment of fibres (Right). (Raedts [38]; Ogura et al. [31])*

In general it follows from research that the flexural strength of the printed concrete increases by the addition of fibres. Also from research conducted by Nematollahi et al. [29] this conclusion is drawn, here three different types of synthetic fibres are tested. For all tested samples an increase in flexural strength is observed compared to the printed geopolymer without fibres. However, also the inter-layer bond strength is tested in this research. By the addition of fibres to a mixture the material properties change, this led to a reduction in interlayer bond strength compared to the plain geopolymer samples. An increase in stiffness of the fresh mixture was observed, hereby the deformation capacity of the layers reduced which led to a more porous interface [29]. It is stated that further research is needed to confirm this statement.

APPENDIX B – DEVELOPMENT BLOWER

To check which fibre types can be used as reinforcement for printed concrete, twenty different fibres are analysed. It is yet unknown which fibre might be suitable to use, therefore a wide variety of fibre types is chosen to start with. Different fibre materials are chosen to determine the influence, such as steel, glass, and synthetic. Different geometries are also observed, with respect to the shape and by testing different lengths of the fibres. For each type of fibre an analysis is made to determine whether it can be used or not. Once the blower is fully operational all fibre types can be tested with the blower to check the output, for the development a selection will be made to improve the device. This selection of fibre types is based on literature research. A list of all the fibres which are tested is given in table B.1, in figure B.1 a picture of all fibres can be found, the corresponding number can be found in the table.

Table B.1: *Fibre types*

Fibre type		Shape	Material	Length (mm)	Diameter (mm)
1.)	Dramix OL 6/.16	Straight	High strength steel	6	0.16
2.)	Dramix OL 13/.20	Straight	High strength steel	13	0.20
3.)	Dramix 3D RC-4530-BL	Hooked-end	High strength steel	30	0.62
4.)	OL 6530 Proef 9635E	Crimped	High strength steel	20	0.30
5.)	Synmix SP55	Waved	Polymer type II	55	0.85
6.)	Duomix M12	Straight	Polymer type IA	12	0.03
7.)	Fibraflex FF/30L6	Flat	High strength steel	30	0.029
8.)	Fibraflex FF/20L6	Flat	High strength steel	20	0.029
9.)	Fibraflex FF/20E0	Flat	High strength steel	20	0.024
10.)	Fibraflex FF/15E0	Flat	High strength steel	15	0.024
11.)	Fibraflex FF/10E0	Flat	High strength steel	10	0.024
12.)	Fibraflex FF/5E0	Flat	High strength steel	5	0.024
13.)	Turbobuild dispergate AC-12-300/D	Straight	Basalt	12	0.04
14.)	Turbobuild integral AC 24-200/I	Straight	Basalt	24	0.12
15.)	Uncoated chopped fibre	Straight	Basalt	12	0.09
16.)	OC reinforcements Anti crak HP 18	Straight	Alkali resistant glass	18	0.16
17.)	OC reinforcements Anti crak HP 24	Straight	Alkali resistant glass	24	0.44
18.)	OC reinforcements Anti crak HP 67/36	Straight	Alkali resistant glass	36	0.54
19.)	Cem-FIL Minibars 24 mm	Twisted	Alkali resistant glass + Thermoset resin	24	0.70
20.)	Cem-FIL Minibars 43 mm	Twisted	Alkali resistant glass + Thermoset resin	43	0.70

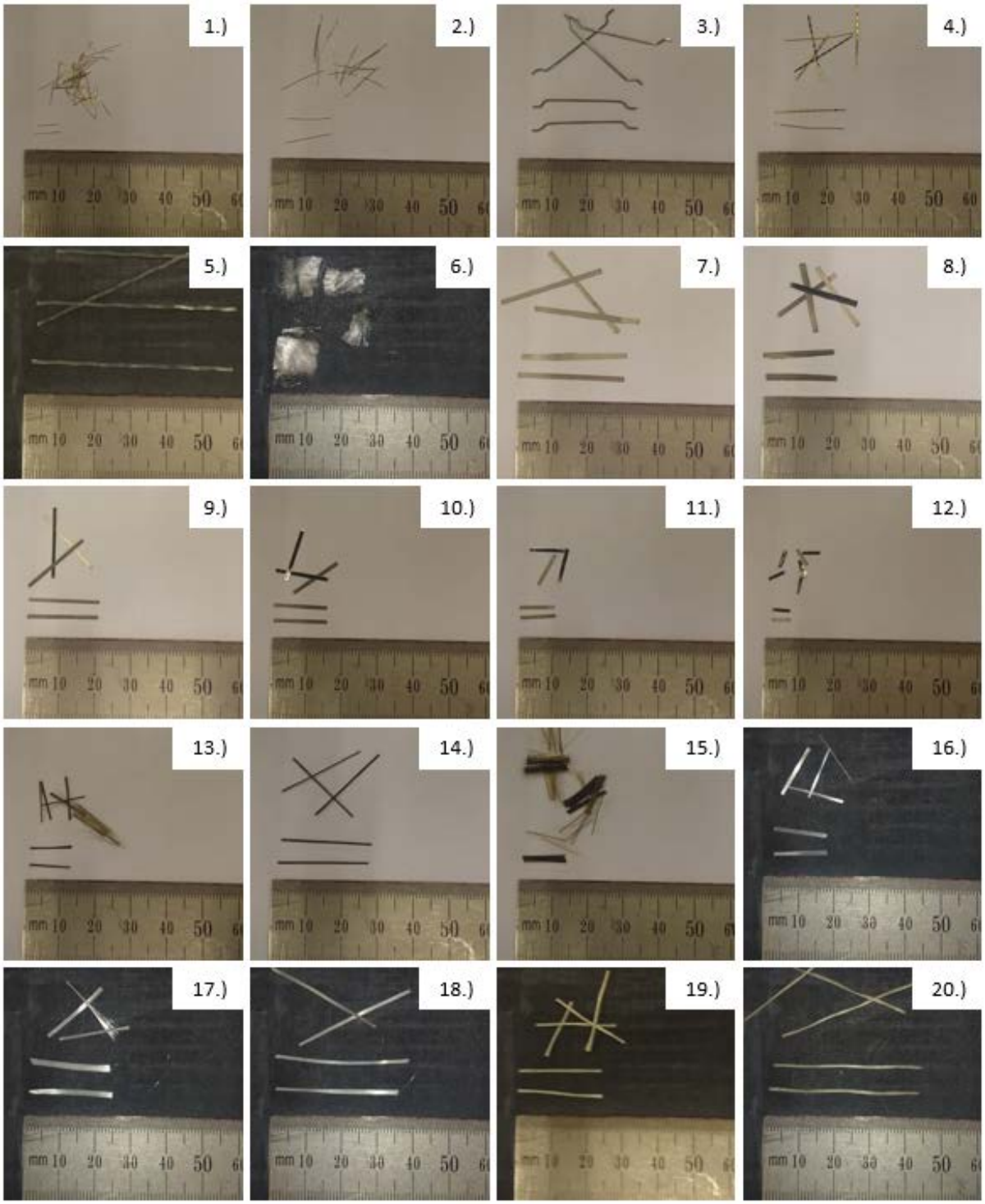

Figure B.1: *Tested fibre types.*

B.1 DEPOSITING METHOD OF FIBRES

To add fibres, or other admixtures, to the process of printing concrete a blower is used. This device transfers the fibres from the storage bucket to the robot arm by means of an air flow. The blower consists of an aluminium casing through which the fibres are blown, an overview of all parts can be seen in figure B.2. During the research several adaptions are made to improve the output of the blower, the final set-up is described here while the made adaptions will be explained later. Inside the chamber a rotary blade is located, this blade creates an air flow from the bottom of the chamber towards the side (figure B.2(a)(b)). The rotor blade is powered by a DC motor which can be controlled by a potentiometer. A display is added to the system in order to check the settings, here the power output of the motor is given. The fibres are added in a storage bucket, which is located under the blower (figure B.2(d)). The storage bucket is continuously vibrated to avoid fibre balling, due to the constant motion entanglement of the fibres is reduced. At the bottom of this bucket a funnel is created to collect all the fibres in the centre of the bucket (figure B.2(c)). Through a hose with a diameter of 60 millimetre the fibres are pulled into the chamber of the blower. From the side of this chamber another hose with a diameter of 50 millimetre is connected which leads to the robot arm (figure B.2(e)). Here the hose is connected to a pipe from which the fibres are blown towards the print path. The pipe is fixed to the robot arm with a distance of approximately 200 millimetre from the print path, from this height no influence on the concrete could be observed. If an influence on the concrete can be observed for different wind speeds, the pipe can be moved in a vertical direction to alter the distance from the print path.

Figure B.2: *Final set-up of fibre blower; a.) Motor and wattage meter; b.) Rotor blade inside aluminium casing; c.) Fixation of input hose and funnel; d.) Vibration bucket; e.) Fixation of output hose at robot arm.*

For now the pipe which is fixed to the robot arm does not rotate, so when the printer makes a turn the fibres are blown next to the layer instead of on top. If the pipe follows the rotation of the nozzle the hose will get entangled with the robot arm. The goal of this research is only to prove that the concept of the blower works, so for the current application the set-up of the device fulfils the requirements. However it might be needed to make an adaption when the device is applied in practice, because in practice it is needed to reinforce the concrete no matter in which direction is printed.

B.2 WORKABILITY TEST

For the current application the fibre has to be able to pass through the blower, therefore all fibres mentioned above are tested for this criterion. Almost all fibres are able to pass thorough the blower, only two types of fibres lead to clogging of the device. The 5.) Synmix SP55 and 20.) Cem-FIL Minibars 43mm get stuck in the device, this is due to the length of the fibres (figure B.3).

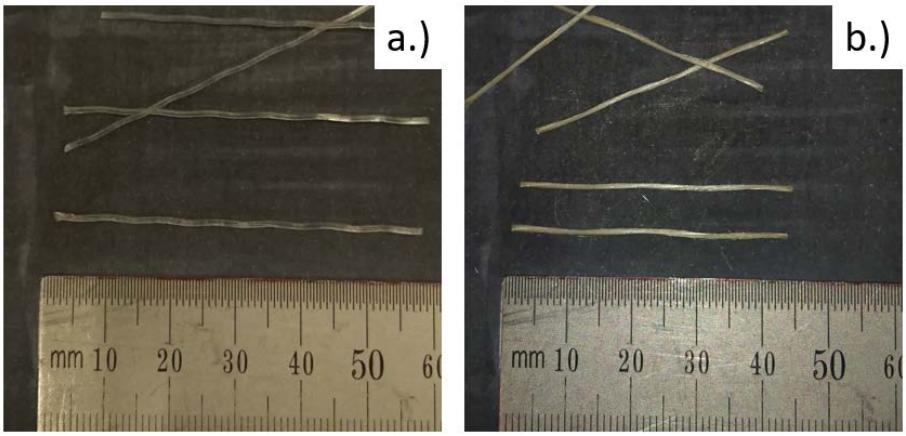

Figure B.3: *Fibres which resulted in clogging of the device; a.) Synmix SP55; b.) Cem-FIL Minibars 43mm.*

The rest of the fibres were able to pass through the blower, however in some cases a deformation of the fibre occurred. For a minority of the 3.) Dramix 3D RC-4530-BL the hooks of the fibre were straightened or the fibres were bend due to the steel rotor blade (figure B.4(a)). Another type of deformation could be observed for all the Fibraflex fibres, in this case a minority got sliced in smaller pieces (figure B.4(b)). Due to the sharp blade and thin shape, the flat fibres got torn to pieces. However these deformations are up to a certain limit still acceptable, the fibre might still be able to improve the material properties. For three types of fibres, 6.) Duomix M12 (figure B.4(c)), 13.) Turbobuild dispergate AC-12-300/D and 15.) Uncoated chopped fibres (figure B.4(d)), the wires got unbundled. Hereby the volume of the fibres increased significantly which lead to the fibres being blown in all direction. For the current application these fibres cannot be used while the majority of the fibres will be blown over the printing table. It is also expected that the part that lands on the print path will be dragged by the nozzle due to the increased volume.

Figure B.4: *Deformation of fibre types due to rotor blade; a.) Dramix 3D RC-4530-BL; b.) Fibraflex FF/30L6; c.) Duomix M12; d.) Uncoated chopped fibres.*

B.2.1 BUCKET TEST

The first test regarding the output of the blower is done with two types of fibres, 1.) Dramix OL 6/.16 and 2.) Dramix OL 13/.20. The rotary knob on the blower makes it possible to vary the wind speed, however there is no exact feedback on what the speed is. Therefore it is chosen to only test two settings, minimum and maximum. Once an extra display can be added to the system it will be easier to replicate the same settings to do multiple tests for settings in between the minimum and maximum. For these first test a stationary test is done where the fibres are blown through the device and collected in a bucket (see figure B.5). The amount of fibres which is collected in the respective time interval is weighted and from this number the weight per volume and area can be calculated as well as the output per minute. To do so a standard print path is considered, the printing speed of the concrete printer is taken as 100 mm/sec. For the standard printing layer a dimension of 60 millimetre in width and 10 millimetre in height is taken. From these number the translation to a weight per volume and a weight per area can be calculated. The obtained results for the first test can be found in table B.2 till B.5.

Figure B.5: *Set-up bucket test.*

Table B.2: *Output blower*

Fibre type:	Dramix OL 6/.16			
Blower setting:	Minimum			
Time	**Output**	**Weight per volume**	**Weight per area**	**Output per minute**
15 sec	72.9 g	81.0 kg/m^3	0.8 kg/m^2	291.6 g/min
30 sec	149.4 g	83.0 kg/m^3	0.8 kg/m^2	298.8 g/min
60 sec	269.4 g	74.8 kg/m^3	0.7 kg/m^2	269.4 g/min
Average	- g	79.6 kg/m^3	0.8 kg/m^2	286.6 g/min
Standard deviation				15.3 g/min

Table B.3: *Output blower*

Fibre type:	Dramix OL 6/.16			
Blower setting:	Maximum			
Time	**Output**	**Weight per volume**	**Weight per area**	**Output per minute**
15 sec	138.9 g	154.3 kg/m^3	1.5 kg/m^2	555.6 g/min
	119.4 g	132.7 kg/m^3	1.3 kg/m^2	477.9 g/min
	131.1 g	145.7 kg/m^3	1.5 kg/m^2	524.4 g/min
30 sec	300.3 g	166.8 kg/m^3	1.7 kg/m^2	600.6 g/min
	257.8 g	143.2 kg/m^3	1.4 kg/m^2	515.6 g/min
	264.2 g	146.8 kg/m^3	1.5 kg/m^2	528.4 g/min
60 sec	566.8 g	157.4 kg/m^3	1.6 kg/m^2	566.8 g/min
	575.3 g	159.8 kg/m^3	1.6 kg/m^2	575.3 g/min
	585.4 g	162.6 kg/m^3	1.6 kg/m^2	585.4 g/min
Average	- g	152.2 kg/m^3	1.5 kg/m^2	547.7 g/min
Standard deviation				39.1 g/min

Table B.4: *Output blower*

Fibre type:	Dramix OL 13/.20			
Blower setting:	Minimum			
Time	**Output**	**Weight per volume**	**Weight per area**	**Output per minute**
15 sec	54.3 g	60.3 kg/m^3	0.6 kg/m^2	217.2 g/min
	45.8 g	50.9 kg/m^3	0.5 kg/m^2	183.2 g/min
	43.1 g	47.9 kg/m^3	0.5 kg/m^2	172.4 g/min
30 sec	114.9 g	63.8 kg/m^3	0.6 kg/m^2	229.8 g/min
	110.9 g	61.6 kg/m^3	0.6 kg/m^2	221.8 g/min
	84.5 g	46.9 kg/m^3	0.5 kg/m^2	169.0 g/min
60 sec	172.0 g	47.8 kg/m^3	0.5 kg/m^2	172.0 g/min
	169.6 g	47.1 kg/m^3	0.5 kg/m^2	169.6 g/min
	172.2 g	47.8 kg/m^3	0.5 kg/m^2	172.2 g/min
Average	- g	52.7 kg/m^3	0.5 kg/m^2	189.7 g/min
Standard deviation				25.5 g/min

Table B.5: *Output blower*

Fibre type:	Dramix OL 13/.20			
Blower setting:	Maximum			
Time	**Output**	**Weight per volume**	**Weight per area**	**Output per minute**
15 sec	70.3 g	78.1 kg/m^3	0.8 kg/m^2	281.2 g/min
	70.2 g	78.0 kg/m^3	0.8 kg/m^2	280.8 g/min
	78.4 g	87.1 kg/m^3	0.9 kg/m^2	313.6 g/min
30 sec	141.5 g	78.6 kg/m^3	0.8 kg/m^2	283.0 g/min
	143.3 g	79.6 kg/m^3	0.8 kg/m^2	286.6 g/min
	146.3 g	81.3 kg/m^3	0.8 kg/m^2	292.6 g/min
60 sec	311.5 g	86.5 kg/m^3	0.9 kg/m^2	311.5 g/min
	285.9 g	79.4 kg/m^3	0.8 kg/m^2	285.9 g/min
	294.6 g	81.8 kg/m^3	0.8 kg/m^2	294.6 g/min
Average	- g	81.2 kg/m^3	0.8 kg/m^2	292.2 g/min
Standard deviation				12.5 g/min

In figure B.6 a graph is given with the average output per minute, the deviation is also shown in this figure. For a higher setting of the blower a larger output is obtain, as could be expected. However for the 1.) Dramix OL 6/.16 fibres this increase is much larger compared to the slightly bigger 2.) Dramix OL 13/.20 fibre. This is most likely due to the weight of the fibre, while a lighter fibre is dragged along more easily. The deviation of this test is also larger compared to the other test, this could be due to clogging of the device, if there are more fibres in the chamber the possibility of clogging increases. In most cases clogging happened at the transition from the chamber to the output hose where the diameter of the opening decreased. To obtain a more constant output, clogging of the device should be avoided.

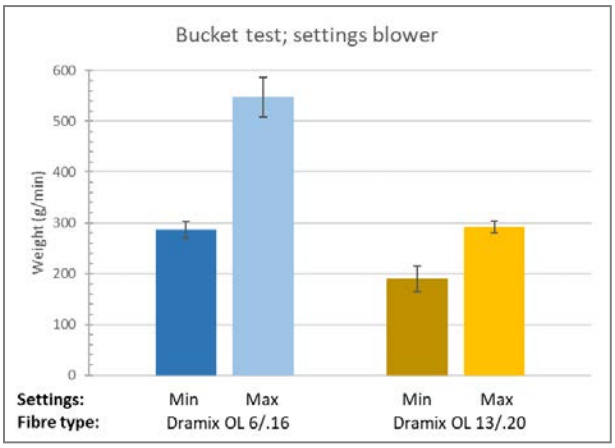

Figure B.6: *Results bucket test; Variation of settings blower.*

To avoid clogging of the system two adaptions are made for the blower, the diameter of the output hose is increased from 30 millimetre to 50 millimetre. By doing so there is no contraction along the path of the fibres where clogging can occur. By increasing the diameter of the output hose the wind pressure changes and thus it is expected that the output of the blower changes. It is expected that the amount of fibres will reduce due to the reduction in wind speed. A second adaption which is done is the addition of a vibration table for the storage bucket (figure B.7). By constantly vibrating the storage bucket the fibres will stay in motion, this avoids fibre balling in the storage bucket. Hereby it is expected that the input of fibres will be more gradual which will also reduce the possibility of clogging. To test the new adaptions another test is executed in the same manner, this time only one type of fibre is

tested 1.) Dramix OL 6/.16. The results of this test can be found in table B.6, for the blower setting there is chosen to only test the maximum setting at this moment.

Figure B.7: *Vibration bucket.*

Table B.6: *Output blower*

Fibre type:	Dramix OL 6/.16			
Blower setting:	Maximum			
Time	**Output**	**Weight per volume**	**Weight per area**	**Output per minute**
15 sec	84.5 g	93.9 kg/m^3	0.9 kg/m^2	338.0 g/min
	112.5 g	125.0 kg/m^3	1.3 kg/m^2	450.0 g/min
	76.0 g	84.4 kg/m^3	0.8 kg/m^2	304.0 g/min
	85.1 g	94.6 kg/m^3	0.9 kg/m^2	340.4 g/min
	65.7 g	73.0 kg/m^3	0.7 kg/m^2	262.8 g/min
30 sec	190.4 g	105.8 kg/m^3	1.1 kg/m^2	380.8 g/min
	175.4 g	97.4 kg/m^3	1.0 kg/m^2	350.8 g/min
	189.1 g	105.1 kg/m^3	1.1 kg/m^2	378.2 g/min
	164.1 g	91.2 kg/m^3	0.9 kg/m^2	328.2 g/min
	190.4 g	105.8 kg/m^3	1.1 kg/m^2	380.8 g/min
60 sec	344.6 g	95.7 kg/m^3	1.0 kg/m^2	344.6 g/min
	363.4 g	100.9 kg/m^3	1.0 kg/m^2	363.4 g/min
	342.9 g	95.3 kg/m^3	1.0 kg/m^2	342.9 g/min
	366.0 g	101.7 kg/m^3	1.0 kg/m^2	366.0 g/min
	405.7 g	112.7 kg/m^3	1.1 kg/m^2	405.7 g/min
Average	- g	98.8 kg/m^3	1.0 kg/m^2	355.8 g/min
Standard deviation				43.3 g/min

With the made adaptions clogging of the system is avoided for this type of fibre, by removing the contraction from the chamber to the output hose the fibres will no longer accumulate in this part of the blower. Also the addition of the vibration table avoids fibre balling in the storage bucket which results in a gradual fibre input. In figure B.8(Left) a comparison is made between this test and the previous test, it can be seen that the output reduces. By increasing the hose diameter the pressure inside the hose is reduced, thus lowering the wind speed. The deviation of both tests remains more or

less the same, which shows that it is still difficult to obtain a constant output. The consistency of the output can also be analysed with respect to the time interval over which the tests are executed. In figure B.8(Right) the average results and deviation are visualised based on three different time intervals. What immediately can be seen is that the deviation for the 15 seconds time interval is larger compared to the other two intervals. This is due to the fact that a 15 second time interval is more susceptible to an error, while for a large time interval an error of 1 second is averaged out. The overall averages of the different time interval are nevertheless constant.

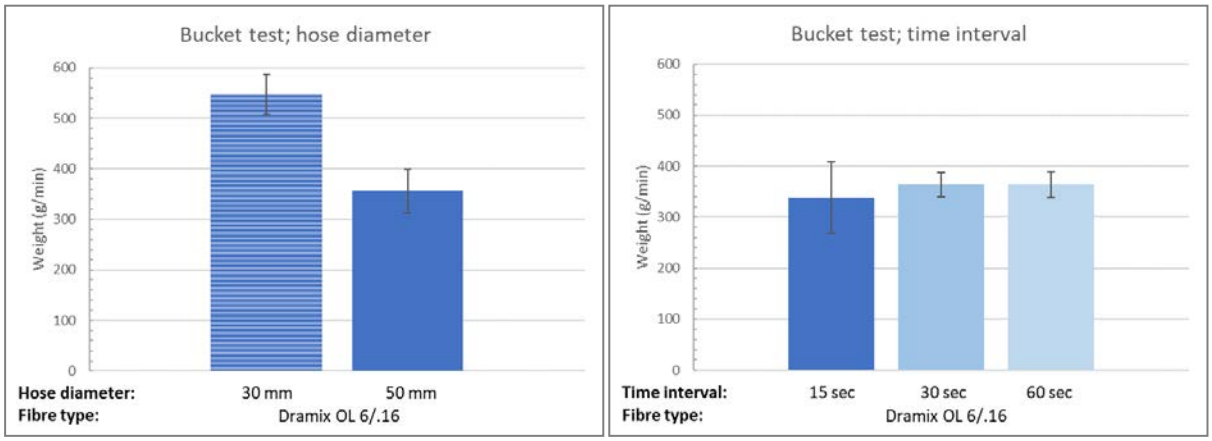

Figure B.8: *Results bucket test; Influence of hose diameter input hose (Left); Influence of time interval on consistency (Right).*

Until now the fibres are collected manually, which could be a reason for the large deviation in output. To remove this factor the hose is fixed to the vibration table by rods and is positioned in the centre of the bucket. A funnel is created in the bucket to assure that the fibres are guided to the centre of the bucket, at the location where the hose is fixed (figure B.9). For these tests two different types of fibres are used, namely 10.) Fibraflex FF/15E0 and 19.) Cem-FIL Minibars 24mm. This is done while it is expected that the structural capacity of these fibres is larger compared to the Dramix OL fibres. Another adaption which is made is the increase of the input hose from 30 millimetre to 60 millimetre. By doing so the possibility arises to use larger fibres which could also improve the structural capacity, by increasing the diameter the chance of clogging is also reduced. The results of the test are shown in the table B.7 and B.8, to start only the minimum speed setting of the blower is tested. While two new types of fibres are tested there is chosen to only perform the test for a 15 second time interval, even though it followed from the previous tests that the scatter for this interval was larger compared to the other intervals. The overall obtained average value is comparable for all tested time intervals.

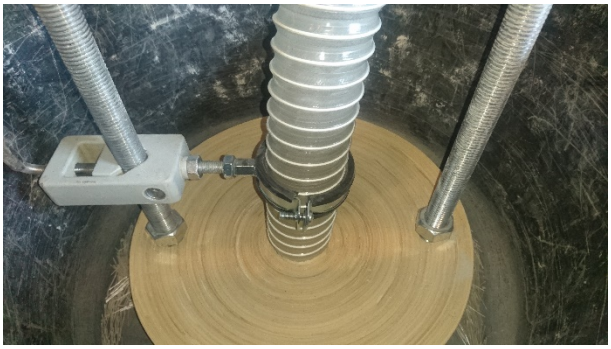

Figure B.9: *Fixation of input hose in vibration bucket.*

Table B.7: *Output blower*

Fibre type:	Fibraflex FF/15E0			
Blower setting:	Minimum; 450 Watt			
Time	**Output**	**Weight per volume**	**Weight per area**	**Output per minute**
15 sec	84.7 g	94.1 kg/m^3	0.9 kg/m^2	338.8 g/min
	80.3 g	89.2 kg/m^3	0.9 kg/m^2	321.2 g/min
	78.5 g	87.2 kg/m^3	0.9 kg/m^2	314.0 g/min
	73.7 g	81.9 kg/m^3	0.8 kg/m^2	294.8 g/min
	84.3 g	93.7 kg/m^3	0.9 kg/m^2	337.2 g/min
Average	- g	89.2 kg/m^3	0.9 kg/m^2	341.2 g/min
Standard deviation				31.8 g/min

Table B.8: *Output blower*

Fibre type:	Cem-FIL Minibars 24mm			
Blower setting:	Minimum; 450 Watt			
Time	**Output**	**Weight per volume**	**Weight per area**	**Output per minute**
15 sec	59.2 g	65.8 kg/m^3	0.6 kg/m^2	236.8 g/min
	55.3 g	61.4 kg/m^3	0.6 kg/m^2	221.2 g/min
	49.8 g	55.3 kg/m^3	0.6 kg/m^2	199.2 g/min
	49.7 g	55.2 kg/m^3	0.6 kg/m^2	198.8 g/min
	57.4 g	63.8 kg/m^3	0.6 kg/m^2	229.6 g/min
Average	- g	60.3 kg/m^3	0.6 kg/m^2	217.1 g/min
Standard deviation				17.4 g/min

By fixing the position of the input hose the output of the blower becomes more constant as can be seen from the results. A deviation of less than 10% compared to the average output can be found, which can be used as an acceptable range at this stage of the research. In figure B.11 the average results for the two types of fibres can be seen. To gain more control over the settings of the blower an energy meter is applied to obtain a more or less fixed power (figure B.10). At the start of each test the power is set to approximately 440-450 Watt, once fibres entered the chamber it could be seen that the power increased to 480-500 Watt. Also the 3.) Dramix 3D RC-4530-BL is tested to obtain a constant output, however for this fibre no constant output could be obtained. This was most likely due to the weight of a single fibre, which is about 10 times larger compared to a Fibraflex fibre for instance. By using the minimum setting of the blower the power was too low to obtain a gradual input. When the power was increased the amount of fibres inside the chamber increased, which resulted in clogging of the fibres due to the hooked-end. Although the output of the blower is more or less constant, the amount is still too large for the current application. To get a proper coverage with sufficient bond between the layers the output should be reduced with a factor of 15-25 depending on the fibre type. The exact coverage which is needed to increase the structural capacity is at this point still unknown, so it is difficult to determine the requirements of the blower. However it can be said with certainty that the output is too high at this moment for each type of fibre.

Figure B.10: *Wattage meter in order to check settings blower.*

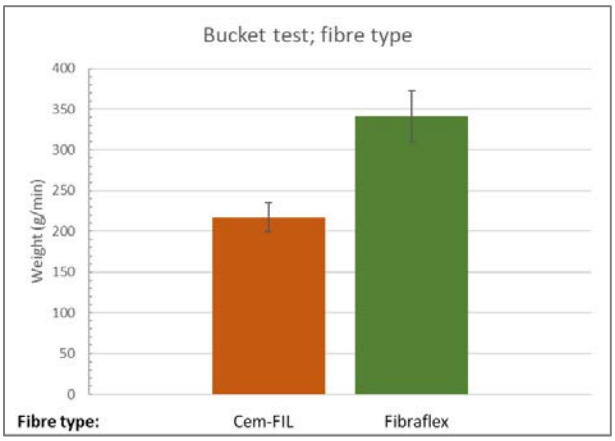

Figure B.11: *Results bucket test; Testing different fibre types.*

For the previous tests the settings of the motor were already at the minimum, thus in order to reduce the output a new motor is installed (figure B.12). This new motor is able to provide much lower wind speeds, so the output of the fibres should be reduced. For the following test there is also chosen to vary with the length of the input hose. The short hose has a length of approximately 1 metre and the long hose is about 6 metre. By enlarging the input hose the wind speed can be further reduced. To test the new motor a next test in performed, also for this test the 10.) Fibraflex FF/15E0 and 19.) Cem-FIL Minibars 24 mm are used. Two different settings are used and for both setting the hose length is varied, the results of this test can be found in table B.9 till B.14.

Figure B.12: *DC motor of blower.*

Table B.9: *Output blower*

Fibre type:	Fibraflex FF/15E0			
Blower setting:	350 Watt, Short input hose			
Time	**Output**	**Weight per volume**	**Weight per area**	**Output per minute**
15 sec	89.6 g	99.6 kg/m^3	1.0 kg/m^2	358.4 g/min
	75.6 g	84.0 kg/m^3	0.8 kg/m^2	302.4 g/min
	78.4 g	87.1 kg/m^3	0.9 kg/m^2	313.6 g/min
Average	- g	90.2 kg/m^3	0.9 kg/m^2	324.8 g/min
Standard deviation				29.6 g/min

Table B.10: *Output blower*

Fibre type:	Fibraflex FF/15E0			
Blower setting:	350 Watt, Long input hose			
Time	**Output**	**Weight per volume**	**Weight per area**	**Output per minute**
15 sec	79.8 g	88.7 kg/m^3	0.9 kg/m^2	319.2 g/min
	71.9 g	79.9 kg/m^3	0.8 kg/m^2	287.6 g/min
	51.5 g	57.2 kg/m^3	0.6 kg/m^2	206.0 g/min
	58.3 g	64.8 kg/m^3	0.6 kg/m^2	233.2 g/min
	71.3 g	79.2 kg/m^3	0.8 kg/m^2	285.2 g/min
Average	- g	74.0 kg/m^3	0.7 kg/m^2	266.2 g/min
Standard deviation				45.7 g/min

Table B.11: *Output blower*

Fibre type:	Fibraflex FF/15E0			
Blower setting:	300 Watt, Short input hose			
Time	**Output**	**Weight per volume**	**Weight per area**	**Output per minute**
15 sec	58.3 g	64.8 kg/m^3	0.6 kg/m^2	233.2 g/min
	80.2 g	89.1 kg/m^3	0.9 kg/m^2	320.8 g/min
	62.3 g	69.2 kg/m^3	0.7 kg/m^2	249.2 g/min
	72.2 g	80.2 kg/m^3	0.8 kg/m^2	288.8 g/min
	66.1 g	73.4 kg/m^3	0.7 kg/m^2	264.4 g/min
Average	- g	75.4 kg/m^3	0.8 kg/m^2	271.3 g/min
Standard deviation				34.4 g/min

Table B.12: *Output blower*

Fibre type:	Fibraflex FF/15E0			
Blower setting:	300 Watt, Long input hose			
Time	**Output**	**Weight per volume**	**Weight per area**	**Output per minute**
15 sec	47.8 g	53.1 kg/m^3	0.5 kg/m^2	191.2 g/min
	49.9 g	55.4 kg/m^3	0.6 kg/m^2	199.6 g/min
	61.5 g	68.3 kg/m^3	0.7 kg/m^2	246.0 g/min
	55.3 g	61.4 kg/m^3	0.6 kg/m^2	221.2 g/min
Average	- g	59.6 kg/m^3	0.6 kg/m^2	214.5 g/min
Standard deviation				24.5 g/min

Table B.13: *Output blower*

Fibre type:	Cem-FIL Minibars 24mm			
Blower setting:	300 Watt, Short input hose			
Time	**Output**	**Weight per volume**	**Weight per area**	**Output per minute**
15 sec	26.1 g	29.0 kg/m^3	0.3 kg/m^2	104.4 g/min
	47.1 g	52.3 kg/m^3	0.5 kg/m^2	188.4 g/min
	40.9 g	45.4 kg/m^3	0.5 kg/m^2	163.6 g/min
	31.7 g	35.2 kg/m^3	0.4 kg/m^2	126.8 g/min
	52.5 g	58.3 kg/m^3	0.6 kg/m^2	210.0 g/min
Average	- g	44.1 kg/m^3	0.4 kg/m^2	158.6 g/min
Standard deviation				43.3 g/min

Table B.14: *Output blower*

Fibre type:	Cem-FIL Minibars 24mm			
Blower setting:	300 Watt, Long input hose			
Time	**Output**	**Weight per volume**	**Weight per area**	**Output per minute**
15 sec	28.2 g	31.3 kg/m^3	0.3 kg/m^2	112.8 g/min
	30.6 g	34.0 kg/m^3	0.3 kg/m^2	122.4 g/min
	17.8 g	19.8 kg/m^3	0.2 kg/m^2	71.2 g/min
	25.9 g	28.8 kg/m^3	0.3 kg/m^2	103.6 g/min
Average	- g	28.5 kg/m^3	0.3 kg/m^2	102.5 g/min
Standard deviation				22.2 g/min

With the new motor it can be seen that the output can be further reduced by using a lower setting. The obtained output of fibres gets closer to an acceptable range which could be used in practice. In figure B.13 the average result per fibre type can be seen. By reducing the power of the blower the output of fibres is reduced as could be expected. Although a lower amount of fibres is obtained, the scatter of the results increases. Especially for the 19.) Cem-FIL Minibars an increase in scatter can be observed, this is most likely due to the weight of the fibres. Once the power is reduced the weight of a single fibre becomes more important, as the blower might not be able to transfer the fibre. By increasing the length of the input hose the output of fibres is reduced in all cases. Due to the longer length the power at the input hose reduces, thus resulting in a lower amount of fibres. When the deviation for these tests is observed no unambiguous result can be found. In some cases the long hose resulted in a large scatter while for the Cem-FIL fibres the shorter hose resulted in a larger scatter.

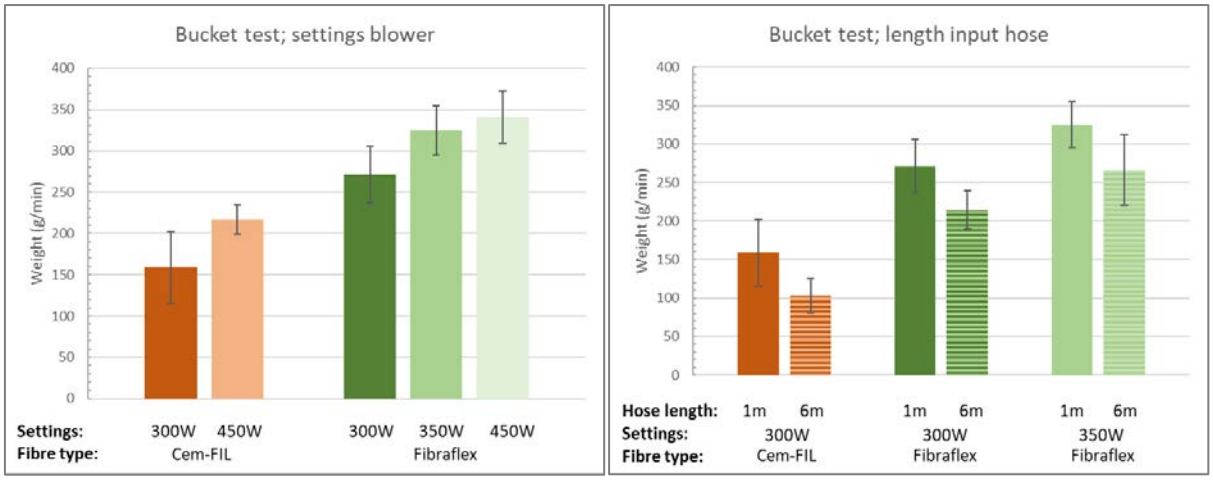

Figure B.13: *Results bucket test; Variation of settings blower (Left); Influence of length input hose (Right).*

B.2.2 CHAMBER TEST

In the previous tests the blower was tested separately from the robot arm, however in practice the hose will move. This movement should also be taken into account while this might affect the output of the blower. So for the next test the output hose is fixed to the robot arm, which moves over a simple print path. To catch the fibres a box is made with several compartments in which the fibres will be collected (figure B.14), after weighing the output the results can be compared with the stationary tests which are executed earlier. For both fibre types multiple tests are performed, the obtained results can be found in table B.15 and B.16. All compartments have a length of approximately of 1 metre, which is equal to 10 seconds with the current printer speed.

Figure B.14: *Set-up of chamber test.*

Table B.15: *Output blower*

Fibre type:	Cem-FIL Minibars 24mm			
Blower setting:	300 Watt			
Run	**Output**	**Weight per volume**	**Weight per area**	**Output per minute**
1	32.2 g	53.7 kg/m^3	0.5 kg/m^2	193.2 g/min
	28.6 g	47.7 kg/m^3	0.5 kg/m^2	171.6 g/min
	15.5 g	25.8 kg/m^3	0.3 kg/m^2	93.0 g/min
	- g	- kg/m^3	- kg/m^2	- g/min
2	37.7 g	62.8 kg/m^3	0.6 kg/m^2	226.2 g/min
	39.7 g	66.2 kg/m^3	0.7 kg/m^2	238.2 g/min
	51.3 g	85.5 kg/m^3	0.9 kg/m^2	307.8 g/min
	44.8 g	74.7 kg/m^3	0.7 kg/m^2	268.8 g/min
3	45.1 g	75.2 kg/m^3	0.8 kg/m^2	270.6 g/min
	28.3 g	47.2 kg/m^3	0.5 kg/m^2	169.8 g/min
	24.3 g	40.5 kg/m^3	0.4 kg/m^2	145.8 g/min
	- g	- kg/m^3	- kg/m^2	- g/min
4	49.3 g	82.2 kg/m^3	0.8 kg/m^2	295.8 g/min
	47.7 g	79.5 kg/m^3	0.8 kg/m^2	286.2 g/min
	16.5 g	27.5 kg/m^3	0.3 kg/m^2	99.0 g/min
	33.6 g	56.0 kg/m^3	0.6 kg/m^2	201.6 g/min
Average	- g	58.9 kg/m^3	0.6 kg/m^2	212.0 g/min
Standard deviation				70.4 g/min

Table B.16: *Output blower*

Fibre type:	Fibraflex FF/15E0			
Blower setting:	300 Watt			
Run	**Output**	**Weight per volume**	**Weight per area**	**Output per minute**
1	57.9 g	96.4 kg/m^3	1.0 kg/m^2	315.5 g/min
	56.8 g	94.7 kg/m^3	0.9 kg/m^2	309.9 g/min
	53.2 g	88.7 kg/m^3	0.9 kg/m^2	290.3 g/min
	54.1 g	90.2 kg/m^3	0.9 kg/m^2	295.3 g/min
2	41.6 g	69.4 kg/m^3	0.7 kg/m^2	227.1 g/min
	41.7 g	69.4 kg/m^3	0.7 kg/m^2	227.2 g/min
	41.0 g	68.4 kg/m^3	0.7 kg/m^2	223.8 g/min
	35.7 g	59.4 kg/m^3	0.6 kg/m^2	194.5 g/min
Average	- g	79.6 kg/m^3	0.8 kg/m^2	260.5 g/min
Standard deviation				47.1 g/min

For these tests a large deviation can be observed between the amount of fibres per chamber. This is most likely due to the longer time interval for which the test was executed. This could lead to fibre balling inside the hose and sometimes even clogging of the device which occurred in two runs for the Cem-FIL Minibars. In figure B.15 a comparison is made with the stationary bucket test which is performed earlier. For the Cem-FIL Minibars an increase in output can be found for the chamber test, this could be due to the movement of the hose. In a stationary test the hose remains curved, once attached to the robot arm the hose stretches several times which reduces the resistance inside the hose. The standard deviation of the chamber test is slightly increased, this is also most likely due to the movement of the robot arm. Although the hose is stretched several times, in some cases the hose is bent. Hereby increasing the resistance inside the hose again, thus a larger scatter is obtained which is related to the position of the robot arm. For the Fibraflex fibre on the other hand no difference can be found between the output of the bucket test and the chamber test. Here a slight increase in standard deviation can be found for the chamber test, which could be due to the movement of the hose. Although it is tried to perform the tests in the same manner, a human error cannot be avoided in the current stadium of the development. It is likely that different parameters play an important role with regard to the output of the blower, like position of the hose, quantity of fibre input, etc.

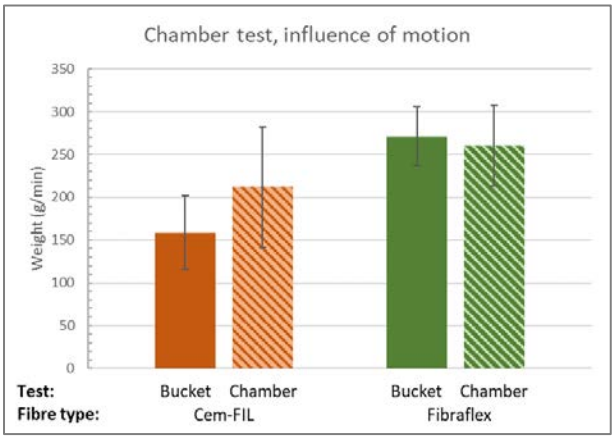

Figure B.15: *Chamber test; Influence of motion robot arm.*

Not all fibres which are transferred by the blower will land on the concrete layer, the output has a certain spread (see figure B.16). In the previous test all fibres were considered, however this number cannot be taken as the fibre ratio. To obtain a more realistic value to amount of fibres which land next to the layer should be subtracted from the total number to obtain the real value of the fibre ratio. To

do this the same test is done over again, only this time a concrete layer is printed simultaneously. By doing so the fibres which land on the concrete layer can be separated from the fibres which land next to the layer. The 10.) Fibraflex FF/15E0 and 19.) Cem-FIL Minibars 24mm are used to test what the ratio will be with the current settings, the results can be found in table B.17 and B.18. The amounts found in these tests are the weight of the fibres next to the layer, thus not the total output of the blower.

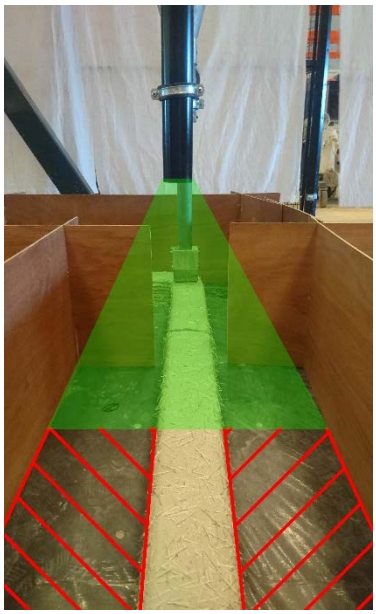

Figure B.16: *Spread of fibre during printing; Schematic flow of fibres (Green); Unusable fibres next to print path (Red).*

Table B.17: *Output blower*

Fibre type:	Fibraflex FF/15E0			
Blower setting:	300 Watt			
Time	**Output**	**Weight per volume**	**Weight per area**	**Output per minute**
10 sec	23.5 g	39.1 kg/m^3	0.4 kg/m^2	140.8 g/min
	20.4 g	34.1 kg/m^3	0.3 kg/m^2	122.6 g/min
	20.6 g	34.3 kg/m^3	0.3 kg/m^2	123.4 g/min
	18.8 g	31.3 kg/m^3	0.3 kg/m^2	112.8 g/min
Average	- g	34.7 kg/m^3	0.3 kg/m^2	124.9 g/min
Standard deviation				11.6 g/min

Table B.18: *Output blower*

Fibre type:	Cem-FIL Minibars 24mm			
Blower setting:	300 Watt			
Time	**Output**	**Weight per volume**	**Weight per area**	**Output per minute**
10 sec	15.5 g	25.9 kg/m^3	0.3 kg/m^2	93.1 g/min
	14.1 g	23.5 kg/m^3	0.2 kg/m^2	84.5 g/min
	16.1 g	26.8 kg/m^3	0.3 kg/m^2	96.4 g/min
	16.4 g	27.3 kg/m^3	0.3 kg/m^2	98.1 g/min
Average	- g	25.8 kg/m^3	0.3 kg/m^2	93.0 g/min
Standard deviation				6.1 g/min

For both fibre types a standard deviation can be found which is less than 10%, thus a relative constant output is obtained. During the tests the hose is guided to make sure no excessive bending occurred which could result in clogging of the device. This resulted in a relatively large standard deviation in the previous chamber test. From a visual analysis on the output of the 10.) Fibraflex FF/15E0, it can be said that a more or less uniform distribution is obtained. Although the amount of fibres resulted in fracture of the interface between the layers as can be seen from figure B.17. Due to the large surface area of this fibre type a large coverage is obtained which resulted in a significant reduction of bond in between the layers. Multiple samples broke in the interface once they were removed from the printing table, for which a smooth crack in the interface can be observed. From the obtained results it can be concluded that the output is too high and further adaptions need to be made to lower this output. Also for the 19.) Cem-FIL Minibars 24mm a uniform distribution is observed from a visual analysis. The weight per minute obtained from this fibre type is comparable to that of the Fibraflex fibres. However a single glass fibre is heavier compared to the steel fibre, thus the total number of fibres is lower. This can also be seen in the fibre distribution in figure B.18, here it is assumed that the bond capacity between the layers is still sufficient.

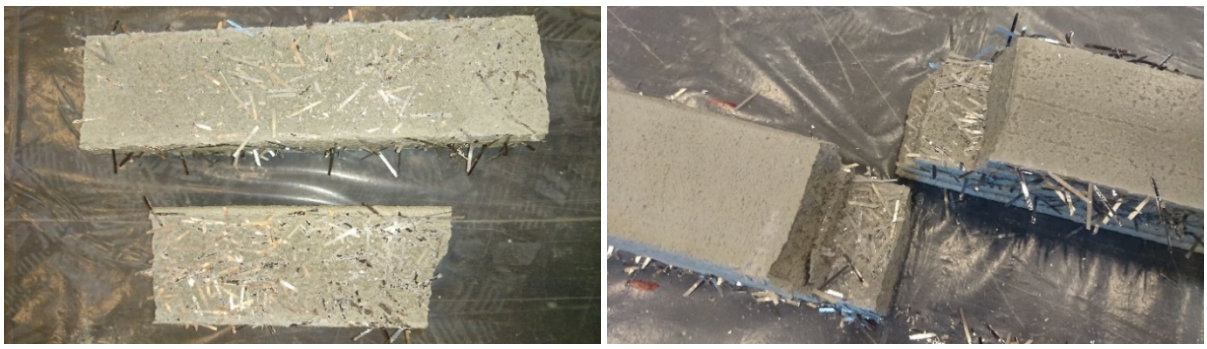

Figure B.17: *Separation of layers due to reduction bond strength for Fibraflex FF/15E0.*

Figure B.18: *Fibre distribution over print path for Cem-FIL Minibars 24mm.*

If the results are compared with the chamber test performed earlier, the total number of fibres can be subtracted by the number of fibres next to the layer (figure B.19). From this an approximation can be made of the amount of fibres inside the concrete element. The total weight of the Cem-FIL fibres is on average 212.0 g/min, from this it can be concluded that approximately 118.9 g/min is deposited on top of the concrete layer. Thus about half of the fibres which are deposited by the fibre blower are lost while they are blown next to the concrete. For the Fibraflex fibres a higher total amount of fibres is obtained, 260.5 g/min. Also for this case about half of the fibres is deposited next to the concrete layers, 135.6 g/min is found for this test. Further testing needs to be conducted while these tests are conducted on different dates. The standard deviation of the test for which the total number of fibres is obtained is relatively high. Several parameters are of importance for the exact output, thus it cannot be said with certainty that the total output of the second chamber test resulted in an equal number.

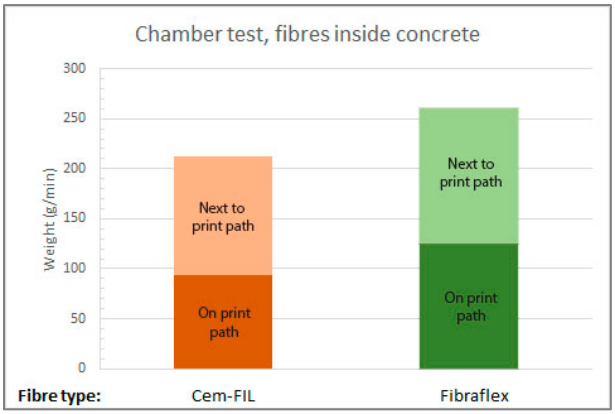

Figure B.19: *Chamber test; spread of output blower.*

By using the blower the fibres are sprinkled over the concrete layers, however due to the spread of the blower not all fibres will land on top of the layer. It can be that a fibre is partly sticking out from a concrete layer or that the fibres are blown to the sides of a filament (figure B.20). These fibres will play little to no influence on the structural behaviour of the concrete element. However they are of importance for the visual appearance of the element, which can be unsuited for application in practice. Also the environmental conditions might play a role while a steel fibre might start to corrode if subjected to a large humidity. If the fibres are added by the current device a surface treatment is required in order to use the concrete element in practice. For now the output of the blower is random, to avoid fibres on the side of the filaments control needs to be gained over this output. Either by controlling the flow of air at the end of the nozzle or by collecting the fibres which land next to the layer before the land on the print table.

Figure B.20: *Fibres on sides of printed element.*

APPENDIX C – IMAGE ANALYSIS

C.1 RESULTS

By using the program MATLAB an image analysis is performed to predict the distribution of the fibres over the print path. For all fibre ratios 10 random distributions are taken and analysed, only in the case for Cem-FIL Minibars 24mm ratio C, 3 random distributions are taken. This is while this ratio is obtained by using the blower. In the following tables the overall results can be found, in table C.1 the average coverage of the concrete layer is found. Table C.2 shows the average number of fibres per cross section, which is taken on three positions per image. And finally in table C.3 the orientation of the fibres is shown, here a horizontal position (0^o) represents a fibre which is orientated parallel to the print direction. It should be noted that with the used code the contrast between the fibres and background (concrete) is of great importance. This contrast should be large enough to make a distinction between the fibres and the concrete. For almost all fibre ratios a white or black background is chosen, for Cem-FIL Minibars 24mm ratio C the background consisted of concrete (grey), which did show in some cases insufficient contrast.

Table C.1: *Fibre coverage*

Fibre type	Ratio		Coverage	Standard deviation
Cem-FIL Minibars 24mm	(A)	0.0632 Kg/m^2	6.6 %	(0.5 %)
	(B)	0.0842 Kg/m^2	8.1 %	(0.3 %)
	(C)	0.2485 Kg/m^2	17.9 %	(2.5 %)
Dramix 3D RC-4530-BL	(A)	0.1559 Kg/m^2	8.0 %	(0.5 %)
	(B)	0.2227 Kg/m^2	9.9 %	(0.5 %)
Fibraflex FF/20L6	(A)	0.0259 Kg/m^2	13.7 %	(0.5 %)
	(B)	0.0388 Kg/m^2	17.7 %	(0.4 %)

Table C.2: *Fibre per cross-section*

Fibre type	Ratio		No. of fibres	Standard deviation
Cem-FIL Minibars 24mm	(A)	0.0632 Kg/m^2	3	(1.20)
	(B)	0.0842 Kg/m^2	4	(1.35)
	(C)	0.2485 Kg/m^2	6	(3.71)
Dramix 3D RC-4530-BL	(A)	0.1559 Kg/m^2	2	(0.94)
	(B)	0.2227 Kg/m^2	4	(1.03)
Fibraflex FF/20L6	(A)	0.0259 Kg/m^2	4	(1.55)
	(B)	0.0388 Kg/m^2	5	(1.31)

Table C.3: *Fibre orientation*

Fibre type	Ratio	Angle	No. of fibres	Standard deviation
Cem-FIL Minibars 24mm	(A) 0.0632 Kg/m^2	0° - 15°	5.8	(2.3)
		15° - 30°	5.8	(1.5)
		30° - 60°	11.3	(3.2)
		60° - 90°	7.1	(2.1)
	(B) 0.0842 Kg/m^2	0° - 15°	9.6	(2.7)
		15° - 30°	7.3	(1.9)
		30° - 60°	13.5	(3.3)
		60° - 90°	10.5	(2.7)
	(C) 0.2485 Kg/m^2	0° - 15°	22.7	(6.4)
		15° - 30°	22.3	(4.7)
		30° - 60°	37.0	(5.2)
		60° - 90°	36.0	(6.2)
Dramix 3D RC-4530-BL	(A) 0.1559 Kg/m^2	0° - 15°	5.5	(2.1)
		15° - 30°	5.1	(2.3)
		30° - 60°	7.6	(2.2)
		60° - 90°	2.8	(1.1)
	(B) 0.2227 Kg/m^2	0° - 15°	8.7	(1.7)
		15° - 30°	7.0	(2.6)
		30° - 60°	8.5	(2.3)
		60° - 90°	5.1	(1.6)
Fibraflex FF/20L6	(A) 0.0259 Kg/m^2	0° - 15°	9.9	(3.2)
		15° - 30°	10.5	(2.6)
		30° - 60°	12.7	(4.8)
		60° - 90°	9.0	(2.1)
	(B) 0.0388 Kg/m^2	0° - 15°	15.3	(3.1)
		15° - 30°	11.5	(4.0)
		30° - 60°	19.0	(3.8)
		60° - 90°	13.2	(4.8)

C.2 MATLAB CODE

```
% Load image
clear all
close all

base = 'directory path';
img = fullfile(base,'File name');
RGB = imread(img);

% Binary image
BW = rgb2gray(RGB);
BW2 = imbinarize(BW);
figure
imshow(BW2)


% Remove noise
h = fspecial('motion',25,50);
filteredBW2 = imfilter(BW2, h);
figure
imshow(filteredBW2)

% Calculate fibre percentage
percentageBlack = (nnz(filteredBW2)/numel(filteredBW2))*100;
figure
imshow(filteredBW2)
title(['Fibre coverage is ' num2str(percentageBlack) '%.'])

% Detect straight lines
close all
[H,T,R] = hough(filteredBW2);
imshow(H,[],'XData',T,'YData',R,'InitialMagnification','fit');
xlabel('\theta'), ylabel('\rho');
axis on, axis normal, hold on;

P = houghpeaks(H,150,'threshold',ceil(0.3*max(H(:))));
x = T(P(:,2));
y = R(P(:,1));
plot(x,y,'s','color','white');

lines = houghlines(filteredBW2,T,R,P,'FillGap',50,'MinLength',350);
figure
imshow(filteredBW2), hold on
max_len = 0;
```

```
for k = 1:length(lines)
        xy = [lines(k).point1; lines(k).point2];
        plot(xy(:,1),xy(:,2),'LineWidth',2,'Color','green');
        plot(xy(1,1),xy(1,2),'x','LineWidth',2,'Color','yellow');
        plot(xy(2,1),xy(2,2),'x','LineWidth',2,'Color','red');
end

% Rewrite coordinates matrix
StartPoint = [];
for k = 1:length(lines)
        StartPoint = [StartPoint; reshape(lines(k).point1,2,numel(lines(k).point1)/2)];
end

EndPoint = [];
for k = 1:length(lines)
        EndPoint = [EndPoint; reshape(lines(k).point2,2,numel(lines(k).point2)/2)];
end

Orientation = [];
for k = 1:length(lines)
        Orientation = [Orientation; reshape(lines(k).theta,1,numel(lines(k).theta/1)]
end

Coordinates = [StartPoint, Endpoint, Orientation];

% If houghlines is unable to detect correct lines they can be selected manually
imshow(RGB)
[xi,yi] = getpts;

Coordinates1 = [xi,yi];
```

APPENDIX D – ANALYTICAL MODEL

D.1. VALIDATION ANALYTICAL MODEL

To validate the analytical model a visual analysis is made for all cracked sections, here the number of fibres per interface is manually counted and given in table D.1. By implementing the number of fibres into the model a distribution factor is determined. A comparison is made between the stress obtained from the experimental curve and the analytical model, this is done at five points on the graph. Overall a good agreement is found between the experimental and analytical curves. In some cases the comparison at a vertical deflection of 1.5 millimetre is neglected, this gave unrealistic numbers is some cases. In figure D.1 till D.4 all conducted experiments are shown, the comparison made between the stress can be found in table D.2 till D.5.

Table D.1: *Manual count of fibres in cracked section per interface*

Sample	**Interface**			
	1	**2**	**3**	**4**
F1_B_6	0	3	0	2
F1_B_7	1	0	1	1
F1_B_8	2	1	0	0
F1_B_9	2	0	0	0
F1_B_10	1	0	0	0
F1_C_1	0	1	5	3
F1_C_2	3	4	0	4
F1_C_3	3	3	0	0
F1_C_4	2	2	2	4
F2_B_6	2	0	1	2
F2_B_7	0	1	1	0
F2_B_8	2	5	1	1
F2_B_9	2	0	3	1
F2_B_10	1	1	2	0
F3_B_6	2	1	2	2
F3_B_7	3	0	2	2
F3_B_8	0	0	0	0
F3_B_9	0	2	1	0
F3_B_10	1	3	0	3

Cem-FIL Minibars 24mm, ratio B = 0.0842 kg/m^2

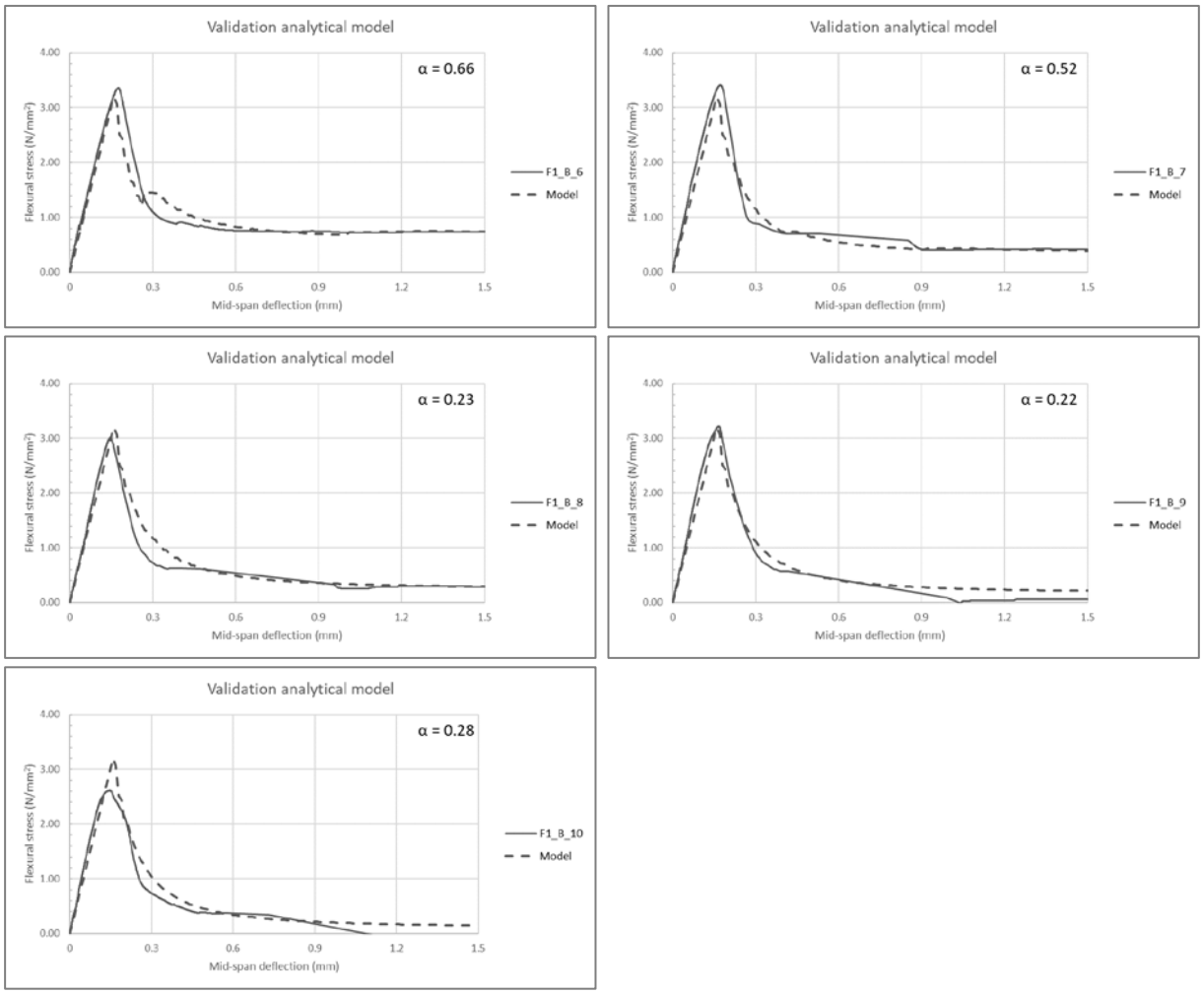

Figure D.1: *Comparison of analytical model with experimental curves, Cem-FIL Minibars, Down-flow nozzle.*

Table D.2: *Comparison between experimental curve and analytical model, Cem-FIL Minibars 24mm*

Test sample	**Deflection** (mm)	**Experimental results** (N/mm^2)	**Analytical model** (N/mm^2)	**Difference** (%)
F1_B_6	0.1	2.17	2.02	7.11
α = 0.66	0.2	2.92	2.43	16.60
	0.3	1.10	1.46	32.53
	0.9	0.75	0.70	6.85
	1.5	0.74	0.74	0.68
F1_B_7	0.1	2.31	2.02	12.77
α = 0.52	0.2	3.27	2.43	25.63
	0.3	0.90	1.19	32.20
	0.9	0.42	0.42	0.34
	1.5	0.41	0.40	4.07
F1_B_8	0.1	2.24	2.02	9.86
α = 0.23	0.2	2.03	2.43	19.94
	0.3	0.74	1.28	73.66
	0.9	0.62	0.36	41.28
	1.5	0.29	0.29	1.01
F1_B_9	0.1	2.33	2.02	13.37
α = 0.22	0.2	2.81	2.43	13.38
	0.3	0.92	1.17	26.52
	0.9	0.57	0.28	50.61
	~~1.5~~	~~0.06~~	~~0.21~~	~~249.81~~
F1_B_10	0.1	2.24	2.02	9.82
α = 0.28	0.2	2.15	2.43	13.13
	0.3	0.74	1.12	51.21
	0.9	0.35	0.22	36.76
	~~1.5~~	~~0.00~~	~~0.15~~	~~572.66~~

Cem-FIL Minibars 24mm, ratio C = 0.2485 kg/m^2

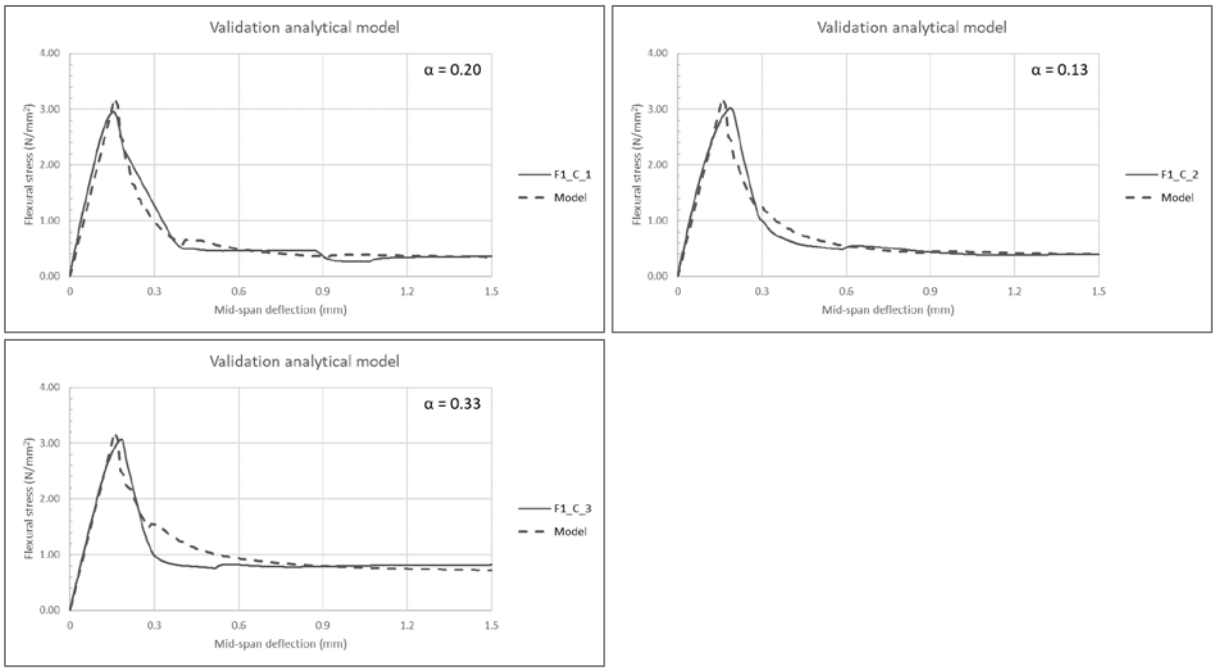

Figure D.2: *Comparison of analytical model with experimental curves, Cem-FIL Minibars, Proof of concept.*

Table D.3: *Comparison between experimental curve and analytical model, Cem-FIL Minibars 24mm*

Test sample	**Deflection** (mm)	**Experimental results** (N/mm^2)	**Analytical model** (N/mm^2)	**Difference** (%)
F1_C_1	0.1	2.31	2.02	12.44
α = 0.20	0.2	2.31	2.43	5.37
	0.3	2.31	1.05	54.38
	0.9	0.37	0.37	0.53
	1.5	0.36	0.35	2.56
F1_C_2	0.1	2.10	2.02	3.85
α = 0.13	0.2	2.94	2.43	17.37
	0.3	1.01	1.30	28.71
	0.9	0.44	0.42	3.92
	1.5	0.40	0.40	0.78
F1_C_3	0.1	2.07	2.02	2.30
α = 0.33	0.2	2.88	2.43	15.46
	0.3	1.00	1.55	55.57
	0.9	0.79	0.80	0.90
	1.5	0.82	0.72	11.72

Dramix 3D RC-4530-BL, ratio B = ratio B = 0.2227 kg/m^2

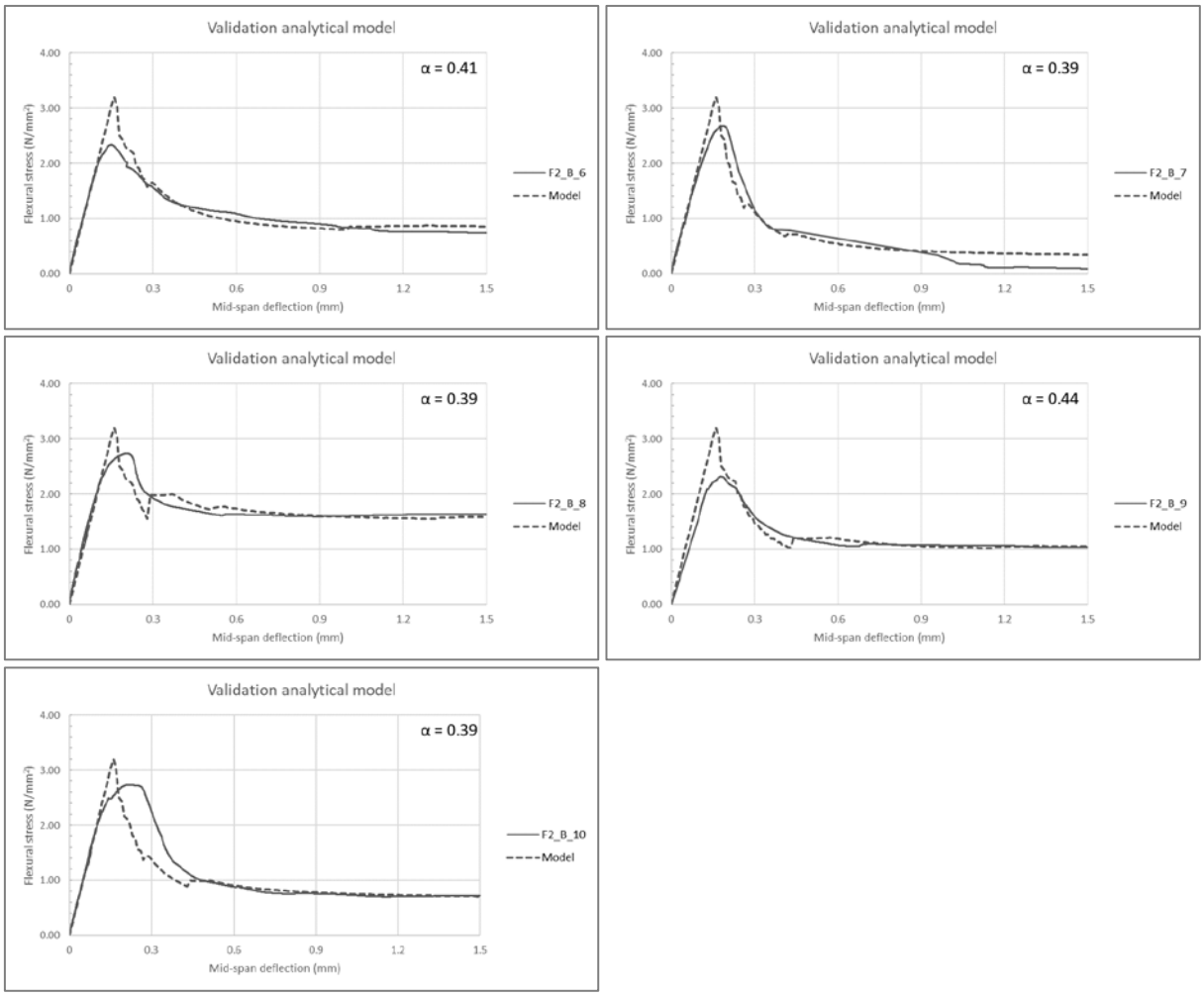

Figure D.3: *Comparison of analytical model with experimental curves, Dramix 3D RC-4530-BL, Down-flow nozzle.*

Table D.4: *Comparison between experimental curve and analytical model, Dramix 3D RC-4530-BL*

Test sample	**Deflection** (mm)	**Experimental results** (N/mm^2)	**Analytical model** (N/mm^2)	**Difference** (%)
F2_B_6	0.1	1.95	2.02	3.66
α = 0.41	0.2	2.05	2.43	18.84
	0.3	1.57	1.56	0.53
	0.9	0.90	0.76	15.97
	1.5	0.57	0.80	6.68
F2_B_7	0.1	1.87	2.02	8.07
α = 0.39	0.2	2.62	2.43	7.31
	0.3	1.29	1.19	8.40
	0.9	0.78	0.42	46.88
	~~1.5~~	~~0.09~~	~~0.35~~	~~278.77~~
F2_B_8	0.1	2.06	2.02	2.06
α = 0.39	0.2	2.74	2.43	11.06
	0.3	1.93	1.99	3.10
	0.9	1.60	1.61	0.74
	1.5	1.64	1.59	2.91
F2_B_9	0.1	1.59	2.02	27.34
α = 0.44	0.2	2.23	2.43	9.27
	0.3	1.59	1.60	0.22
	0.9	1.08	1.06	1.91
	1.5	1.04	1.05	0.97
F2_B_10	0.1	1.97	2.02	2.66
α = 0.39	0.2	2.72	2.43	10.67
	0.3	2.25	1.44	36.06
	0.9	0.76	0.78	2.81
	1.5	0.72	0.71	0.86

Fibraflex FF/20L6, ratio B = 0.0388 kg/m^2

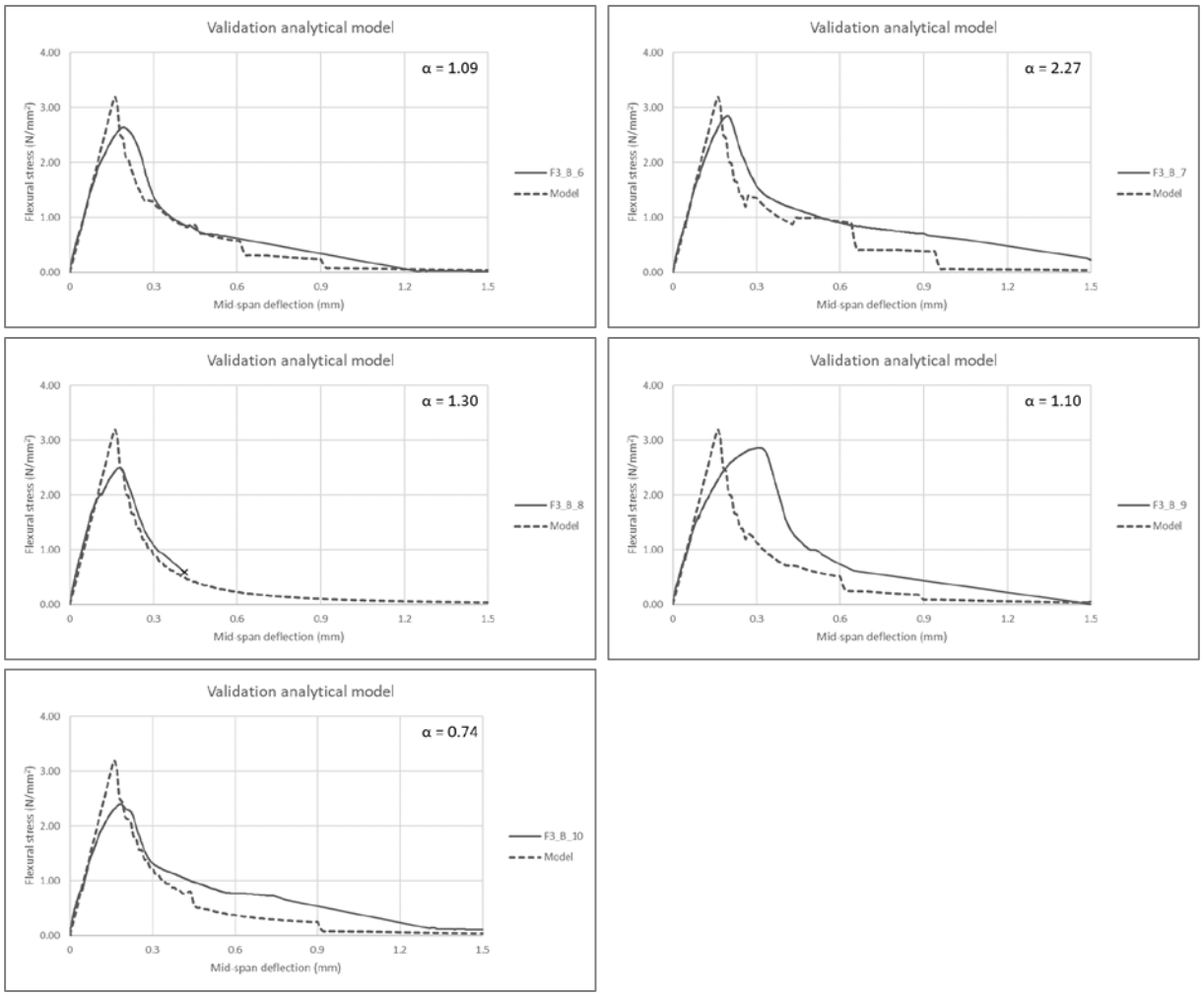

Figure D.4: *Comparison of analytical model with experimental curves, Fibraflex FF/20L6, Down-flow nozzle.*

Table D.5: *Comparison between experimental curve and analytical model, Fibraflex FF/20L6*

Test sample	**Deflection** (mm)	**Experimental results** (N/mm^2)	**Analytical model** (N/mm^2)	**Difference** (%)
F3_B_6	0.1	1.89	2.02	7.11
α = 1.09	0.2	2.62	2.43	7.29
	0.3	1.39	1.39	0.45
	0.9	0.66	0.28	57.51
	~~1.5~~	~~0.02~~	~~0.10~~	~~474.72~~
F3_B_7	0.1	1.85	2.02	9.19
α = 2.27	0.2	2.84	2.43	1434
	0.3	1.58	1.82	15.28
	0.9	0.70	0.39	44.69
	1.5	0.23	0.17	24.37
F3_B_8	0.1	1.94	2.02	4.21
α = 1.30	0.2	2.32	2.43	5.04
	0.3	1.10	1.02	7.34
	0.9	-	-	-
	1.5	-	-	-
F3_B_9	0.1	1.69	2.02	19.78
α = 1.10	0.2	2.55	2.43	4.73
	0.3	2.85	1.21	57.49
	0.9	0.62	0.12	80.70
	1.5	0.05	0.04	30.34
F3_B_10	0.1	1.76	2.02	14.87
α = 0.74	0.2	2.34	2.43	4.15
	0.3	1.32	1.24	6.15
	0.9	0.65	0.16	75.39
	1.5	0.11	0.11	0.04

APPENDIX E – DIMENSIONS

The data obtained from the Instron bench is load vs. deflection. To translate the load into a stress the dimensions of the test samples are needed. All samples are measured using a calliper, at the start of the paragraph a sketch is given to indicate at which location the measurements are taken. All data is given in the following tables, the average values are taken into account to calculate the stresses in the report.

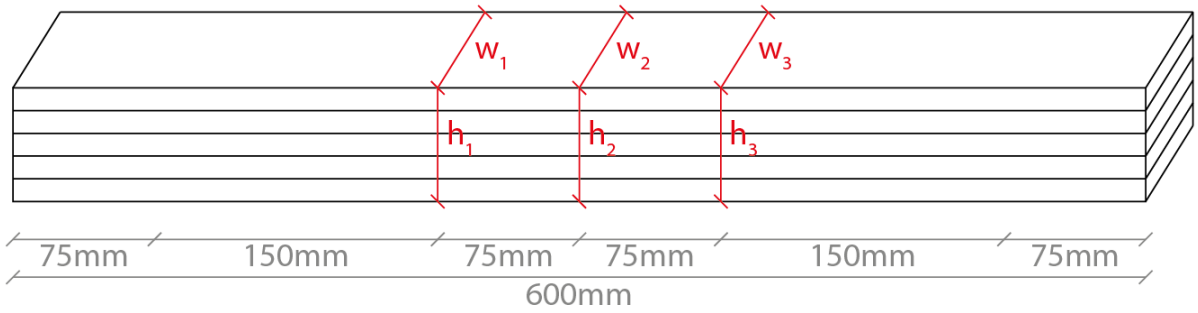

Figure E.1: *Dimensions of four-point bending test.*

E.1. HYBRID NOZZLE

Plain concrete

Table E.1: *Dimensions; plain concrete, ratio A*

Label	Height (mm)				Width (mm)			
	h_1	h_2	h_3	Average	w_1	w_2	w_3	Average
F0_A_1	61.71	62.10	62.38	62.06	41.04	40.61	40.24	40.63
F0_A_2	61.10	61.34	61.17	61.20	40.47	40.38	39.94	40.26
F0_A_3	58.71	59.39	59.58	59.23	38.70	38.62	38.69	38.67
F0_A_4	60.14	60.28	59.54	59.99	39.31	39.26	39.00	39.19
F0_A_5	60.40	60.57	60.26	60.41	40.31	40.37	40.48	40.39
F0_A_6	60.32	60.54	60.48	60.45	40.20	40.32	40.64	40.39

Table E.2: *Data; plain concrete, ratio A*

Label	Nozzle type	Print date	Test date	Hardening time (days)
F0_A_1	Hybrid nozzle	21/11/2018	28/11/2018	7
F0_A_2	Hybrid nozzle	30/11/2018	07/12/2018	7
F0_A_3	Hybrid nozzle	05/12/2018	12/12/2018	7
F0_A_4	Hybrid nozzle	05/12/2018	12/12/2018	7
F0_A_5	Hybrid nozzle	30/11/2018	07/12/2018	7
F0_A_6	Hybrid nozzle	30/11/2018	07/12/2018	7

Cem-FIL Minibars 24mm, ratio A = 0.0632 kg/m^2

Table E.3: *Dimensions; Cem-FIL Minibars 24mm, ratio A = 0.0632 kg/m^2*

Label	Height (mm)				Width (mm)			
	h_1	h_2	h_3	Average	w_1	w_2	w_3	Average
F1_A_1	60.25	59.89	60.06	60.07	40.44	40.38	39.94	40.25
F1_A_2	60.71	60.17	60.28	60.39	40.76	40.77	40.73	40.75
F1_A_3	58.19	58.25	58.96	58.47	40.85	40.92	41.09	40.95
F1_A_4	59.26	58.90	58.96	59.04	40.13	40.91	41.14	40.73
F1_A_5	59.40	59.97	60.03	59.80	41.18	40.71	40.00	40.63

Table E.4: *Data; Cem-FIL Minibars 24mm, ratio A = 0.0632 kg/m^2*

Label	Nozzle type	Print date	Test date	Hardening time (days)
F1_A_1	Hybrid nozzle	30/11/2018	07/12/2018	7
F1_A_2	Hybrid nozzle	30/11/2018	07/12/2018	7
F1_A_3	Hybrid nozzle	30/11/2018	07/12/2018	7
F1_A_4	Hybrid nozzle	30/11/2018	07/12/2018	7
F1_A_5	Hybrid nozzle	30/11/2018	07/12/2018	7

Dramix 3D RC-4530-BL, ratio A = 0.1559 kg/m^2

Table E.5: *Dimensions; Dramix 3D RC-4530-BL, ratio A = 0.1559 kg/m^2*

Label	Height (mm)				Width (mm)			
	h_1	h_2	h_3	Average	w_1	w_2	w_3	Average
F2_A_1	59.95	59.98	59.29	59.74	39.21	39.25	39.02	39.16
F2_A_2	59.40	59.08	59.07	59.18	37.89	37.72	37.51	37.71
F2_A_3	59.23	58.81	58.54	58.86	38.54	38.64	38.69	38.62
F2_A_4	58.93	58.68	58.21	58.61	38.71	38.66	38.44	38.60
F2_A_5	59.76	59.60	59.61	59.66	39.21	39.22	38.88	39.10

Table E.6: *Data; Dramix 3D RC-4530-BL, ratio A = 0.1559 kg/m^2*

Label	Nozzle type	Print date	Test date	Hardening time (days)
F2_A_1	Hybrid nozzle	05/12/2018	12/12/2018	7
F2_A_2	Hybrid nozzle	05/12/2018	12/12/2018	7
F2_A_3	Hybrid nozzle	05/12/2018	12/12/2018	7
F2_A_4	Hybrid nozzle	05/12/2018	12/12/2018	7
F2_A_5	Hybrid nozzle	05/12/2018	12/12/2018	7

Dramix 3D RC-4530-BL, ratio B = 0.2227 kg/m^2

Table E.7: *Dimensions; Dramix 3D RC-4530-BL, ratio B = 0.2227 kg/m^2*

Label	Height (mm)				Width (mm)			
	h_1	h_2	h_3	Average	w_1	w_2	w_3	Average
F2_B_1	61.13	61.42	61.87	61.47	38.59	38.57	38.49	38.55
F2_B_2	60.37	60.51	60.71	60.53	40.15	40.04	39.97	40.05
F2_B_3	60.93	60.61	60.34	60.63	40.22	40.37	40.12	40.24
F2_B_4	61.42	61.15	60.76	61.11	39.94	39.98	40.17	40.03
F2_B_5	60.86	61.13	61.44	61.14	40.15	40.04	39.74	39.98

Table E.8: *Data; Dramix 3D RC-4530-BL, ratio B = 0.2227 kg/m^2*

Label	Nozzle type	Print date	Test date	Hardening time (days)
F2_B_1	Hybrid nozzle	05/12/2018	12/12/2018	7
F2_B_2	Hybrid nozzle	05/12/2018	12/12/2018	7
F2_B_3	Hybrid nozzle	05/12/2018	12/12/2018	7
F2_B_4	Hybrid nozzle	05/12/2018	12/12/2018	7
F2_B_5	Hybrid nozzle	05/12/2018	12/12/2018	7

Fibraflex FF/20L6, ratio A = 0.0259 kg/m^2

Table E.9: *Dimensions; Fibraflex FF/20L6, ratio A = 0.0259 kg/m^2*

Label	Height (mm)				Width (mm)			
	h_1	h_2	h_3	Average	w_1	w_2	w_3	Average
F3_A_1	62.21	62.47	62.71	62.46	41.07	41.84	42.26	42.72
F3_A_2	59.95	60.53	60.61	60.36	40.86	41.38	41.77	41.34
F3_A_3	62.06	62.54	62.85	62.48	40.98	41.80	42.56	41.78
F3_A_4	63.02	62.59	62.11	62.57	41.60	41.01	40.73	41.11
F3_A_5	62.23	62.28	62.50	62.34	40.68	41.05	41.46	41.06

Table E.10: *Data; Fibraflex FF/20L6, ratio A = 0.0259 kg/m^2*

Label	Nozzle type	Print date	Test date	Hardening time (days)
F3_A_1	Hybrid nozzle	30/11/2018	07/12/2018	7
F3_A_2	Hybrid nozzle	30/11/2018	07/12/2018	7
F3_A_3	Hybrid nozzle	30/11/2018	07/12/2018	7
F3_A_4	Hybrid nozzle	30/11/2018	07/12/2018	7
F3_A_5	Hybrid nozzle	30/11/2018	07/12/2018	7

Fibraflex FF/20L6, ratio B = 0.0388 kg/m^2

Table E.11: *Dimensions; Fibraflex FF/20L6, ratio B = 0.0388 kg/m^2*

Label	Height (mm)				Width (mm)			
	h_1	h_2	h_3	Average	w_1	w_2	w_3	Average
F3_B_1	60.50	60.48	60.58	60.52	39.20	39.72	40.03	39.65
F3_B_2	57.20	59.50	59.86	58.85	39.75	39.59	39.13	39.49
F3_B_3	60.33	61.41	62.10	61.28	39.92	39.75	39.34	39.67
F3_B_4	60.90	60.75	60.53	60.73	38.66	39.27	39.58	39.17
F3_B_5	60.27	60.99	62.06	61.11	40.26	39.69	39.08	39.68

Table E.12: *Data; Fibraflex FF/20L6, ratio B = 0.0388 kg/m^2*

Label	Nozzle type	Print date	Test date	Hardening time (days)
F3_B_1	Hybrid nozzle	30/11/2018	07/12/2018	7
F3_B_2	Hybrid nozzle	30/11/2018	07/12/2018	7
F3_B_3	Hybrid nozzle	30/11/2018	07/12/2018	7
F3_B_4	Hybrid nozzle	30/11/2018	07/12/2018	7
F3_B_5	Hybrid nozzle	30/11/2018	07/12/2018	7

E.2. DOWN-FLOW NOZZLE

Plain concrete

Table E.13: *Dimensions; plain concrete, ratio A*

Label	Height (mm)				Width (mm)			
	h_1	h_2	h_3	Average	w_1	w_2	w_3	Average
F0_A_7	61.34	61.16	60.78	61.09	38.75	39.16	39.45	39.12
F0_A_8	60.30	60.46	60.39	60.38	38.82	39.01	39.07	38.97
F0_A_9	60.79	60.67	60.52	60.66	39.12	39.31	39.53	39.32

Table E.14: *Data; plain concrete, ratio A*

Label	Nozzle type	Print date	Test date	Hardening time (days)
F0_A_7	Down-flow nozzle	13/02/2019	20/02/2019	7
F0_A_8	Down-flow nozzle	13/02/2019	20/02/2019	7
F0_A_9	Down-flow nozzle	13/02/2019	20/02/2019	7

Cem-FIL Minibars 24mm, ratio B = 0.0842 kg/m^2

Table E.15: *Dimensions; Cem-FIL Minibars 24mm, ratio B = 0.0842 kg/m^2*

Label	Height (mm)				Width (mm)			
	h_1	h_2	h_3	Average	w_1	w_2	w_3	Average
F1_B_6	60.08	60.95	61.33	60.79	39.45	39.25	38.94	39.21
F1_B_7	60.08	60.23	60.17	60.17	39.78	39.49	39.17	39.48
F1_B_8	60.91	60.61	60.60	60.60	39.33	39.33	39.77	39.38
F1_B_9	60.38	60.92	60.89	60.89	39.59	39.28	39.10	39.32
F1_B_10	61.11	60.73	60.71	60.71	38.50	38.64	38.66	38.60

Table E.16: *Data; Cem-FIL Minibars 24mm, ratio B = 0.0842 kg/m²*

Label	Nozzle type	Print date	Test date	Hardening time (days)
F1_B_6	Down-flow nozzle	13/02/2019	20/02/2019	7
F1_B_7	Down-flow nozzle	13/02/2019	20/02/2019	7
F1_B_8	Down-flow nozzle	13/02/2019	20/02/2019	7
F1_B_9	Down-flow nozzle	13/02/2019	20/02/2019	7
F1_B_10	Down-flow nozzle	13/02/2019	20/02/2019	7

Dramix 3D RC-4530-BL, ratio B = 0.2227 kg/m²

Table E.17: *Dimensions; Dramix 3D RC-4530-BL, ratio B = 0.2227 kg/m²*

Label	Height (mm)				Width (mm)			
	h_1	h_2	h_3	Average	w_1	w_2	w_3	Average
F2_B_6	59.40	60.02	60.07	59.83	38.63	38.66	39.13	38.81
F2_B_7	57.34	57.79	58.16	57.76	38.72	38.90	39.19	38.94
F2_B_8	59.93	59.79	59.77	59.83	38.88	38.62	38.67	38.72
F2_B_9	59.45	59.69	59.82	59.65	38.83	39.08	39.21	39.04
F2_B_10	59.75	59.59	59.38	59.57	38.79	39.06	39.36	39.07

Table E.18: *Data; Dramix 3D RC-4530-BL, ratio B = 0.2227 kg/m²*

Label	Nozzle type	Print date	Test date	Hardening time (days)
F2_B_6	Down-flow nozzle	13/02/2019	20/02/2019	7
F2_B_7	Down-flow nozzle	13/02/2019	20/02/2019	7
F2_B_8	Down-flow nozzle	13/02/2019	20/02/2019	7
F2_B_9	Down-flow nozzle	13/02/2019	21/02/2019	8
F2_B_10	Down-flow nozzle	13/02/2019	21/02/2019	8

Fibraflex FF/20L6, ratio B = 0.0388 kg/m²

Table E.19: *Dimensions; Fibraflex FF/20L6, ratio B = 0.0388 kg/m²*

Label	Height (mm)				Width (mm)			
	h_1	h_2	h_3	Average	w_1	w_2	w_3	Average
F3_B_6	61.06	60.66	60.57	60.76	40.48	40.06	39.76	40.10
F3_B_7	60.47	60.31	60.18	60.32	40.35	40.14	39.77	40.09
F3_B_8	59.93	60.44	60.66	60.34	39.63	39.88	40.26	39.92
F3_B_9	59.97	60.50	60.84	60.44	40.45	40.23	39.95	40.21
F3_B_10	60.62	60.52	60.15	60.43	39.19	39.23	39.21	39.21

Table E.20: *Data; Fibraflex FF/20L6, ratio B = 0.0388 kg/m²*

Label	Nozzle type	Print date	Test date	Hardening time (days)
F3_B_6	Down-flow nozzle	13/02/2019	21/02/2019	8
F3_B_7	Down-flow nozzle	13/02/2019	21/02/2019	8
F3_B_8	Down-flow nozzle	13/02/2019	21/02/2019	8
F3_B_9	Down-flow nozzle	13/02/2019	21/02/2019	8
F3_B_10	Down-flow nozzle	13/02/2019	21/02/2019	8

E.3. PROOF OF CONCEPT

Cem-FIL Minibars 24mm, ratio C = 0.2485 kg/m^2

Table E.21: *Dimensions; Cem-FIL Minibars 24mm, ratio C = 0.2485 kg/m^2 (Blower)*

Label	Height (mm)				Width (mm)			
	h_1	h_2	h_3	Average	w_1	w_2	w_3	Average
F1_C_1	60.46	61.05	61.44	60.98	38.35	38.55	38.58	38.49
F1_C_2	59.45	59.47	59.31	59.41	38.48	39.48	38.41	38.46
F1_C_3	57.78	58.10	58.02	57.97	39.14	39.02	38.91	39.02

Table E.22: *Data; Cem-FIL Minibars 24mm, ratio C = 0.2485 kg/m^2 (Blower)*

Label	Nozzle type	Print date	Test date	Hardening time (days)
F1_C_1	Down-flow nozzle	13/02/2019	20/02/2019	7
F1_C_2	Down-flow nozzle	13/02/2019	20/02/2019	7
F1_C_3	Down-flow nozzle	13/02/2019	20/02/2019	7

APPENDIX F – TEST RESULTS

The test results of all performed test are given in the following tables, the most relevant information is taken from the raw data obtained by the Instron bench. The corresponding graphs are also shown for all test series.

F.1. HYBRID NOZZLE

Plain concrete

Table F.1: *Test results; Plain concrete, ratio A*

Label	Maximum stress (N/mm^2)	Deflection at max stress (mm)	Fracture energy (N/mm)
F0_A_1	3.10	0.16	-
F0_A_2	3.37	0.16	-
F0_A_3	4.36	0.22	-
F0_A_4	4.23	0.20	-
F0_A_5	3.49	0.18	-
F0_A_6	3.54	0.19	-
Average	3.68	0.18	-
Standard deviation	(0.59)	(0.03)	-

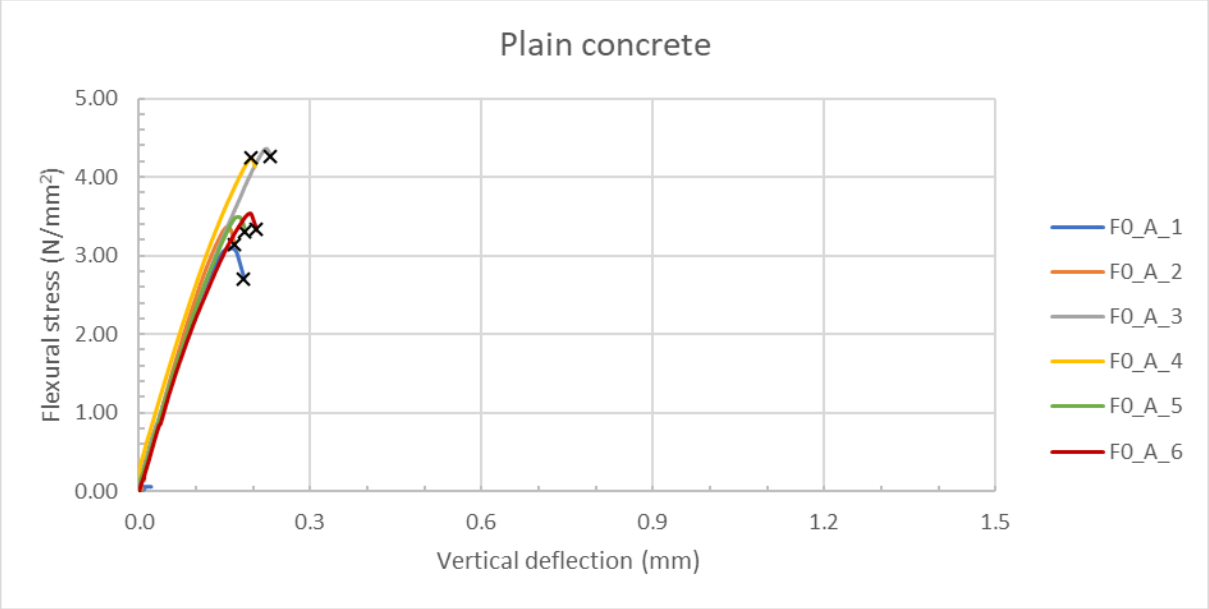

Figure F.1: *Stress-Deflection diagram, Plain concrete, Printed with a hybrid nozzle.*

Cem-FIL Minibars 24mm, ratio A = 0.0632 kg/m^2

Table F.2: *Test results; Cem-FIL Minibars 24mm, ratio A = 0.0632 kg/m^2*

Label	**Maximum stress** (N/mm^2)	**Deflection at max stress** (mm)	**Fracture energy** (N/mm)
F1_A_1	4.59	0.21	1.000
F1_A_2	4.24	0.19	-
F1_A_3	4.41	0.22	-
F1_A_4	3.46	0.19	-
F1_A_5	3.32	-	-
Average	4.00	0.20	1.000
Standard deviation	(0.57)	(0.01)	-

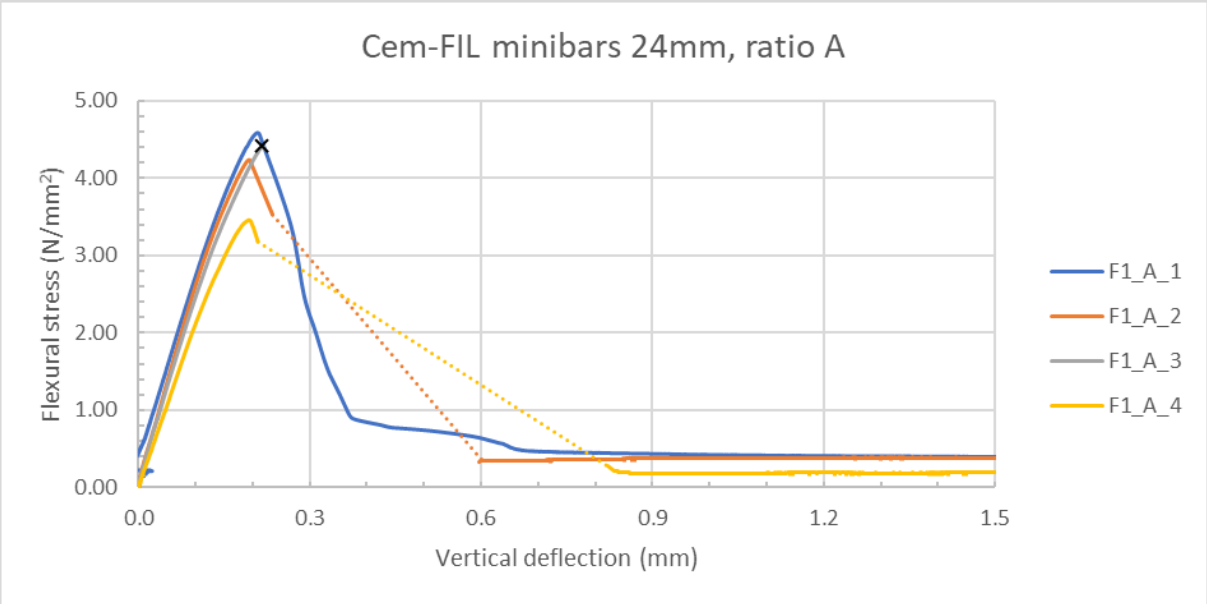

Figure F.2: *Stress-Deflection diagram, Cem-FIL Minibars 24mm, ratio A = 0.0632 kg/m^2, Printed with a hybrid nozzle.*

Dramix 3D RC-4530-BL, ratio A = 0.1559 kg/m²

Table F.3: *Test results; Dramix 3D RC-4530-BL, ratio A = 0.1559 kg/m²*

Label	Maximum stress (N/mm²)	Deflection at max stress (mm)	Fracture energy (N/mm)
F2_A_1	3.54	0.20	1.083
F2_A_2	3.88	0.23	-
F2_A_3	4.23	0.23	-
F2_A_4	3.76	0.19	-
F2_A_5	3.74	0.19	0.939
Average	3.83	0.21	1.011
Standard deviation	(0.25)	(0.01)	-

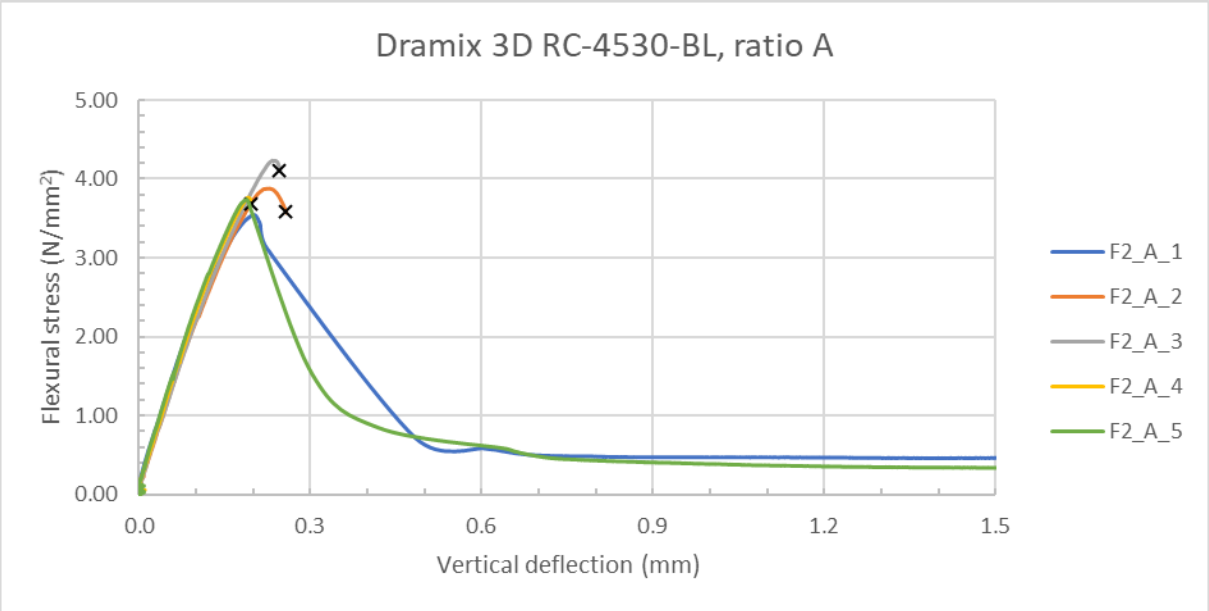

Figure F.3: *Stress-Deflection diagram, Dramix 3D RC-4530-BL, ratio A = 0.1559 kg/m², Printed with a hybrid nozzle.*

Dramix 3D RC-4530-BL, ratio B = 0.2227 kg/m^2

Table F.4: *Test results; Dramix 3D RC-4530-BL, ratio B = 0.2227 kg/m^2*

Label	Maximum stress (N/mm^2)	Deflection at max stress (mm)	Fracture energy (N/mm)
F2_B_1	4.09	0.22	-
F2_B_2	3.34	0.21	-
F2_B_3	3.63	0.21	1.092
F2_B_4	3.51	0.20	1.260
F2_B_5	3.28	0.21	1.079
Average	3.57	0.21	1.144
Standard deviation	(0.32)	(0.01)	(0.101)

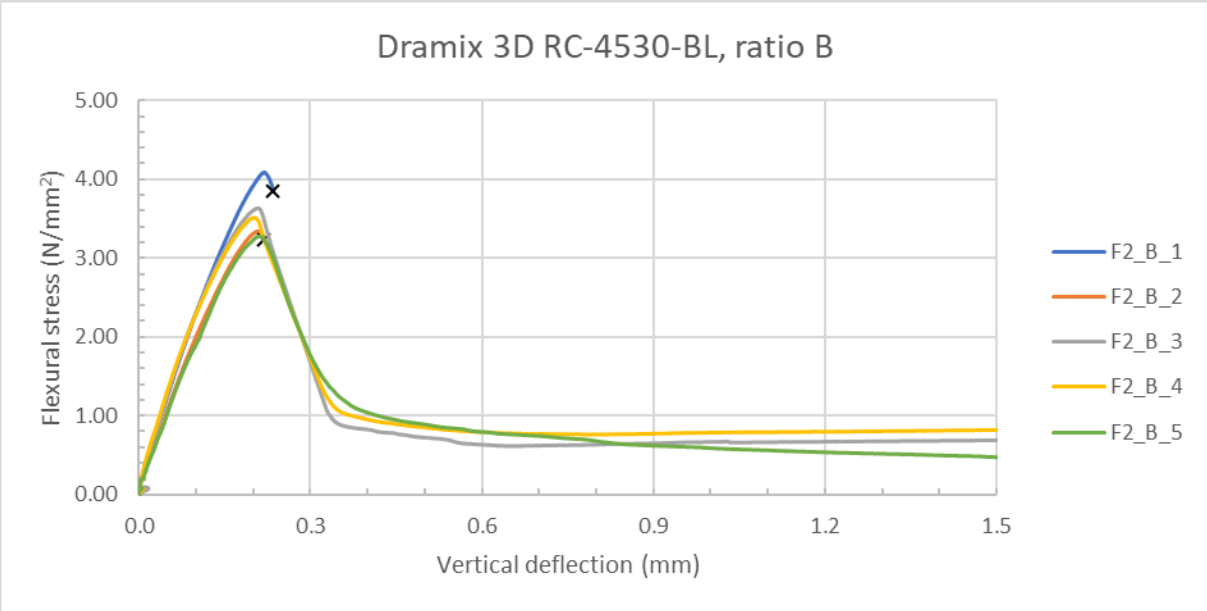

Figure F.4: *Stress-Deflection diagram, Dramix 3D RC-4530-BL, ratio B = 0.2227 kg/m^2, Printed with a hybrid nozzle.*

Fibraflex FF/20L6, ratio A = 0.0259 kg/m^2

Table F.5: *Test results; Fibraflex FF/20L6, ratio A = 0.0259 kg/m^2*

Label	Maximum stress (N/mm^2)	Deflection at max stress (mm)	Fracture energy (N/mm)
F3_A_1	3.03	0.18	0.505
F3_A_2	3.27	0.23	0.520
F3_A_3	3.05	0.20	0.682
F3_A_4	3.06	0.19	-
F3_A_5	2.86	0.19	0.597
Average	3.05	0.20	0.576
Standard deviation	(0.15)	(0.02)	(0.070)

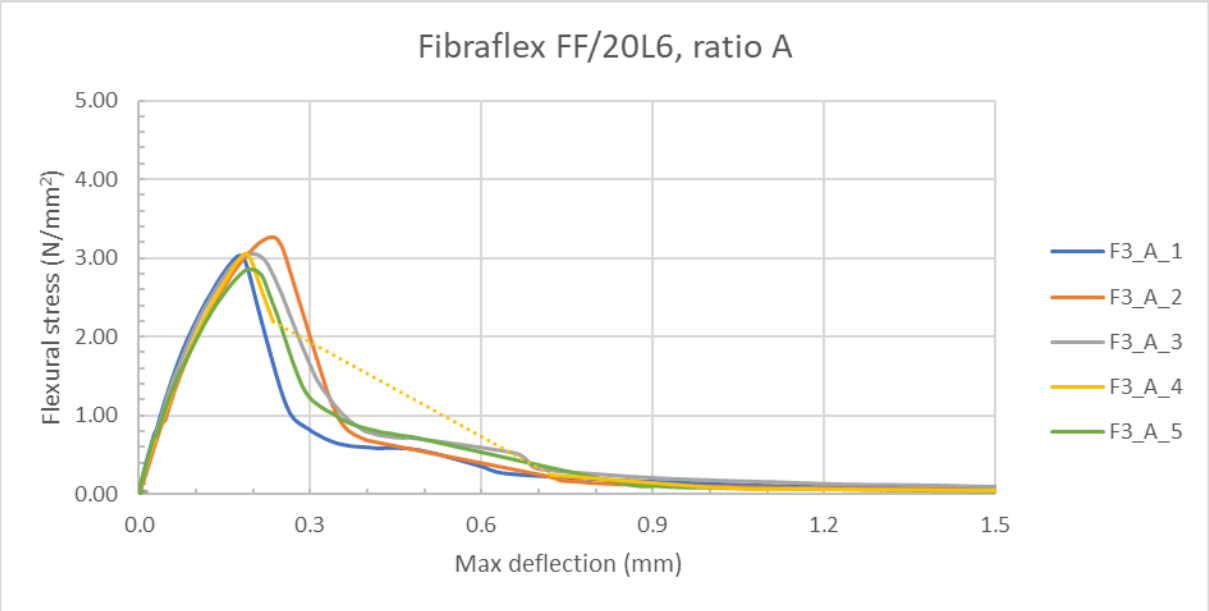

Figure F.5: *Stress-Deflection diagram, Fibraflex FF/20L6, ratio A = 0.0259 kg/m^2, Printed with a hybrid nozzle.*

Fibraflex FF/20L6, ratio B = 0.0388 kg/m^2

Table F.6: *Test results; Fibraflex FF/20L6, ratio B = 0.0388 kg/m^2*

Label	Maximum stress (N/mm^2)	Deflection at max stress (mm)	Fracture energy (N/mm)
F3_B_1	3.19	0.23	0.731
F3_B_2	2.93	0.22	0.691
F3_B_3	2.97	0.22	0.485
F3_B_4	2.48	0.18	0.528
F3_B_5	2.87	0.22	0.654
Average	2.89	0.21	0.618
Standard deviation	(0.26)	(0.02)	(0.106)

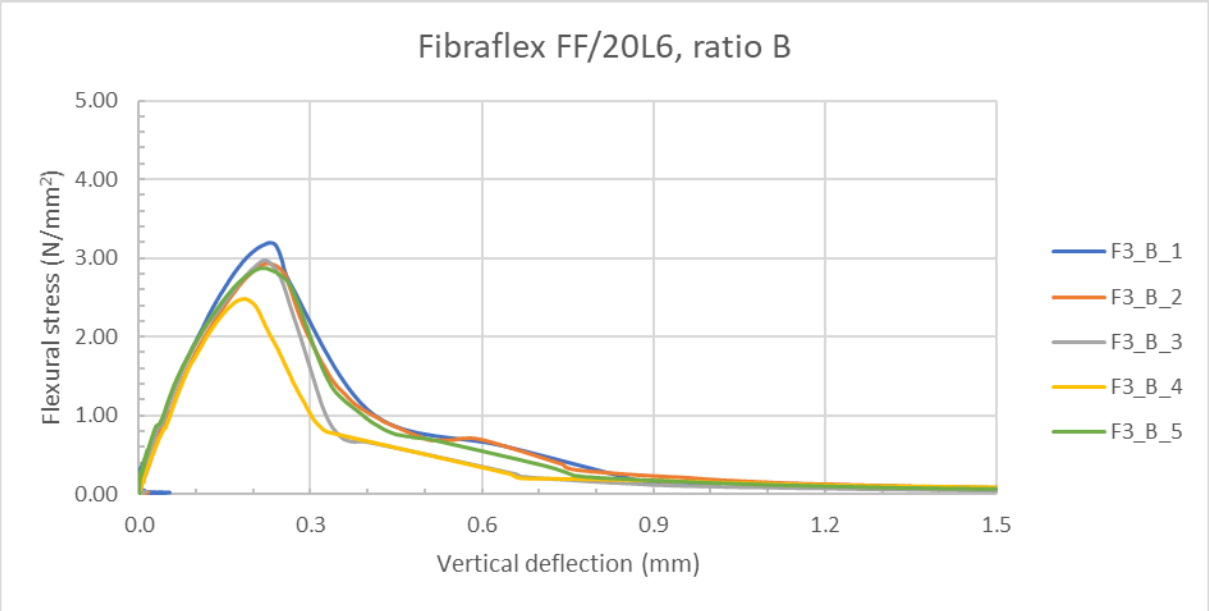

Figure F.6: *Stress-Deflection diagram, Fibraflex FF/20L6, ratio B = 0.0388 kg/m^2, Printed with a hybrid nozzle.*

F.2. DOWN-FLOW NOZZLE

Plain concrete

Table F.7: *Test results; Plain concrete, ratio A*

Label	Maximum stress (N/mm^2)	Deflection at max stress (mm)	Fracture energy (N/mm)
F0_A_7	2.11	0.14	-
F0_A_8	2.36	0.14	-
F0_A_9	2.78	0.17	-
Average	2.41	0.15	-
Standard deviation	(0.34)	(0.02)	-

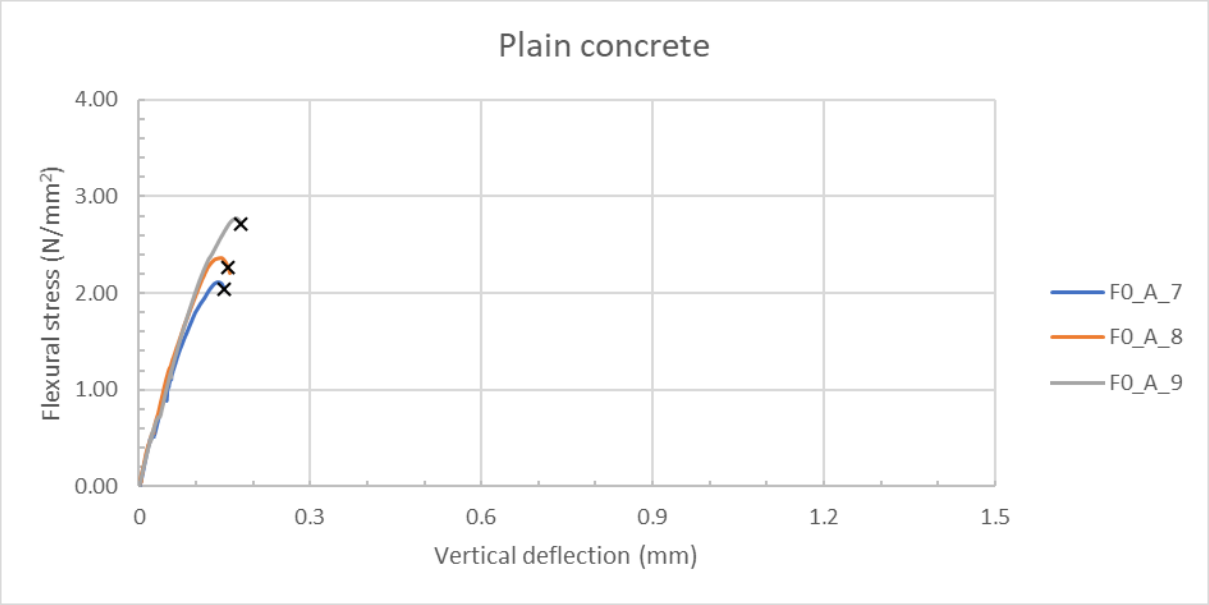

Figure F.7: *Stress-Deflection diagram, Plain concrete, Printed with a down-flow nozzle.*

Cem-FIL Minibars 24mm, ratio B = 0.0842 kg/m^2

Table F.8: *Test results; Cem-FIL Minibars 24mm, ratio B = 0.0842 kg/m^2*

Label	**Maximum stress** (N/mm^2)	**Deflection at max stress** (mm)	**Fracture energy** (N/mm)
F1_B_6	3.36	0.18	1.179
F1_B_7	3.41	0.17	0.891
F1_B_8	3.01	0.15	0.746
F1_B_9	3.22	0.17	0.550
F1_B_10	2.61	0.15	0.501
Average	3.12	0.16	0.774
Standard deviation	(0.33)	(0.01)	(0.275)

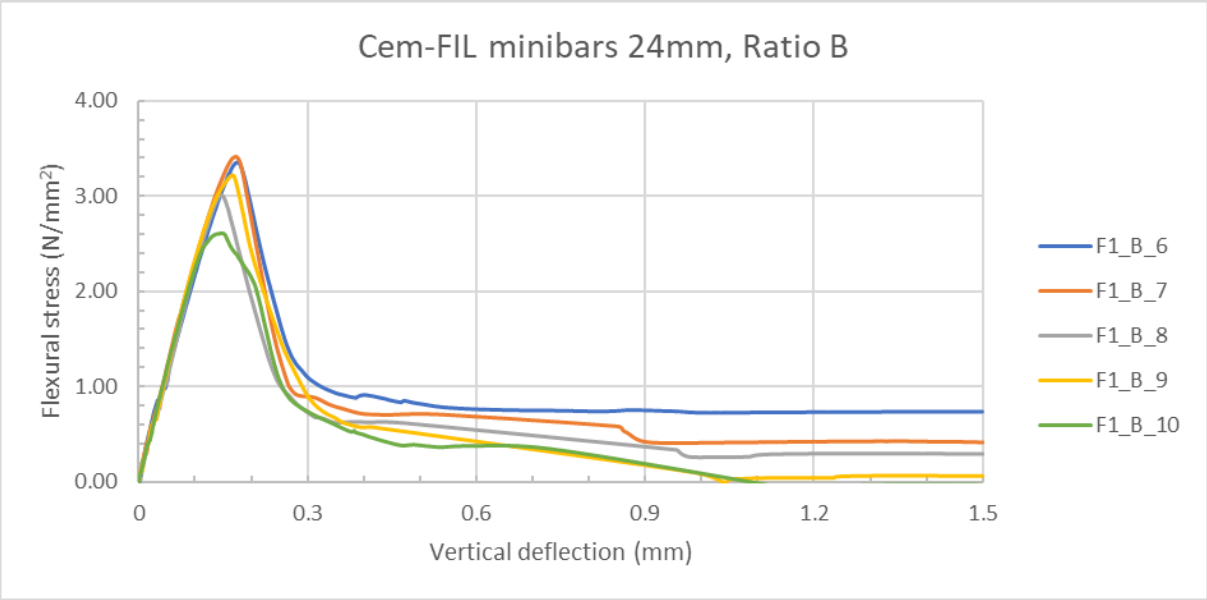

Figure F.8: *Stress-Deflection diagram, Cem-FIL Minibars 24mm, ratio B = 0.0842 kg/m^2, Printed with a down-flow nozzle.*

Dramix 3D RC-4530-BL, ratio B = 0.2227 kg/m^2

Table F.9: *Test results; Dramix 3D RC-4530-BL, ratio B = 0.2227 kg/m^2*

Label	**Maximum stress** (N/mm^2)	**Deflection at max stress** (mm)	**Fracture energy** (N/mm)
F2_B_6	2.34	0.15	1.429
F2_B_7	2.68	0.19	0.706
F2_B_8	2.74	0.21	2.186
F2_B_9	2.32	0.18	1.579
F2_B_10	2.74	0.22	1.250
Average	2.56	0.19	1.430
Standard deviation	(0.22)	(0.03)	(0.536)

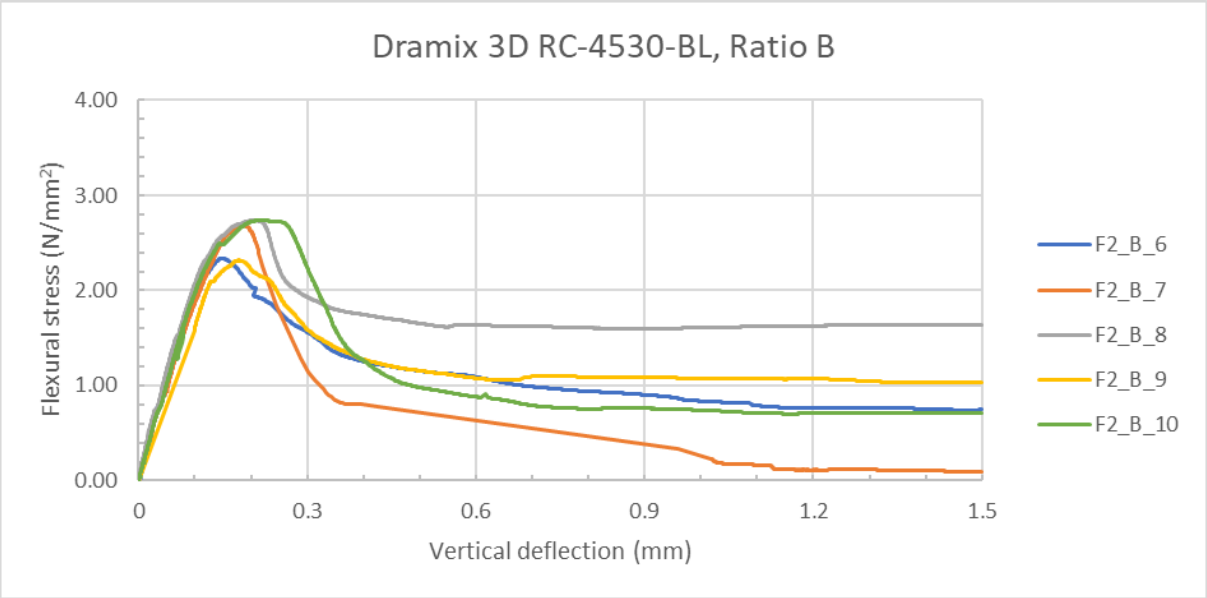

Figure F.9: *Stress-Deflection diagram, Dramix 3D RC-4530-BL, ratio B = 0.2227 kg/m^2, Printed with a down-flow nozzle.*

Fibraflex FF/20L6, ratio B = 0.0388 kg/m^2

Table F.10: *Test results; Fibraflex FF/20L6, ratio B = 0.0388 kg/m^2*

Label	Maximum stress (N/mm^2)	Deflection at max stress (mm)	Fracture energy (N/mm)
F3_B_6	2.64	0.19	0.699
F3_B_7	2.85	0.20	1.099
F3_B_8	2.50	0.18	0.308
F3_B_9	2.86	0.30	0.742
F3_B_10	2.40	0.18	0.883
Average	2.65	0.21	0.746
Standard deviation	(0.20)	(0.05)	(0.291)

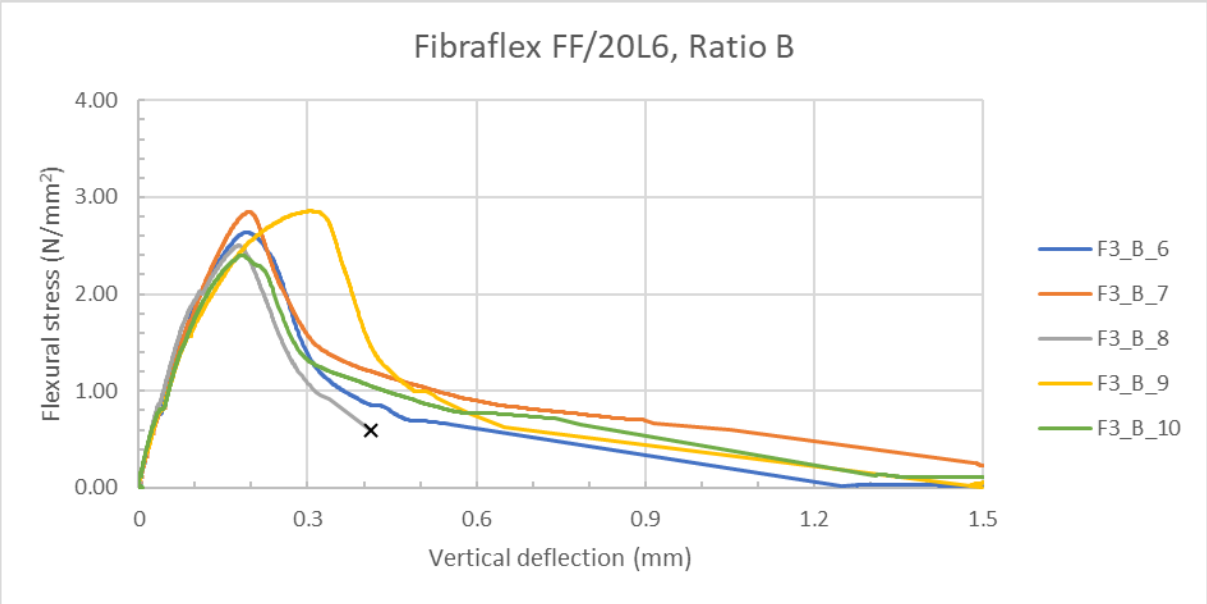

Figure F.10: *Stress-Deflection diagram, Fibraflex FF/20L6, ratio B = 0.0388 kg/m^2, Printed with a down-flow nozzle.*

F.3. PROOF OF CONCEPT

Cem-FIL Minibars 24mm, ratio C = 0.2485 kg/m^2

Table F.11: *Test results; Cem-FIL Minibars 24mm, ratio C = 0.2485 kg/m^2 (Blower)*

Label	**Maximum stress** (N/mm^2)	**Deflection at max stress** (mm)	**Fracture energy** (N/mm)
F1_C_1	2.96	0.16	0.805
F1_C_2	3.02	0.19	0.797
F1_C_3	3.06	0.18	1.193
Average	3.02	0.17	0.931
Standard deviation	(0.05)	(0.02)	(0.226)

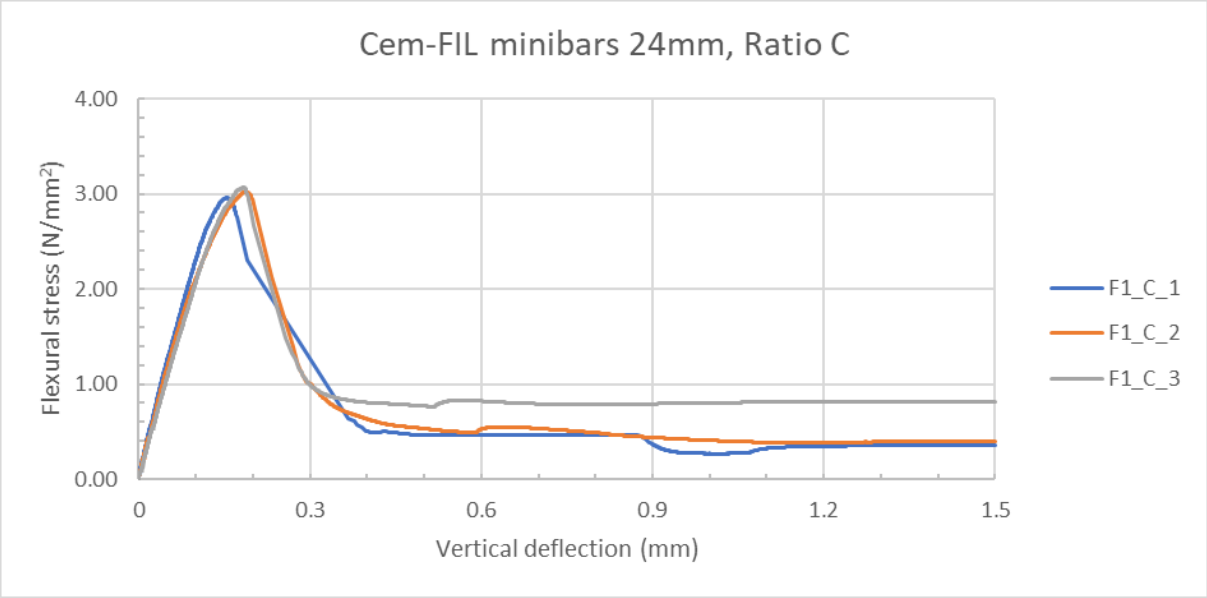

Figure F.11: *Stress-Deflection diagram, Cem-FIL Minibars 24mm, ratio C = 0.2485 kg/m^2, Printed with a down-flow nozzle.*